The Dissertation Committee for Adam Keith Ekenseair certifies that this is the approved version of the following dissertation:

A Fundamental Investigation of Non-Fickian and Case II

Penetrant Transport in Glassy Polymers

Committee:

Nicholas A. Peppas, Supervisor

Donald R. Paul

Benny D. Freeman

Douglas R. Lloyd

Richard A. Ketcham

A Fundamental Investigation of Non-Fickian and Case II

Penetrant Transport in Glassy Polymers

by

Adam Keith Ekenseair, B.S. Ch.E.

Dissertation

Presented to the Faculty of the Graduate School of

The University of Texas at Austin

in Partial Fulfillment

of the Requirements

for the Degree of

Doctor of Philosophy

The University of Texas at Austin

August 2010

Dedication

This work is dedicated to my wonderful wife, beautiful daughter, and supportive parents without whom my graduate career would not have been possible.

Acknowledgements

Thanks so much to my loving wife, Chelsea, for her patience, love, and caring throughout my graduate career, and my beautiful daughter, Anna, for bringing a smile to my face every day. My parents also never spared their expression of how proud they are of me, and never hesitated to lend a hand when times got hard. Their support made this entire Austin experience possible.

My path of academic experiences might not have progressed beyond undergrad if it had not been for the support and guidance provided by Professor Edgar C. Clausen at the University of Arkansas. He gave me the opportunity, as an undergraduate, to experience what independent graduate research was like, facilitated my efforts to participate in external research experiences through the NSF-REU program, and gave me the necessary tools and understanding to be successful in my PhD research.

Special thanks to my advisor Professor Nicholas A. Peppas for his guidance, patience, encouragement, and advice throughout my graduate career. This work would not have been possible without the countless hours of time spent by Professor Peppas providing guidance and instruction for my research. I would like to thank Dr. Richard A. Ketcham for his time and efforts running and assisting in the analysis of the X-ray computed tomography experiments. I would also like to thank my thesis committee for lending their valuable time and expertise in reviewing this thesis and my defense.

Life would not have been quite as enjoyable without my labmates to serve as an outlet for all the frustrations and assist in solving experimental difficulties. Special thanks go to Don Owens and Steve Marek for their consultations regarding polymer chemistry and experimental procedures.

Finally, this work would not have been possible if not for the tireless efforts of the remarkable undergraduate assistants that I had the pleasure of working with over the course of my studies. Thank you, Michael Nelson, Yi-Hsuan Chen, Akshar Patel, Kevin Fernandes, and especially Megan Kittle, Alexandra Corona, Robert Seidel, and Craig Fredrich. I wish you all the best of luck on your future endeavors.

A Fundamental Investigation of Non-Fickian and Case II

Penetrant Transport in Glassy Polymers

Publication No._____

Adam Keith Ekenseair, Ph.D.

The University of Texas at Austin, 2010

Supervisor: Nicholas A. Peppas

The relative rates of the diffusional and relaxational processes during the absorption of penetrant molecules in glassy polymers determine the nature of the transport process and lead to Fickian, Case II, and anomalous absorption behavior. While previous models account for anomalous behavior, there is still a disconnect between theory and experiment, as data must be fit to the model with previously determined independent parameters. With trends leading to smaller device scales and increasingly complex polymer structures, there is a need for a quantitative understanding of the manner in which a polymer's network structure alters both the rate and the mode of penetrant transport.

To this end, samples of glassy poly(methyl methacrylate), poly(2-hydroxyethyl methacrylate), and poly(vinyl alcohol) were synthesized primarily by an *iniferter*-mediated, thermally-initiated free radical polymerization procedure. The thermal and mechanical properties of these polymers, as well as the polymer network structure, were varied through crosslinking and confirmed by detailed characterization. The

dynamics of small molecule penetrant transport were examined in each polymer, with an emphasis on the occurrence of non-Fickian and Case II transport.

The degree of crosslinking and choice of crosslinking molecule were shown to be powerful tools in tuning the observed penetrant transport process. For instance, the transport dynamics were altered from Fickian to Case II by increasing the degree of crosslinking and from Case II to Fickian by increasing the crosslinking interchain bridge length. Within the purely Case II regime, the rate of penetrant transport, or the Case II front velocity, was shown to scale with the square root of the degree of crosslinking in all systems investigated.

A novel procedure for the *in situ* examination of penetrant transport in glassy polymers was developed utilizing high-resolution X-ray computed tomography. This completely nondestructive technique was used to visualize features in the interior of opaque solid objects and obtain digital information on their 3-D structure and properties. In this manner, the time-dependent penetrant concentration profiles throughout a swelling polymer were determined and analyzed.

Table of Contents

List of Tables

List of Figures

xv

xvi

xvii

Chapter 1: Introduction

Glassy polymers are increasingly relied upon in the construction and fabrication of high-tech devices. These devices are often used in applications, such as membrane separations, barrier packaging, microfluidics, artificial hearts, bones, & tissues, and controlled drug delivery, where the polymers come into contact with fluids, either liquids or vapors, capable of penetrating the polymer network. When such a situation arises, the penetrant, either a solvent or a non-solvent, diffuses into the polymer over time until an equilibrium concentration is reached. The process of diffusion of one material into another is generally described by Fick's 2nd Law:

$$\frac{\partial C_A}{\partial t} = -D_{AB} \frac{d^2 C_A}{dz^2} \tag{1}$$

Where C_A is the concentration of the diffusing species, t is time, z is the distance in the direction of transport, and D_{AB} is the binary diffusion coefficient for the specific polymer-penetrant combination [1, 2].

This relationship is valid for most systems where one fluid is diffusing into another and even applies to penetrant diffusion into rubbery polymers, or polymers that are above their glass transition temperature, T_g, and behave as viscoelastic fluids. However, it was discovered early on that some penetrants when brought into contact with glassy polymers, rigid polymers below their T_g, at certain conditions show anomalous, or non-Fickian transport behavior [3]. While there is generally agreement on the mechanisms that underlie the appearance of anomalous transport, how to model and predict this behavior is still a topic of much debate.

The manner in which penetrant molecules enter and move through polymers, and the associated physical ramifications, is of general importance in the development of plastic structures that may be exposed to organic chemicals, especially those used in

food and barrier packaging [4, 5]. Even at very low organic vapor concentrations, deviations from Fickian transport behavior can be seen in many commercially relevant polymers, including polystyrene and poly(methyl methacrylate) [6-9]. This goes so far as to result in material failure in the form of cracking or crazing when exposed to a penetrant that favors a strongly non-Fickian transport mechanism [9-12]. A better understanding of the interrelation of penetrant and polymer properties with the occurrence of non-Fickian behavior would enable more appropriate material design and selection in the early stages of product development.

With the advent of glassy polymer-based, high-tech devices in fields such as microelectronics and microfluidics, as well as the associated continuous drive towards smaller and more complex designs, the effects of penetrant transport into these polymers are becoming increasingly significant. Microfluidics, in particular, has seen much work this decade pursuing "Lab on a Chip" devices, which would necessarily incorporate many features where fluids are transported through and processed in polymeric channels and reservoirs [13-17]. In addition to potential penetrant transport into the wall material, membranes are being utilized for component separation, and swellable polymers are being employed as microvalves, which often respond to environmental stimuli and imbibe fluid to the point that bulk liquid flow is stopped [18-20]. Moreover, microfluidic devices are promising for basic chemical reactions, whether as part of a "Lab on a Chip" device or not, in which the fluids used may go so far as to induce crack and craze formation in the channels, leading to device failure [21].

In the field of controlled drug delivery, traditional polymer network structures, and their associated structure-property relationships, are quickly becoming obsolete. The polymers of choice are usually heavily crosslinked and often include long-chain crosslinks and grafted substituent chains. In order to produce "smart" polymers, the polymer networks generally include dissociable hydrogen bonding groups from complementary comonomers or are made from interpenetrating polymer networks [22-

31]. Thus, the need for new structure-property relationships and investigations into the fundamental penetrant transport mechanisms is evident.

It is therefore the intent of this author to explore, as part of this thesis, penetrant transport in glassy polymers with both traditional and complex network structures from a fundamental viewpoint to increase the general understanding of such processes, with a particular emphasis on non-Fickian behavior. In addition, novel *in situ* techniques will be pursued to visualize and quantify the transport mechanisms within these materials. The experimental results of this work will facilitate the formulation of new scaling relationships and lay the groundwork for experimental validation of a property-based predictive theory for anomalous penetrant transport in glassy polymers.

REFERENCES

1.   Crank, J., *The Mathematics of Diffusion*. 2nd ed. 1975, New York: Oxford University Press. p. 47.
2.   Crank, J. and G.S. Park, *Diffusion in Polymers*. 1968, New York: Academic Press.
3.   Alfrey, T., E.F. Gurnee, and W.G. Lloyd, *Diffusion in Glassy Polymers.* Journal of Polymer Science, Part C: Polymer Symposia, 1966. **12**: p. 249-261.
4.   Cayot, N., C. Dury-Brun, T. Karbowiak, G. Savary, and A. Voilley, *Measurement of transport phenomena of volatile compounds: A review.* Food Research International, 2008. **41**(4): p. 349-362.
5.   Zaki, O., B. Abbes, and L. Safa, *Non-Fickian diffusion of amyl acetate in polypropylene packaging: Experiments and modelling.* Polymer Testing, 2009. **28**(3): p. 315-323.
6.   Gall, T.P., R.C. Lasky, and E.J. Kramer, *Case-II Diffusion - Effect of Solvent Molecule Size.* Polymer, 1990. **31**(8): p. 1491-1499.
7.   Jacques, C.H.M. and H.B. Hopfenberg, *Kinetics of Vapor and Liquid Transport in Glassy Polyblends of Polystyrene and Poly (2,6-Dimethyl 1,4-Phenylene Oxide) .2.* Polymer Engineering and Science, 1974. **14**(6): p. 449-455.
8.   Lasky, R.C., E.J. Kramer, and C.Y. Hui, *The Initial-Stages of Case-II Diffusion at Low Penetrant Activities.* Polymer, 1988. **29**(4): p. 673-679.
9.   Rosen, B., *Time-Dependent Tensile Properties. Part III. Microfracture and Non-Fickian Vapor Diffusion in Organic Glasses.* Journal of Polymer Science, 1961. **49**: p. 177-188.
10.   Hopfenberg, H.B., R.H. Holley, and V. Stannett, *The Effect of Penetrant Activity and Temperature on Anomalous Diffusion of Hydrocarbons and Solvent Crazing in Polystyrene .1. Biaxially Oriented Polystyrene.* Polymer Engineering and Science, 1969. **9**(4): p. 242-&.
11.   Kambour, R.P., C.L. Gruner, and E.E. Romagosa, *Solvent Crazing of Dry Polystyrene and Dry Crazing of Plasticized Polystyrene.* Journal of Polymer Science Part B-Polymer Physics, 1973. **11**(10): p. 1879-1890.
12.   Kambour, R.P., E.E. Romagosa, and C.L. Gruner, *Swelling, Crazing, and Cracking of an Aromatic Copolyether-Sulfone in Organic Media.* Macromolecules, 1972. **5**(4): p. 335-&.
13.   Abgrall, P. and A.M. Gue, *Lab-on-chip technologies: making a microfluidic network and coupling it into a complete microsystem - a review.* Journal of Micromechanics and Microengineering, 2007. **17**(5): p. R15-R49.
14.   Gunther, A. and K.F. Jensen, *Multiphase microfluidics: from flow characteristics to chemical and materials synthesis (vol 6, pg 1487, 2006).* Lab on a Chip, 2007. **7**(7): p. 935-935.
15.   Haeberle, S. and R. Zengerle, *Microfluidic platforms for lab-on-a-chip applications.* Lab on a Chip, 2007. **7**(9): p. 1094-1110.

16.   Hu, G.Q. and D.Q. Li, *Multiscale phenomena in microfluidics and nanofluidics.* Chemical Engineering Science, 2007. **62**(13): p. 3443-3454.

17.   Situma, C., M. Hashimoto, and S.A. Soper, *Merging microfluidics with microarray-based bioassays.* Biomolecular Engineering, 2006. **23**(5): p. 213-231.

18.   Chaterji, S., I.K. Kwon, and K. Park, *Smart polymeric gels: Redefining the limits of biomedical devices.* Progress in Polymer Science, 2007. **32**(8-9): p. 1083-1122.

19.   de Jong, J., R.G.H. Lammertink, and M. Wessling, *Membranes and microfluidics: a review.* Lab on a Chip, 2006. **6**(9): p. 1125-1139.

20.   Zhang, C.S., D. Xing, and Y.Y. Li, *Micropumps, microvalves, and micromixers within PCR microfluidic chips: Advances and trends.* Biotechnology Advances, 2007. **25**(5): p. 483-514.

21.   Geyer, K., J.D.C. Codee, and P.H. Seeberger, *Microreactors as tools for synthetic chemists - The chemists' round-bottomed flask of the 21st century?* Chemistry - A European Journal, 2006. **12**(33): p. 8434-8442.

22.   Brannon-Peppas, L. and N.A. Peppas, *Solute and Penetrant Diffusion in Swellable Polymers .9. The Mechanisms of Drug Release from Ph-Sensitive Swelling-Controlled Systems.* Journal of Controlled Release, 1989. **8**(3): p. 267-274.

23.   Brannon-Peppas, L. and N.A. Peppas, *Equilibrium Swelling Behavior of Dilute Ionic Hydrogels in Electrolytic Solutions.* Journal of Controlled Release, 1991. **16**(3): p. 319-330.

24.   Brazel, C.S. and N.A. Peppas, *Modeling of drug release from swellable polymers.* European Journal of Pharmaceutics and Biopharmaceutics, 2000. **49**(1): p. 47-58.

25.   Langer, R. and N.A. Peppas, *Advances in biomaterials, drug delivery, and bionanotechnology.* AIChE Journal, 2003. **49**(12): p. 2990-3006.

26.   Langer, R. and D.A. Tirrell, *Designing materials for biology and medicine.* Nature, 2004. **428**(6982): p. 487-492.

27.   Losi, E., R. Bettini, P. Santi, F. Sonvico, G. Colombo, K. Lofthus, P. Colombo, and N.A. Peppas, *Assemblage of novel release modules for the development of adaptable drug delivery systems.* Journal of Controlled Release, 2006. **111**(1-2): p. 212-218.

28.   Peppas, N.A., *Intelligent biomaterials as pharmaceutical carriers in microfabricated and nanoscale devices.* MRS Bulletin, 2006. **31**(11): p. 888-893.

29.   Peppas, N.A., P. Bures, W. Leobandung, and H. Ichikawa, *Hydrogels in pharmaceutical formulations.* European Journal of Pharmaceutics and Biopharmaceutics, 2000. **50**(1): p. 27-46.

30.   Peppas, N.A., J.Z. Hilt, A. Khademhosseini, and R. Langer, *Hydrogels in biology and medicine: From molecular principles to bionanotechnology.* Advanced Materials, 2006. **18**(11): p. 1345-1360.

31.   Peppas, N.A. and A.R. Khare, *Preparation, Structure and Diffusional Behavior of Hydrogels in Controlled-Release.* Advanced Drug Delivery Reviews, 1993. **11**(1-2): p. 1-35.

Chapter 2: Background

INTRODUCTION

The intent of this chapter is to present a qualitative understanding of non-Fickian penetrant transport dynamics in glassy polymers. To this end, the basic mechanical aspects of and the major experimental findings concerning Case II transport are reviewed. Additionally, anomalous mechanisms are described and some qualitative relationships between the various transport mechanisms are discussed.

NON-FICKIAN AND CASE II TRANSPORT

Phenomenological Aspects of Case II Transport

Deviations from the expected diffusive behavior in regards to the transport of small penetrant molecules, either vapors or liquids, into glassy polymers have long been reported. These penetrant-polymer systems exhibit a wide array of dynamic sorption behavior, which will be discussed below. First, it is constructive to define clearly Case II behavior and discuss all of its ramifications, as it is often referred to as a second, limiting case for the transport of small molecules into glassy polymers (transport obeying Fick's 2nd law being Case I, or often simply Fickian, transport).

The basic notion is that, in glassy polymers, the relaxation and chain disentanglement process necessary for sample expansion and sorption of penetrants can be a rate-controlling step [1, 2]; thus the transport of the penetrant would proceed at a rate dependent on the mechanical properties of the polymer glass and its thermodynamic compatibility with the penetrant. Case II transport, which has been presented as a limiting case of complete relaxational control over the transport dynamics, has five phenomenological traits, all of which are necessary conditions for the occurrence of this mechanism [3, 4].

First, the most common indication of a Case II transport mechanism is the significant deviation from Fick's 2nd Law in the early portion of an integral sorption experiment (an integral sorption experiment is here defined as one in which a dry polymer is initially immersed in a penetrant-rich environment held at a constant external activity and is subsequently allowed to absorb penetrant until an equilibrium degree of swelling is reached). While the early time penetrant uptake of a system following Fick's 2nd Law is proportional to the square root of time, $t^{1/2}$, [5] Case II transport exhibits a direct proportionality to time, t, [3] as illustrated in Figure 2.1. Also unlike Fickian dynamics, this initial time dependence persists until equilibrium is reached.

Second, during the penetrant sorption process, there is a sharp front separating a dry polymer core and an outer, penetrant-swollen region. This front and its inward propagation during the sorption process are generally visible to the naked eye due to the refractive index difference between dry and swollen polymer materials [6]. In some cases, an opaque polymer may even become transparent behind the advancing front if a sufficient penetrant concentration is met in the swollen polymer. However, the existence of this sharp, inwardly propagating front during integral sorption is not by itself a conclusive indication of Case II behavior. Indeed, sharp penetrant fronts can be observed in most penetrant sorption studies into glassy polymers owing to the strong concentration-dependence of the diffusion coefficient in such cases [1, 7, 8].

Third, the penetrant concentration in the swollen region behind the advancing front must maintain a constant concentration throughout the sorption process and constitute an essentially equilibrium degree of swelling. However, it should be noted that this equilibrium degree of swelling need not be the same as that of the final end-state of the polymer-penetrant system, as will be discussed below.

Fourth, the sharp front separating dry polymer from fully-swollen polymer must advance at a constant rate through the sample until the two fronts (one from each face in a planar integral sorption experiment) meet in the center and sorption ends. In this

7

manner, the transport kinetics are forced to scale with t and not $t^{1/2}$. In Fickian transport behavior, the rate of penetrant sorption is continually decreasing as the concentration of the penetrant in the polymer increases (or in other words as the overall driving force for sorption is decreased). However, Case II transport exhibits a seemingly concentration independent behavior, which is a result of the second through fourth features. Thus, there is still a concentration-differential driving force for transport to occur; however, it is localized at the sorption front, remains constant, and propagates spatially through the polymer.

Fifth, there is a Fickian precursor, or foot, that precedes the sharp penetrant front through the polymer. The presence of this precursor was first predicted from theories and later experimentally verified by numerous authors [9-14]. Basically, this precursor represents passive Fickian diffusion of the penetrant into the free volume of the glassy polymer and is responsible for initiating, through solvent-plasticization, the very rapid expansion of the polymer network over the front region. The presence of this Fickian precursor also necessitates another commonly observed trait of Case II transport; namely that there is an induction time associated with sorption in glassy polymers, where the dominance of a particular rate-controlling mechanism has not yet been established. This induction time can be very short and sometimes impossible to experimentally observe [15]; however, more often it is a significant component of the transport dynamics and its magnitude can be related to the properties of the polymer and penetrant [16]. Figure 2.2 illustrates the overall Case II transport mechanism when compared to a Fickian mechanism.

An additional aspect of diffusion of penetrants into glassy polymers that should be noted is the anisotropy of dimensional swelling. This anisotropic swelling will often occur even in Fickian or anomalous transport and is not related specifically to Case II behavior, though it always accompanies it [17]. Consequently, when the dimensional swelling profiles of a disc or film are examined, one will see that the initial rate of thickness expansion is much greater than the rate of expansion along the edge surface

8

area. This trend will continue until the glassy core has disappeared, at which point the thickness will begin to recede, while the diameter expansion will accelerate. Interestingly, though, the overall rate of volume expansion through this process is often constant in a Case II mechanism, owing to the fact that the swollen polymer is already at its equilibrium degree of swelling [17].

This dimensional swelling behavior is a result of the difference in mechanical properties of the dry, glassy core and a more-swollen, surrounding gel layer [18]. As the outer layers of the polymer swell, through a Case II or a non-Case II mechanism, each differential layer of expanding polymer chains exerts an outward force on the next layer in. This is due to the fact that, at least in polymers above the critical molecular weight for entanglements, each differential layer of chains is entangled with the layer in front of and behind it. Thus, if one differential element expands, it will exert a force on the next element, encouraging it to also expand. However, if there is a glassy polymer core, whether completely dry or just at a low enough penetrant concentration to remain glassy, the chains in this segment of the polymer sample will not expand. This effectively stresses the surrounding swollen polymer layers and orients the swelling process in the direction of greatest surface area. Thus, for a thin film placed in a penetrant solution, the dynamic dimensional expansion process will be anisotropic, as illustrated in Figure 2.3. Despite this dynamic anisotropy, once the glassy core has disappeared, the stresses it imposed on the surrounding swollen layer will dissipate and the sample will undergo bulk structural rearrangement towards a seemingly isotropically swollen end-state (so long as the polymer end-state is rubbery and thereby allows this rearrangement to occur in an accessible time frame) [19].

This anisotropic swelling is one of the many reasons given for the appearance of another common integral transport phenomenon; namely the polymer may initially absorb more penetrant than is thermodynamically ideal and will subsequently expel some penetrant near the end of the sorption process. In this manner, the mass uptake of penetrant by the polymer can "overshoot" its equilibrium value. In most cases, this is

likely due to a difference in the equilibrium of a stressed (by the dry polymer core) and a non-stressed swollen polymer [19, 20]. In fact, evidence suggests that the equilibrium penetrant content is generally higher in oriented or stretched polymers than in homogeneous or annealed polymers [21] (assuming of course that there were no additional associated structural changes to the polymer such as an increase in crystallinity). In addition, other possible reasons for the observation of an overshoot in the integral sorption penetrant uptake are solvent-actuated crystallization of the polymer in the swollen state and the desorption of an initially present species such as unreacted monomer or solvent that was entrapped in the polymer core [22].

Significant Experimental Findings

One recurring difficulty and area of occasional confusion in discussing and attempting to model Case II and anomalous transport surrounds the presence of a glass/rubber transition during the sorption process. Many authors mention and subsequently utilize as a key assumption in their model derivations that the swollen end-state of the polymer must be rubbery. In other words, the polymer must be able to absorb enough penetrant to depress the glass transition temperature of the then-plasticized polymer below the experimental temperature. However, it has been shown experimentally by a number of authors [23-26] that Case II transport can occur regardless of the equilibrium state of the swollen polymer (glassy or rubbery). This implies that the key considerations in determining whether Case II transport will occur and at what rate lie in the polymer's glassy-state properties.

Another key parameter that has been heavily investigated is the activity of the penetrant molecule (when most authors refer to the activity as such they are referring to the equilibrium concentration of the penetrant in the polymer rather than the external concentration) [27]. Generally speaking, a high penetrant activity is required. Normally, this means that a relatively high concentration of the penetrant is necessary to observe anomalous or Case II transport, though this tendency will also be altered by

the molecular size of the penetrant and other mitigating factors including specific interactions such as hydrogen bonds [28]. The rationale is simply that a strong driving force, consistent with a high external concentration or strong intermolecular interactions between penetrant and polymer, is necessary for the dramatic and rapid expansion of the polymer chains that is observed in Case II transport. In other words, the activation energy for the formation and propagation of a Case II front is significant. However, it should be noted that Case II transport has been observed for even very modest penetrant uptakes as low as 6 – 8 wt % [23, 24].

Additionally, it has been observed and confirmed numerous times that desorption of penetrant from the swollen polymer following a Case II transport mechanism is always Fickian in nature [25, 27, 29-31]. In other words, the formation and propagation of a Case II penetrant front must necessarily be an irreversible process that is tied exclusively to a positive expansion of the glassy polymer. The fact that Case II transport occurs regardless of the end-state of the polymer (glassy or rubbery) adds to this conclusion and supports an anelastic deformation mechanism as the underlying physical process responsible for Case II behavior.

Many authors have reported on the temperature dependence of the rate of Case II transport, more commonly referred to as the Case II front velocity. This velocity has been shown to obey an Arrhenius dependence on temperature with an activation energy that has ranged from 17 – 50 kcal/mol depending on the polymer-penetrant system [11, 32, 33]. Even for the same polymer-penetrant system, however, the published values can still vary greatly (for example, Case II methanol sorption into poly(methyl methacrylate) has reported activation energies from 17 – 30 kcal/mol). The values of these activation energies are generally higher than those expected from a purely Fickian diffusive process [34, 35]. This is not a surprising result, considering that the expansion of the polymer chains will add to the diffusive energy required for swelling.

The Case II front velocity has also been shown to be independent of molecular weight for both monodisperse and polydisperse polymers above the critical molecular weight for entanglements [29, 36]. Some authors have previously introduced the polymer viscosity as a key mechanical parameter that should control Case II dynamics [14]. However, if that was true, the rate of Case II transport should depend on the polymer molecular weight, just as the polymer viscosity does. Once again this leads us to the notion that the properties of the polymer in the glassy state are the rate-controlling factors, not the properties in the interim region of expansion or in the swollen end-state.

Additionally, the Case II front velocity has been shown to accelerate in oriented or stressed polymer systems, when compared to homogeneous or annealed polymers [37-39]. Likewise, the cooling rate through the glass transition has been shown to affect the rate of transport, namely a faster cooling rate (leading to a polymer with a higher degree of free volume) increases the velocity of the propagating penetrant front [26]. These results, and those indicating that annealing of polymer samples decreases sorption rates [40], indicate a history-dependence of the transport dynamics and support a deformation-controlled mechanism. Basically, an oriented/stressed or less annealed polymer will have a higher free volume and a lower resistance to chain expansion.

Finally, crazing and cracking of a polymer upon exposure to a penetrant have been described as extensions of Case II transport [23]. Crazing fronts have been shown to propagate through a polymer sample at constant velocities, much in the same way as a Case II front, though generally at higher penetrant activities. Cracking can then occur as a further extension of crazing [23, 41, 42]. More commonly, material fracture will occur as the result of a build-up of stresses inside the polymer sample due to network expansion in the presence of the dry polymer core. As mentioned, the core stresses the surrounding swollen polymer, and if the penetrant activity is sufficiently high, the polymer structure may destructively relieve those stresses.

Anomalous Penetrant Transport

Thus far, discussion of non-Fickian penetrant transport into glassy polymers has been centered on the limiting scenario of Case II transport. However, a wide array of behaviors can be seen in between the two extremes of Fickian and Case II. It is useful at this point to consider a simple mechanistic tool; namely the power-law model:

$$\frac{M_t}{M_\infty} = kt^n \tag{2.1}$$

where M_t is the mass of penetrant absorbed at a time t, M_∞ is the equilibrium mass of absorbed penetrant, k is a proportionality constant, and n is the power law exponent. This equation was derived from the short time ($M_t/M_\infty < 0.60$) approximation of the rigorous solution to Fick's 2nd Law, where the binary diffusion coefficient is contained within k and n = 0.5 [5]. As discussed, in Case II transport, the fractional mass uptake (M_t/M_∞) is directly proportional to time, and n is thus 1.0. Figure 2.4 shows the general behavior for Case I and Case II transport as predicted by the power law model. Any behavior that falls between these two extremes is assumed to involve a blending or superposition of the two mechanisms and is often simply referred to as anomalous behavior, with power law exponent values of 0.5 < n < 1.0 [21].

One specific deviation from Case II transport often encountered is referred to as two-stage sorption [43]. In this case, the relaxational time scale is sufficiently longer than the diffusional time scale such that diffusion initially occurs into the free volume and elastic capacity of the polymer structure before approaching a pseudo-equilibrium value. At this point, the penetrant will have sufficiently plasticized the polymer such that it will begin to undergo structural relaxation and further network expansion [44, 45], often in a linear pseudo-Case II manner. This behavior is illustrated in Figure 2.1.

On the opposite end of the spectrum, one can encounter anomalous scenarios where the rate of diffusion limits the transport process and results in deviations from Case II behavior. This effect was initially elucidated by Thomas and Windle in their

13

investigations of methanol sorption into PMMA [33]. They noticed that as the temperature of the system was increased, the dynamics shifted from Case II to anomalous (a power-law exponent between 0.5 and 1.0). When the time-dependent concentration profiles within the polymer were examined, they noted that the concentration of penetrant immediately behind the advancing front decreased over time as the front moved inward. This was accompanied by an associated decrease in the front velocity, as it is directly related to the penetrant activity behind it [33] (or the local driving force for sorption and network expansion). This in turn caused curvature to appear in the fractional mass uptake curve. The conclusion was that as the temperature increased, the front velocity increased substantially and the rate of diffusion of penetrant through the swollen polymer could not keep up. As a result, the penetrant concentration at the advancing front could not be maintained.

In a similar manner, apparent thickness dependencies of the penetrant transport mechanism have been associated with diffusional limitations in the swollen polymer [33]. Basically, as the thickness is increased, the distance that the penetrant must travel from the external supply to the advancing front increases. Since the characteristic diffusion time is defined by Equation 2.2, increasing the sample thickness can lead to a deviation from Case II transport similar in nature to the one just discussed:

$$\theta = \frac{D_{12}}{L^2} \tag{2.2}$$

where θ is the characteristic diffusion time, D_{12} is the binary diffusion coefficient of the penetrant in the polymer, and L is the diffusion path length (generally the initial half-thickness in integral sorption experiments).

A final commonly encountered anomalous transport effect is referred to as super-Case II behavior. In super-Case II transport, the integral sorption process follows precisely Case II dynamics until near the very end of the sorption process (or when the fronts are very near the core of the polymer), at which point the fronts seemingly

rapidly accelerate towards one another leading to an uptick in the fractional mass uptake curve and a power-law exponent greater than unity. There has been discussion in the literature over the years as to whether or not this is a true mechanistic feature [32]; however, there are cases where it seems plausible that it is. Specifically, in the limit of very slow Case II transport dynamics with an associated lengthy induction period and very sizeable Fickian precursor, a mechanistic interpretation of super-Case II transport can be made.

Basically, as the fronts approach one another in the center of the specimen, the large Fickian precursors meet well in advance of these two fronts and begin to overlap. Once this happens, the dry, glassy core can disappear along with the associated stresses it imposed on the surrounding material [26]. Since Case II transport and front propagation necessarily require the presence of a restricting core, the behavior then shifts towards Fickian diffusion for the remainder of the sorption profile and results in an increase in rate (Fickian diffusion will necessarily occur faster than Case II transport since the assumption is that the chain expansion process was the limiting rate). Additionally, purely Case II dynamics from a molecular stand point have been shown to appear as super-Case II transport from a macroscopic view when the geometry of the polymer is altered from a planar configuration to a spherical one [32]. Thus, it is not surprising that super-Case II transport has often been seen in sorption into powders.

Interrelation of Mechanisms

As complicated as each of the individual transport mechanisms can be, the ultimate goal is to be able to predict which mechanism and rate a given polymer and penetrant will exhibit at the desired experimental conditions. This has led to quite a large number of attempts to model and predict these phenomena. These efforts have been well-reviewed by many authors, and their analyses will not be repeated here [15, 18, 21, 26, 34, 46]. However, some qualitative understandings that have developed from these theoretical efforts are helpful in comprehending the observed behaviors.

One useful relationship that has been developed by Vrentas and Duda from the notion that the diffusion and relaxational processes are competing for control over the transport process is the dimensionless Deborah number [47]:

$$De = \frac{\lambda}{\theta} \qquad (2.3)$$

where λ is the characteristic relaxation time of the polymer and θ is the characteristic diffusion time (Equation 2.2). Anomalous penetrant transport would then be expected to occur when the time scales of diffusion and relaxation are comparable, or when De $\approx$ 1 [48]. When De is much less than unity, the relaxational processes of the polymer are rapid when compared to the penetrant diffusion, with the result that the penetrant is always diffusing into an equilibrated structure and the dynamics are Fickian in nature. Finally, when De is much greater than unity, a variety of behaviors can occur, as illustrated in Figure 2.5 [47]. Here a Deborah number of unity is associated with the glass transition region in polymers. Well below the glass transition, Fickian diffusion will occur if the penetrant activity is low enough or the polymer relaxational times long enough such that no relaxation of the polymer structure occurs in an experimentally accessible time frame. Additionally, extreme anomalous effects can be seen, which include Case II transport, crazing, and cracking. Finally, there is a transition region from Fickian transport to Case II transport as the penetrant activity and/or temperature are increased.

Hopfenberg, Holley, and Stannett rationalized that all anomalous transport behaviors are connected and can be seen for any given penetrant-polymer pair if the appropriate experimental conditions are met [23]. Of course, in many instances, material limitations, including penetrant freezing and boiling points as well as the fact that external penetrant concentrations have an upper limit, will interfere with the observation of some behaviors. Finally, the observed behaviors were put into a convenient graphical format by Hopfenberg and Frisch [27] (Figure 2.6), which

16

summarizes nicely the observed experimental trends with temperature and penetrant activity.

SUMMARY

Despite the vast literature on the subject of non-Fickian transport processes in glassy polymers and the scores of theories and models that have been developed, there remains no satisfactory means by which to determine what transport behavior a given penetrant-polymer system will exhibit. The formulation of an accessible model to this end remains a challenge. Even to date, there is debate on the most basic underlying physics involved in determining the appearance and rate of Case II transport. The prevailing notion is that the propagation of a Case II front is an anelastic deformation process, similar in nature to a rapid, solvent-actuated creep of the polymer network caused by an osmotic pressure (or osmotic suction) [14, 26, 33, 49, 50]. However, some authors maintain that Case II transport can be modeled satisfactorily through a highly concentration-dependent diffusion coefficient and accounting for volume effects [15]. Development of a truly predictive theory has been hindered over the years by the sheer number of mathematical formulations and methodologies that can be utilized to reproduce sharp concentration fronts and linear time dependencies [46].

REFERENCES

1. Fujita, H. and A. Kishimoto, *Diffusion-Controlled Stress Relaxation in Polymers. II. Stress Relaxation in Swollen Polymers.* Journal of Polymer Science, 1958. **28**(118): p. 547-567.
2. Hartley, G.S., *Diffusion and Swelling of High Polymers. Part III. Anisotropic Swelling in Oriented Polymer Film.* Transactions of the Faraday Society, 1949. **45**: p. 820-832.
3. Alfrey, T., E.F. Gurnee, and W.G. Lloyd, *Diffusion in Glassy Polymers.* Journal of Polymer Science, Part C: Polymer Symposia, 1966. **12**: p. 249-261.
4. Hartley, G.S., *Diffusion and Swelling of High Polymers. Part I. The Swelling and Solution of a High Polymer Solid Considered as a Diffusion Process.* Transactions of the Faraday Society, 1946. **42**: p. B006-B011.
5. Crank, J., *The Mathematics of Diffusion*. 2nd ed. 1975, New York: Oxford University Press. p. 47.
6. King, G., *Sorption of Vapours by Keratin and Wool.* Transactions of the Faraday Society, 1945. **41**: p. 325-332.
7. Ferry, J.D., *Viscoelastic Properties of Polymers*. 3rd ed. 1980, New York: John Wiley & Sons.
8. Sinclair, G.W. and N.A. Peppas, *Analysis of Non-Fickian Transport in Polymers Using Simplified Exponential Expressions.* Journal of Membrane Science, 1984. **17**(3): p. 329-331.
9. Hui, C.Y., K.C. Wu, R.C. Lasky, and E.J. Kramer, *Case-II Diffusion in Polymers .1. Transient Swelling.* Journal of Applied Physics, 1987. **61**(11): p. 5129-5136.
10. Hui, C.Y., K.C. Wu, R.C. Lasky, and E.J. Kramer, *Case-II Diffusion in Polymers .2. Steady-State Front Motion.* Journal of Applied Physics, 1987. **61**(11): p. 5137-5149.
11. Lasky, R.C., E.J. Kramer, and C.Y. Hui, *Temperature-Dependence of Case-Ii Diffusion.* Polymer, 1988. **29**(6): p. 1131-1136.
12. Lasky, R.C., E.J. Kramer, and C.Y. Hui, *The Initial-Stages of Case-II Diffusion at Low Penetrant Activities.* Polymer, 1988. **29**(4): p. 673-679.
13. Peterlin, A., *Diffusion in a Network with Discontinuous Swelling.* Polymer Letters, 1965. **3**: p. 1083-1087.
14. Thomas, N.L. and A.H. Windle, *A Theory of Case-II Diffusion.* Polymer, 1982. **23**(4): p. 529-542.
15. Vrentas, J.S. and C.M. Vrentas, *Integral sorption in glassy polymers.* Chemical Engineering Science, 1998. **53**(4): p. 629-638.
16. Jacques, C.H.M., H.B. Hopfenberg, and V.T. Stannett, *Super Case II Transport of Organic Vapors in Glassy Polymers.* Abstracts of Papers of the American Chemical Society, 1974: p. 51-51.

17. Thomas, N. and A.H. Windle, *Discontinuous Shape Changes Associated with Case-2 Transport of Methanol in Thin Sheets of PMMA.* Polymer, 1977. **18**(11): p. 1195-1195.

18. Lustig, S.R., *A Continuum Thermodynamics Theory for Transport in Polymer/Fluids Systems*, in *Chemical Engineering*. 1989, Purdue University.

19. Thomas, N.L. and A.H. Windle, *Diffusion Mechanics of the System PMMA-Methanol.* Polymer, 1981. **22**(5): p. 627-639.

20. Treloar, L.R.G., *The Physics of Rubber Elasticity*. 3rd ed. 1975, New York: Oxford University Press.

21. Crank, J. and G.S. Park, *Diffusion in Polymers*. 1968, New York: Academic Press.

22. Joshi, S. and G. Astarita, *Diffusion-Relaxation Coupling in Polymers Which Show 2-Stage Sorption Phenomena.* Polymer, 1979. **20**(4): p. 455-458.

23. Hopfenberg, H.B., R.H. Holley, and V. Stannett, *The Effect of Penetrant Activity and Temperature on the Anomalous Diffusion of Hydrocarbons and Solvent Crazing in Polystyrene Part I: Biaxially Oriented Polystyrene.* Polymer Engineering and Science, 1969. **9**(4): p. 242-249.

24. Jacques, C.H.M. and H.B. Hopfenberg, *Vapor and Liquid Equilibria in Glassy Polyblends of Polystyrene and Poly(2,6-Dimethyl-1,4-Phenylene Oxide) .1.* Polymer Engineering and Science, 1974. **14**(6): p. 441-448.

25. Jacques, C.H.M., H.B. Hopfenberg, and V. Stannett, *Vapor Sorption and Liquid Interactions with Glassy Polyblends of Polystyrene and Poly(2,6-Dimethyl-1,4-Phenylene Oxide).* Polymer Engineering and Science, 1973. **13**(2): p. 81-87.

26. Thomas, N.L. and A.H. Windle, *A Deformation Model for Case-II Diffusion.* Polymer, 1980. **21**(6): p. 613-619.

27. Hopfenberg, H.B. and H.L. Frisch, *Transport of Organic Micromolecules in Amorphous Polymers.* Journal of Polymer Science, Part B: Polymer Letters, 1969. **7**(6): p. 405-409.

28. Gall, T.P., R.C. Lasky, and E.J. Kramer, *Case-II Diffusion - Effect of Solvent Molecule Size.* Polymer, 1990. **31**(8): p. 1491-1499.

29. Baird, B.R., H.B. Hopfenberg, and V. Stannett, *The Effect of Molecular Weight and Orientation on the Sorption of n-Pentane by Glassy Polystyrene.* Polymer Engineering and Science, 1971. **11**(4): p. 274-283.

30. Crank, J. and G.S. Park, *Diffusion in High Polymers: Some Anomalies and their Significance.* Transactions of the Faraday Society, 1951. **47**: p. 1072-1084.

31. Holley, R.H., H.B. Hopfenberg, and V. Stannett, *Anomalous Transport of Hydrocarbons in Polystyrene.* Polymer Engineering and Science, 1970. **10**(6): p. 376-382.

32. Lee, P.I., *Temperature-Dependence of Methanol Transport in Spherical PMMA Beads.* Polymer, 1993. **34**(11): p. 2397-2400.

33. Thomas, N. and A.H. Windle, *Transport of Methanol in Poly(Methyl Methacrylate).* Polymer, 1978. **19**(3): p. 255-265.

34. Hopfenberg, H.B. and V. Stannett, in *Physics of Glassy Polymers*, R.N. Haward, Editor. 1973, Applied Science: London.

35. Nicolais, L., E. Drioli, H.B. Hopfenberg, and D. Tidone, *Characterization and Effects of N-Alkane Swelling of Polystyrene Sheets.* Polymer, 1977. **18**(11): p. 1137-1142.

36. Hassan, M.M. and C.J. Durning, *Effects of polymer molecular weight and temperature on Case II transport.* Journal of Polymer Science Part B-Polymer Physics, 1999. **37**(22): p. 3159-3171.

37. Harmon, J.P., S. Lee, and J.C.M. Li, *Methanol Transport in PMMA - the Effect of Mechanical Deformation.* Journal of Polymer Science Part A - Polymer Chemistry, 1987. **25**(12): p. 3215-3229.

38. Nicolais, L., E. Drioli, H.B. Hopfenberg, and A. Apicella, *Effects of Orientation on the Penetration, Crazing, and Dissolution of Polystyrene by N-Hexane.* Polymer, 1979. **20**(4): p. 459-464.

39. Zhou, Q.Y., A.S. Argon, and R.E. Cohen, *Enhanced Case-II diffusion of diluents into glassy polymers undergoing plastic flow.* Polymer, 2001. **42**(2): p. 613-621.

40. Enscore, D.J., H.B. Hopfenberg, V.T. Stannett, and A.R. Berens, *Effect of Prior Sample History on N-Hexane Sorption in Glassy Polystyrene Microspheres.* Polymer, 1977. **18**(11): p. 1105-1110.

41. Hayes, M.J. and G.S. Park, *Diffusion of Benzene in Rubber. I. Low Concentrations of Benzene.* Transactions of the Faraday Society, 1955. **51**: p. 1134-42.

42. Michaels, A.S., H.J. Bixler, and H.B. Hopfenberg, *Controllably Crazed Polystyrene - Morphology and Permeability.* Journal of Applied Polymer Science, 1968. **12**(5): p. 991-&.

43. Bagley, E. and F.A. Long, *Two-stage Sorption and Desorption of Organic Vapors in Cellulose Acetate.* Journal of the American Chemical Society, 1955. **77**(2172-2178).

44. Kokes, R.J., F.A. Long, and J.L. Hoard, *Diffusion of Acetone into Polyvinyl Acetate above and below the Second-Order Transition.* Journal of Chemical Physics, 1952. **20**(11): p. 1711-1716.

45. Long, F.A. and D. Richman, *Concentration Gradients for Diffusion of Vapors in Glassy Polymers and their Relation to Time Dependent Diffusion Phenomena.* Journal of the American Chemical Society, 1960. **82**: p. 513-519.

46. Frisch, H.L., *Sorption and Transport in Glassy-Polymers - Review.* Polymer Engineering and Science, 1980. **20**(1): p. 2-13.

47. Vrentas, J.S., C.M. Jarzebski, and J.L. Duda, *Deborah Number for Diffusion in Polymer-Solvent Systems.* AIChE Journal, 1975. **21**(5): p. 894-901.

48. Vrentas, J.S. and J.L. Duda, *Diffusion in Polymer-Solvent Systems .3. Construction of Deborah Number Diagrams.* Journal of Polymer Science Part B-Polymer Physics, 1977. **15**(3): p. 441-453.

49.   Argon, A.S., R.E. Cohen, and A.C. Patel, *A mechanistic model of case II diffusion of a diluent into a glassy polymer.* Polymer, 1999. **40**(25): p. 6991-7012.

50.   Durning, C.J., D.A. Edwards, and D.S. Cohen, *Perturbation analysis of Thomas and Windle's model of case II transport.* AIChE Journal, 1996. **42**(7): p. 2025-2035.
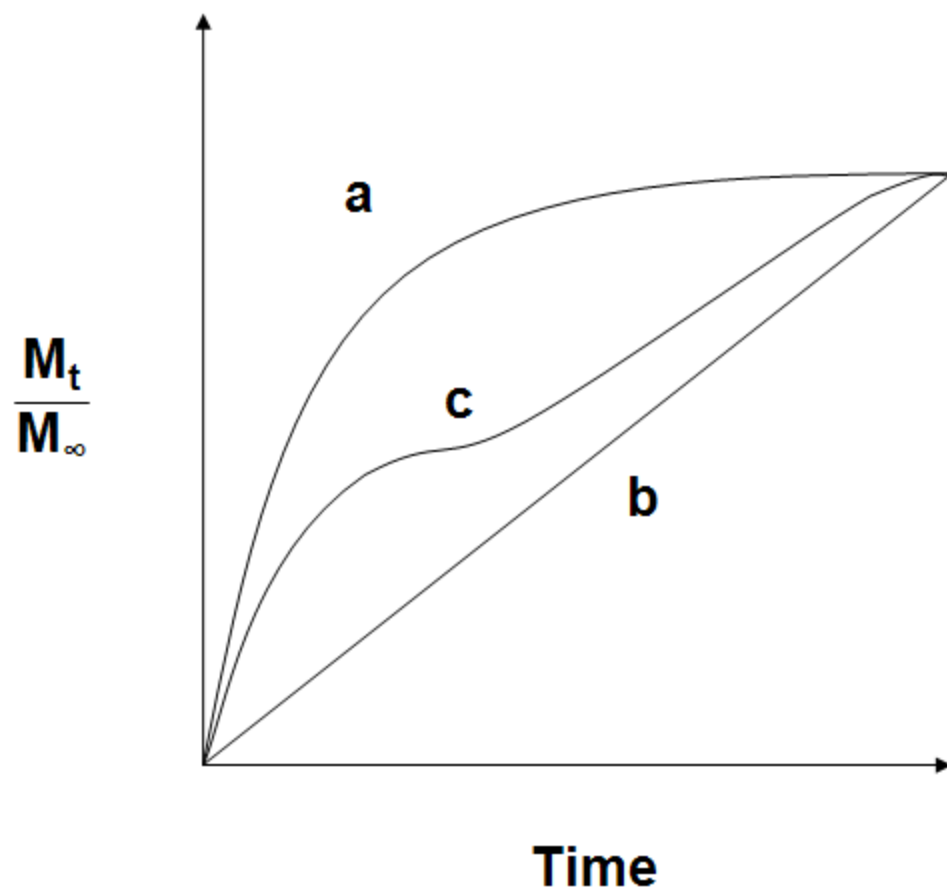
Figure 2.1: Comparison of representative fractional mass uptake curves for Fickian (a), Case II (b), and two-stage (c) penetrant transport behaviors.

$C_i = 0$

Fickian
Transport

Crosslinked Polymer Film Exposed to Penetrant
Concentration C_{bulk} at Time $= 0$

$C = C_f$

Case II
Transport

$C_f \neq C_{bulk}$

Case II Boundaries Move at ~Constant Velocity
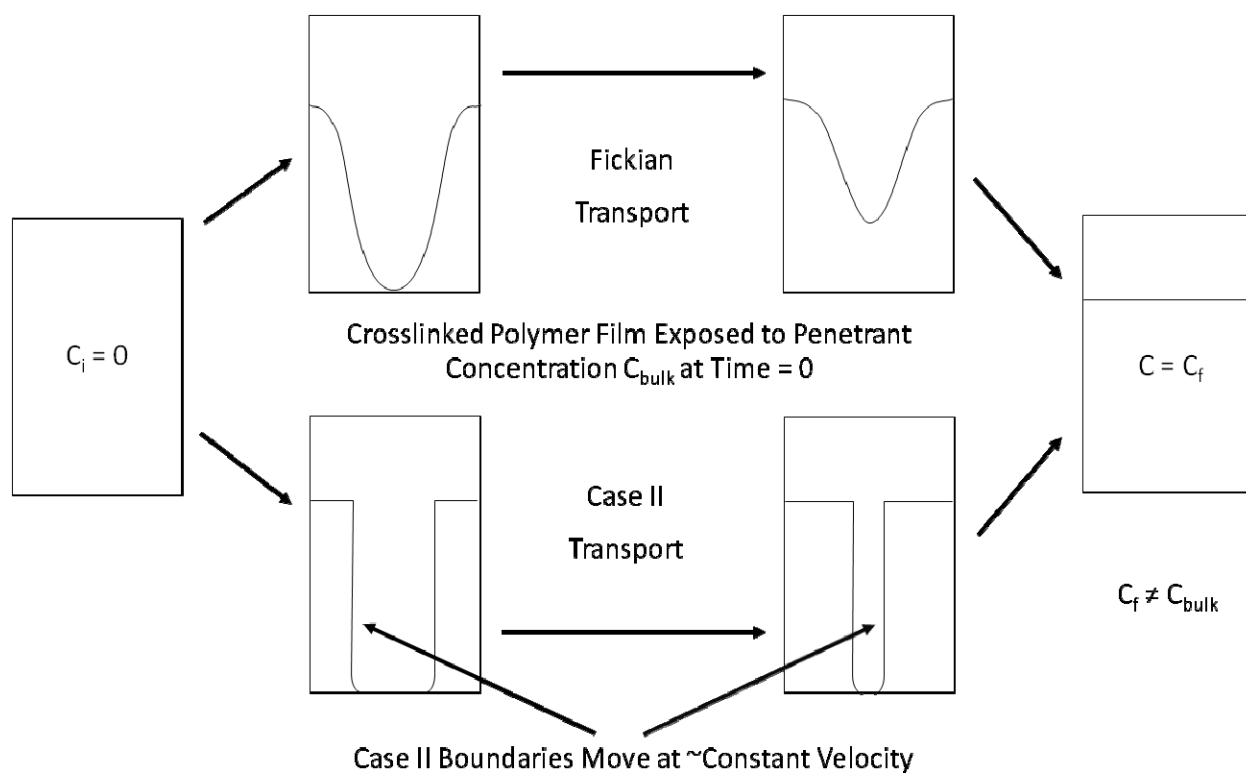
Figure 2.2: Comparison of typical penetrant concentration profiles in polymer films during sorption by Fickian and Case II transport mechanisms.

Swelling Anisotropy
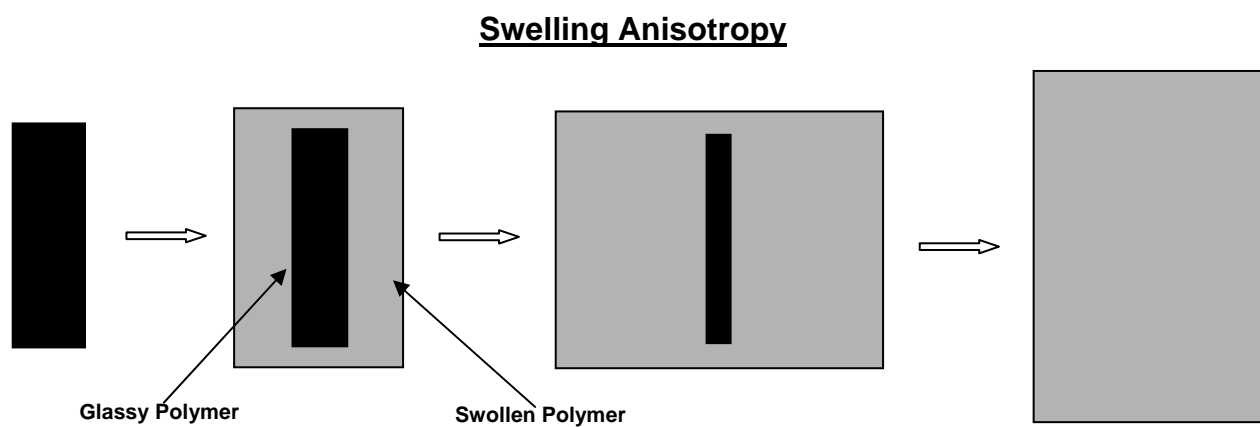
Figure 2.3: Anisotropic expansion of a polymer film (side view).

Fickian vs. Case II: Swelling Kinetics

Power Law Model: $$\frac{M_t}{M_\infty} = k\,t^n$$

$\frac{M_t}{M_\infty}$

$k\uparrow$

time

Fickian Diffusion

n = 0.5

$\frac{M_t}{M_\infty}$

$k\uparrow$

time
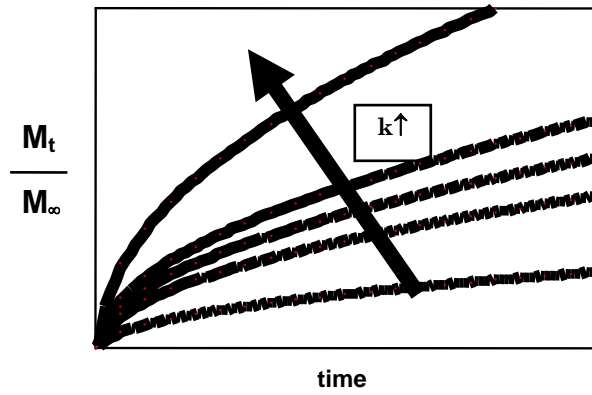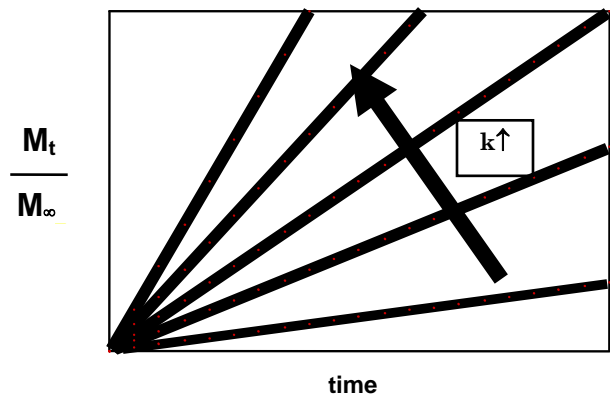
Case II Diffusion

n = 1.0

Figure 2.4: Comparison of Fickian and Case II penetrant uptake behavior according to the power law expression.
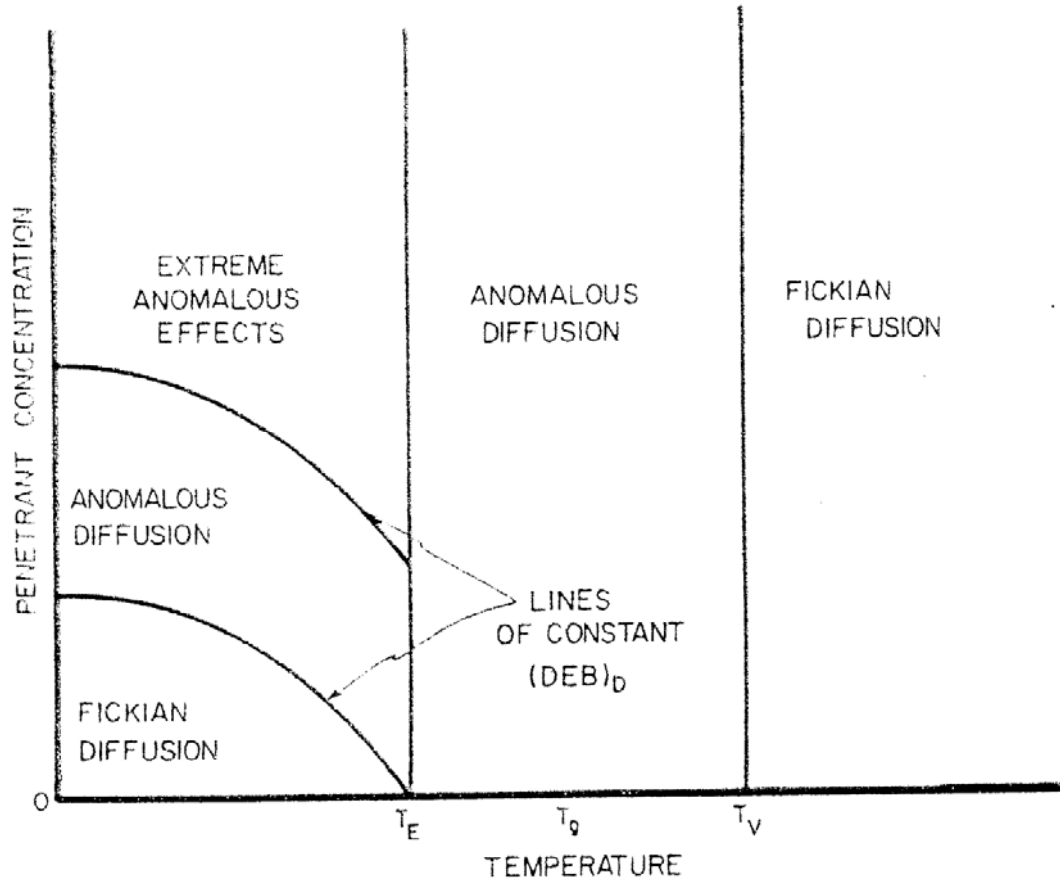
Figure 2.5: Concentration vs. temperature diagram showing the three regions associated with the diffusional Deborah number (Vrentas, Jarzebski and Duda, 1975 [47]).
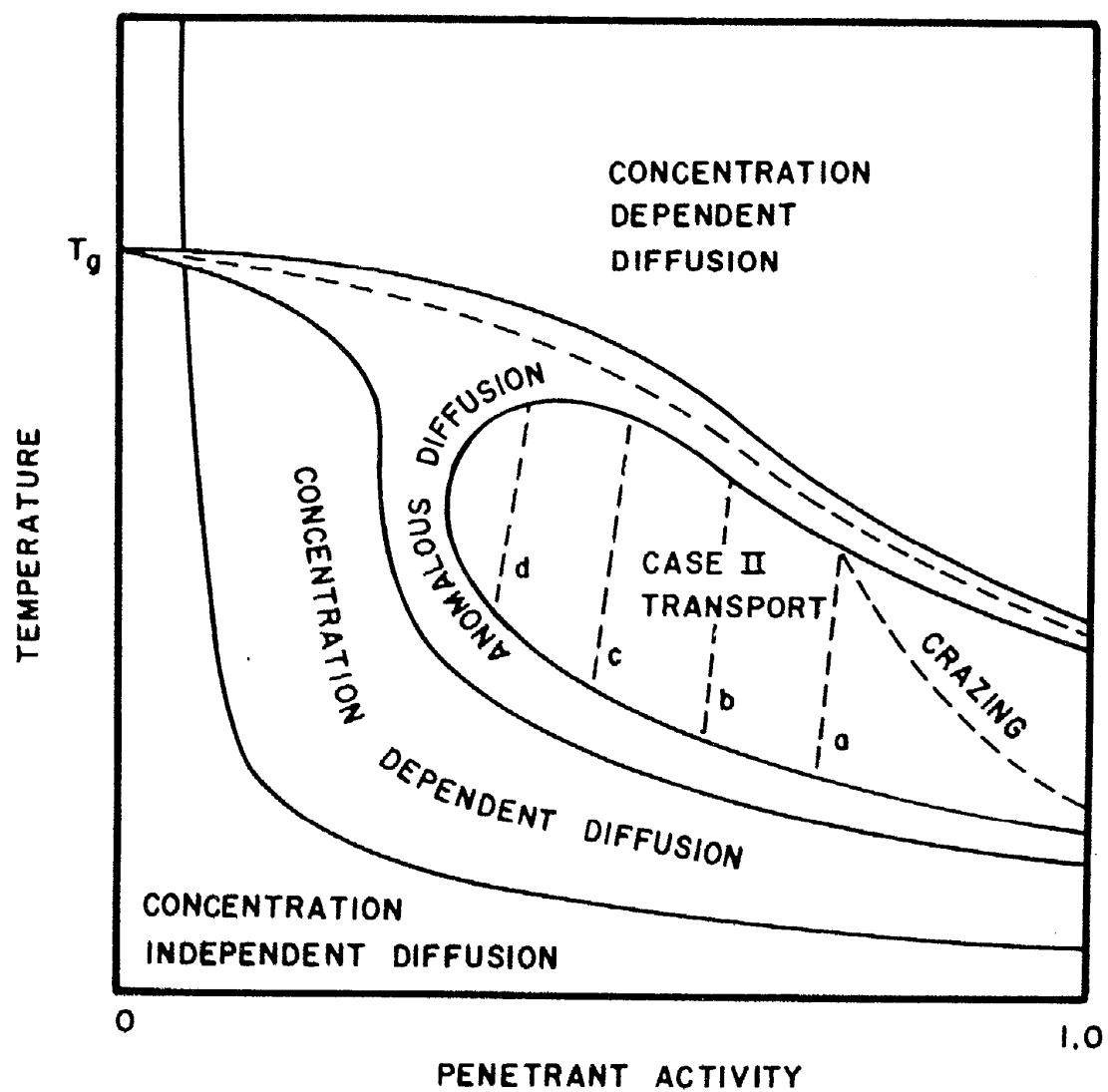
Figure 2.6: Temperature vs. penetrant activity diagram showing the full range of behaviors that can be seen in a given polymer-penetrant combination (Hopfenberg and Frisch, 1969 [27]).

Chapter 3: Research Objectives

The goals of this Ph.D. thesis were to (i) synthesize and characterize glassy polymers in a controlled manner in order to create a variety of polymer network structures and microenvironments; (ii) examine the effect of network structural parameters on the transport dynamics of small penetrant molecules during sorption of methanol into poly(methyl methacrylate); (iii) pursue novel *in situ* experimental techniques to visualize and quantify the penetrant transport process; (iv) investigate the penetrant transport dynamics in hydrophilic and semi-crystalline polymers; and (v) formulate new scaling relationships and lay the groundwork for experimental validation of a property-based predictive theory for anomalous penetrant transport in glassy polymers.

The aim of the study presented in Chapter 4 was to synthesize and characterize poly(methyl methacrylate) with precise control over the polymer network structure. The objective was to alter the degree of crosslinking through a bulk, controlled free radical polymerization process by altering the degree of incorporation of difunctional methacrylate comonomers with varying interchain crosslinking bridge lengths. The resulting polymer network structure was examined via differential scanning calorimetry, dynamic mechanical analysis, and equilibrium swelling measurements to determine an efficiency of crosslinking and directly relate the polymerization feed to the polymer network structure and mechanical behavior.

The aim of the study presented in Chapter 5 was to investigate the transport dynamics of methanol sorption into glassy poly(methyl methacrylate). The objective was to elucidate the effects of network structural parameters on both the transport mechanism observed and the kinetics. The effects of polymerization and preparation procedures and the effects of temperature were determined. Control over the penetrant transport mechanism encountered by changing the polymer network

structure was demonstrated, and scaling relationships between the Case II front velocity and polymer network structure were established.

The aim of the study in Chapter 6 was to pursue novel *in-situ* experimental techniques to visualize and quantify the penetrant transport process. The objective was to evaluate the use of high resolution X-ray computed tomography to observe and analyze the anomalous transport of methanol into plasticized poly(methyl methacrylate). Using this adapted experimental technique, the concentration profiles of methanol in poly(methyl methacrylate), the anisotropic dimensional swelling mechanics, and the overall integral sorption dynamics were determined in a completely non-destructive manner.

The aim of the study presented in Chapter 7 was to extend the investigation of Chapter 5 to hydrophilic and semi-crystalline polymers. The objective was to synthesize and characterize poly(2-hydroxyethyl methacrylate) and poly(vinyl alcohol) with varying network structures and polymer microenvironments. The scaling relationships determined in Chapter 5 were validated, and the effects of crystallinity on the transport process were investigated.

Chapter 4: Synthesis and Characterization of
Poly(Methyl Methacrylate)

INTRODUCTION

There is no way to accurately predict *a priori* the velocity of a Case II penetrant front in an integral sorption experiment from the basic material properties of the polymer and penetrant. The vast majority of investigations have focused on characterizing the qualitative features of Case II transport profiles and attempting to model a transition from Fickian to non-Fickian dynamics, with the result that much is still unknown about how basic material properties affect the transport dynamics within the purely Case II regime. In particular, the effects of the polymer network structure and relaxational behavior have not been sufficiently studied.

In order to study the effects of basic network parameters, including the molecular weight between crosslinks, M_c, and the polymer mesh size, ξ, control over these parameters is necessary. Traditionally, investigators in this field have purchased polymer samples from industrial companies for sorption studies, with the result that little was known or reported on the network structure and other general properties of those polymers. In this investigation, polymer samples were synthesized in house and the polymer network structure was altered by varying both the molar incorporation of crosslinks into the polymer chains and the length of the crosslink interchain bridge. Additionally, a controlled, living free radical polymerization mechanism was utilized to both increase crosslinking efficiency and avoid autoacceleration by controlling the concentration of growing polymer chains.

The most-studied penetrant-polymer system in the literature exhibiting Case II transport is methanol sorption into poly(methyl methacrylate) (PMMA). This system consistently displays Case II transport dynamics at easily accessible experimental conditions and was chosen as the primary system for this investigation. Therefore,

samples of PMMA crosslinked during bulk polymerization by the incorporation of difunctional methacrylate comonomers were synthesized. These polymers were then characterized by gel permeation chromatography, equilibrium sorption data, differential scanning calorimetry, and dynamic mechanical analysis to determine basic material properties and verify the polymer network structures produced.

MATERIALS AND METHODS

Materials

Ethylene glycol dimethacrylate (EGDMA), diethylene glycol dimethacrylate (di(EG)DMA), triethylene glycol dimethacrylate (tri(EG)DMA), tetraethylene glycol dimethacrylate (tetra(EG)DMA), lauroyl peroxide (LP), and tetraethylthiuram disulfide (TED) were purchased from Sigma-Aldrich (St. Louis, MO) and used as received. Methyl methacrylate (MMA, inhibited with 100 ppm monomethyl ether of hydroquinone (MEHQ)), was purchased from Sigma-Aldrich and passed through a pre-packed inhibitor removal column (Sigma-Aldrich) and into a chilled, amber collection flask to remove the inhibitor prior to polymerization. All MMA monomer was used within two weeks of inhibitor removal. The molecular structures of chemicals used in the synthesis of PMMA are shown in Figure 4.1. All other chemicals were ACS reagent grade and were used as received.

Synthesis

In a typical polymerization, the MMA monomer was combined with 2.5 mol % EGDMA (or another crosslinker), 0.5 wt % LP, and a 1:1 molar ratio of TED:LP in a glass jar, which was then capped to prevent evaporation. This jar was placed in a Labconco controlled environment glove box (Labconco, Kansas City, MO) and the glove box was then purged with nitrogen gas until the concentration of oxygen was less than 0.05 %, as measured by a Handi™ Maxtec oxygen sensor (Maxtec, Inc., Salt Lake City, UT). Nitrogen gas was then bubbled through the monomer solution for five minutes to purge

the solution of oxygen. The monomer solution was then transferred to a 26 mm diameter cylindrical glass tube, which had been previously silanized utilizing a Siliclad® solution (Gelest, Morrisville, PA) purchased from Fisher Scientific (Pittsburgh, PA), and sealed with a rubber stopper. The reaction vessel was then placed into a water bath maintained at 60°C by a re-circulating immersion heater and the solution was allowed to polymerize for 44 hours (2.6 initiator half-lives) [1]. Once the reaction was complete, the polymer cylinder was removed from the glass tube and stored in a desiccator. Finally, the polymer cylinders were sectioned into 1 mm thick discs by a Buehler® Isomet™ Low-Speed Saw (Buehler®, Lake Bluff, IL) with diamond wafering blades, polished to remove surface defects by an abrasive slurry (Novus #2 Fine Scratch Remover, Savage, MN), and stored in a desiccator until use. It should be noted that in all cases, discs used were from a small central region of the cylinder to avoid any potential vertical variations or edge effects.

Characterization

The molecular weights and molecular weight distribution of uncrosslinked polymer samples were determined by a gel permeation chromatography (GPC) system consisting of a refractometer (Optilab DSP, Wyatt Technology, Santa Barbara, CA) and a multi-angle laser light scattering (MALLS) detector (DAWN EOS, Wyatt Technology). The system used a series of 2 identical Polymer Labs columns packed with crosslinked polystyrene beads (5 μm bead size, mixed-C pore size). For PMMA, samples of polymer were dissolved in tetrahydrofuran (THF) at a concentration of 5-10 mg/mL, and 60 μL of this solution was injected into the GPC system with THF as the carrier solvent.

The thermal properties of the polymer samples were characterized by differential scanning calorimetry (Perkin Elmer DSC 7, Perkin Elmer, Waltham, MA) using a heat/cool/heat method. A sample of each polymer batch to be tested was either crushed into a fine powder with a mortar and pestle or cut into a small section with tin snips. Once ready, 10-15 mg samples were placed into the DSC, heated from 50°C to

180°C (or higher temperatures as needed), and then cooled back to 50°C at a rate of 10°C/min in order to erase any thermal histories present in the polymer and to remove unreacted monomer and moisture that might interfere with the signal. The samples were then heated a second time from 50°C to 180°C and the glass transition temperature, T_g, was determined as the halfway point during the change in heat capacity of the polymer associated with the transition from glass to rubber (1/2 ΔC_p method).

Additionally, dynamic mechanical analysis (DMA 983, TA Instruments, and New Castle, DE) was used to determine basic mechanical properties. Rectangular samples (~2 mm x 8 mm x 20 mm) were cut for each polymer to be tested. Once prepared, the samples were placed into the DMA device and the device was run on resonant mode from 60°C to 180°C (or higher temperatures as needed). In this manner, the shear storage modulus, G'; the shear loss modulus, G''; the onset T_g based on G'; and the tanδ peak T_g were determined.

Finally, equilibrium polymer swelling experiments were run in methanol and acetone. For this study, PMMA discs with a 1 mm nominal thickness were first suspended in methanol on a metal mesh in a glass jar, the jars were immersed in a constant-temperature water bath, and the samples were allowed to equilibrate. Since the PMMA samples synthesized fractured when placed in pure acetone from the dry state, a stair-step procedure was utilized to take discs swollen in pure methanol to pure acetone. In this manner, equilibrium swelling data were collected for 100:0, 80:20, 60:40, 40:60, 20:80, and 0:100 volumetric ratios of methanol:acetone penetrant solutions. After equilibrating in methanol, discs were switched over and allowed a number of days to re-equilibrate successively in each new penetrant solution. The disc weight in air, weight in a non-solvent, thickness, and diameter were all recorded in each state and used to calculate sample volume and polymer volume fraction.

RESULTS AND DISCUSSION

Inhibitor Removal Verification

In order to verify that MEHQ, the inhibitor, was completely removed by passage through the inhibitor removal column, a Lambda 10 UV/Vis Spectrometer (Perkin Elmer) was utilized to measure the inhibitor concentration both before and after treatment. Experimental quantification of the MEHQ concentration based on absorbance of light at a wavelength of 420 nm was performed according to the American Society for Testing and Materials (ASTM) standard test method [2]. A calibration curve was first created as is shown in Figure 4.2. Using this calibration curve, the concentration of MEHQ present in the untreated methyl methacrylate was 89 ppm (this value falls within the calibration range and is equivalent to 0.084 g/L), which agrees with the approximate manufacturer specification of 100 ppm. After treatment, the concentration of MEHQ was determined to be 2 ppm. Thus, a single pass through the pre-packed inhibitor removal column (with a residence time in the column of 10-15 seconds) was sufficient to eliminate MEHQ from MMA.

Iniferter Chemistry and Gel Permeation Chromatography

An *iniferter*-mediated mechanism was utilized to control the polymerizations and circumvent autoacceleration. *Iniferter* (*ini*tiator-chain trans*fer-ter*mination) compounds typically contain a labile bond, such as a carbamate or disulfide bond, that leads to the formation of stable sulfur radicals [3]. For the case of a carbamate-based molecule or the case of the combination of a disulfide molecule with a traditional free radical initiator, the availability of both carbon and sulfur radicals leads to a reversible capping mechanism and living polymerization scheme, whereby the growing chains are successively terminated via combination with a free sulfur radical and then reinitiated by the cleavage of the newly formed, yet labile, bond [4-7]. This mechanism is

illustrated in Figure 4.3 for the case of a disulfide *iniferter* molecule along with a typical free radical initiator.

The efficacy of this mechanism stems from the fact that the sulfur radicals formed are relatively less reactive than carbon radicals towards the double bonds found in monomers and thus do not initiate growing polymer chains to a significant extent [8-10]. Additionally, while bimolecular termination of two growing chains can still occur, the cross-termination of a sulfur radical with a carbon radical is preferred even at low conversions when the diffusion resistances are negligible [11]. This preference is only heightened as conversion increases due to increased viscosity and subsequent diffusion limitations which affect the growing polymer macromolecules to a much greater extent than the small radical sulfur compounds. The low conversion preference has been attributed by some to a higher activation energy for carbon-carbon radical termination versus carbon-sulfur radical termination [12]. As a result of this behavior, the often problematic phenomenon of autoacceleration can be largely avoided [12].

Autoacceleration is brought about by an increase in the concentration of propagating carbon radicals due to a decrease in the rate of long-chain termination once a polymerizing solution has begun to vitrify. However, in the case of *iniferter*-mediated polymerizations, the concentration of free carbon radicals is kept low at all times due to the relatively minor impact of increased viscosity on the diffusion of the small molecule sulfur radicals and associated carbon-sulfur radical termination [13]. In addition to the circumvention of autoacceleration, this polymerization mechanism was chosen for its ease of use in bulk polymerizations, as no solvent was required, its negligible addition of impurities such as heavy metals, and previously demonstrated use in polymerizations of 2-hydroxyehtyl methacrylate and methyl methacrylate [13-16].

One particular concern with the exothermic polymerization of PMMA in bulk was supplying adequate heat transfer so that autoacceleration as a result of a high core temperature does not occur. This deficiency resulted in significant spatial dependencies of the molecular weights, as shown in Figure 4.4 for a typical PMMA cylinder

35

polymerization without the addition of an *iniferter* compound. However, the addition of an *iniferter* compound, like TED, had the ultimate effect of retarding the reaction kinetics, thus preventing temperature-induced autoacceleration and giving homogeneous polymer cylinders as shown in Figure 4.5. The results of the GPC analysis for both cases are presented in Table 4.1 and show that the addition of an *iniferter* compound significantly reduced the overall molecular weight, which was consistent with the elimination of autoacceleration.

Reactivity Ratio Calculations

For this analysis, a theoretical degree of crosslinking was first computed utilizing the reactivity ratios of MMA and EGDMA. Reactivity ratios for MMA with di(EG)DMA, tri(EG)DMA, and tetra(EG)DMA were not found; however, it was expected that they will be similar in nature and magnitude to those for MMA and EGDMA. Thus, values for MMA and EGDMA were used in all cases in this chapter. Conflicting reports were found for the values of r_1 and r_2 for MMA (1) and EGDMA (1). Odian [1] describes the free radical copolymerization of MMA and EGDMA as one of the rare ideal copolymerizations, were $r_1 = r_2 = 1$ and the copolymer composition, F_1 and F_2, is the same as the feed composition, f_1 and f_2. However, the Q-e scheme was utilized to estimate the reactivity ratios by Equations 4.1 and 4.2, and the resulting values were $r_1 = 0.789$ and $r_2 = 1.236$:

$$r_1 = \frac{Q_1}{Q_2} \exp\left[-e_1\left(e_1 - e_2\right)\right] \qquad (4.1)$$

$$r_2 = \frac{Q_2}{Q_1} \exp\left[-e_2\left(e_2 - e_1\right)\right] \qquad (4.2)$$

where $Q_1 = 0.78$, $e_1 = 0.40$, $Q_2 = 0.88$, and $e_2 = 0.24$ [17, 18]. These values of the reactivity ratios still yielded an ideal polymerization with near random placement of the comonomers in the polymer chains ($r_1 r_2 = 0.975$). However, EGDMA will be

36

preferentially consumed during the polymerization, and the instantaneous feed ratios will change throughout the polymerization process

Finally, a recent investigation by Mao, et al. concluded from experimental data that the reactivity ratios for a free radical polymerization of MMA and EGDMA are 0.674 (± 0.045) and 1.34 (± 0.18), respectively [19]. From these values it was again seen that both MMA and EGDMA would rather react with EGDMA at a nearly commensurate rate, leading to a polymerization with an r_1r_2 value of 0.90 (compared to r_1r_2 = 1 for an ideal reaction). For this investigation, these experimental values were chosen for theoretical copolymer composition, F_1 and F_2, calculations.

The copolymerization equation was used to determine the copolymer composition based on instantaneous monomer concentrations [1]:

$$F_1 = \frac{r_1 f_1^2 + f_1 f_2}{r_1 f_1^2 + 2 f_1 f_2 + r_2 f_2^2} \tag{4.3}$$

Figure 4.6 shows the ultimate effect that the preferential depletion of EGDMA had on the theoretical, weight-averaged incorporation of crosslinks in PMMA when the reaction was run to 97 % conversion, with a linear data regression shown. Thus, the weight-averaged copolymer composition of crosslinks, F_2, was 10.3 % greater than the actual polymerization feed composition, f_2.

Here it should be noted that all subsequent feed compositions of crosslinking dimethacrylate comonomers (f_2 values) mentioned in this thesis refer to the composition of crosslinkable functionalities. Every dimethacrylate comonomer has the ability to add to two different polymer chains or to add two segments to the same chain. Thus, an ideal copolymerization with 2.5 mol % EGDMA in the reaction feed will have a crosslinkable functionality feed composition of 4.88 mol %, or f_2 = 0.0488.

DSC and DMA

Differential scanning calorimetry and dynamic mechanical analysis experiments were performed on the synthesized polymers after drying and annealing in order to determine both the thermal and mechanical properties of the samples prior to use in sorption investigations. One key parameter of any polymer is its glass transition temperature, T_g, or the temperature above which long-range relaxational motions of polymer chains are likely to happen. DSC and DMA offer just two of many methods to determine this transition temperature, and the reported value of the T_g for a given polymer will depend on the experimental method chosen, the method of T_g data analysis utilized, and such experimental parameters as the heating rate in DSC or the frequency in DMA. Thus, care must be taken when determining, using, and comparing glass transition temperatures of polymers.

For this investigation, the critical aspect of the polymer's T_g was not its absolute value, but the rate at which the T_g changed with changing network structure. Some representative DSC thermograms are shown in Figure 4.7 for PMMA crosslinked with EGDMA with varying crosslinker feed compositions. Values of the glass transition temperature calculated by the ½ ΔC_p extrapolated analysis method are shown. Additionally, DMA can itself yield several measures of the T_g. Typical DMA experimental curves are presented in Figure 4.8 for both the shear storage modulus, G', and tanδ for a PMMA sample crosslinked with EGDMA with f_2 = 0.0488. Shown are oft-reported values of the T_g from DMA experiments: the onset of the approximately 3-order-of-magnitude drop in G' and the peak of the tanδ curve.

The variation of these three values of the glass transition temperature with increasing crosslinker feed compositions (from 0.2 – 26.1 mol %) is shown in Figure 4.9. Even though the absolute value of the T_g differed for each method, increasing the crosslinking density by incorporating more crosslinking moieties affected each method in the same, linear manner. This behavior is generally expected and predicted by the Fox-Loshaek Equation [20]:

38

$$T_g = T_g^0 + K_c\rho_c \qquad\qquad (4.4)$$

where T_g^0 is the glass transition temperature of the uncrosslinked polymer, ρ_c is the crosslinking density of the polymer, and K_c is a polymer-specific constant.

However, there is a secondary contribution to the increase in T_g that is masked by this expression when a significant amount of a comonomer is used to crosslink the system. Namely, the addition of a comonomer itself can alter the T_g, for example the generally reported value of T_g for neat PMMA is 105°C [21] while the temperature for poly(EGDMA) has been reported as 271°C [22]. A further complication is that neat poly(EGDMA) will itself necessarily be highly crosslinked, such that you must obtain T_g values of the equivalent, uncrosslinked polymer.

Glass transition temperatures determined by DSC for PMMA samples with 1.98, 4.88, and 9.52 mol % feed compositions, f_2, of crosslinkers with varying bridge lengths EGDMA, di(EG)DMA, tri(EG)DMA, and tetra(EG)DMA) are shown in Figure 4.10. Increasing the bridge length of the crosslinking comonomer lowered the T_g in all cases. This was expected since increasing the bridge length loosens the network structure and the energy necessary for relaxational motion will be reduced. However, the negligible change in the T_g with increasing crosslinking density for tri(EG)DMA and tetra(EG)DMA could not be explained by this phenomenon alone. This behavior was also seen in T_g values determined by DMA from both G′ and tanδ.

One potential contributing factor tested was whether or not the inherent decrease in crosslinking density as the bridge length was increased contributed substantially to this behavior. Basically, even though the number of crosslinks was in theory the same for all samples with 9.52 mol % crosslinker feed, the larger crosslinkers contributed additional mass and volume to the system, thereby reducing the number of crosslinks per unit volume. This led to a theoretical decrease in crosslinking density of 1.7 %, 3.6 %, and 5.6 % for polymers crosslinked with di(EG)DMA, tri(EG)DMA, and tetra(EG)DMA, respectively, when compared to polymers crosslinked with EGDMA. The

T_g values were plotted against the resulting theoretical crosslinking densities in Figure 4.11. There was essentially no change in the T_g behavior, indicating that this change in crosslinking density played no substantive role.

The negligible changes in T_g for the longer crosslinkers was rather the additive result of the "copolymer effect" and the "crosslinking effect" [23].   Crosslinks traditionally raise the glass transition temperature by acting as points of resistance to relaxational motion, thereby increasing the average chain energy necessary to transition from a glass to a rubber. This has been referred to as the "crosslinking effect" and the magnitude of the ΔT_g per additional crosslink will decrease as the crosslinks are increased in length using increasingly flexible oligo(ethylene glycol) bridges, as the ability of the crosslinks to restrict chain motion is diminished. With this behavior, the T_g will still always increase with increasing degree of crosslinking. However, crosslinking comonomers have an additional effect on the T_g, dubbed the "copolymer effect" [23].

As the crosslinker length is increased, it becomes a more substantial component of the network structure. Since poly(ethylene glycol) has a substantially lower T_g than PMMA (-67°C [17]), increasing the quantity and length of the crosslinker will lower the T_g of the copolymer. Thus, you have two opposing factors that can lead to negligible changes in T_g as the degree of crosslinking is increased, and will eventually lead to reductions in the T_g at higher crosslinking comonomer compositions or longer bridge lengths.

Finally, values of the shear storage modulus, G', are shown in Figure 4.12 for two series of PMMA samples with varying theoretical copolymer crosslinker compositions determined by reactivity ratio calculations. The two series represent two different batches of synthesized PMMA cylinders. As shown, G' increased monotonically after a critical crosslinker composition is reached. This indicated that at and below molar amounts of 1.0 mol % crosslinker in the copolymer the increase in commoner concentration was creating crosslink points at a much greater rate than after this critical

region. This effect was due to the entrapment of entanglements in the network structure.

Values for the molecular weight between entanglements in uncrosslinked polymer, M_e^0, are given in Ferry [24] as 4,700, 10,000, and 4,800 g/mol for conventionally synthesized, atactic PMMA. These entanglements act as temporary, physical crosslinks in the rubbery state. However, as chemical crosslinks are added to the network structure, some of these entanglements become entrapped, thereby creating permanent physical crosslinks that add to the effective crosslinking density of the polymer. As the degree of chemical crosslinking continues to increase, eventually all of the entanglements present become locked into place and contribute to polymer properties dependent on the crosslinking density. Thus, shear modulus profiles like the one shown in Figure 4.12 were expected from theory [24]. Additionally, the latter portion of the curve in Figure 4.12 was fitted to a linear profile (shown). The resulting y-intercept returned a value of M_e^0 = 4,690 g/mol for the polymer samples used in this study. This value was in excellent agreement with values typically reported for PMMA and was utilized in this investigation to determine the extent of chemical crosslinking.

Figure 4.13 shows the variation of G' with degree of crosslinking for di(EG)DMA, tri(EG)DMA, and tetra(EG)DMA. Figure 4.14 contains the same data plotted alongside the values for polymers of Series 2 crosslinked with EGDMA. There was no appreciable change in the modulus of PMMA when the length of the crosslinking interchain bridge was increased. This was in contrast to the T_g results, and showed that the shear storage modulus was not significantly affected by the "copolymer effect" in this investigation, while it changed monotonically with the number of crosslinks in the polymer above a critical value.

DETERMINATION OF M_c

Equilibrium Swelling Measurements

Verification of the polymer network structure created in the synthesis of crosslinked PMMA samples was necessary for this investigation. To this end, equilibrium swelling measurements were collected in triplicate for PMMA with varying molar amounts of EGDMA, di(EG)DMA, tri(EG)DMA, and tetra(EG)DMA added in the polymerization feed.

Equilibrium penetrant sorption measurements can be related to the crosslinking density of a crosslinked polymer sample by considering a free energy balance between the energy of mixing and the elastic resistance to expansion of the polymer mesh and following the derivation of Flory and Rehner [25]:

$$\Delta G = \Delta G_{mix} + \Delta G_{el} \tag{4.5}$$

By assuming the deformation process occurs without a significant change in enthalpy and drawing from rubber elasticity theories, the change in elastic free energy becomes:

$$\Delta G_{el} = -T\Delta S_{el} = \frac{RT\upsilon_e}{(f/2)}\left[\alpha_x^2 + \alpha_y^2 + \alpha_z^2 - 3 - \ln\alpha_x\alpha_y\alpha_z\right] \tag{4.6}$$

where R is the ideal gas constant, ΔS_{el} is the entropy change of network expansion, T is temperature in Kelvin, υ_e is the effective number of mols of chain segments in the polymer network, f is the functionality of the crosslinker used (f = 4 for dimethacrylates), and α_i is the extension ratio in a given direction. For dimethacrylates, f = 4, since each double bond provides two "functional sites" and can create 2 new bonds when reacted. One can further relate the extension ratio to the penetrant volume fraction at equilibrium, ϕ_2, if an isotropic end-state expansion is assumed:

$$\alpha_x = \alpha_y = \alpha_z = \frac{1}{\phi_2^{1/3}} \tag{4.7}$$

Combining equations 4.6 and 4.7 then gives the following result:

$$\Delta G_{el} = \frac{RT\upsilon_e}{(f/2)}\left[\frac{3}{\phi_2^{2/3}} - 3 + \ln\phi_2\right] \qquad (4.8)$$

Next, the elastic chemical potential of the polymer, μ_1, can be derived from equations 4.9 and 4.10 to give the result shown in equation 4.11:

$$\mu_1 - \mu_1^0 = \frac{\partial(\Delta G_m)}{\Delta n_1} \qquad (4.9)$$

$$\phi_2 = \frac{V_0}{V_0 + n_1 V_1} \qquad (4.10)$$

$$\left(\mu_1 - \mu_1^0\right)_{el} = \frac{RTV_1}{(f/2)}\left(\frac{\nu_e}{V_0}\right)\left[2\phi_2^{1/3} - \phi_2\right] \qquad (4.11)$$

where n_1 is the number of moles of penetrant, V_0 is the volume of the polymer prior to expansion, and V_1 is the molar volume of the penetrant.

The change in the free energy of mixing can be evaluated separately from the Flory-Huggins theory [26-28]:

$$\left(\mu_1 - \mu_1^0\right)_{mix} = RT\left[\ln(1-\phi_2) + \left(1 - \frac{1}{x}\right)\phi_2 + \chi\phi_2^2\right] = RT\ln a_1 \quad (4.12)$$

where x is the degree of polymerization of the polymer chain, a_1 is the activity of the penetrant supply, and χ is the Flory-Huggins interaction parameter. For high polymers $x \gg 1$, and this simplifies to equation 4.13:

$$\ln a_1 = \ln(1-\phi_2) + \phi_2 + \chi\phi_2^2 \qquad (4.13)$$

Combining the elastic and mixing components to the free energy balance, the Flory-Rehner equation [25] is returned:

$$\ln a_1 = \left[\ln(1-\phi_2) + \phi_2 + \chi\phi_2^2\right] + \frac{V_1}{(f/2)}\left(\frac{v_e}{V_0}\right)\left[2\phi_2^{1/3} - \phi_2\right] \quad (4.14)$$

where v_e/V_0 is the crosslinking density of the polymer. Next, if the activity of the penetrant is assumed to be 1 (equivalent to a polymer immersed in a pure liquid), the crosslinking density is written in terms of the molecular weight between crosslinks (equation 4.16), and the presence of chain ends is corrected for (equation 4.15), the final result shown in equation 4.17 can be derived:

$$\upsilon_e = \upsilon\left(1 - \frac{\overline{M}_c}{\overline{M}_n}\right) \quad (4.15)$$

$$\upsilon = \frac{\overline{V}}{\overline{\upsilon}\overline{M}_c} \quad (4.16)$$

$$\frac{1}{\overline{M}_c} = \frac{2}{\overline{M}_n} - \frac{\dfrac{\overline{\upsilon}}{V_1}\left[\ln(1-\phi_2) + \phi_2 + \chi\phi_2^2\right]}{\dfrac{1}{(f/2)}\left[2\phi_2^{1/3} - \phi_2\right]} \quad (4.17)$$

where M_n is the number-average molecular weight of the uncrosslinked polymer chains, v is the number of mols of network chain segments including chain ends, V_1 is the total volume of the sample, and v-bar is the specific volume of the polymer.

For this investigation, values for equilibrium swelling in both pure methanol and pure acetone were utilized. The relevant parameter values are listed in Table 4.2. The values of the Flory-Huggins interaction parameter, χ, also commonly referred to as the chi factor and χ_{12}, were calculated using the Hansen Solubility Parameter equation [29]:

$$\chi_{12} = \frac{V_1 A_{12}}{RT} \quad (4.18)$$

where A_{12} is defined by equation 4.19:

$$A_{12} = \left[\left(\delta_{D2} - \delta_{D1} \right)^2 + \left(\delta_{P2} - \delta_{P1} \right)^2 + \left(\delta_{H2} - \delta_{H1} \right)^2 \right] \quad (4.19)$$

where δ_{Di}, δ_{Pi}, and δ_{Hi} are solubility parameter contributions of dispersion, polar, and hydrogen-bonding forces, respectively for solvent (1) and polymer (2). Values of these constants and the calculated values of the Flory-Huggins interaction parameter are listed in Table 4.2. Finally, values of the equilibrium polymer volume fraction were determined by Archimedes' principle:

$$\phi_2 = \frac{V_{2,d}}{V_{2,s}} = \frac{W_{air,d} - W_{non-solvent,d}}{W_{air,s} - W_{non-solvent,s}} \quad (4.20)$$

where $V_{2,d}$ and $V_{2,s}$ are the polymer sample volumes in the dry and completely swollen states, respectively and W_i are weights in air and a non-solvent (for PMMA the chosen non-solvent was pure water).

The results of the equilibrium swelling calculations for PMMA crosslinked with EGDMA (Series 2) with varying molar crosslinker feed compositions, f_2, are presented in Table 4.3. Given for comparison are theoretical values for the molecular weight between crosslinks. The first theoretical value was calculated from the crosslinker feed compositions by:

$$M_c = \frac{M_r}{2 f_2} \quad (4.21)$$

where M_r is the molecular weight of the repeat unit (100.12 g/mol for MMA) and f_2 is the molar fraction of the crosslinking functionalities in the polymerization feed. The weighted r_1, r_2 value was calculated as discussed previously, and the initial r_1, r_2 value is the copolymer composition formed during the initial stages of the polymerization.

The Flory-Rehner theory provided a poor estimate for the molecular weight between crosslinks in this instance. Equilibrium swelling calculations using this model are only valid when swelling in a penetrant with a chi factor value of 0.5 of less. Thus, the poor results for swelling in methanol could be expected; however, the poor

correlation for acetone was due to the assumption of a Gaussian distribution of network chain segments in the development of the Flory-Rehner theory. This assumption breaks down in systems that are highly crosslinked, as many in this investigation were, and when the degree of network expansion is modest. Acetone is a good solvent for PMMA, but still only exhibited a modest expansion with a weight-swelling ratio of 1.4 - 2.4 over the dry polymer, depending on the degree of crosslinking. In this low state of expansion, it is reasonable to say that there will not be a Gaussian distribution of chain segments. To remedy this, other models have been previously developed by Peppas and Lucht [30] (equation 4.22) and Kovac [31] (equation 4.23) assuming non-Gaussian network segment distributions:

$$\frac{1}{\overline{M}_c} = \frac{2}{\overline{M}_n} - \frac{\dfrac{\overline{\upsilon}}{V_1}\left[\ln(1-\upsilon_{2,s})+\upsilon_{2,s}+\chi\upsilon_{2,s}^2\left[1-\dfrac{1}{N}\upsilon_{2,s}^{2/3}\right]\right]^3}{\dfrac{1}{(f/2)}\left[2\upsilon_{2.s}^{1/3}-\upsilon_{2,s}\left[1+\dfrac{1}{N}\upsilon_{2,s}^{1/3}\right]\right]^2} \tag{4.22}$$

$$\overline{M}_c = \frac{V_1}{\overline{\upsilon}}\left[\ln(1-\phi_2)+\phi_2+\chi\phi_2^2\left[1-\frac{\phi_2^{-2/3}}{N}\right]\right]^{-1} \tag{4.23}$$

where N is defined as:

$$N = \frac{\lambda\overline{M}_c}{M_r} \tag{4.24}$$

where λ = 2 for vinyl polymers.

The results of calculations from the Peppas-Lucht and Kovac methods are also reported in Table 4.3. The Peppas-Lucht model had an improved correlation with the values based on reactivity ratio calculations; however, the Kovac model offered the best correlation of the three. Furthermore, all values of M_c calculated from equilibrium swelling models included the effects of physical crosslinks due to chain entanglements.

The molecular weight between entanglements was determined to be 4,690 g/mol previously in this chapter. While it might be expected that some entanglements will relax during network expansion, the motion of these physical crosslinks are restricted due to the presence of neighboring chemical crosslinks and need to be accounted for. If the physical entanglements were subtracted out from the values for the Kovac model in Table 4.3, then a value for the crosslinking efficiency could be calculated. For PMMA crosslinked with EGDMA in this investigation, the equilibrium swelling results gave a crosslinking efficiency of 43.5 % (Figure 4.15). Since the earliest polymer produced will have the highest degree of crosslinking and ultimately limit overall network expansion during swelling, equilibrium swelling measurements must be compared to the theoretical copolymer composition at low conversions.

Results are similarly presented in Table 4.4 for PMMA crosslinked with di(EG)DMA, tri(EG)DMA, and tetra(EG)DMA. Reactivity ratios for these systems were not found and the ratios for MMA and EGDMA were used in the calculations. As can be seen from the table and Figure 4.16, the results largely mimicked those of crosslinking with EGDMA. The Kovac model with entanglements subtracted out once again gave a good fit with a crosslinking efficiency of 42 %. The decreased goodness of the fit over results for PMMA with EGDMA was most likely due to the absence of accurate reactivity ratios and the lack of a method in current models to account for the effects of changing the length of the crosslinker interchain bridge.

Attempts were made to determine the latter effect, including the previously discussed evaluation of changes in crosslinking density inherent to increasing the bridge length and correlating this with the observed values of equilibrium polymer volume fraction (shown in Figure 4.17). However, there was no conclusive trend, as changes were inconsistent and within experimental error. It should also be mentioned that equilibrium swelling in acetone was achieved by a stair-step procedure from samples swollen first in methanol, since immersion of dry PMMA in pure acetone resulted in sample destruction due to fracturing. The pathway taken by PMMA samples crosslinked

47

with multi(EG)DMAs from pure methanol to pure acetone is shown in Figure 4.18 and was non-linear in nature.

Finally, values for the polymer network mesh size were calculated. The mesh size, ξ, in Å^2 gives an estimate for the effective area available for diffusion of penetrant molecules into the polymer. The mesh size can be calculated from the unperturbed root-mean-squared (RMS) end-to-end distance and polymer volume fraction (ϕ_2):

$$\xi = \phi_2^{1/3} \left(\overline{r_0^2} \right)^{1/2}$$
(4.25)

where the unperturbed RMS end-to-end distance can be calculated from the RMS end-to-end distance in the freely jointed state and the Flory characteristic ratio (C_n):

$$\left(\overline{r_0^2} \right)^{1/2} = C_n^{1/2} \left(\overline{r^2} \right)^{1/2}$$
(4.26)

where:

$$\left(\overline{r^2} \right)^{1/2} = \ell n^{1/2}$$
(4.27)

where l is the bond length, which for vinyl polymers is the carbon-carbon bond length of 1.52 Å and n is the number of bonds in a polymer network segment given by:

$$n = \frac{1}{X}$$
(4.28)

Combining equations 4.25 through 4.28 gives the final result:

$$\xi = \phi_2^{1/3} \left(\frac{\ell^2 C_n}{X} \right)^{1/2}$$
(4.29)

With a C_n value of 8.65 for PMMA [17], the variation of ξ with X is shown in Figure 4.19 for PMMA crosslinked with EGDMA and swollen in Methanol at 25°C. Thus, there was a diminishing return on continuing to increase X in terms of restricting the ability of molecules to diffusion through the polymer network.

Differential Scanning Calorimetry

In addition to equilibrium swelling models, DSC measurements of T_g were used to calculate the crosslinking density and M_c through the Fox-Loshaek Equation (Equation 4.4) and appropriate data. For PMMA crosslinked with EGDMA in a free-radical polymerization, the Fox-Loshaek constant has been calculated to give [23]:

$$\Delta T_g = \left(0.78 \text{x} 10^5\right)\rho_c \tag{4.30}$$

Thus, for PMMA crosslinked with EGDMA, the T_g values from Figure 4.9 were used to calculate ρ_c and M_c. Table 4.5 reports the DSC-calculated values of M_c and F_2. Figure 4.20 compares these values of M_c with the weight-averaged theoretical values expected from the reactivity ratios with a crosslinking efficiency of 40 %. In this case, as opposed to equilibrium swelling measurements, the weight-averaged value of M_c was the appropriate one to use in comparison, since the T_g is a measure of a chain's ability to move relative to neighbors.

Dynamic Mechanical Analysis

Finally, since the DSC analysis could not easily be repeated for multi(EG)DMAs due to a lack of data on the relative contributions of the "copolymer effect" and "crosslinker effect" for these systems, DMA analysis was also utilized to determine M_c. Using rubber elasticity theories, the following equation can be derived [32]:

$$\rho_e = \frac{E_1}{6RT} \tag{4.31}$$

Where ρ_e is the total entanglement (chemical and physical) density and E_1 is the bulk storage modulus in the rubbery plateau region, which can be related to the shear storage modulus (G') by:

$$E_1 = G'\left(1 + \mu\right) \tag{4.32}$$

where μ is Poisson's ratio, which for PMMA is 0.44 [17]. Finally, the effects of chain ends were removed and ρ_e was related to M_e through equations 4.13 and 4.14. Table 4.6 reports values of G', M_c from weight-averaged reactivity ratio calculations (using r_1,r_2 for MMA and EGDMA) and M_c from DMA experiments (M_e with entanglements subtracted assuming $M_{e,0}$ = 4,690 g/mol). The M_c values were then used to calculate a mol % of crosslinker incorporated into the polymer chains (F_2). The resulting typical crosslinking efficiency was 38 %. Figure 4.21 compares DMA-calculated values of M_c for PMMA crosslinked with EGDMA with the expected value based on weight-averaged reactivity ratio calculations with a crosslinking efficiency of 37 %. Overall, the DMA results showed excellent agreement with equilibrium swelling calculations and DSC results considering experimental error.

CONCLUSIONS

Samples of PMMA were successfully synthesized by an *iniferter*-mediated free radical polymerization pathway to yield polymers with controlled variations in network structure by changing the molar amount and bridge length of difunctional comonomers in the reaction feed. The network structures of crosslinked PMMA were characterized by DSC, DMA, and equilibrium swelling measurements and displayed qualitative and quantitative agreement with the expected network parameters calculated from knowledge of the EGDMA and MMA reactivity ratios and typical crosslinker efficiencies (typically around 30-70 % for PMMA crosslinked with EGDMA [33]). DMA and DSC measurements were shown to correlate well to weight-averaged values of the degree of crosslinking, while equilibrium swelling measurements correlated to the degree of crosslinking produced in the very early stages of polymerization.

Overall, the equilibrium swelling measurements using a highly non-Gaussian model for network segment distribution gave the best fits; however, this was also the most labor and calculation intensive procedure. DSC and especially DMA showed

increased scatter from experimental error but captured the behavior well, though DSC could not be used for crosslinking with multi(EG)DMAs. The results suggested an average efficiency of crosslinking for PMMA in this investigation of 40 %.

Additionally, for PMMA crosslinked with multi(EG)DMAs, values of the rubbery plateau modulus were shown to be essentially insensitive to the copolymer effect which greatly depressed T_g. Increasing the crosslinker bridge length also had little discernable impact on the equilibrium polymer volume fraction. It was hypothesized that there would be a measurable change due to the inherent decrease in crosslinking density as the bridge length was increased; however, the change in going from EGDMA to tetra(EG)DMA was too modest and showed no consistent trends outside of experimental error.

The knowledge of the polymer network structure of the samples synthesized in this investigation will be used to examine the role that network parameters such as mesh size and relaxational timescales play in the dynamics of non-Fickian and especially Case II transport. Of particular interest will be the results from the multi(EG)DMAs, as tri(EG)DMA and tetra(EG)DMA allowed for increased degrees of crosslinking and higher moduli without an associated increase in T_g.

REFERENCES

1.   Odian, G., *Principles of Polymerization*. 4th ed. 2004, Hoboken, NJ: John Wiley & Sons, Inc.

2.   ASTM Standard D3125-97 (2001), *Monomethyl Ether of Hydroquinone in Colorless monomeric Acrylate Esters and Acrylic Acid.* ASTM International, West Conshohocken, PA, 2001, DOI: 10.1520/D3125-97R01, w ww.astm.org.

3.   Otsu, T. and A. Matsumoto, *Controlled Synthesis of Polymers Using the Iniferter Technique: Developments in Living Radical Polymerization*. Advances in Polymer Science. Vol. 136. 1998, New York: Springer. 75-137.

4.   Otsu, T., *Iniferter concept and living radical polymerization.* Journal of Polymer Science, Part A: Polymer Chemistry, 2000. **38**(12): p. 2121-2136.

5.   Ward, J.H., R. Bashir, and N.A. Peppas, *Micropatterning of biomedical polymer surfaces by novel UV polymerization techniques.* Journal of Biomedical Materials Research, 2001. **56**(3): p. 351-360.

6.   Ward, J.H. and N.A. Peppas, *Kinetic gelation modeling of controlled radical polymerizations.* Macromolecules, 2000. **33**(14): p. 5137-5142.

7.   Ward, J.H., A. Shahar, and N.A. Peppas, *Kinetics of 'living' radical polymerizations of multifunctional monomers.* Polymer, 2002. **43**(6): p. 1745-1752.

8.   Kazmaier, P.M., K.A. Moffat, M.K. Georges, R.P.N. Veregin, and G.K. Hamer, *Free-Radical Polymerization for Narrow-Polydispersity Resins - Semiempirical Molecular-Orbital Calculations as a Criterion for Selecting Stable Free-Radical Reversible Terminators.* Macromolecules, 1995. **28**(6): p. 1841-1846.

9.   Lambrinos, P., M. Tardi, A. Polton, and P. Sigwalt, *The Mechanism of the Polymerization of Normal-Butyl Acrylate Initiated with N,N-Diethyl Dithiocarbamate Derivatives.* European Polymer Journal, 1990. **26**(10): p. 1125-1135.

10.   Otsu, T., T. Matsunaga, A. Kuriyama, and M. Yoshioka, *Living Radical Polymerization through the Use of Iniferters - Controlled Synthesis of Polymers.* European Polymer Journal, 1989. **25**(7-8): p. 643-650.

11.   Manga, J.D., A. Polton, M. Tardi, and P. Sigwalt, *Living Character of the Polymerization of Butyl Acrylate Initiated by a Model N,N-Diethyldithiocarbamate.* Journal of Macromolecular Science-Pure and Applied Chemistry, 1995. **A32**: p. 695-703.

12.   Kannurpatti, A.R., S.X. Lu, G.M. Bunker, and C.N. Bowman, *Kinetic and mechanistic studies of iniferter photopolymerizations.* Macromolecules, 1996. **29**(23): p. 7310-7315.

13.   Zaremskii, M.Y., A.V. Olenin, Y.S. Garina, S.I. Kuchanov, V.B. Golubev, and V.A. Kabanov, *Mechanism of Photoinitiated Radical Polymerization of Styrene in the Presence of Benzyldithiocarbamate Iniferter.* Vysokomolekulyarnye Soedineniya Seriya A, 1991. **33**(10): p. 2167-2175.

14.   Luo, N., A.T. Metters, J.B. Hutchison, C.N. Bowman, and K.S. Anseth, *A methacrylated photoiniferter as a chemical basis for microlithography: Micropatterning based on photografting polymerization.* Macromolecules, 2003. **36**(18): p. 6739-6745.

15.   Otsu, T. and M. Yoshida, *Role of Initiator-Transfer Agent-Terminator (Iniferter) in Radical Polymerizations - Polymer Design by Organic Disulfides as Iniferters.* Makromolekulare Chemie, Rapid Communications, 1982. **3**(2): p. 127-132.

16.   Turner, S.R. and R.W. Blevins, *Photoinitiated Block Copolymer Formation Using Dithiocarbamate Free-Radical Chemistry.* Macromolecules, 1990. **23**(6): p. 1856-1859.

17.   *Polymer Handbook*. Third ed, ed. J. Brandrup and E.H. Immergut. 1989, New York: John Wiley & Sons.

18.   E., H.G., *Copolymerization*. 1964, New York: Interscience Publishers.

19.   Mao, R.S., Y. Liu, M.B. Huglin, and P.A. Holmes, *Determination of Monomer Reactivity Ratios in the Cross-Linking Copolymerization of Methyl-Methacrylate with Ethylene Dimethacrylate.* Macromolecules, 1995. **28**(20): p. 6739-6744.

20.   Fox, T.G. and S. Loshaek, *Influence of Molecular Weight and Degree of Crosslinking on the Specific Volume and Glass Temperature of Polymers.* Journal of Polymer Science, 1955. **15**: p. 371-390.

21.   Rehberg, C.E. and C.H. Fisher, *Properties of Monomeric and Polymeric Alkyl Acrylates and Methacrylates.* Journal of Industrial and Engineering Chemistry, 1948. **40**: p. 1429-33.

22.   Bowman, C.N. and N.A. Peppas, *Polymers for Information-Storage Systems .2. Polymerization Kinetics for Preparation of Highly Cross-Linked Polydimethacrylates.* Journal of Applied Polymer Science, 1991. **42**(7): p. 2013-2018.

23.   Loshaek, S., *Crosslinked Polymers. II. Glass Temperatures of Copolymers of Methyl Methacrylate and Glycol Dimethacrylates.* Journal of Polymer Science, 1955. **15**: p. 391-404.

24.   Ferry, J.D., *Viscoelastic Properties of Polymers*. 3rd ed. 1980, New York: John Wiley & Sons.

25.   Flory, P.J. and R. Rehner, Jr., *Statistical Mechanics of Crosslinked Polymer Networks. I. Rubberlike Elasticity.* Journal of Chemical Physics, 1943. **11**: p. 521.

26.   Huggins, M.L., *Some Properties of Solutions of Long-chain Compounds.* Journal of Physical Chemistry, 1942. **46**: p. 151-158.

27.   Flory, P.J., *Thermodynamics of High-Polymer Solutions.* Journal of Physical Chemistry, 1942. **10**: p. 51-61.

28.   Flory, P.J. and W.R. Krigbaum, *Thermodynamics of High Polymer Solutions.* Annual Review of Physical Chemistry, 1951. **2**: p. 383-402.

29.   Hansen, C.M., *Hansen Solubility Parameters: A User's Handbook*. 2nd ed. 2007, Boca Raton: CRC Press.

30. Peppas, N.A. and L.M. Lucht, *Macromolecular Structure of Coals. I. The Organic Phase of Bituminous Coals as a Macromolecular Network.* Chemical Engineering Communications, 1984. **30**(3-5): p. 291-310.

31. Kovac, J., *Modified Gaussian Model for Rubber Elasticity.* Macromolecules, 1978. **11**(2): p. 362-365.

32. Sekkar, V., K. Narayanaswamy, K.J. Scariah, P.R. Nair, K.S. Sastri, and H.G. Ang, *Evaluation by various experimental approaches of the crosslink density of urethane networks based on hydroxyl-terminated polybutadiene.* Journal of Applied Polymer Science, 2007. **103**(5): p. 3129-3133.

33. Loshaek, S. and T.G. Fox, *Cross-linked Polymers. I. Factors Influencing the Efficiency of Cross-linking in Copolymers of Methyl Methacrylate and Glycol Dimethacrylates.* Journal of the American Chemical Society, 1953. **75**: p. 3544.

34. *DIPPR 801 Database of Physical and Thermodynamical Properties of Pure Chemicals*, BYU DIPPR Thermodynamical Properties Laboratory. Web. May 2010.

Table 4.1: Spatial comparison of molecular weights and molecular weight distributions for PMMA samples polymerized with and without the presence of an *iniferter* molecule.

		M_n	M_w	PDI
Free Radical Polymerization	*Inner Section*	892,800	1,615,000	1.81
	Outer Section	2,012,000	2,986,000	1.48
	Total	1,467,000	2,342,000	1.60
***Iniferter*-mediated Free-Radical Polymerization**	*Total*	139,200	221,000	1.59

Table 4.2: Parameter values for equilibrium swelling calculations for PMMA swollen in methanol and acetone at 25°C and 30°C.

		Methanol	Acetone
25°C	V_1 (cm^3/mol)^a	40.56	73.84
	v-bar (cm^3/g)^b	0.817	0.817
	χ	1.01	0.344
30°C	V_1 (cm^3/mol)^a	40.83	74.38
	v-bar (cm^3/g)^b	0.822	0.822
	χ	0.994	0.338
	f^c	4	4
	M_n^d	139,000	139,000
A$_{12}$^{e}	δ_{D1}	15.1	15.5
	δ_{P1}	12.3	10.4
	δ_{H1}	22.3	7
	δ_{D2}	18.6	18.6
	δ_{P2}	10.2	10.2
	δ_{H2}	8.6	8.6

^{a}Values taken from the DIPPR Database [34]
^{b}Values from the Polymer Handbook [17]
^{c}Value for difunctional crosslinking molecules
^{d}Value determined by GPC earlier in this chapter
^{e}Values from Hansen Solubility Parameter Handbook [29]

Table 4.3: Theoretical and experimental values of the molecular weight between crosslinks determined by equilibrium swelling models for PMMA crosslinked with EGDMA and swollen at 30°C.

| Crosslinker Feed, f_2 (mol %) | M_c Based on Monomer Feed Ratios | | | M_c Based on Equilibrium Swelling Models | | | | | |
| | Theoretical | Weighted r_1,r_2 | Initial r_1,r_2 | Flory –Rehner (Equation 4.17) | | Peppas-Lucht (Equation 4.22) | | Kovac (Equation 4.23) | |
				Methanol	Acetone	Methanol	Acetone	Methanol	Acetone
1.02	4,920	4,470	3,850	404	1,433	583	1,680	899	4,290
3.00	1,670	1,520	1,310	293	718	467	976	665	1,980
3.93	1,280	1,160	1,000	251	581	422	729	576	1,480
4.86	1,030	937	810	227	492	396	642	525	1,240
4.88	1,030	933	806	250	491	421	640	575	1,240
5.83	858	781	675	229	421	398	572	529	1,050
7.69	651	593	514	191	326	357	478	451	805
9.52	526	479	416	181	286	345	439	429	706
11.32	442	403	351	198	244	364	396	464	602

Table 4.4: Theoretical and experimental values of the molecular weight between crosslinks determined by equilibrium swelling models for PMMA crosslinked with multi(EG)DMAs and swollen at 25°C.

| Crosslinker | Feed, f_2 (mol %) | M_c Based on Monomer Feed Ratios | | | M_c Based on Equilibrium Swelling Models | | | | | |
| | | | | | Flory –Rehner (Equation 4.17) | | Peppas-Lucht (Equation 4.22) | | Kovac (Equation 4.23) | |
		Theoretical	Weighted r_1,r_2	Initial r_1,r_2	Methanol	Acetone	Methanol	Acetone	Methanol	Acetone
di(EG)DMA	2.00	2,500	2,270	1,960	376	944	554	1,120	840	2,580
di(EG)DMA	4.87	1,030	935	808	233	536	403	679	538	1,360
di(EG)DMA	9.55	524	478	415	194	320	360	495	457	806
tri(EG)DMA	1.95	2,570	2,330	2,010	384	950	563	1,110	858	2,590
tri(EG)DMA	4.86	1,030	936	809	238	535	408	692	548	1,360
tri(EG)DMA	9.51	526	480	416	189	325	354	495	445	814
tetra(EG)DMA	2.02	2,470	2,250	1,940	360	842	537	1,000	805	2,260
tetra(EG)DMA	4.87	1,030	934	807	260	488	431	650	594	1,240
tetra(EG)DMA	9.52	526	479	416	183	300	348	473	434	754

Table 4.5: Comparison of M_c and copolymer crosslinker composition (F_2) determined by DSC measurements with those expected from weight-averaged r_1, r_2 calculations for PMMA crosslinked with EGDMA.

f_2 (mol %)	T_g (DSC)	ϕ_p (Equil.)	M_c (r_1, r_2)	M_c (DSC)	F_2 (mol %) DSC	F_2 (mol %) r_1, r_2
0.21	114.6	0.724	21,500	38,700	0.13	0.23
0.41	115.1	0.724	11,100	22,500	0.22	0.45
0.60	115.5	0.731	7,510	17,600	0.28	0.68
0.81	115.9	0.735	5,580	13,700	0.36	0.90
1.00	115.6	0.737	4,520	16,000	0.31	1.11
1.49	116.1	0.741	3,040	12,900	0.39	1.65
1.99	118.2	0.747	2,280	5,970	0.84	2.20
2.96	120.2	0.754	1,530	4,320	1.16	3.27
4.88	125.6	0.767	930	2,190	2.29	5.68
9.57	132.5	0.779	474	1,470	3.40	10.56
13.98	142.5	0.798	325	883	5.67	15.41
18.17	153.1	0.822	250	673	7.43	20.03
22.23	179.8	0.832	204	447	11.20	24.51
26.07	182.0	0.843	174	399	12.57	28.75

Table 4.6: Comparison of M_c and copolymer crosslinker composition (F_2) determined by DMA measurements without entanglements with those expected from weight-averaged r_1, r_2 calculations for PMMA crosslinked with multi(EG)DMAs.

x(EG) DMA	f_2, (mol %)	Log[G'], (Pa)	M_c (r_1, r_2)	M_c (DMA)	F_2, (mol %) DMA	F_2, (mol %) r_1, r_2
di	2.00	5.91	2,270	10,000	0.50	2.20
di	4.87	6.12	935	2,960	1.69	5.36
di	9.55	6.53	478	1,180	4.25	10.48
tri	1.95	5.93	2,330	10,000	0.50	2.15
tri	4.86	6.31	936	2,820	1.78	5.35
tri	9.51	6.56	480	1,180	4.25	10.44
tetra	2.02	5.86	2,250	10,700	0.47	2.23
tetra	4.87	6.30	934	2,410	2.08	5.36
tetra	9.52	6.53	479	1,340	3.74	10.44
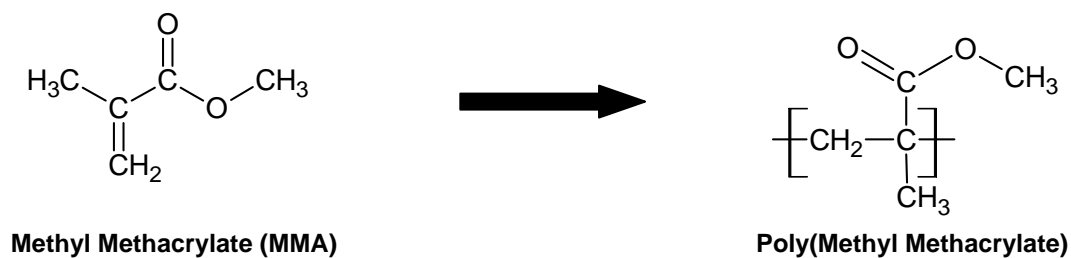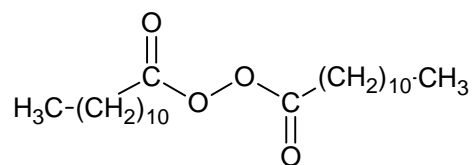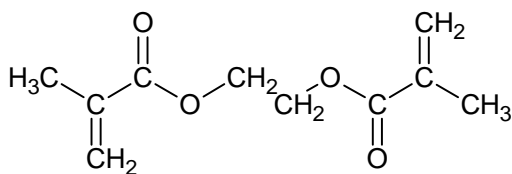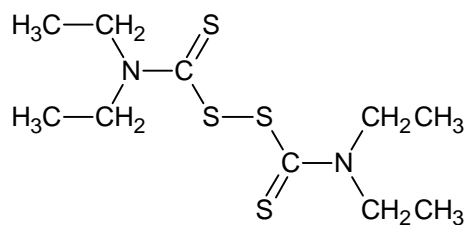
Figure 4.1: Materials used in the synthesis of crosslinked poly(methyl methacrylate).
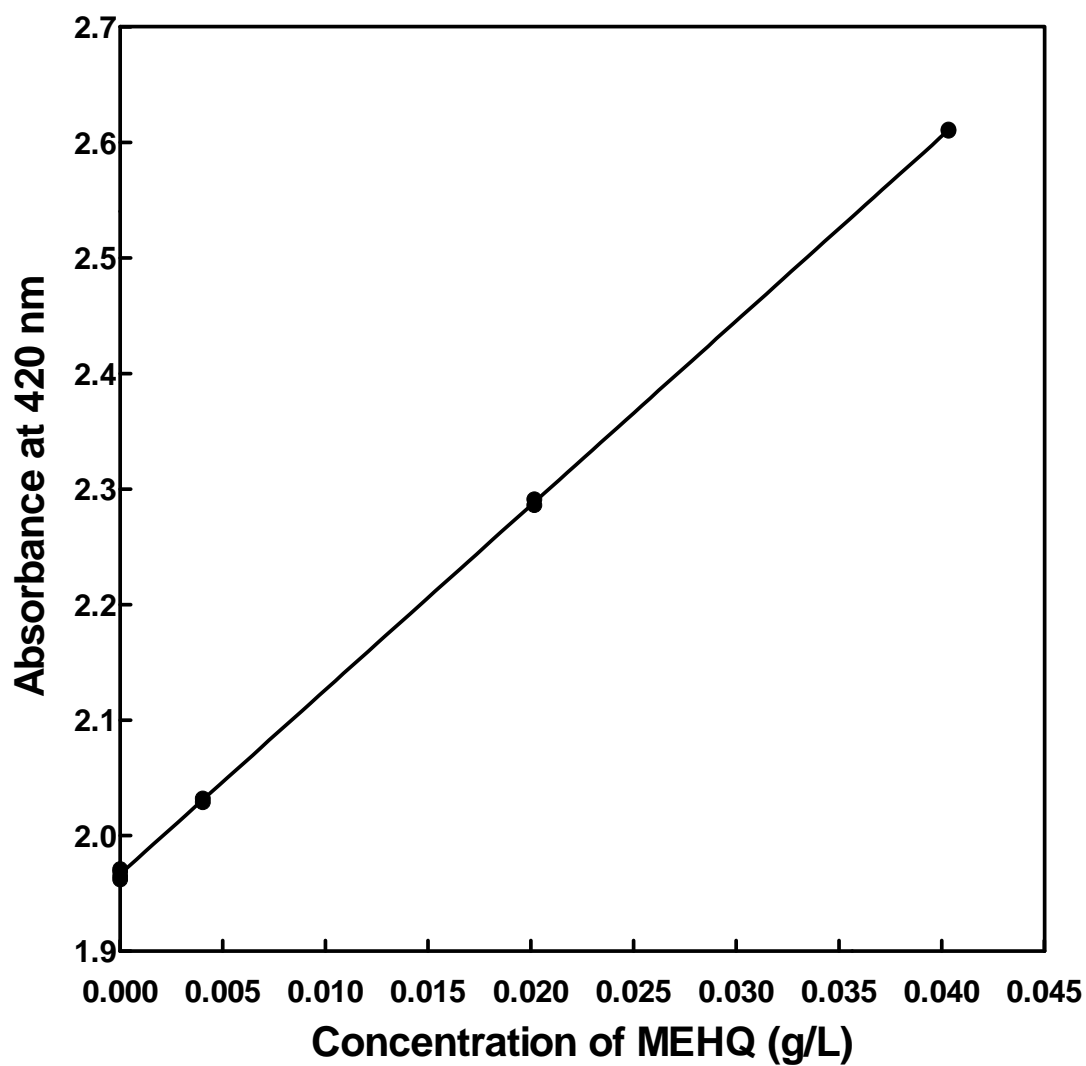
Figure 4.2: Linear calibration curve for determination of MEHQ concentration in methyl methacrylate monomer by UV/Vis Spectroscopy.

Initiation

Propagation

$$Initiator \rightarrow 2R\bullet$$

$$RM\bullet + M_n \rightarrow RM_nM\bullet$$

$$Iniferter \rightarrow 2R'S\bullet$$

Termination

$$R\bullet + M \rightarrow RM\bullet$$

$$RM_nM\bullet + R'S\bullet \leftrightarrow RM_{n+1}SR'$$
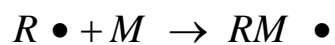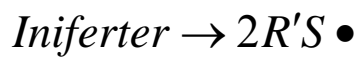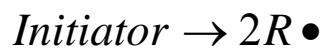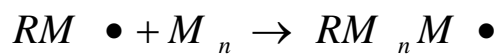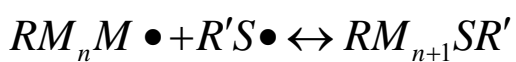
Figure 4.3: Representative mechanism of an *iniferter*-mediated polymerization [4].
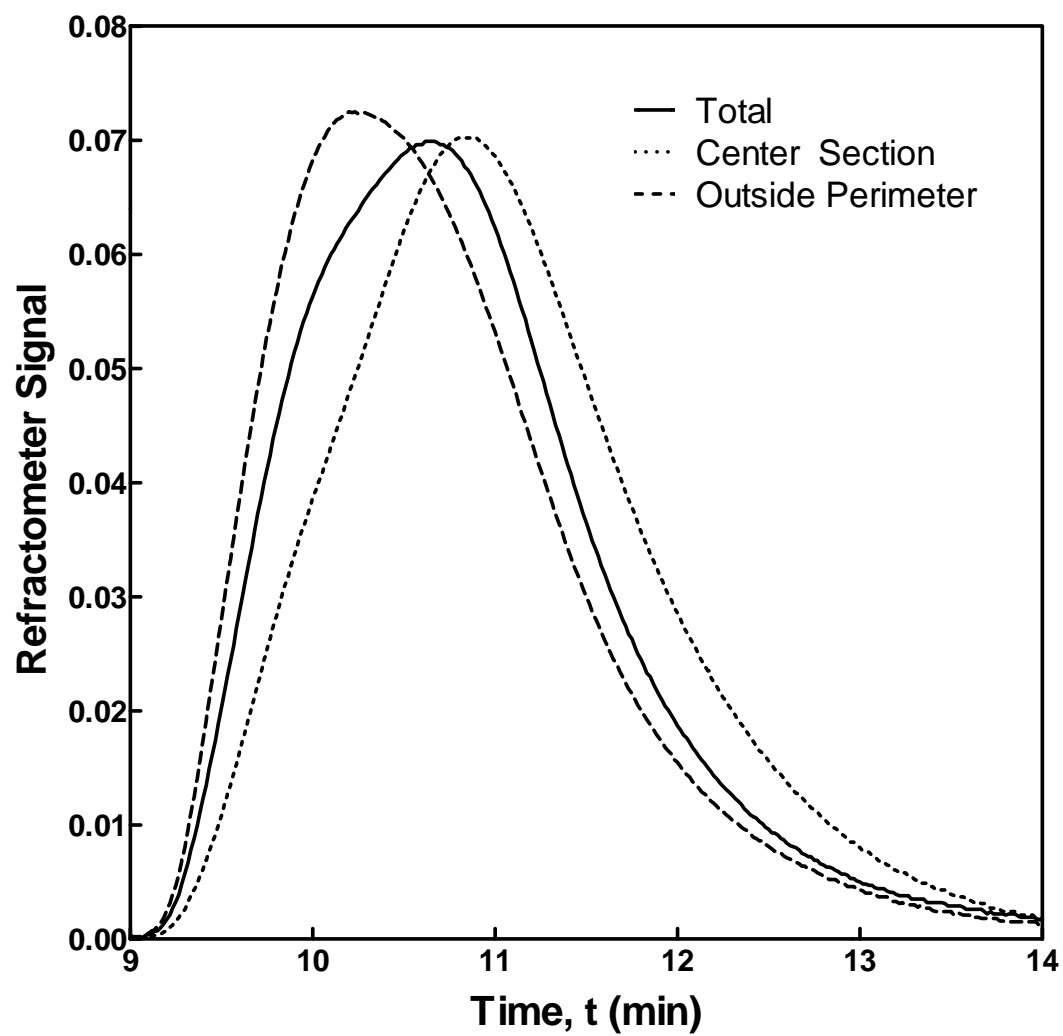
Figure 4.4: GPC output for PMMA polymerized without *iniferter* present.
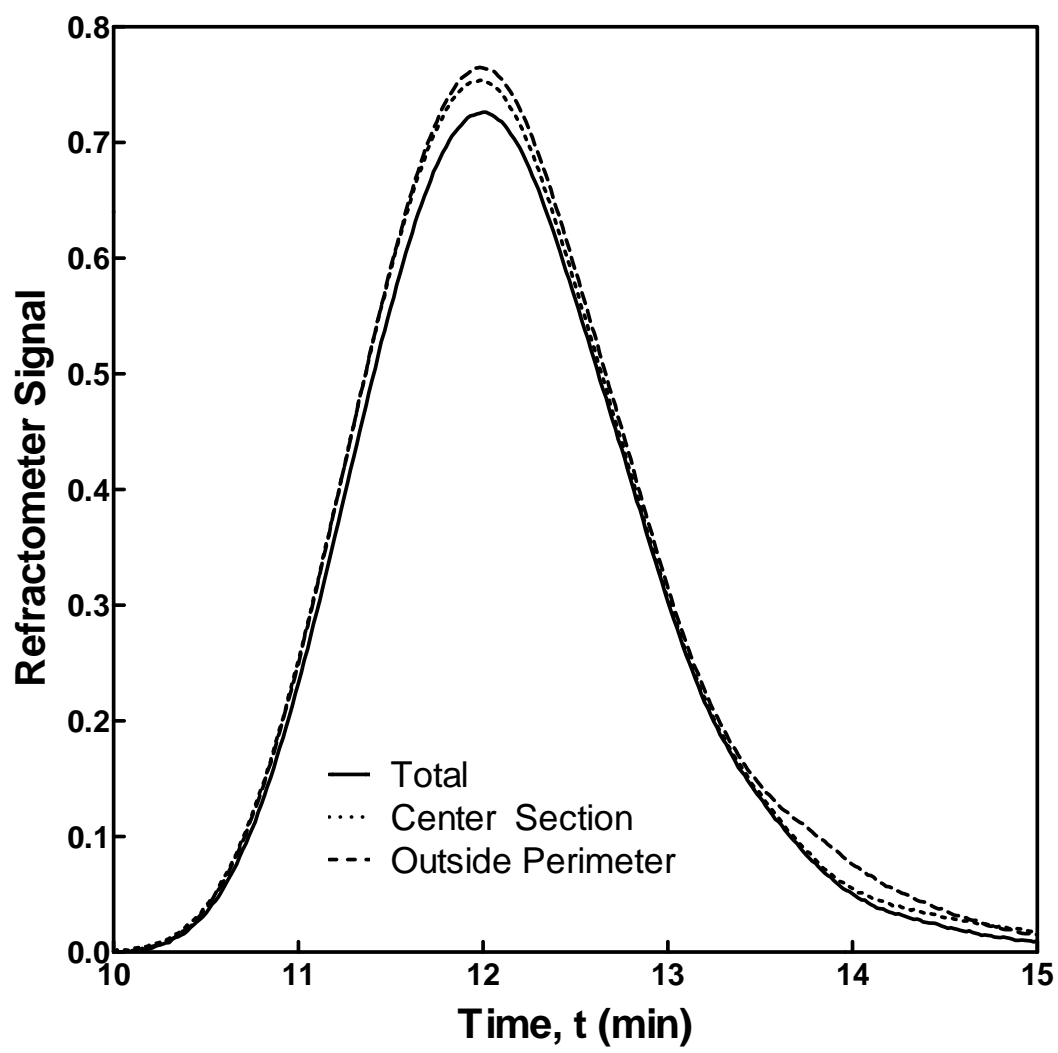
Figure 4.5: GPC output for PMMA polymerized with *iniferter* present.
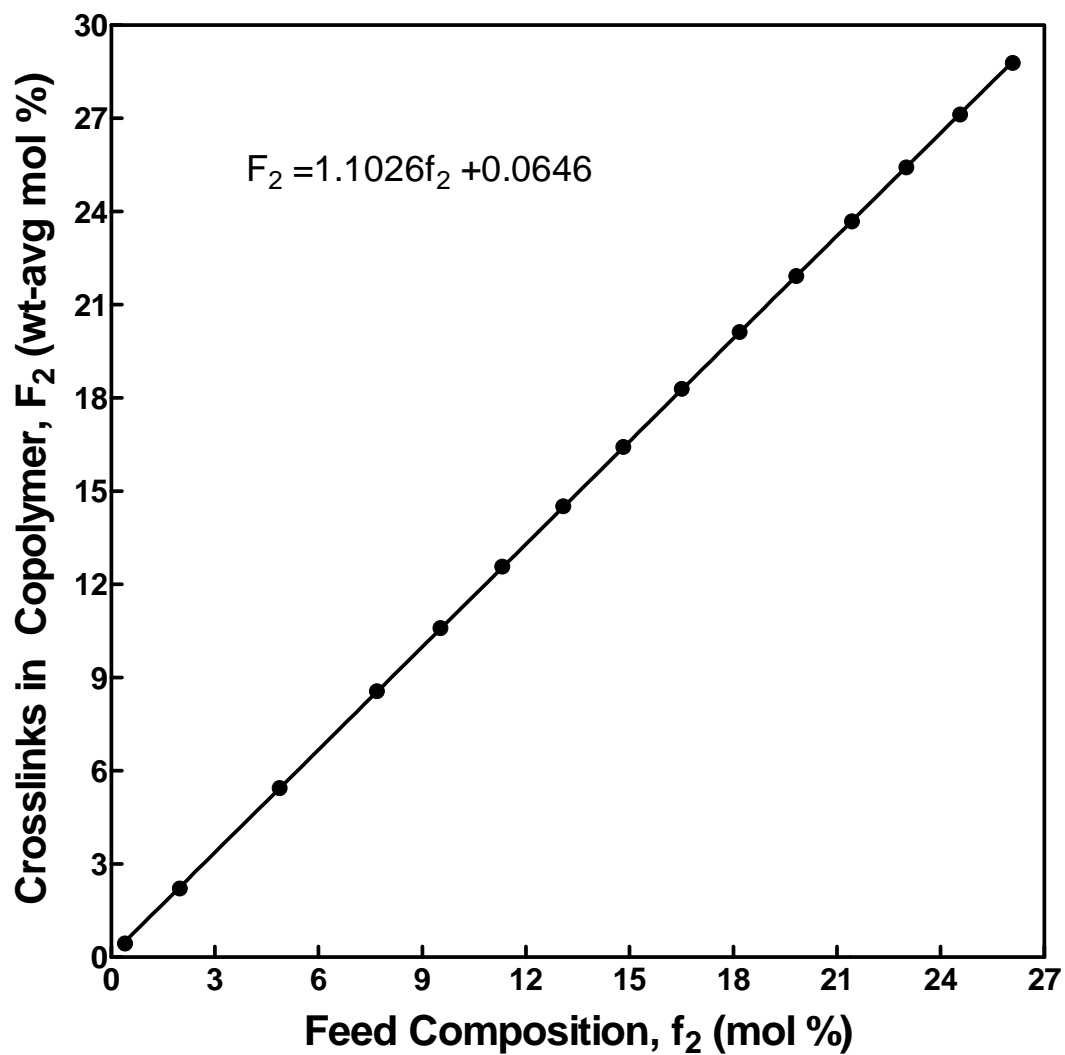
Figure 4.6: Comparison and linear regression of the theoretical, weight-averaged crosslinker composition (F_2) of the copolymer versus the crosslinkable functionality composition of the monomer feed (f_2) for PMMA crosslinked with EGDMA.
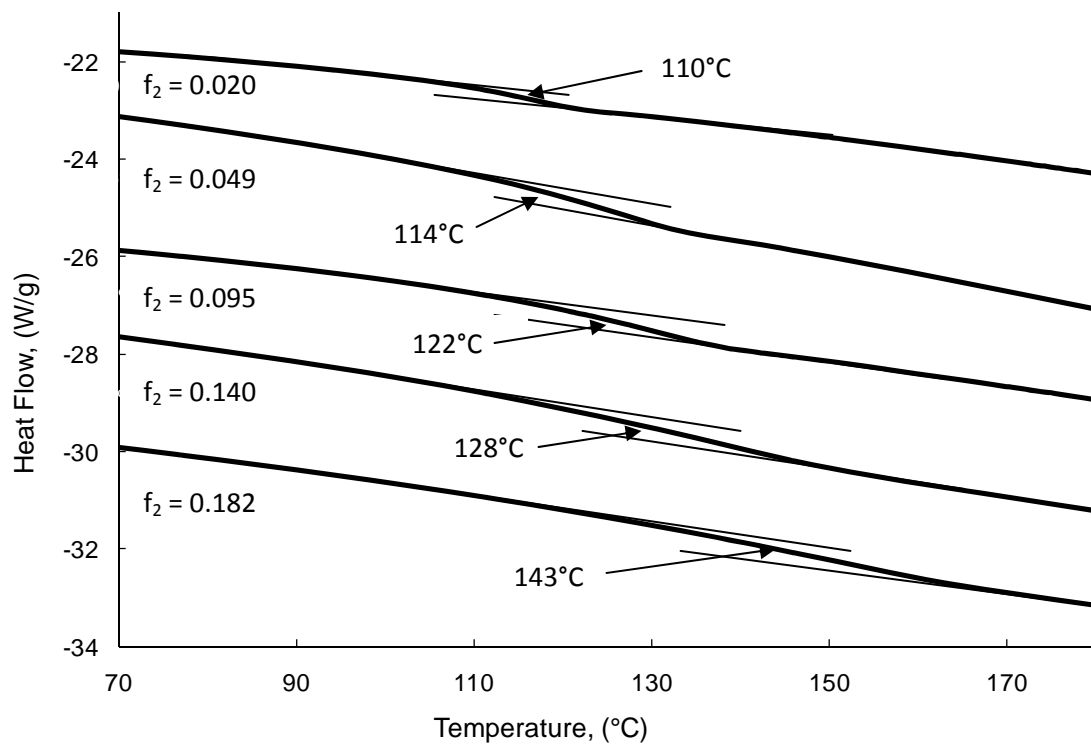
Figure 4.7: DSC thermograms for PMMA crosslinked with varying molar crosslinker feed compositions (f_2).
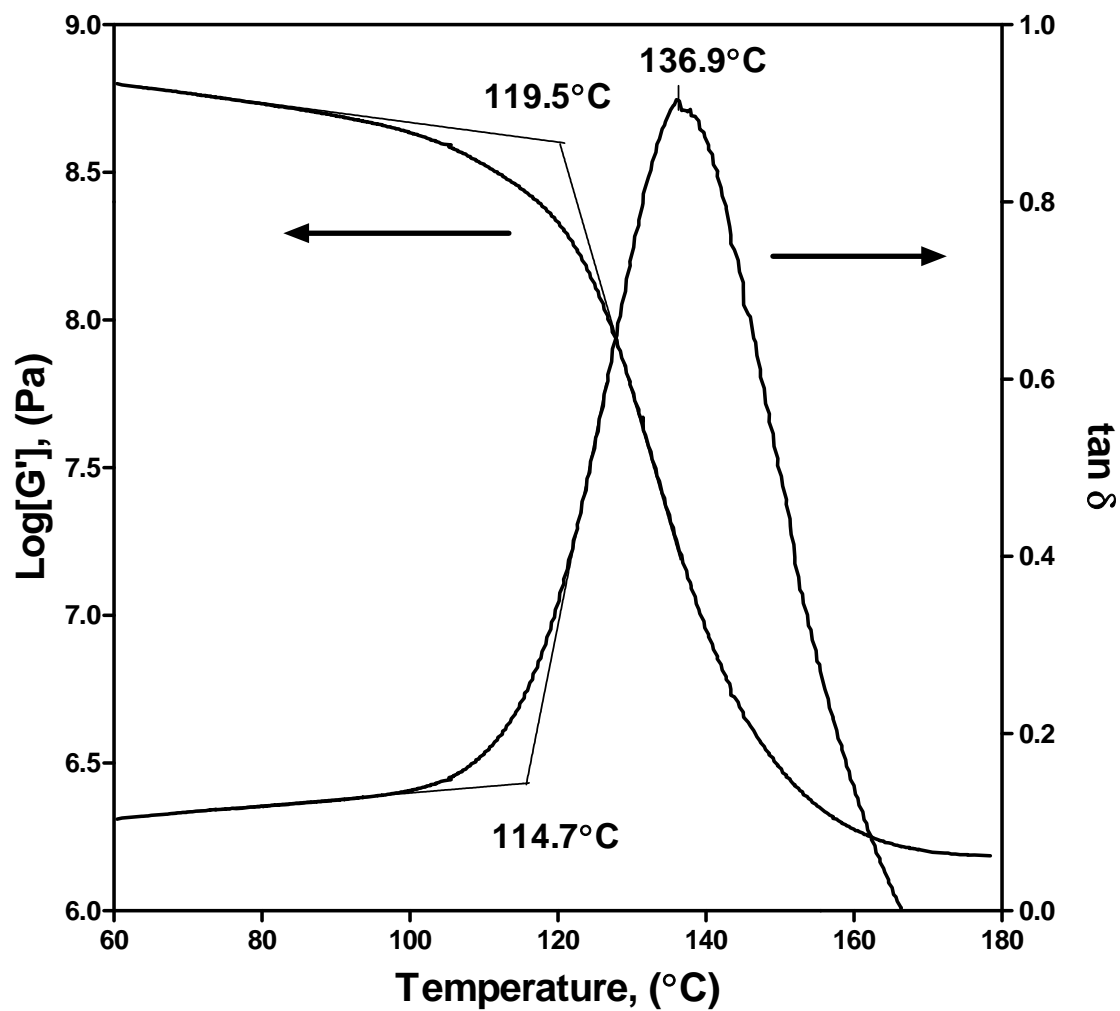
Figure 4.8: DMA resonant curve for PMMA crosslinked with EGDMA with f_2 = 0.0488 from 60°C to 180°C.
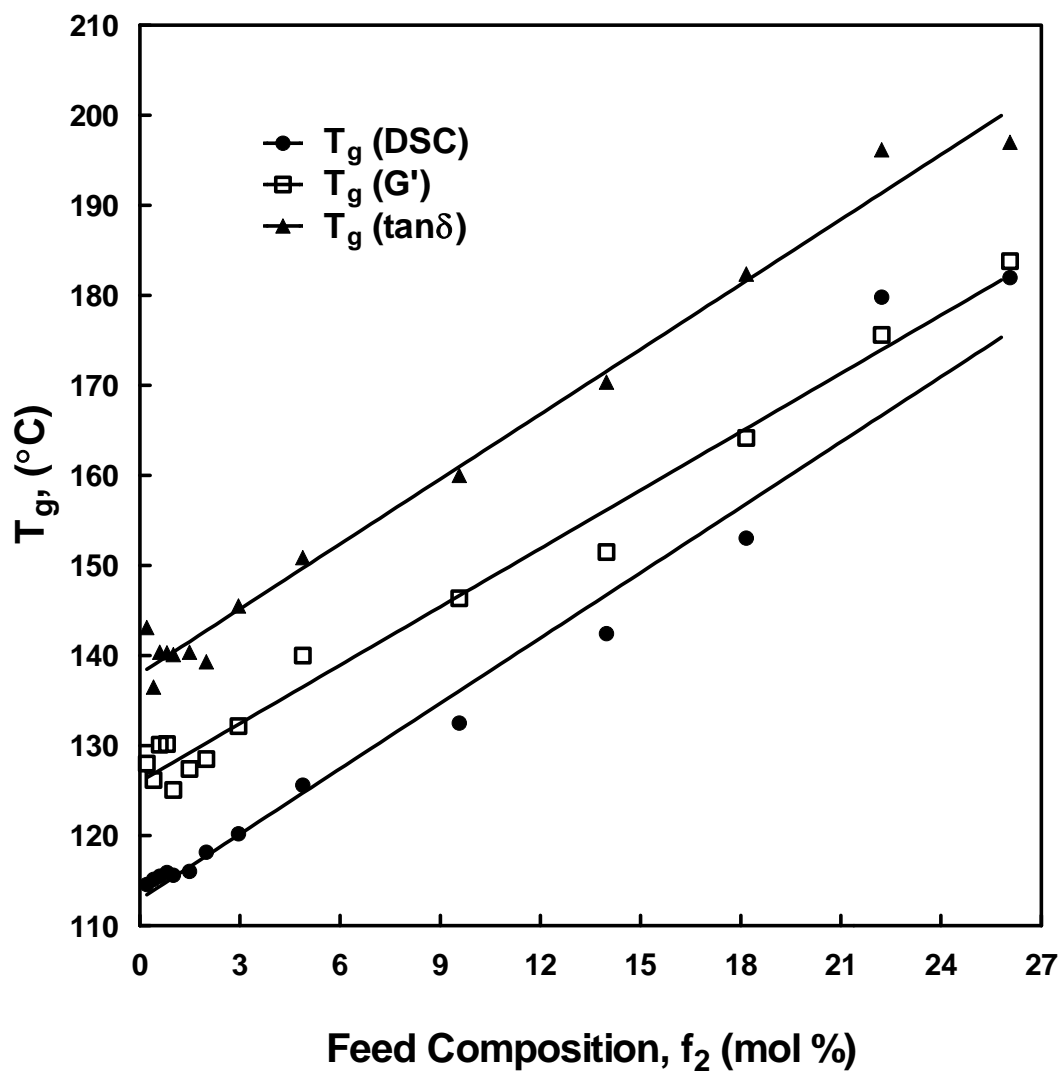
Figure 4.9: Values of T_g determined for PMMA with varying molar crosslinker feed compositions (f_2) by DSC and DMA (G' and tanδ).
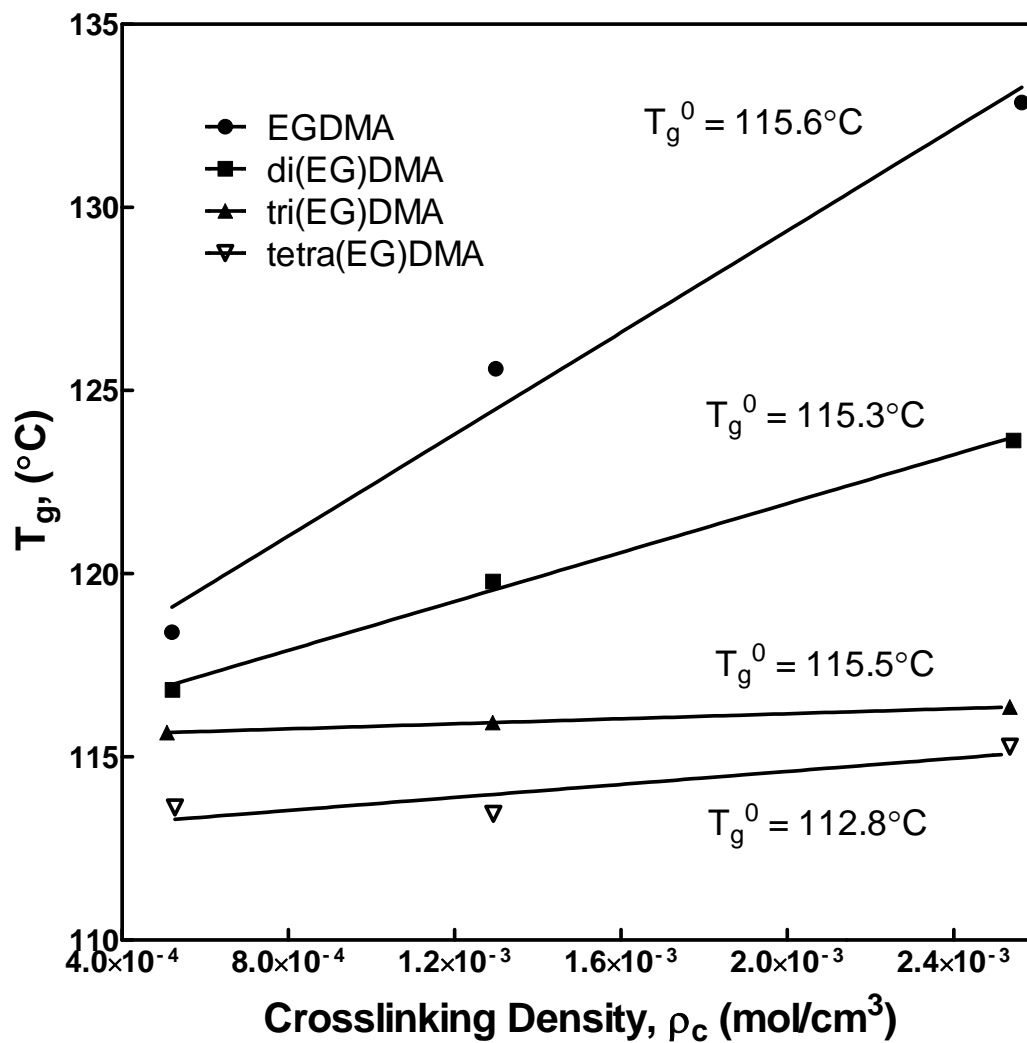
Figure 4.10: Values of T_g determined for PMMA crosslinked with multi(EG)DMAs by DSC with linear regressions and y-intercepts shown plotted against theoretical crosslinking densities determined from weight-averaged reactivity ratio calculations.
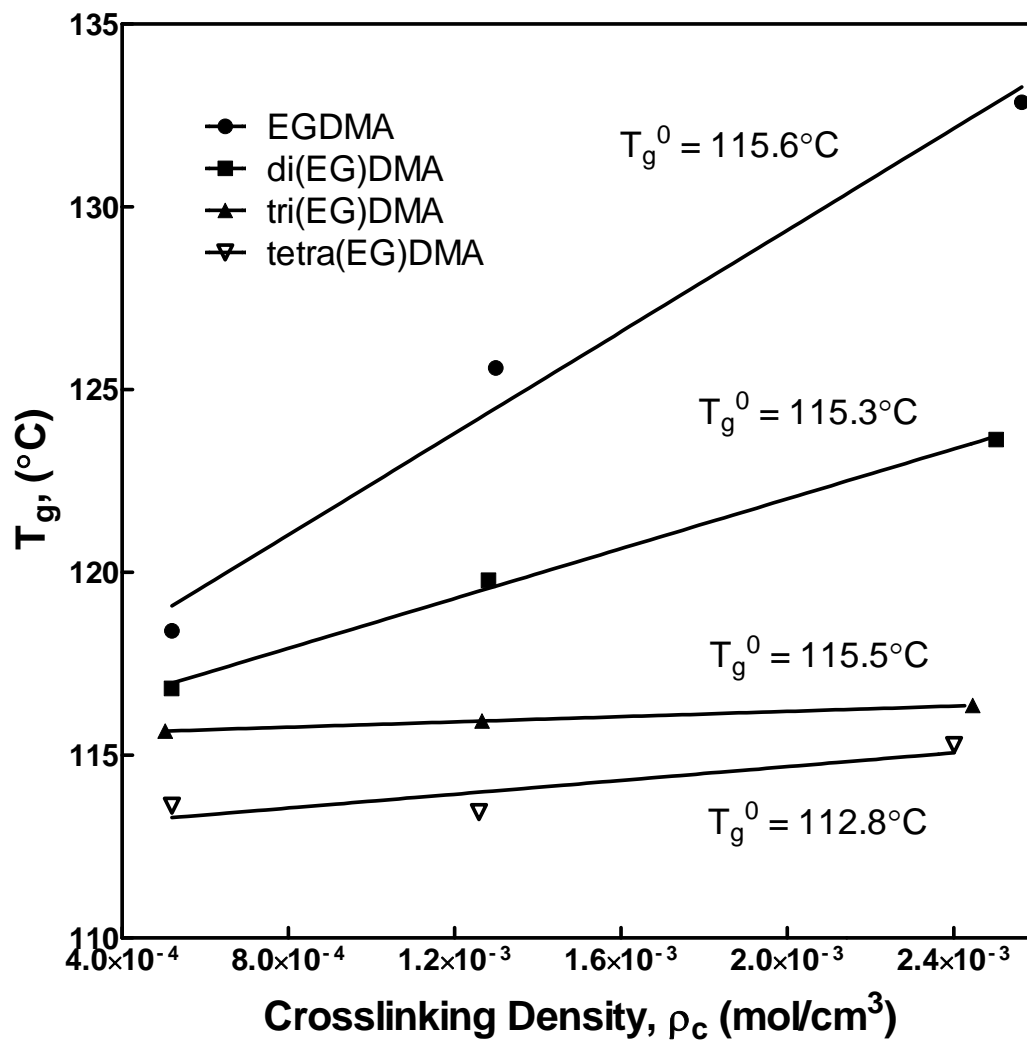
Figure 4.11: Values of T_g determined for PMMA crosslinked with multi(EG)DMAs by DSC with linear regressions and y-intercepts shown plotted against adjusted theoretical crosslinking densities determined from weight-averaged reactivity ratio calculations.
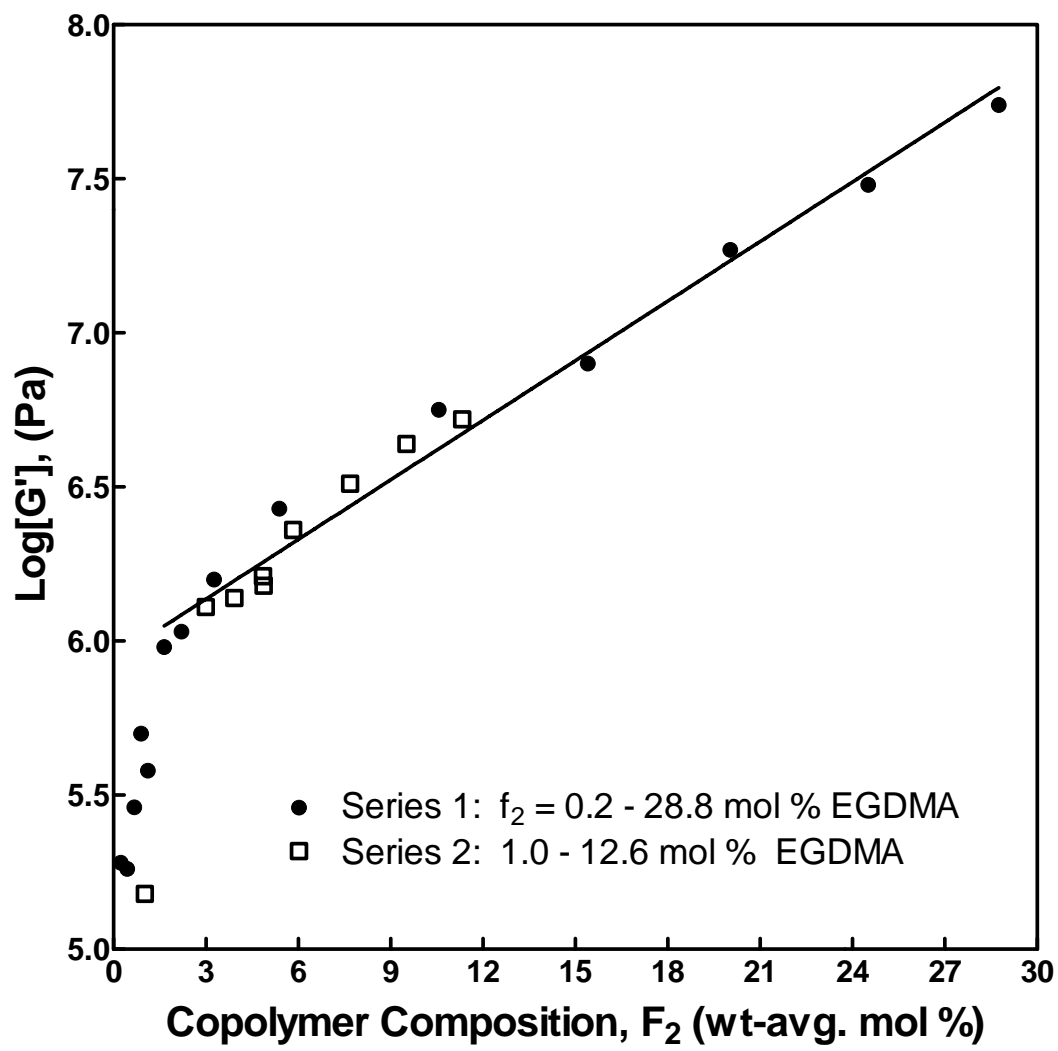
Figure 4.12: Values of the rubbery plateau shear storage modulus determined by DMA for PMMA crosslinked with EGDMA with varying theoretical copolymer crosslinker compositions (F_2) for 2 series of synthesized polymers.
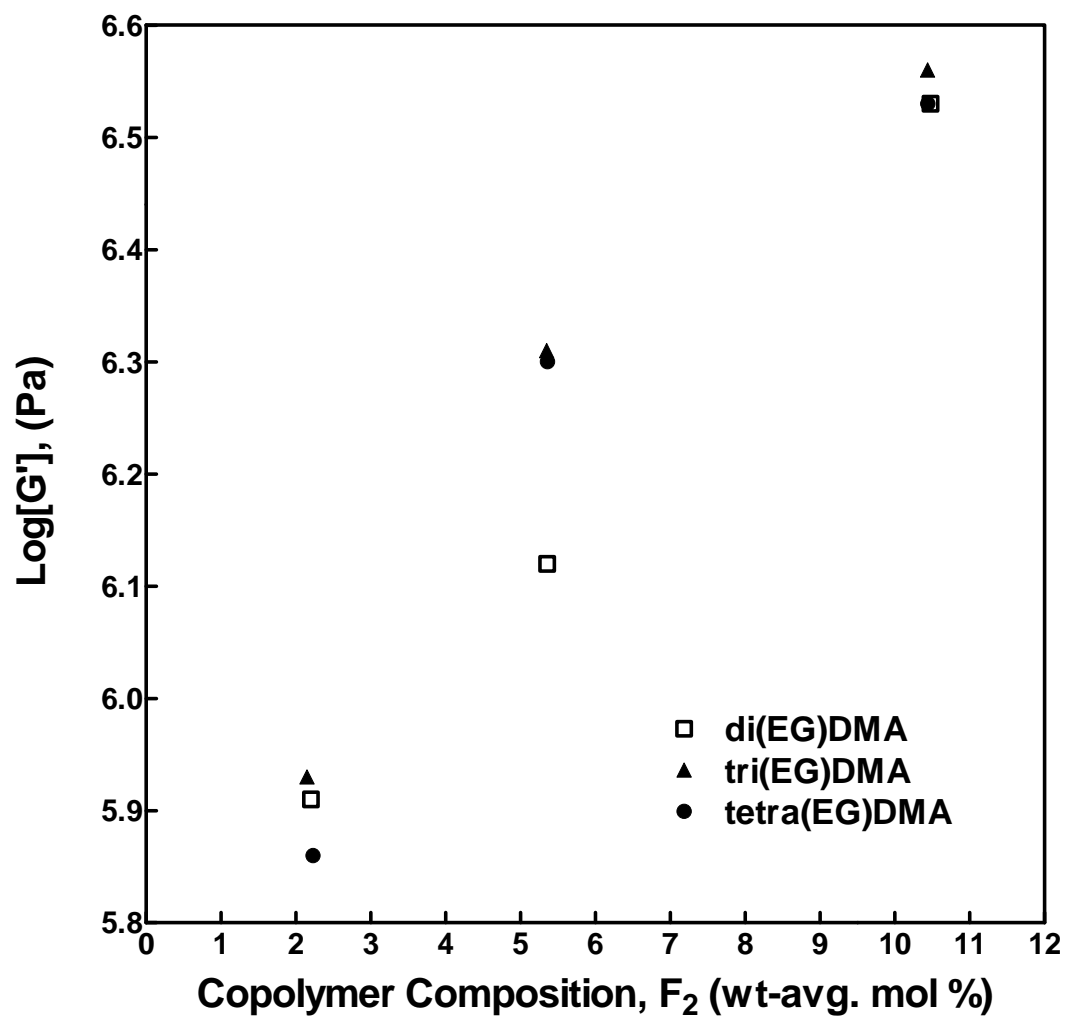
Figure 4.13: Values of G′ determined by DMA for PMMA with multi(EG)DMAs with varying theoretical copolymer crosslinker compositions (F_2).
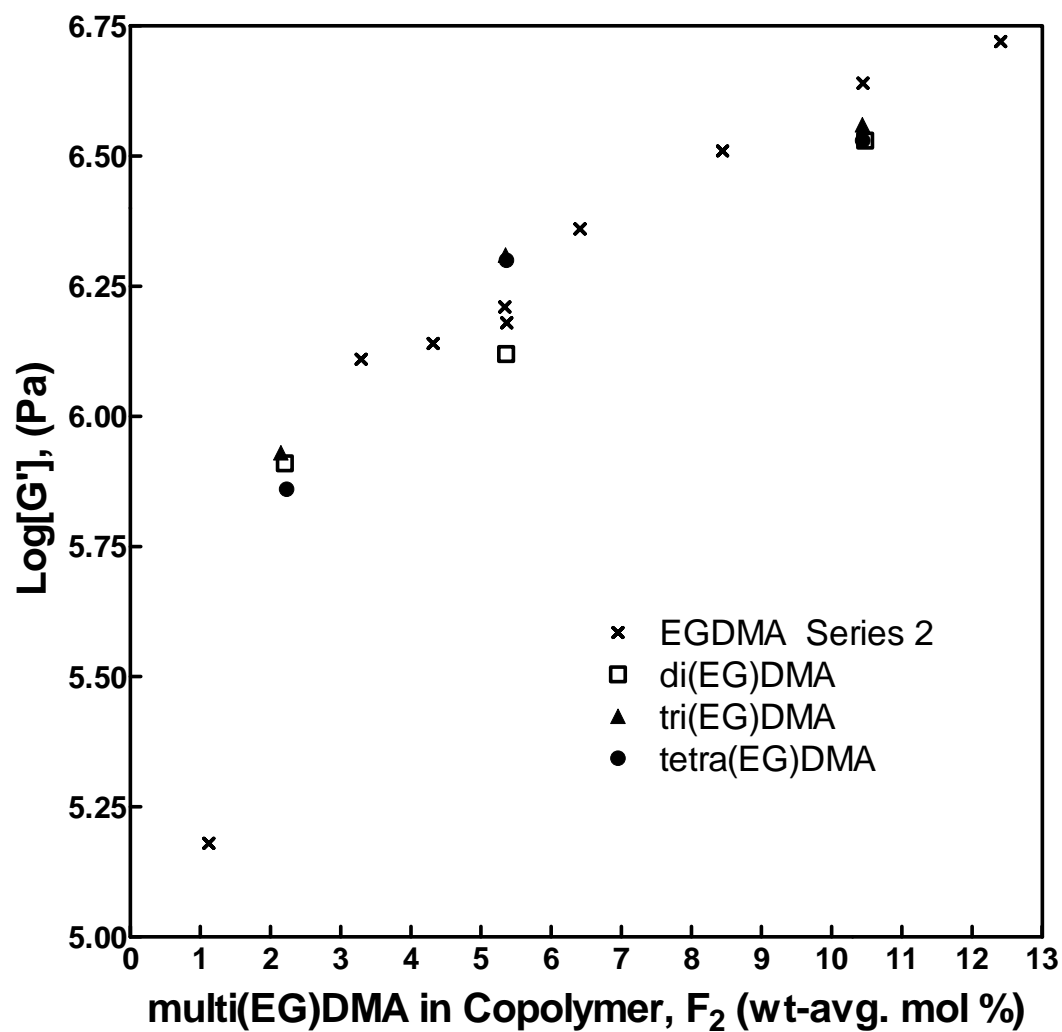
Figure 4.14: Values of G' determined by DMA for PMMA with multi(EG)DMAs with varying theoretical copolymer crosslinker compositions (F_2) compared with EGDMA Series 2.
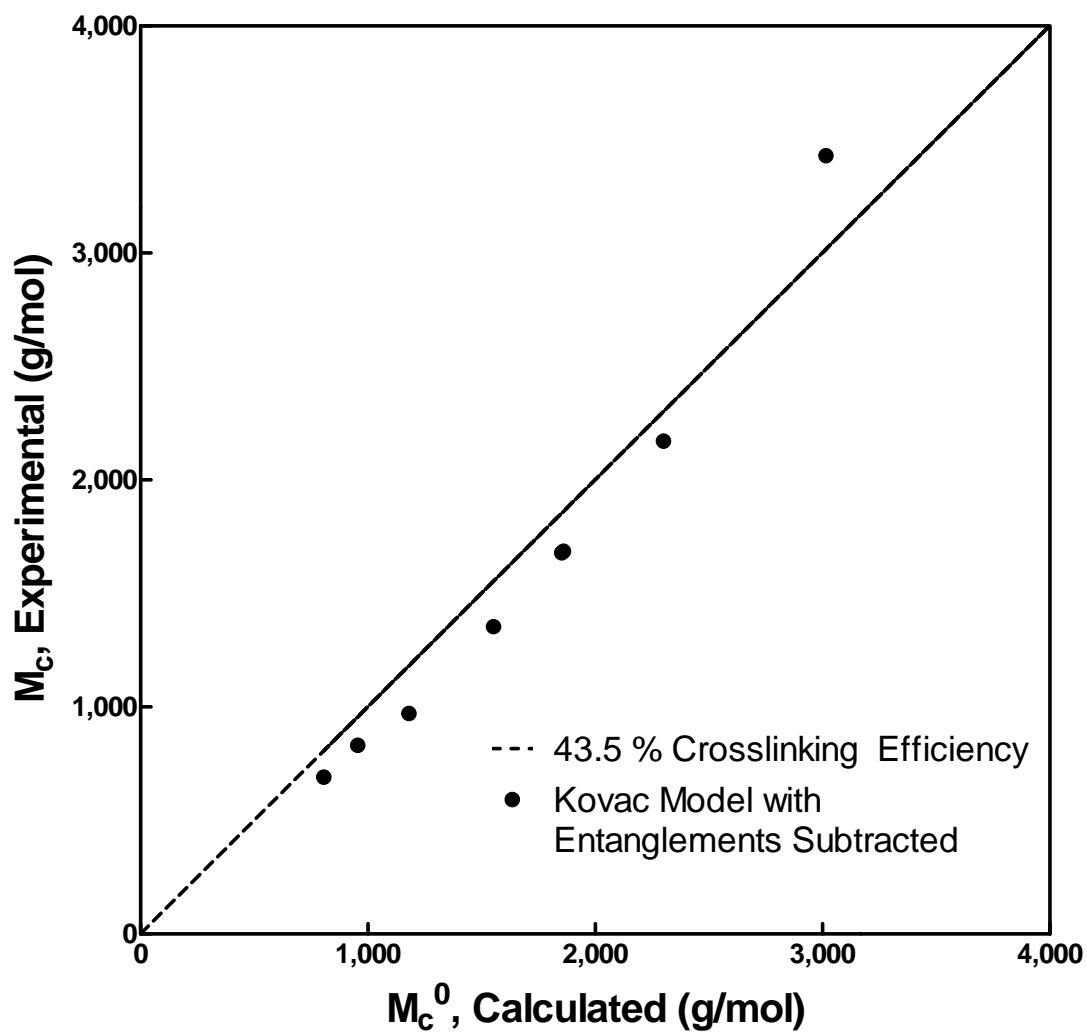
Figure 4.15: Comparison of molecular weights between crosslinks (M_c) derived from Kovac model equilibrium swelling calculations versus monomer reactivity ratios at low conversions with a crosslinking efficiency of 43.5 % for PMMA crosslinked with EGDMA.
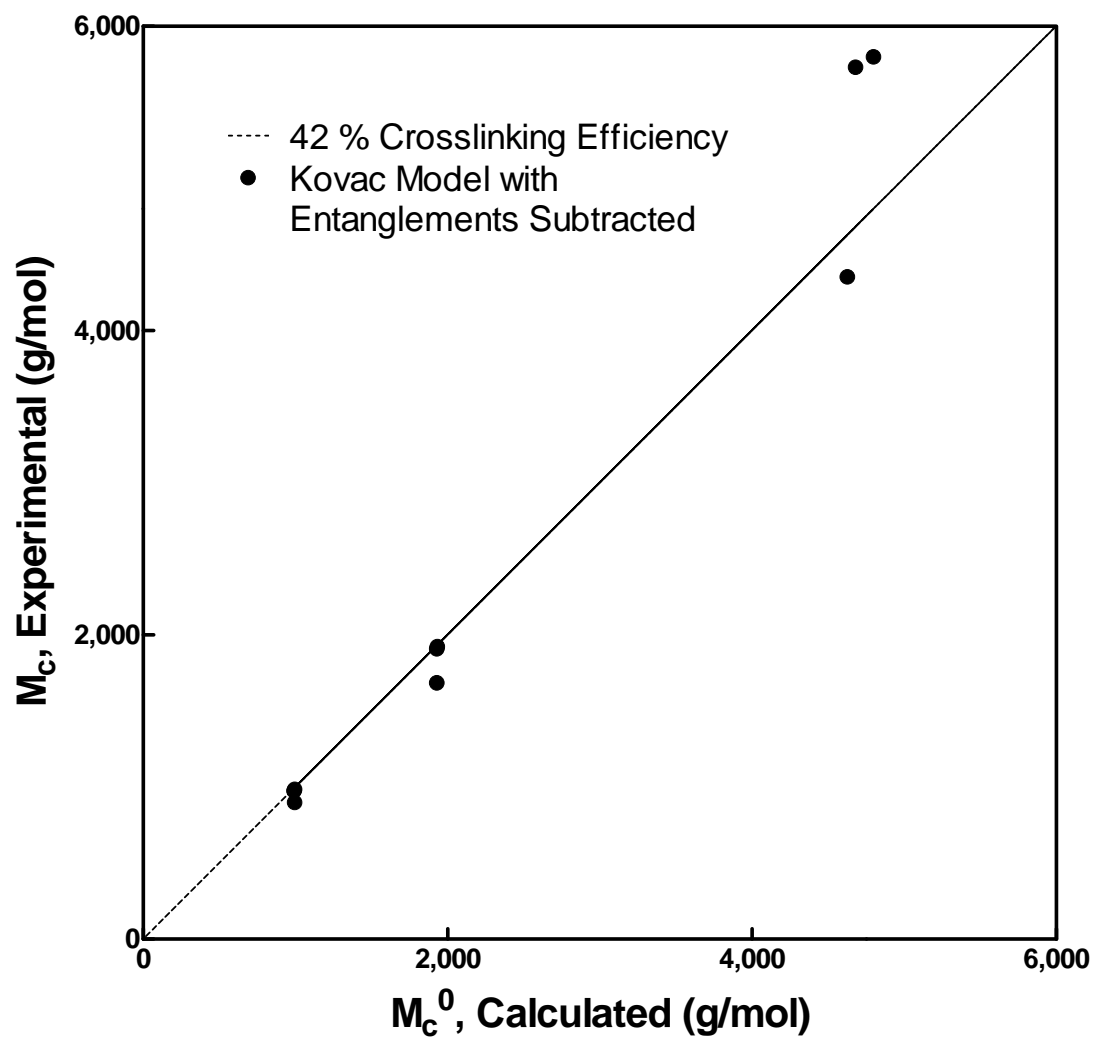
Figure 4.16: Comparison of molecular weights between crosslinks (M_c) derived from Kovac model equilibrium swelling calculations versus monomer reactivity ratios at low conversions with a crosslinking efficiency of 42 % for PMMA crosslinked with multi(EG)DMAs.
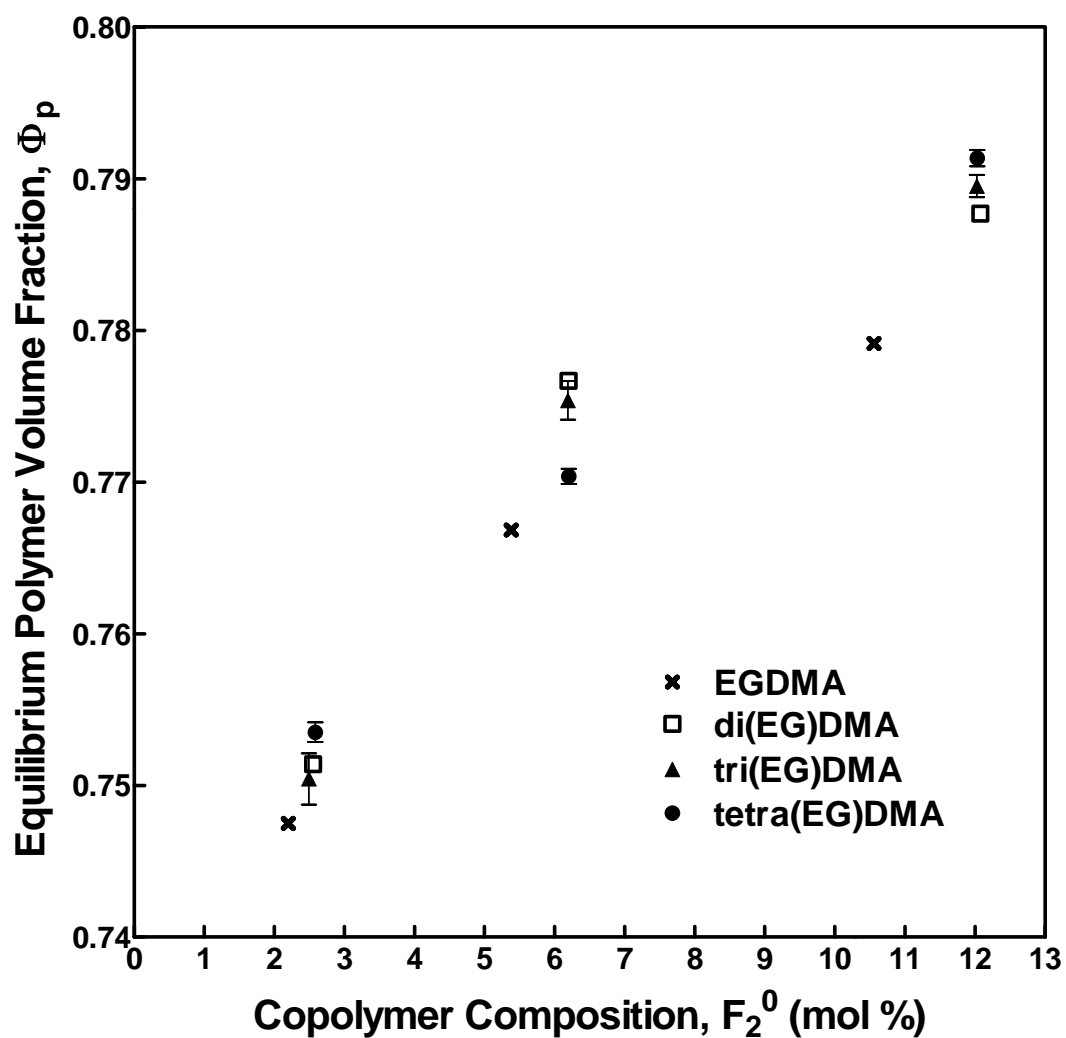
Figure 4.17: Equilibrium polymer volume fraction for PMMA crosslinked with multi(EG)DMAs swollen in Methanol at 25°C versus crosslinker copolymer composition (F_2) calculated for low conversions from reactivity ratios.
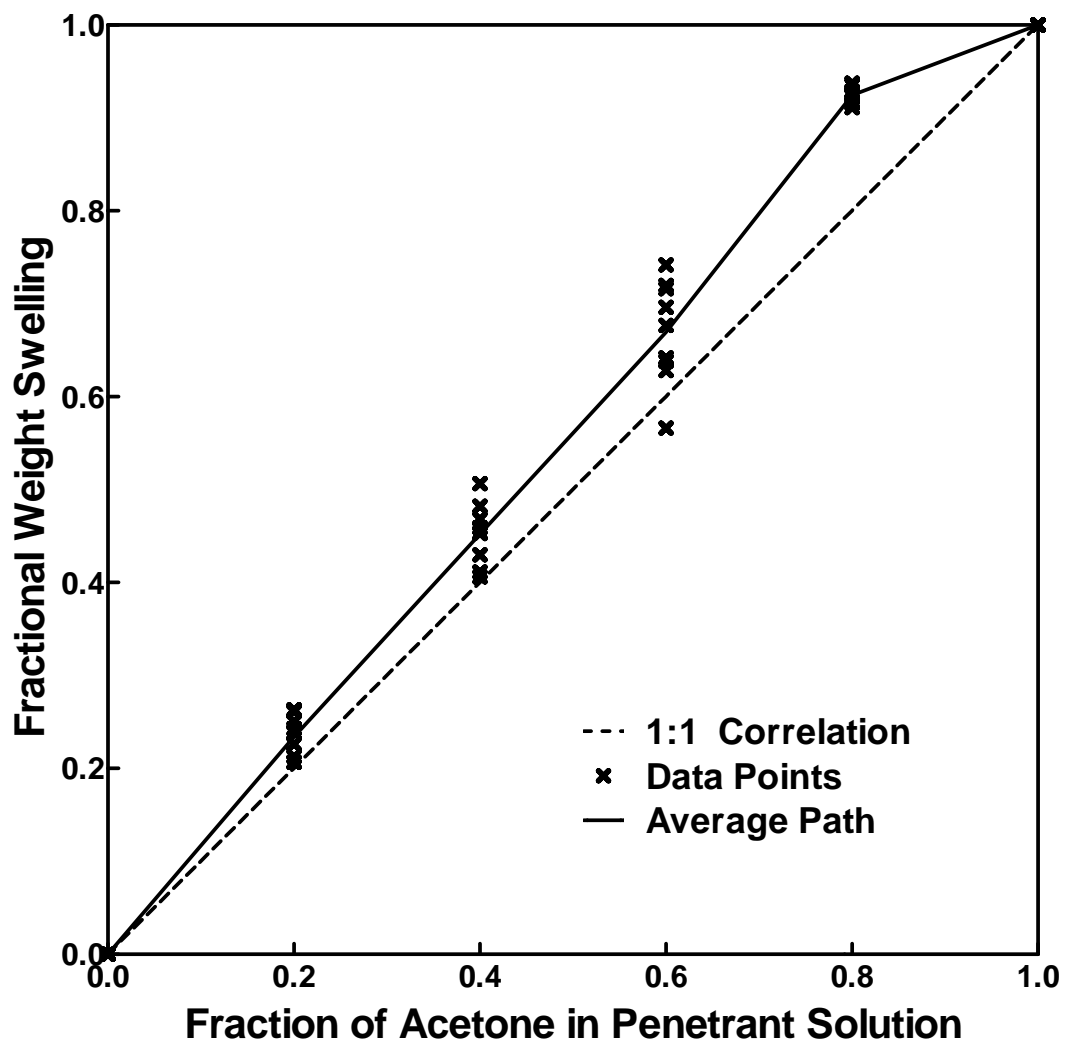
Figure 4.18: Fractional equilibrium swelling increase of PMMA crosslinked with multi(EG)DMAs in transition from pure methanol to pure acetone.
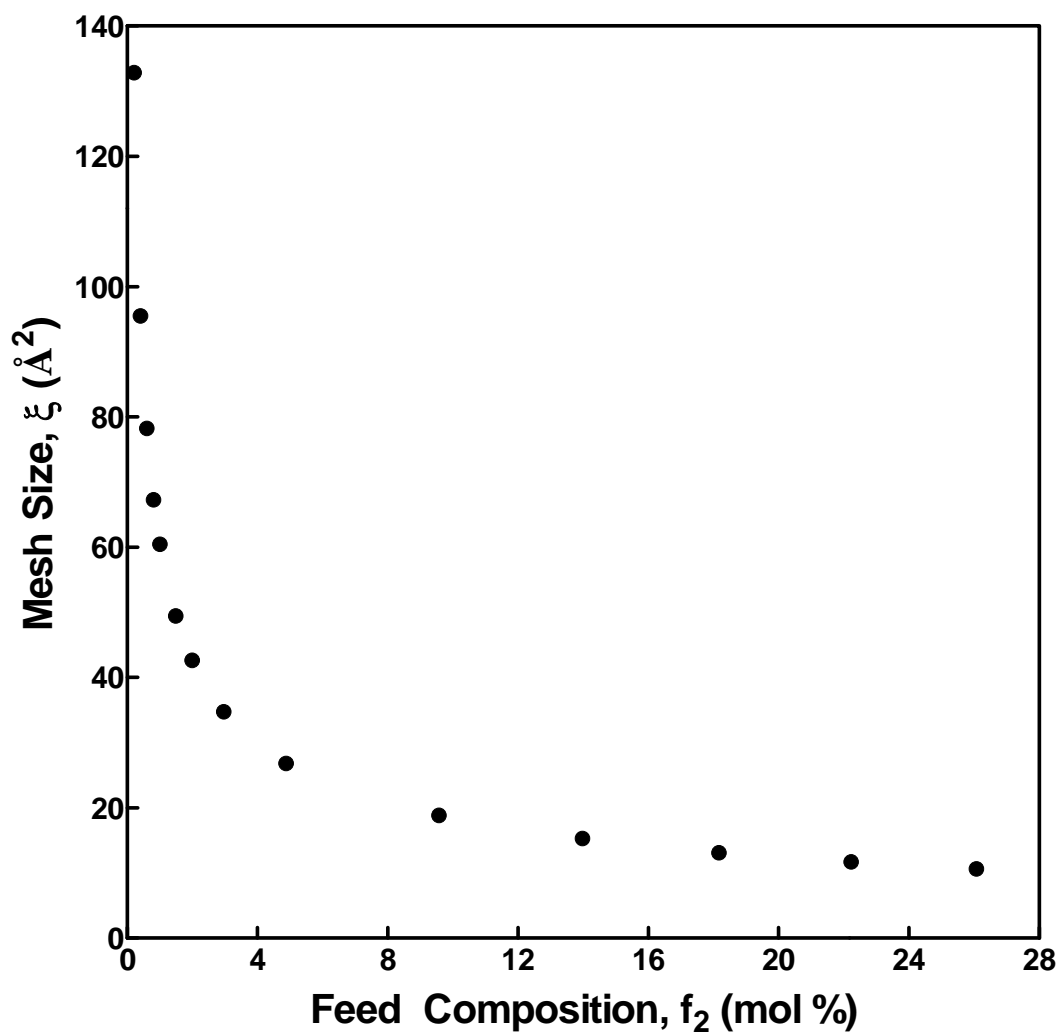
Figure 4.19: Change in polymer network mesh size (ξ) with increasing incorporation of crosslinks into the polymer structure for PMMA crosslinked with EGDMA and swollen in Methanol at 25°C.
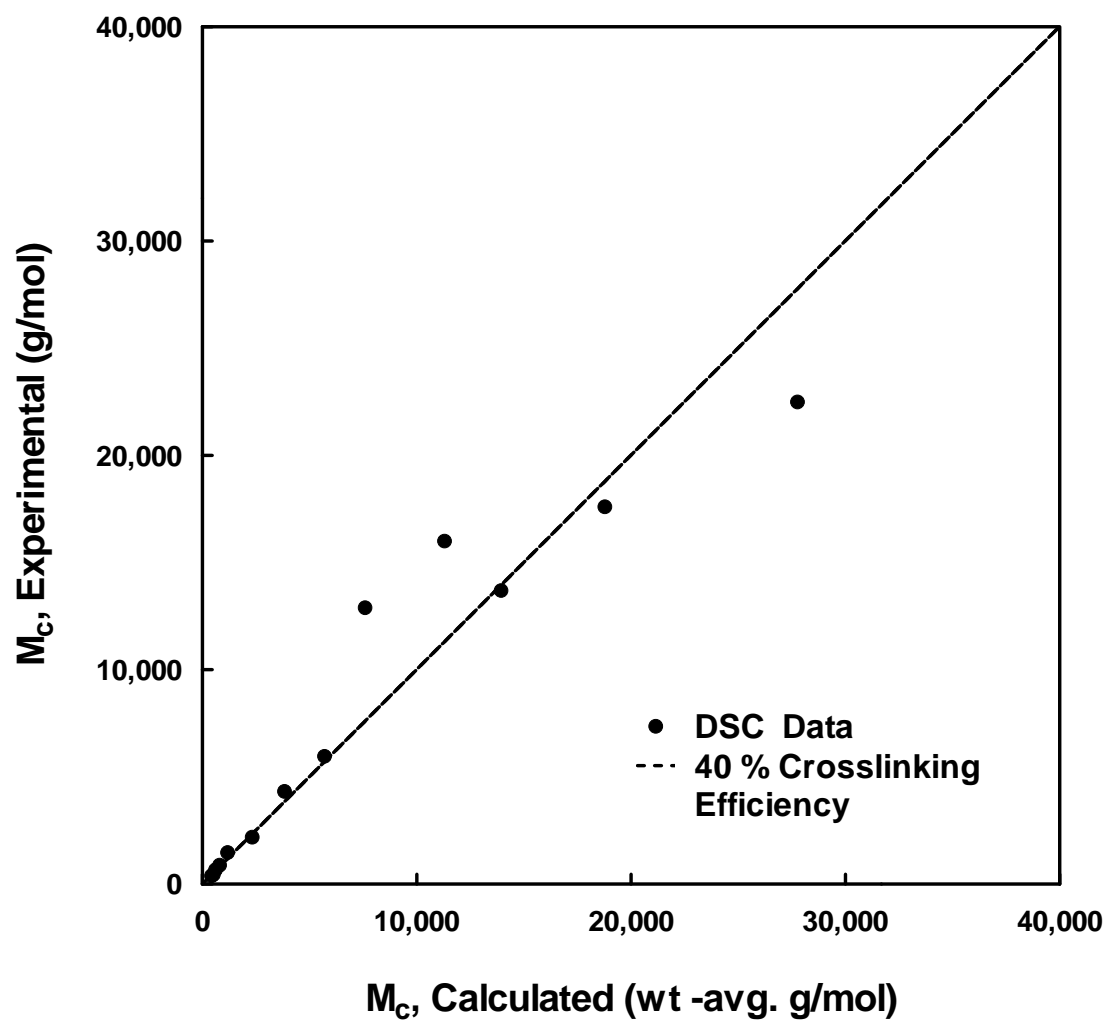
Figure 4.20: Comparison of molecular weights between crosslinks derived from DSC T_g measurements and weight-averaged reactivity ratio calculations with a crosslinking efficiency of 40 % for PMMA crosslinked with EGDMA.
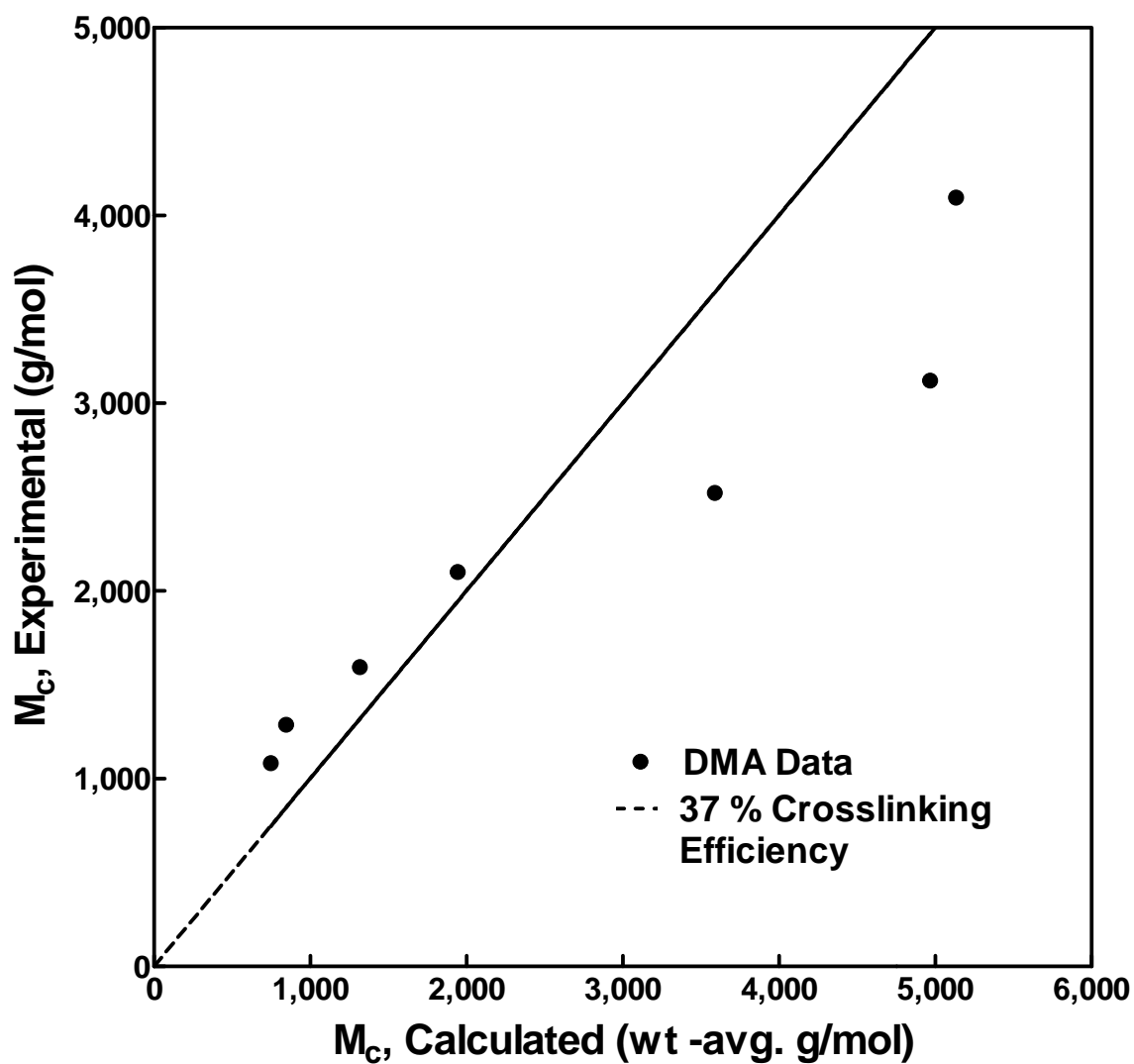
Figure 4.21: Comparison of molecular weights between crosslinks derived from DMA G′ measurements and weight-averaged reactivity ratio calculations with a crosslinking efficiency of 37 % for PMMA crosslinked with EGDMA.

Chapter 5: Penetrant Transport into Glassy Poly(Methyl Methacrylate)

INTRODUCTION

Despite decades of effort and over 1,000 publications on the subject, there remains no means by which to predict *a priori* the transport mechanism for a given polymer-penetrant system. In particular, the effects of basic system parameters on either the front velocity in Case II transport or the transitions between mechanisms are not well understood. In this investigation, the effects of the chosen polymer synthesis and preparation methods on the transport mechanism and kinetics of integral sorption of methanol into poly(methyl methacrylate) (PMMA) were evaluated. Additionally, the effects of temperature were studied and the behavior compared to previous investigations.

A major novel effort of this chapter was a detailed analysis of the effects of crosslinking on the mechanisms of penetrant transport and on the Case II front velocity. There has previously been a paucity of investigations in this regard. The most significant finding in terms of how polymer structural parameters affect the transport process has been a determination that the molecular weight of the polymer has no effect on the Case II front velocity beyond the critical molecular weight for entanglements [1]. This implies that number of chain ends and even the related degree of initial free volume have limited or no control over the Case II mechanics for identical thermal histories. However, the fact that the front velocity was dependent on molecular weight below the critical molecular weight for entanglements tells us that the presence of stable entanglements, or points of resistance to chain motion and network expansion, can directly influence the transport kinetics. Thus, adding additional points of resistance though chemical crosslinks should likewise alter the Case II front velocity.

Previously, Kwei and Zupko [2] noted that increasing the crosslinking density of a polymer while keeping other factors constant resulted in a change from Fickian dynamics at a single lower degree of crosslinking to Case II dynamics at a single higher degree of crosslinking. Additionally, Peppas and Urdahl [3] detailed the effects of crosslinking density on the presence of overshoots in integral sorption experiments; namely that the overshoots were diminished in magnitude and eventually disappeared completely as the degree of crosslinking was increased.

This investigation sought to add to these previous studies by directly examining first the effects of the degree of crosslinking on the Case II front velocity (to our knowledge this has never been investigated). Secondly, Kwei and Zupko's [2] observation that the transport mechanism can be changed simply by altering the crosslinking density will expounded upon (their investigation included just 2 degrees of crosslinking for 2 different penetrant-polymer systems). Finally, the effects of the type of crosslinking structure used will be examined through increasing the interchain bridge length.

MATERIALS AND METHODS

Sample Preparation

Homopolymers of methyl methacrylate (MMA) (Sigma-Aldrich, St. Louis, MO) were synthesized using an *iniferter*-mediated, thermally-initiated free radical polymerization. The crosslinking agents used were ethylene glycol dimethacrylate (EGDMA) (Sigma-Aldrich), diethylthene glycol dimethacrylate (di(EG)DMA) (Sigma-Aldrich), triethylene glycol dimethacrylate (tri(EG)DMA) (Sigma-Aldrich), and tetraethylene glycol dimethacrylate (tetra(EG)DMA) (Sigma-Aldrich). All crosslinkers were used as received, and MMA was passed through a pre-packed inhibitor removal column (Sigma-Aldrich) to remove hydroquinone prior to polymerization. All MMA monomer was used within two weeks of inhibitor removal. Either lauroyl peroxide (LP) (Fluka/Sigma-Aldrich) or 2,2-azobisisobutyronitrile (AIBN) (Sigma-Aldrich) was added as

a thermal initiator in the amount of 0.5 wt % of the total monomer content. Tetraethylthiuram disulfide (TED) (Sigma-Aldrich) was added as an *iniferter* compound in a 1:1 molar ratio with the thermal initiator.

The components were prepared in a cylindrical glass reaction vessel which was silanized prior to use with Siliclad^{TM} (Gelest, Morrisville, PA). The mixture was placed in an oxygen-free environment inside a sealed glove box and bubbled with nitrogen for 5 min to remove dissolved oxygen. The vessel was then sealed and placed in a water bath maintained at 60°C and allowed to polymerize for 48 hours (~2.3 initiator half-lives). Following synthesis, the polymer cylinders (approximately 25 mm in diameter) were sliced into discs with a nominal thickness of 1 mm by a Isomet^{TM} Low-Speed Saw with diamond wafering blades (Buehler®, Lake Bluff, IL), polished to remove surface defects by an abrasive slurry (Novus #2 Fine Scratch Remover, Savage, MN), and dried and/or annealed in a vacuum oven under varying conditions.

Gravimetric Studies

Discs of PMMA were suspended in methanol (Certified ACS Grade, Fisher Scientific, Pittsburgh, PA) in a glass jar on a raised aluminum mesh that occluded less than 3% of the lower disc surface. The glass jars were placed in a constant-temperature water bath and allowed to absorb penetrant. Weight measurements were taken at time intervals by removing a disc from the penetrant, drying the surface with a paper towel, and recording both the weight in air and the weight in a non-solvent (water) using an Ohaus Analytical Plus balance (Ohaus, Pine Brook, NJ). For each experiment, sets of three discs were immersed at the same time and all discs were measured at each time point. Additionally, thickness and diameter measurements were taken both prior to immersion in methanol and once the discs had reached equilibrium using a digital caliper (Brown and Sharpe, North Kingstown, RI).

Data Analysis

Data analysis of gravimetric integral sorption experiments was accomplished primarily by application of the power law model:

$$\frac{M_t}{M_\infty} = kt^n$$

(5.1)

where M_t is the mass of penetrant absorbed at a time t, M_∞ is the equilibrium mass of absorbed penetrant, k is a proportionality constant, and n is the power law exponent [4]. This equation is derived from the short time ($M_t/M_\infty < 0.60$) approximation of the rigorous solution to Fick's 2nd Law [4], where the binary diffusion coefficient is contained within k and n = 0.5. In Case II transport, the fractional mass uptake, M_t/M_∞, is directly proportional to time, and n is thus 1.0. Figure 5.1 shows the general behavior for Case I and Case II transport as predicted by the power law model. Any behavior that falls between these two extremes is generally assumed to involve a combination or superposition of the two mechanisms and is simply referred to as anomalous behavior, with power law exponent values of 0.5 < n < 1.0.

Additionally, glassy polymers undergoing integral sorption almost always go through an induction time, where the dominance of a particular transport mechanism has not yet begun. In Case II transport, this corresponds with the fact that the relaxational process must be initiated by a Fickian precursor, where this initial, passive diffusion into the free volume of the polymer is soon followed by the establishment of advancing fronts. To account for the presence of induction times in integral sorption studies, Equation 5.1 was modified by a time-shift to get:

$$\frac{M_t}{M_\infty} = k(t - \tau)^n$$

(5.2)

where τ is the induction time. Data covering the first 60% of sorption were fit to Equation 5.2 through a non-linear regression and values of k, τ, and n were calculated for all investigations.

Systems exhibiting Fickian or near-Fickian fractional mass uptake, M_t/M_∞, profiles were further analyzed to determine the binary diffusion coefficient, D_{12}, through Equation 5.3:

$$D_{12} = \frac{k^2 \pi^2}{16} \tag{5.3}$$

where k was determined from Equation 5.2 or a linear regression of the data plotted vs. $t^{1/2}$. In addition, Fickian profiles were normalized with respect to sample thickness by dividing time by the square of the initial disc thickness. The rationale for this transformation was that the characteristic diffusion time in Fickian transport varies with both the diffusion coefficient and the diffusion path length (Equation 2.2). In this way, fractional mass uptake curves for triplicate discs like those shown in Figure 5.2 could be collapsed onto a single curve, as shown in Figure 5.3.

Systems exhibiting Case II transport profiles were analyzed to determine the Case II front velocity by equation 5.4:

$$V_{II} = \left(\frac{dW}{dt}\right)\left(\frac{h_0}{W_0}\right) \tag{5.4}$$

where V_{II} is the Case II front velocity, W is the weight of the disc, dW/dt is the rate of mass uptake of the swelling disc, h_0 is the initial disc thickness, and W_0 is the initial weight of the disc. This expression is valid for Case II transport in the limit where one-dimensional planar transport into the disc can be assumed. Since Case II transport involves a steady-state front propagation into a dry polymer core, the initial thickness, initial polymer mass, and rate of mass uptake are all linked.

Finally, the initial and final disc volumes and polymer and penetrant volume fractions were calculated by Archimedes' principle (Equation 4.20); the molecular weight between crosslinks, M_c, and polymer mesh size, ξ, were determined as discussed in Chapter 4; and the tendency of the sorbing polymer to "overshoot" its equilibrium

value, having absorbed more penetrant than is thermodynamically ideal and subsequently expelling fluid until equilibrium is reached, was recorded.

RESULTS AND DISCUSSION

Preliminary Investigations

Preliminary investigations for this thesis involved elucidating the effects of polymerization and preparation procedures on the transport process. For these studies, discs of PMMA were synthesized and dried/annealed at 10°C below the T_g for 24 hours to remove any moisture and residual stresses induced during polymerization [5]. In this manner, approximately 0.25 wt % of moisture was removed from the discs prior to immersion in methanol. Essentially no unreacted monomer was removed from the PMMA discs at this temperature over this very short timescale, and between 2.0 and 2.5 wt % of unreacted monomer remained in the polymer discs. Also due to the short exposure times, the distribution of this unreacted monomer in the discs will only have been disturbed very near the surface of the discs, which had the ultimate effect of increasing induction times and transient behavior during the very early stages of transport through the thin, drier polymer skin. Additionally, unless otherwise stated, all polymer discs were synthesized with 2.5 mol % of EGDMA in the reaction feed (which corresponds to a crosslinker functionality feed concentration, f_2, of 4.88 mol %) and were immersed in methanol at 30°C.

Figure 5.4 shows the effect that initiator choice had on the ultimate transport process. There was no appreciable difference between polymers synthesized with LP or AIBN. A reaction temperature of 60°C was chosen to optimize the activity of the *iniferter* molecule, TED. At 60°C, AIBN and LP were the only two readily available thermal initiators with experimentally relevant half-lives (21.5 hours and 20.9 hours, respectively [6]). With no ultimate difference in transport behavior, LP was chosen as the thermal initiator for all additional polymerizations of PMMA, as AIBN evolves

87

nitrogen gas during the reaction and can lead to the formation of small bubbles in the polymer.

With the initiator chosen, the next parameter investigated was the amount of initiator included in the polymerization feed. Thus, the amount of LP added was varied from 0.1 – 0.5 wt % of the total monomer content, and the results for sorption in methanol are presented in Figures 5.5 and 5.6 for 30°C and in Figure 5.7 for 20°C. As the amount of LP is increased, the concentration of growing polymer chains increased and the resulting average chain molecular weight decreased. However, it is known that molecular weight has no effect on either Fickian [7] or Case II [1] transport dynamics above the critical molecular weight for entanglements (approximately 4,700 g/mol in this investigation). In Figures 5.6 - 5.7, there was no change in transport behavior going from 0.5 wt % to 0.4 wt %. However, with 0.25 wt % and 0.1 wt %, the transport process became more rapid and displayed a shorter induction period. These effects in this instance were attributed to a greater amount of unreacted monomer remaining in the polymer. Below a certain ratio of initiator to monomer, there was not a sufficient number of growing polymer chains to reach the highest monomer conversion possible over the time-span of polymerization (48 hours). An initiator concentration of 0.5 wt % was thus chosen for all subsequent polymerizations.

Another parameter investigated was the polymer disc diameter. Figure 5.8 and 5.9 present results from PMMA discs with 12.5, 16.25, 20.5, and 24.5 mm diameters. As the disc diameter was decreased, while maintaining a constant nominal thickness of 1 mm, the disc moved away from one-dimensional planar diffusion and towards one-dimensional cylindrical diffusion. Fickian cylindrical diffusion gives a value of n = 0.45, as opposed to n = 0.50 for planar diffusion, and this value passes through a minimum of approximately n = 0.43 at an aspect ratio of 1 [8]. It was not surprising then that as the diameter of the discs was decreased, lower values of n were seen. A nominal disc diameter of 24.5 mm was chosen as the standard for subsequent investigations in this thesis.

Drying and Annealing

In order to remove the unreacted monomer from the PMMA samples, discs were first dried at 10°C below their T_g in a vacuum oven for an extended period of time until the weight stabilized. This resulted in a pseudo-Fickian desorption profile and required 6 months to complete the drying process. The greatest change in polymer disc weight, and amount of monomer removed, occurred in the first two weeks. Figure 5.10 shows the effect that drying had on the sorption kinetics of methanol at 30°C. Within the first 24 hours there was an initial loss of ~0.25 wt % of polymer mass which was attributed to removal of moisture from the PMMA discs. PMMA is highly moisture absorptive due to its carbonyl groups and can absorb up to 2 wt % in moisture [9], though this will be reduced with increased molecular weight and crosslinking. Additionally, the polymers synthesized in this investigation were primarily stored in a standard desiccator loaded with Drierite moisture absorbent (W.A. Hammond Drierite Co., Xenia, OH), and as such would be expected to retain only a small percentage of water.

Furthermore, since water is a much smaller compound than methyl methacrylate monomer (MMA), it will desorb at a much faster rate than MMA. From that point on, weight loss was significantly slower and followed pseudo-Fickian kinetics, with a power-law fitted n value of 0.28. During desorption of MMA, the outer region of the polymer discs will be dried to a much greater extent than the interior of the discs early on in the process. This results in the creation of a drier skin that increasingly restricts diffusion of MMA from the interior region of the polymer, thereby leading to a power-law exponent less than 0.5.

Table 5.1 summarizes the power-law model results for the drying curves in Figure 5.10. As more MMA was removed from the polymer discs, the behavior began to shift from Fickian (n = 0.5) to non-Fickian (n = 0.71), or anomalous, transport kinetics. In addition, the diffusion coefficient, as determined by the kinetic parameter k, decreased and the induction time necessary to establish the transport profiles increased with continued drying. After 4 months of drying time, uncrosslinked PMMA displayed purely

Case II transport kinetics (shown in Figure 5.11). Thus, the polymers did not have to be completely dry to show Case II behavior, as drying was completed in 6 months.

Initially, sub-T_g drying was desired so as to not induce major structural rearrangements in the polymer and instead slowly anneal away any residual stresses from shrinkage during polymerization (MMA experiences a shrinkage of 20.7 vol % upon polymerization to PMMA [10]). However, given the incredibly long time-scales for drying and the fact that nearly all polymers tested were substantially crosslinked, super-T_g drying was also tested. Figure 5.12 shows the effects that super-T_g drying had on the transport kinetics of crosslinked PMMA discs in methanol at 30°C. The Case II front velocity, V_{II}, was decreased as drying continues from 7 to 28 days. After 4 weeks, the discs were completely dry and no change was noticed in the transport dynamics. It cannot readily be seen in Figure 5.12, but Figure 5.13 displays the Fickian mechanism seen once again with no drying of the polymer discs.

As a result, all discs used in subsequent studies in this investigation were dried above their T_g for 4 weeks. Additionally, since cooling below the T_g after drying results in a non-equilibrium state, the polymer discs were annealed for 2 weeks after drying. However, this annealing process, aside from one outlier, was found to have no appreciable effect on the transport mechanism or V_{II}, as shown in Figure 5.14.

Effect of Temperature

The effects of temperature on the penetrant transport process have been previously studied. However, it was desired to verify that the PMMA samples synthesized in this investigation behave in a comparable manner. Briefly, Thomas and Windle [11] noted several key effects that temperature had on methanol transport into PMMA samples. First, the rate of mass uptake displayed the typical Arrhenius dependence on temperature (Equation 5.5), though in this case the Case II front velocity, V_{II}, was the parameter of interest rather than the binary diffusion coefficient:

$$V_{II} = V_{II,0} \exp\left(-\frac{E_a}{RT}\right) \qquad (5.5)$$

where $V_{II,0}$ is the Case II front velocity at 0 K, E_a is the activation energy of Case II penetrant transport, T is the temperature in K, and R is the ideal gas constant (R = 1.987 cal/mol/K).

Secondly, as the temperature was increased further, deviations from Case II dynamics were observed. Basically, as the Case II front velocity continued to increase, at some point the diffusion of methanol through the swollen layer behind the Case II front could no longer maintain a constant methanol concentration at the front. As a result, the Case II front diminished in magnitude as it propagated through the polymer, and the velocity of the front decreased concomitantly. Finally, in the purely Case II regime, Thomas and Windle reported an activation energy for transport, E_a, of 25 kcal/mol and a Case II front velocity, V_{II}, of 1.86 nm/s at 24°C [11, 12].

Figure 5.15 displays the penetrant transport curves for methanol into PMMA from 25°C to 35°C. As can be seen from the power-law analysis of the data (Figure 5.16), all samples displayed Case II transport, except the data at 35°C, which showed a slight deviation from Case II dynamics. Additionally, as the temperature was increased, the front velocity increased and the magnitude of the induction time decreased. Figure 5.17 shows the values of V_{II} plotted versus 1/T with a linear regression to the transformed Arrhenius expression (Equation 5.6):

$$\ln(V_{II}) = \ln(V_{II,0}) - \left(\frac{E_a}{R}\right)\left(\frac{1}{T}\right) \qquad (5.6)$$

The value of the activation energy calculated from Figure 5.17 was 25.5 kcal/mol, which is in excellent agreement with previous research.

To compare the Case II front velocity, V_{II}, obtained in this investigation with those found by Thomas and Windle (1.86 nm/s at 24°C) [12], sorption studies on

uncrosslinked samples of PMMA were analyzed (Figure 5.11) and temperature-shifted to 24°C by the calculated activation energy for transport. The resulting value was 1.31 nm/s.

An additional consideration that was taken into account was the effect that the equilibrium penetrant volume fraction, ϕ_s, had on the front velocity. Figure 5.18 shows the dependence of ϕ_s on inverse temperature plotted according to the van't Hoff equation [13], and Figure 5.19 plots the Case II front velocity versus ϕ_s. The linear regression of Figure 5.18 gave a value of the enthalpy of solution of methanol in PMMA of 1.65 kcal/mol. This value was somewhat lower than those previously reported for methanol in PMMA (3.0 [11] and 2.8 [14] kcal/mol). It has also been reported that the velocity of the Case II front varies linearly with ϕ_s with a unit slope [11]. Thus, the value of ϕ_s should always be taken into account. If the data is then normalized by ϕ_s, the trend is essentially unchanged and the recalculated activation energy is 23.8 kcal/mol.

Finally, in an analogous manner, the dependence of the diffusion coefficient on temperature for polymer discs dried/annealed at 10°C below T_g for 24 hours was determined by an Arrhenius expression:

$$\ln(D_{12}) = \ln(D_0) - \left(\frac{E_a}{R}\right)\left(\frac{1}{T}\right) \tag{5.7}$$

where D_{12} is the binary diffusion coefficient, and D_0 is the binary diffusion coefficient at 0 K. In this instance, the polymer discs all displayed Fickian sorption kinetics due to the plasticizing effect of the 2.0 − 2.5 wt % of unreacted monomer that remained. Figure 5.20 plots these data versus the square root of time and shows linear regressions of the data (all regressions had an R^2 value of greater than 0.99). When these data were fit to Equation 5.7, the activation energy was calculated as 24.5 kcal/mol (shown in Figure 5.21).

This result implies that transport of methanol into glassy PMMA had the same activation energy whether the transport followed a Case II or Fickian regime for dry or

plasticized samples, respectively. This similarity was at first unexpected. Indeed, the fact that Case II transport exhibited an apparent activation energy higher than those typically associated with Fickian diffusion and comparable to those reported for creep of glassy PMMA (17-30 kcal/mol) has been used occasionally as evidence to support the notion that Case II transport is a creep-deformation controlled, viscoelastic response of the polymer to an osmotic pressure (or an osmotic suction) created by the penetrant activity differential [12]. The results reported here call this rationalization into question without compromising the broader qualitative interpretation. Additionally, values for the activation energy of methanol diffusion into rubbery PMMA have been measured in the infinite dilution limit as 19 kcal/mol [15]. Finally, some authors have even reported activation energies for case II transport into glassy PMMA as low as 20 kcal/mol [16]. It was reasonable to assume that many of the discrepancies present in the literature are a result of differing PMMA sample properties and varying thermal histories, and that the results of this investigation were accurate and not contradictory to previous data.

Effects of Crosslinking with EGDMA

One polymer property that has not been studied in sufficient detail as to its impact on penetrant transport in glassy polymers, is the crosslinking density (or the degree of crosslinking). In this investigation, two series of PMMA cylinders were synthesized with varying molar amounts of EGDMA included in the polymerization feed. Chapter 4 presents the results of those polymerizations in terms of the overall crosslinking efficiency, which was on average 40 %. Figure 5.22 presents the results of four degrees of copolymer crosslinking, F_2, from Series 2 swollen in methanol at 30°C. For these lower degrees of crosslinking (F_2 less than about 0.05), the methanol-PMMA system displayed purely Case II transport dynamics, as was expected.

However, at degrees of crosslinking greater than 0.05, deviations from Case II transport were seen (Figure 5.23). The early portions of these profiles have also been magnified in Figure 5.24. As the degree of crosslinking was increased past $F_2 = 0.05$,

several phenomena occurred. First, whereas prior to this point increasing the degree of crosslinking led to a reduction in the initial rate of penetrant transport, continuing to increase the degree of crosslinking led to faster initial rates of sorption. Second, the nature of the early transport mechanism also changed from Case II toward Fickian as F_2 continued to increase. Returning to Figure 5.23, the late-time behavior can also be analyzed. Once past the initial, anomalous portion of the integral sorption curve, the rate of transport leveled out, seemingly returning to Case II dynamics in the interim region, before rapidly accelerating in rate toward the end of the sorption process.

The behavior of the samples with low degrees of crosslinking ($F_2 < 0.05$) could easily be understood, as the resistance to chain relaxation was increased with increasing crosslinking and the rate of transport ought to have decreased. However, the behavior for higher degrees of crosslinking was far more complex. Figure 5.25 plots the equilibrium polymer volume fraction, ϕ_p, versus the shear storage modulus, G', and sheds light on this transition in behavior from low to high crosslinking densities. Typically, as methanol was imbibed into the polymer, at some critical concentration the glass transition temperature of the now plasticized PMMA dropped below the experimental temperature. This resulted in an end-state that was a rubbery, methanol-swollen PMMA disc.

When the degree of crosslinking was increased, the amount of penetrant that can ultimately be sorbed by the polymer sample was decreased. At some point, the polymer could no longer absorb sufficient penetrant to go through this glass/rubber transition. For methanol sorption in PMMA this point has been reported as a polymer volume fraction of approximately 0.80 [11]. Clearly, the deviations from Case II transport in this instance occurred only once the polymer-penetrant end-state was glassy rather than rubbery (the deviations occurred significantly in the last three points in Figure 5.25 and to a lesser degree in the point prior to the last three).

On first examination, this lent credence to the idea that a glassy polymer must have a rubbery end-state for Case II transport to occur. However, it has been shown by

several previous investigators [12, 17, 18] that Case II transport can occur regardless of whether or not the swollen polymer end-state is rubbery or glassy. What occurred in this case was that the increased relaxational resistances of the polymer forced the establishment of a very significant Fickian precursor. Thus, initial sorption into the polymer was due entirely to the establishment of the precursor. Once the edge of the polymer had absorbed enough penetrant to relax and expand further, a sorption front was established and propagated inward, leading to the steady-rate portion of the integral sorption curve. This continued until the significant Fickian precursors met one another in the center of the polymer and began to overlap. Once this occurred, the dry polymer core disappeared along with the associated stresses that were necessary for the sorption front to propagate. This led to a rapid increase in the sorption of penetrant by Fickian diffusion, as the polymer disc underwent structural rearrangement towards an effectively isotropically swollen end-state. Ultimately, the behavior seen here was essentially a temporal stacking of a two-stage and a super Case II transport mechanism.

Returning to Figure 5.25, the equilibrium polymer volume fraction, ϕ_p, varied linearly with G', meaning that ϕ_p was dependent on the total number of effective crosslinks (chemical crosslinks and trapped entanglements). In contrast, when the Case II front velocity, V_{II}, (normalized by ϕ_s) is plotted versus G' (Figure 5.26 for Series 1 polymers up to $F_2 = 0.057$), a change in slope after the point at which all entanglements have been entrapped (as discussed in Chapter 4) was observed. This indicated that the Case II front velocity depended not on the total number of effectively permanent crosslinks, but on the number of effective crosslinks in the glassy state. In the glassy state, all entanglements act as crosslink points, not just the ones that are permanently entrapped.

Thus, it was more appropriate to plot the normalized Case II front velocity versus the simple degree of copolymer crosslinking (F_2) (Figure 5.27). The normalized velocity decreased monotonically, though at increasingly diminished rates, as the crosslinking density was increased. A non-linear power-law model regression of this curve gave an

exponent, n, of 0.52. Thus, the Case II front velocity, V_{II}, varied linearly with the square root of the degree of copolymer crosslinking, F_2 (as shown in Figure 5.28). To the best of our knowledge this was a novel finding of this thesis. Figure 5.29 further confirmed this relationship for PMMA polymers crosslinked with EGDMA (Series 2) and swollen in methanol at 30°C.

Additionally, the effects of crosslinking with EGDMA were investigated in plasticized samples of PMMA (discs dried/annealed for 24 hours at 10°C below T_g). Figure 5.30 displays the complete profiles of these plasticized polymers swelling in methanol at 30°C. Shown also are the early time (first 60 % of swelling) power-law model exponents. In a similar manner to the fully dried polymers, the integral sorption curves for crosslinking greater than $F_2 = 0.05$ were initially Fickian, moved towards a constant rate uptake, and finally rapidly accelerated near the end of swelling. As was the case when examining the temperature dependence, plasticizing the polymer with unreacted monomer greatly reduced the relative time scales of the processes occurring and moved transport dynamics from Case II to Fickian at low degrees of crosslinking.

However, at higher degrees of crosslinking, analogous behavior to that of the fully dried polymer was seen in terms of the transport mechanism. This indicated that as the degree of crosslinking continued to increase, a limit was reached where the presence of a plasticizing species had a reduced effect on the relative increase of chain motion. In other words, at some point there was a sufficient quantity of crosslinks such that the crosslinks themselves became the limiting factor in chain motion. The presence of the unreacted monomer will increase the free volume present in the polymer and enhance the rate of diffusion of a penetrant into the polymer. However, with more crosslinking points per chain, a higher concentration of penetrant will be required to initiate a propagating sorption front. Thus, a more substantial Fickian precursor was formed, and once again there was an uptick in sorption rate once the precursors met in the center of the polymer and spatial rearrangement began.

96

Finally, an additional consequence of the two-stage/super Case II mechanism was that the polymers no longer overshot their final equilibrium penetrant concentration (as shown in Figure 5.30), which agreed in nature with the results of Peppas and Urdahl [3]. This demonstrated that the presence of the overshoots in these systems was initially a result of the anisotropic swelling nature of sorption in glassy polymers. In other words, the equilibrium degree of penetrant sorption was higher in the stressed polymer gel than in the final polymer end-state.

Effect of Crosslinker Interchain Bridge Length

In addition to studying the effects of degree of bulk crosslinking, the effect of increasing the crosslinking interchain bridge length was investigated. It was expected that increasing the bridge length with successively longer and more flexible oligo(ethylene glycol) segments would decrease the resistance to expansion of the polymer and favor a Fickian transport mechanism. This expectation is borne out in Figure 5.31 for PMMA crosslinked with EGDMA, di(EG)DMA, tri(EG)DMA, and tetra(EG)DMA and swollen in methanol at 30°C. For di(EG)DMA, the transport mechanism was still Case II, though at an elevated rate compared to that of EGDMA. Continuing to increase the crosslinker bridge length moved the transport mechanism towards Fickian transport. Additionally, when an analogous analysis was applied to di(EG)DMA as was previously done for EGDMA, the resulting trend was the same (Figure 5.32); namely that the normalized Case II front velocity depended on the square root of the degree of crosslinking.

When the same experiments were run at 25°C, Case II transport was seen in all cases for bridge lengths up to tetra(EG)DMA. Figure 5.33 plots the results of the Case II front velocities evolved vs. $F_2^{0.5}$. Once again, the velocities showed a linear dependence. However, as the bridge length increased, the overall rate of transport at all degrees of crosslinking increased. The slopes of the V_{II}/ϕ_s vs. $F_2^{0.5}$ curves are plotted in Figure 5.34 against the number of ethylene glycol linkages in the crosslinker bridge. There was a

97

general upward trend as expected from the data; however, the degree of error was too great to assign a specific nature to the trend. Additionally, attempts were made to determine if the effects of bridge length were related to the associated changes in the glass transition temperature. The idea was that at the same degree of crosslinking, the reduced resistance to relaxational motion from the increased bridge length might scale with the T_g or the distance from the T_g. However, no meaningful correlation could be ascertained between T_g and V_{II}.

CONCLUSIONS

Poly(methyl methacrylate) samples were synthesized, dried, annealed, and the integral sorption of methanol into PMMA discs was examined via gravimetric methods. The synthesis procedure employed allowed for precise control over the polymer network structure, and polymerization and sample preparation procedures were optimized so as not to influence the observed transport mechanisms or rates. The PMMA samples produced displayed similar transport behavior to previous investigations of methanol sorption into PMMA. The Case II front velocities calculated were comparable to those reported by Thomas and Windle [12], and the activation energy of Case II transport of methanol in PMMA was calculated as 25 kcal/mol, which agreed quantitatively with several previous investigations [1, 11].

One of the primary findings of this chapter was the degree to which the transport process can be manipulated and altered through simple crosslinking of the polymer. It was shown that polymer systems can be taken from Fickian transport to anomalous to Case II transport and then beyond that to a two-stage/super Case II mechanism simply by increasing the number of chemical crosslinks. Additionally, samples exhibiting Case II transport mechanisms were altered to give anomalous or Fickian mechanisms at the same degree of crosslinking simply by using a longer, more flexible crosslinking comonomer.

This chapter showed that control over the Case II front velocity was determined by the properties of the polymer in the glassy state. This was demonstrated clearly from data indicating that the front velocity was determined not by the number of permanent crosslinks (chemical crosslinks plus entrapped entanglements), but by the total number of entanglement points in the glassy state (including crosslinks, free entanglements, and entrapped entanglements). The fact that altering the crosslinking density while keeping the degree of crosslinking constant through increasing the crosslinker interchain bridge length, also supported the notion that the controlling factor was the resistance to chain expansion in the glassy state.

This glassy control of the dynamics has also been shown previously, as Thomas and Windle have reported that the appearance of Case II transport and its rate progression as the temperature was lowered followed the same trends and scaling whether the polymer end-state was glassy or rubbery [12]. The polymer end-state did, though, alter the transport phenomena observed at long times. When the polymer remained glassy at the equilibrium degree of sorption, the ability of the polymer to undergo major structural rearrangement from an anisotropically swelling dynamic gel to an isotropically swollen end-state was hindered and the long-time dynamics were anomalous.

Additionally, similarities between the underlying controlling processes for methanol sorption into both dry and plasticized PMMA were noted. The activation energy for transport was found to be the same regardless of whether the mechanism was Fickian or Case II. This indicated again that the primary resistance to sorption that must be overcome is the expansion of the glassy polymer chains. While the properties of the polymer will change with plasticization, the initial resistance of the polymer chains to expansion remains the same so long as each case is well below the T_g. Further similarities were noted with the transport behavior encountered at very high degrees of crosslinking.

Finally, this chapter showed that the ultimate scaling of the dynamics of Case II transport with network structure was straightforward; namely the Case II front velocity was proportional to the square root of the degree of crosslinking (the number of crosslinks per chain, or $V_{II} \propto F_2^{0.5}$). As a result of the interrelation of the degree of crosslinking, the molecular weight between crosslinks, and the polymer mesh size, this conclusion led directly to two analogous scalings: the Case II front velocity was proportional to the molecular weight between crosslinks to the -0.5 power ($V_{II} \propto M_c^{-0.5}$) and proportional to the polymer mesh size ($V_{II} \propto \xi$).

REFERENCES

1. Hassan, M.M. and C.J. Durning, *Effects of polymer molecular weight and temperature on Case II transport.* Journal of Polymer Science Part B-Polymer Physics, 1999. **37**(22): p. 3159-3171.
2. Kwei, T.K. and H.M. Zupko, *Diffusion in Glassy Polymers. I.* Journal of Polymer Science, Part A-2: Polymer Physics, 1969. **7**(5): p. 867-877.
3. Peppas, N.A. and K.G. Urdahl, *Anomalous Penetrant Transport in Glassy-Polymers .7. Overshoots in Cyclohexane Uptake in Cross-Linked Polystyrene.* Polymer Bulletin, 1986. **16**(2-3): p. 201-207.
4. Crank, J., *The Mathematics of Diffusion*. 2nd ed. 1975, New York: Oxford University Press. p. 47.
5. Yoshida, H. and Y. Kobayashi, *Effect of Tacticity on Relaxation Process with Sub-Tg Annealing in Poly(Methyl Methacrylate).* Polymer Journal, 1982. **14**(11): p. 925-926.
6. Brandrup, J., E.H. Immergut, and E.A. Grulke, eds. *Polymer Handbook*. 4th ed. 1999, John Wiley & Sons: New York.
7. Crank, J. and G.S. Park, *Diffusion in Polymers*. 1968, New York: Academic Press.
8. Ritger, P.L. and N.A. Peppas, *Transport of Penetrants in the Macromolecular Structure of Coals .4. Models for Analysis of Dynamic Penetrant Transport.* Fuel, 1987. **66**(6): p. 815-826.
9. Chen, J.K., S.W. Kuo, H.C. Kao, and F.C. Chang, *Thermal properties, specific interactions, and surface energies of PMMA terpolymers having high glass transition temperatures and low moisture absorptions.* Polymer, 2005. **46**(7): p. 2354-2364.
10. Rodriguez, F., C. Cohen, C.K. Ober, and L.A. Archer, *Principles of Polymer Systems*. 5th ed. 2003, New York: Taylor & Francis.
11. Thomas, N. and A.H. Windle, *Transport of Methanol in Poly(Methyl Methacrylate).* Polymer, 1978. **19**(3): p. 255-265.
12. Thomas, N.L. and A.H. Windle, *A Deformation Model for Case-II Diffusion.* Polymer, 1980. **21**(6): p. 613-619.
13. Nicolais, L., E. Drioli, H.B. Hopfenberg, and G. Caricati, *Diffusion-Controlled Penetration of Polymethyl Methacrylate Sheets by Monohydric Normal Alcohols.* Journal of Membrane Science, 1978. **3**(2-4): p. 231-245.
14. Hopfenberg, H.B., L. Nicolais, and E. Drioli, *Relaxation Controlled (Case Ii) Transport of Lower Alcohols in Poly(Methylmethacrylate).* Polymer, 1976. **17**(3): p. 195-198.
15. Arnould, D. and R.L. Laurence, *Size Effects on Solvent Diffusion in Polymers.* Industrial & Engineering Chemistry Research, 1992. **31**(1): p. 218-228.
16. Lee, S.B. and T.M. Fu, *Methanol Transport in Cross-Linked Poly(Methyl Methacrylate).* Polymer, 1995. **36**(20): p. 3975-3978.

17. Jacques, C.H.M. and H.B. Hopfenbenberg, *Vapor and Liquid Equilibria in Glassy Polyblends of Polystyrene and Poly(2,6-Dimethyl-1,4-Phenylene Oxide) .1.* Polymer Engineering and Science, 1974. **14**(6): p. 441-448.

18. Jacques, C.H.M., H.B. Hopfenberg, and V.T. Stannett, *Super Case II Transport of Organic Vapors in Glassy Polymers.* Abstracts of Papers of the American Chemical Society, 1974: p. 51-51.
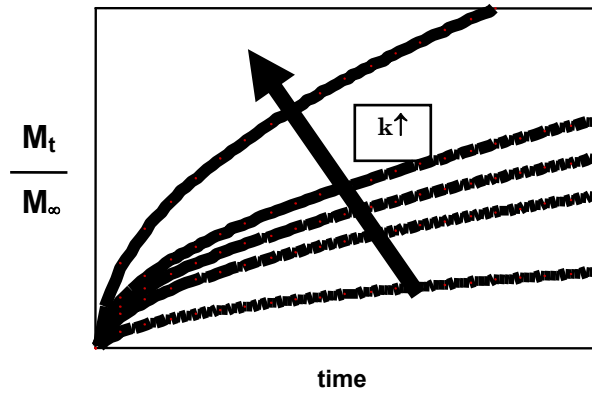
Table 5.1: Effect of annealing/drying time on power-law model coefficients for PMMA discs with 2.29 mol % crosslinking (EGDMA) and 0.5 wt % initiator annealed at 10°C below T_g and swollen in methanol at 30°C.

	n	k	τ (h/mm^2)
~1/2 day	0.53	0.234	0.43
~1 day	0.49	0.195	0.77
~2 days	0.57	0.166	0.67
~7 days	0.58	0.137	1.42
~13 days	0.71	0.107	1.38

Fickian vs. Case II: Swelling Kinetics

Power Law Model: $\dfrac{M_t}{M_\infty} = k\,t^n$

$\dfrac{M_t}{M_\infty}$

time

Fickian Diffusion

n = 0.5

$\dfrac{M_t}{M_\infty}$

time
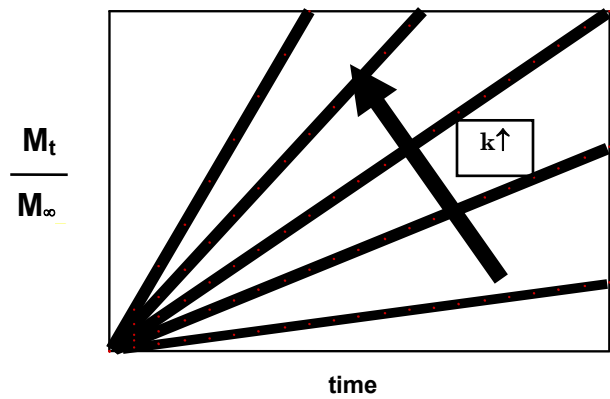
Case II Diffusion

n = 1.0

Figure 5.1: Comparison of Fickian and Case II penetrant uptake behavior according to the power law expression.

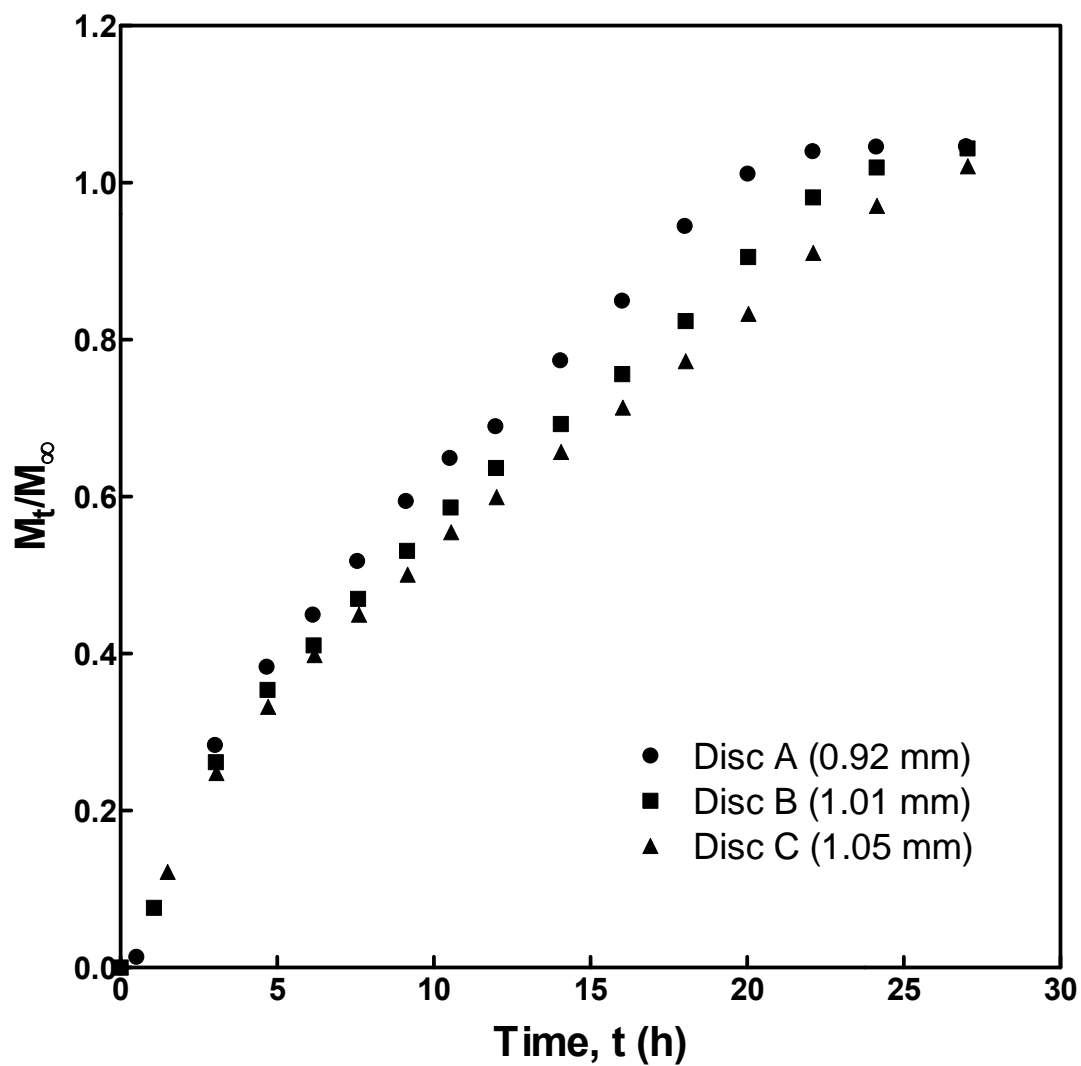Figure 5.2: Examples of experimental scatter due to slight variations in disc thickness for PMMA discs with 2.29 mol % crosslinking (EGDMA) and 0.5 wt % initiator annealed for 24 hours and swollen in methanol at 30°C.
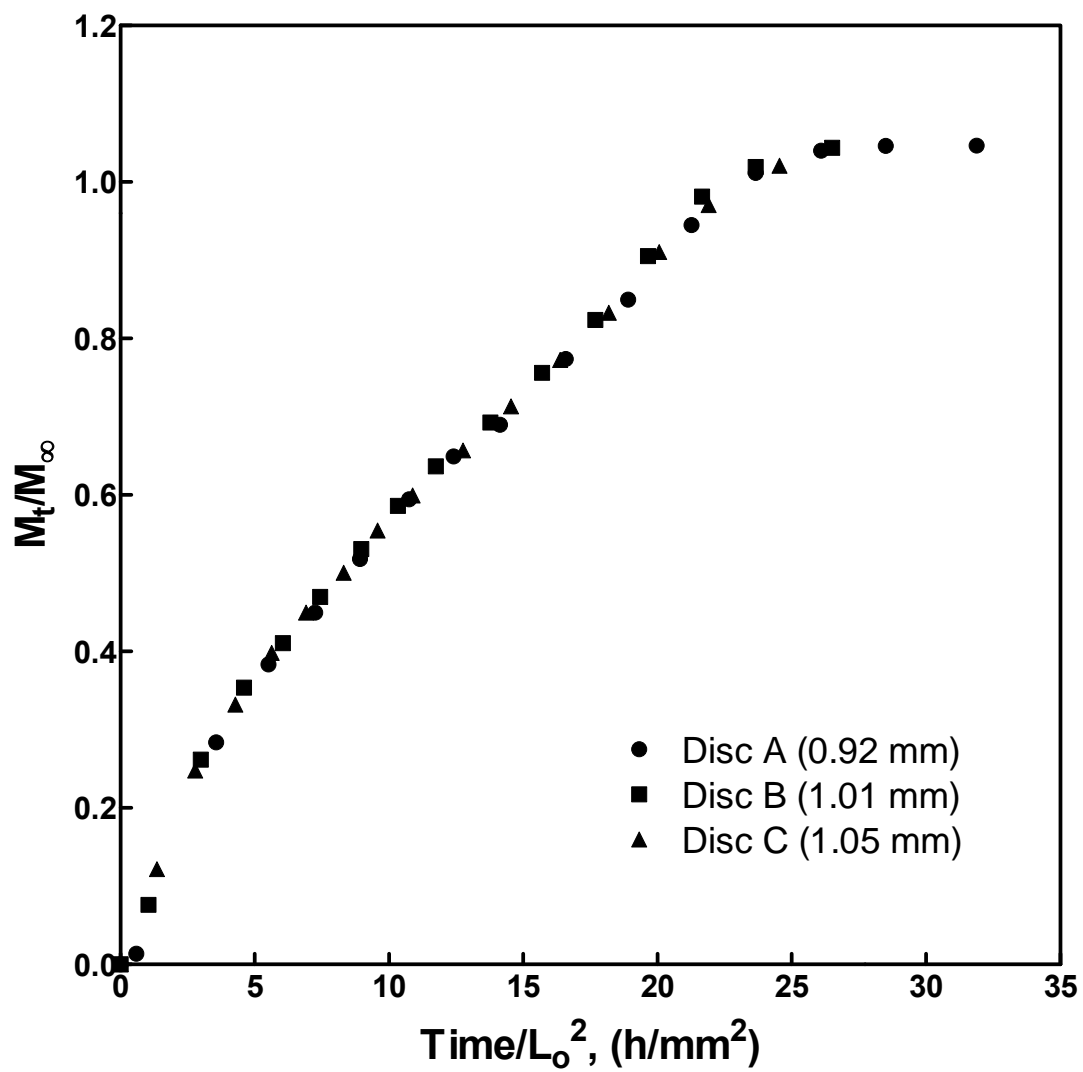
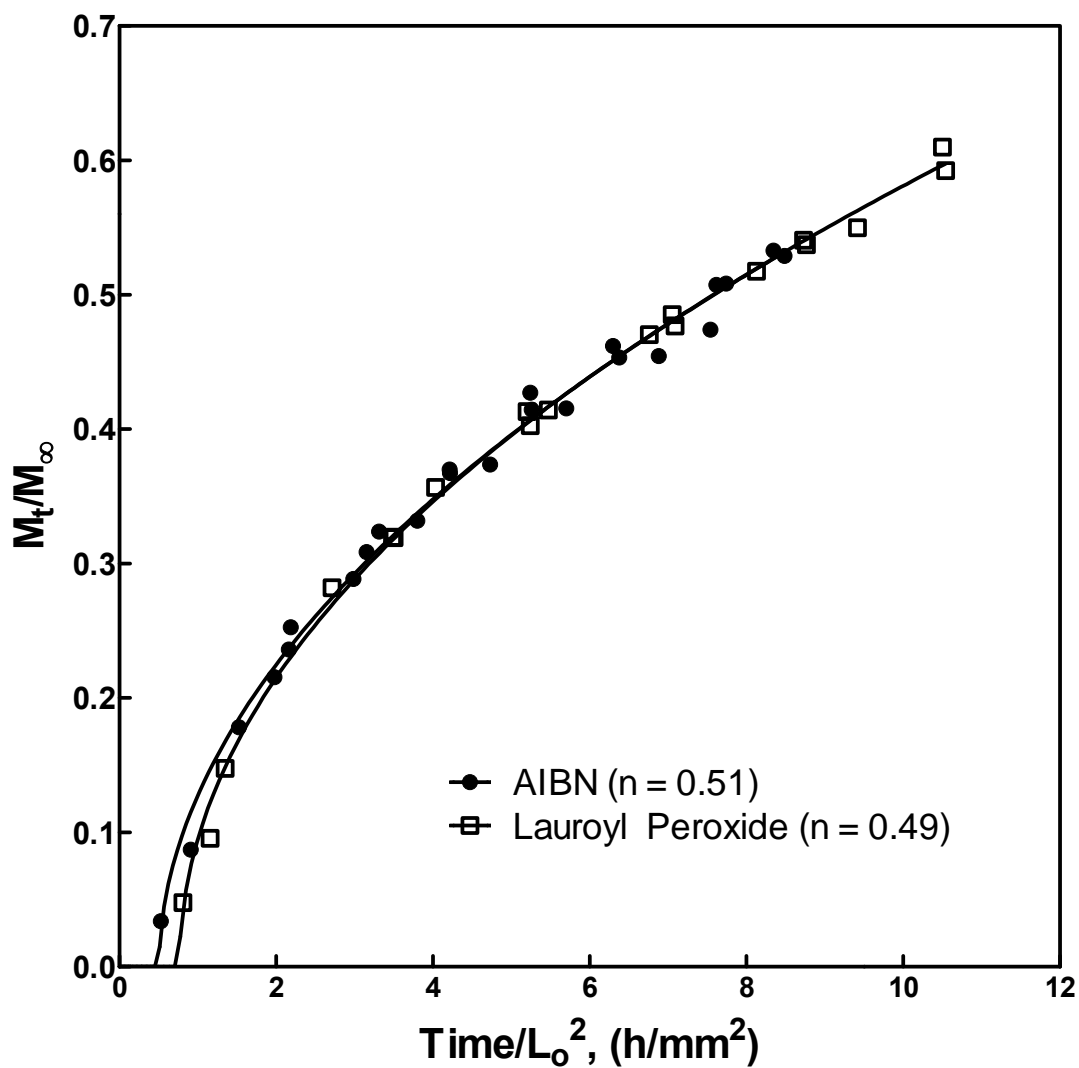Figure 5.3: Data from Figure 5.2 normalized by the square of the initial disc thickness.

Figure 5.4: Power-law model analysis of the effect of initiator choice on the integral sorption dynamics of PMMA discs with 2.29 mol % crosslinking (EGDMA) swelling in methanol at 30°C.
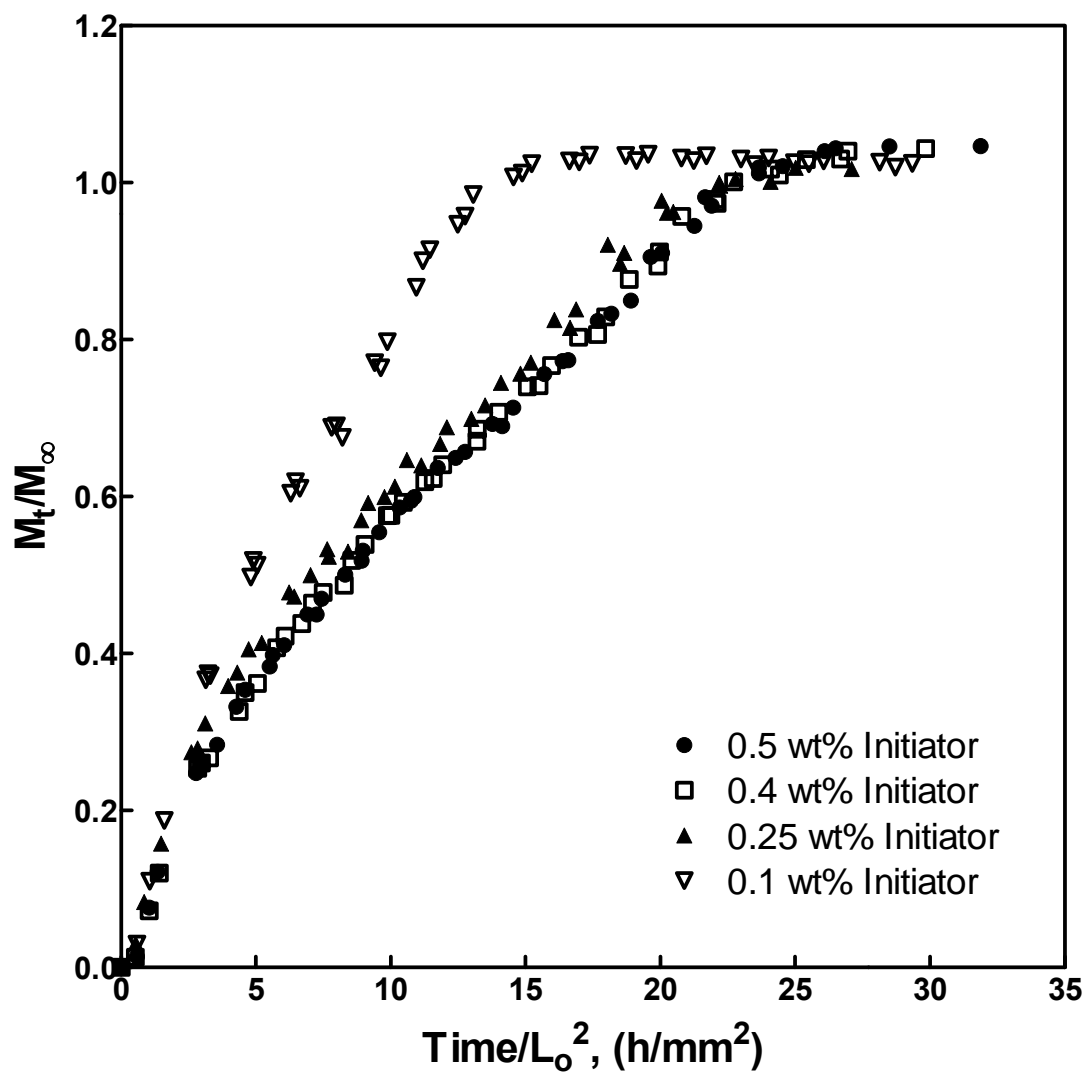
Figure 5.5: The effect of initiator concentration on the integral sorption dynamics of PMMA discs with 2.29 mol % crosslinking (EGDMA) swelling in methanol at 30°C.

Figure 5.6: Power-law model analysis of the effect of initiator concentration on the integral sorption dynamics of PMMA discs with 2.29 mol % crosslinking (EGDMA) swelling in methanol at 30°C.
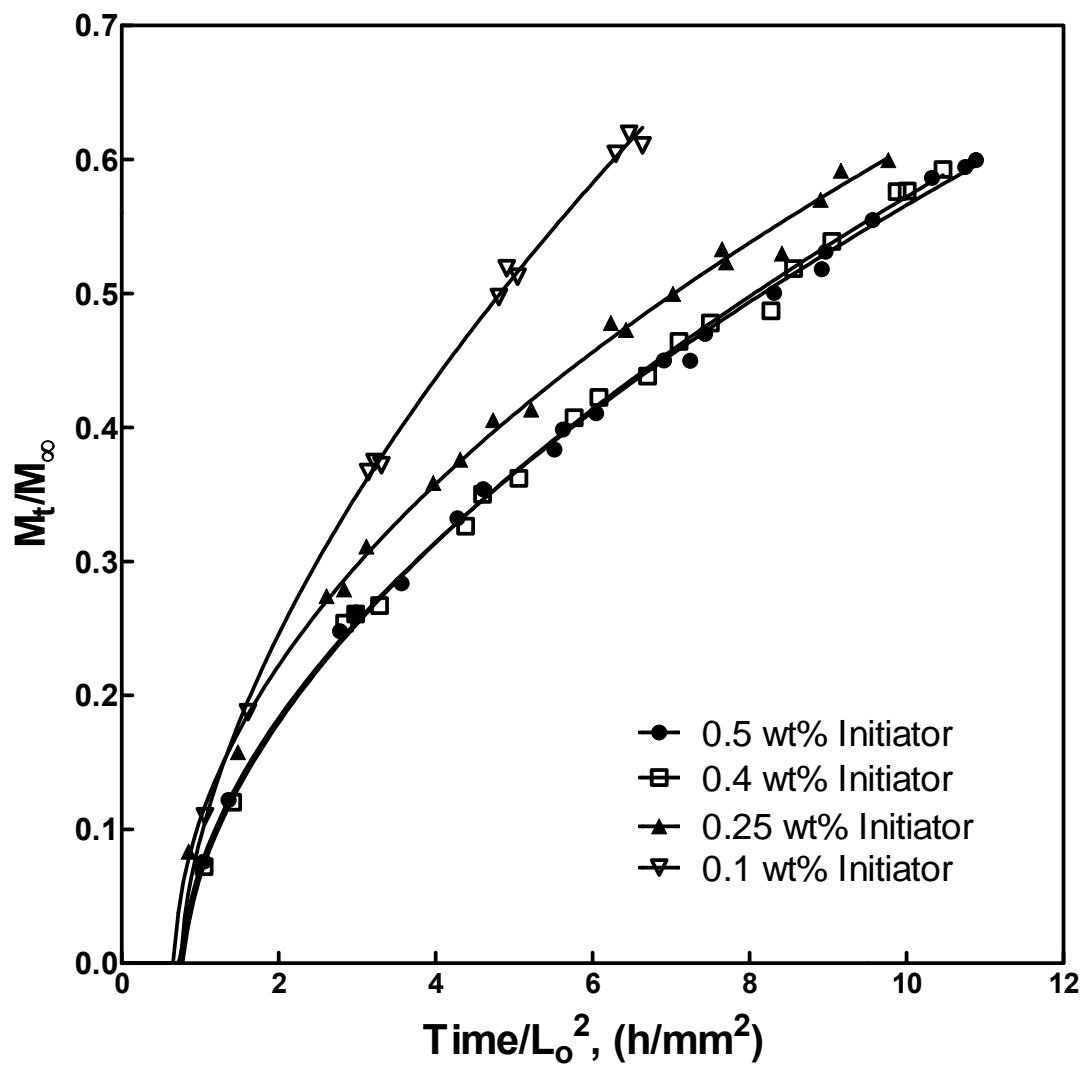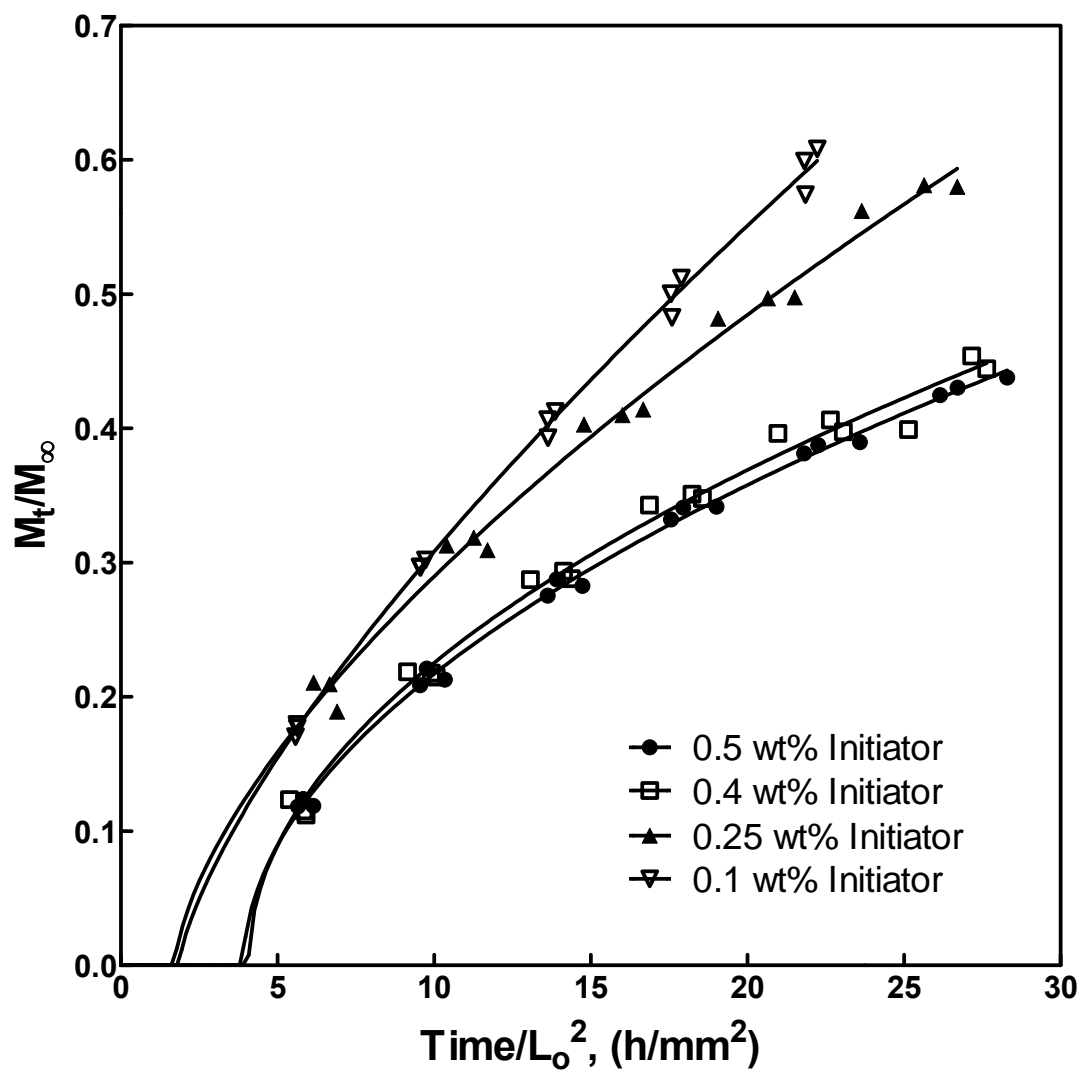
Figure 5.7: Power-law model analysis of the effect of initiator concentration on the integral sorption dynamics of PMMA discs with 2.29 mol % crosslinking (EGDMA) swelling in methanol at 25°C.
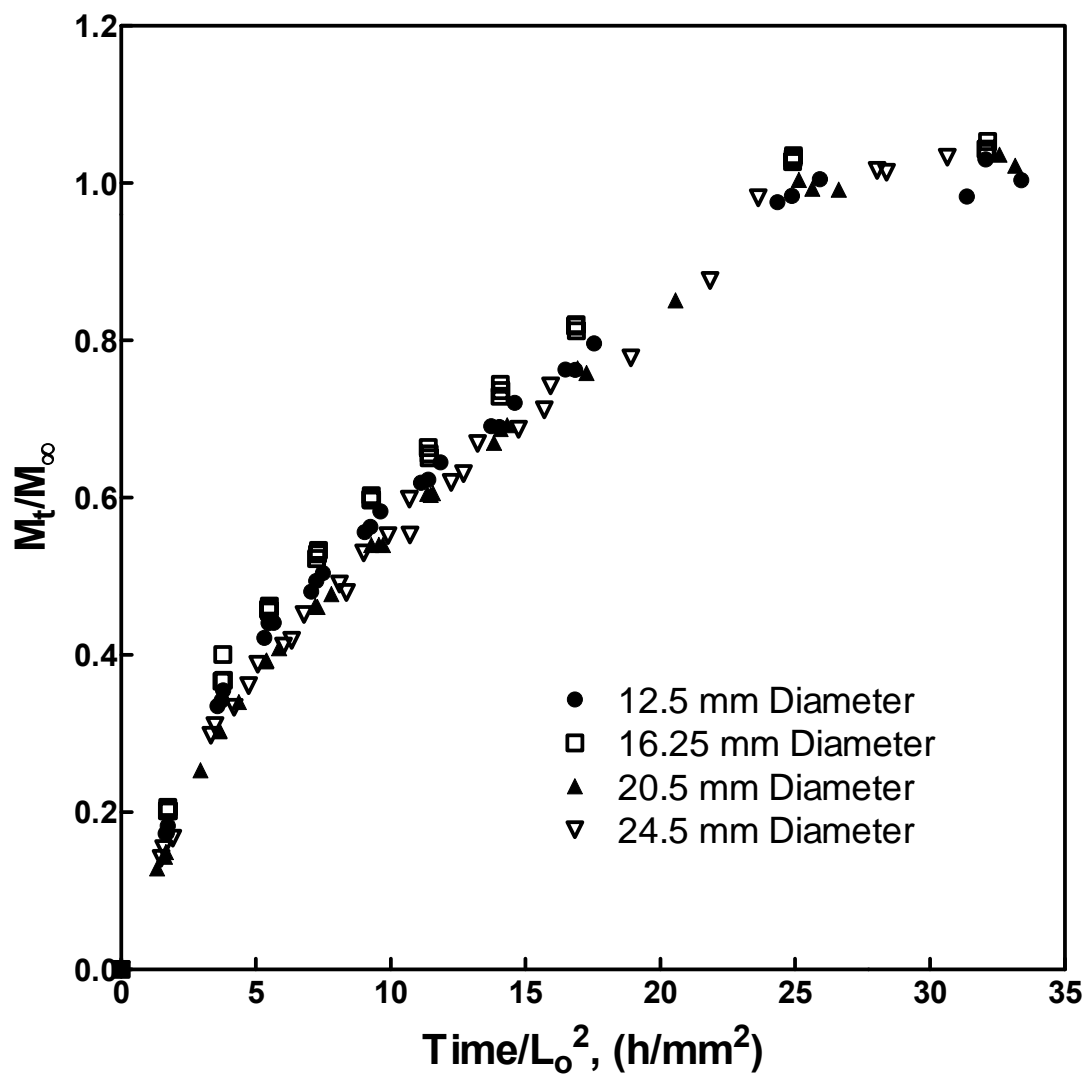
Figure 5.8: The effect of disc diameter on the integral sorption dynamics of PMMA discs with 2.29 mol % crosslinking (EGDMA) swelling in methanol at 30°C.
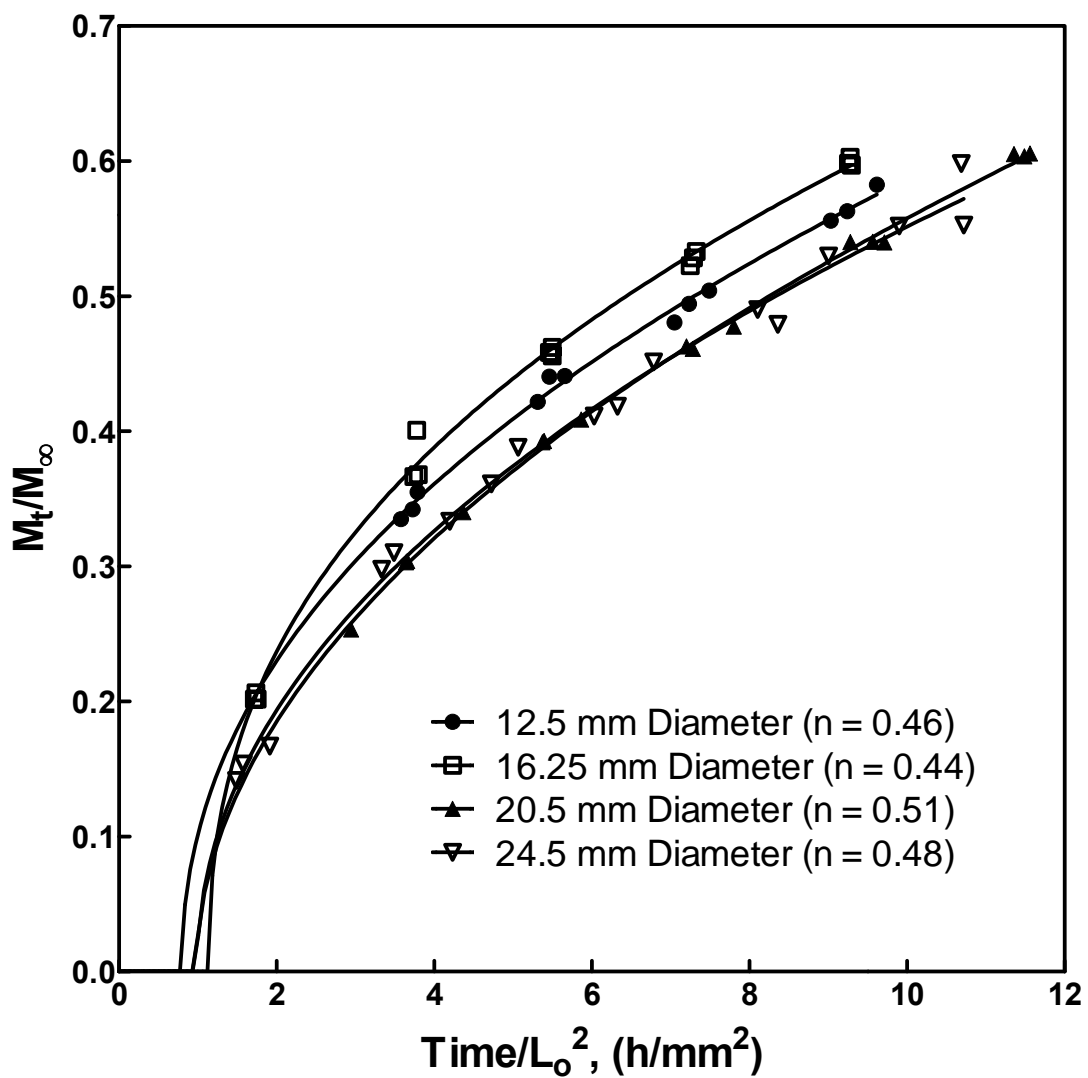
Figure 5.9: Power-law model analysis of the effect of disc diameter on the integral sorption dynamics of PMMA discs with 2.29 mol % crosslinking (EGDMA) swelling in methanol at 30°C.
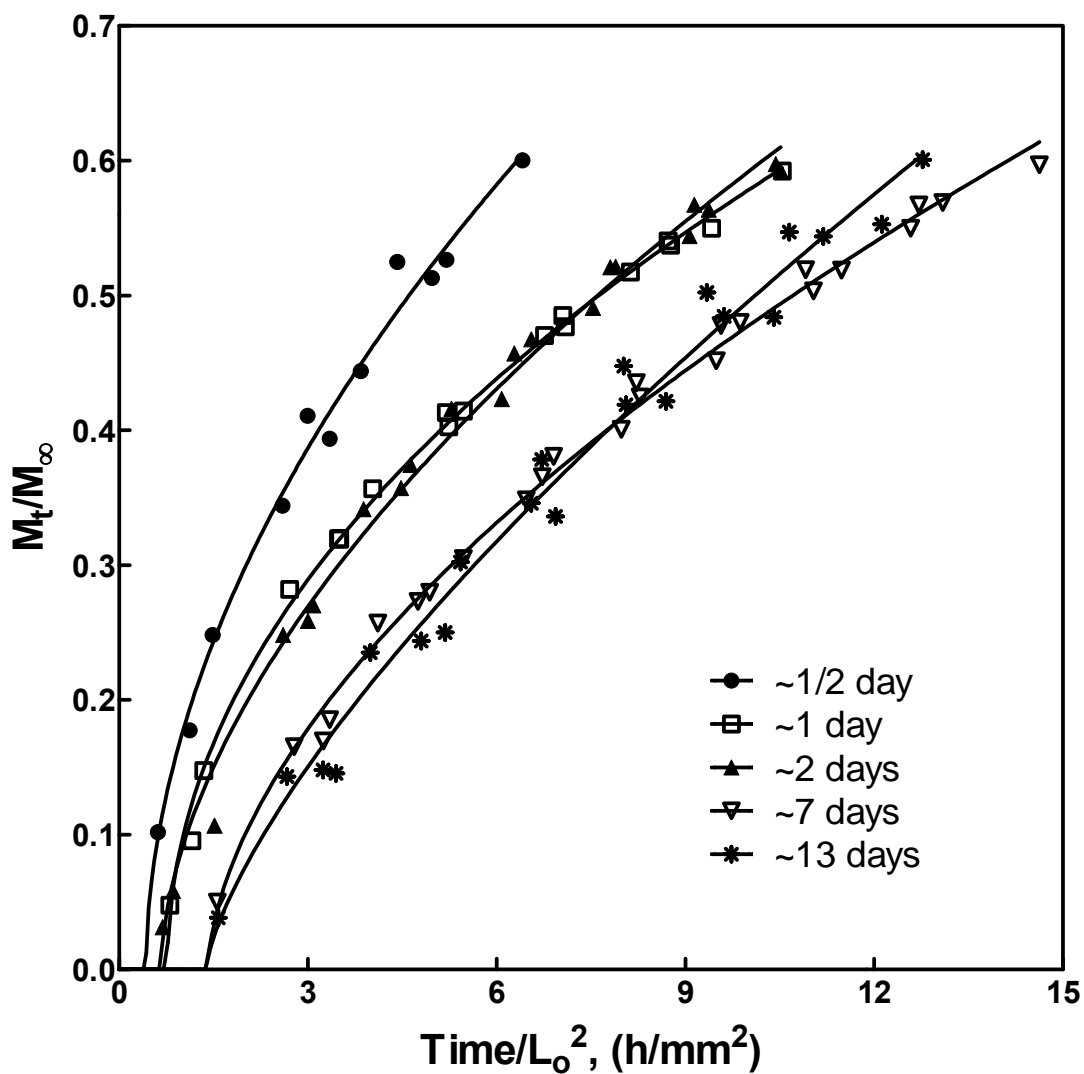
Figure 5.10: Power-law model analysis of the effect of annealing/drying time on PMMA discs with 2.29 mol % crosslinking (EGDMA) annealed at 10°C below T_g and swollen in methanol at 30°C.
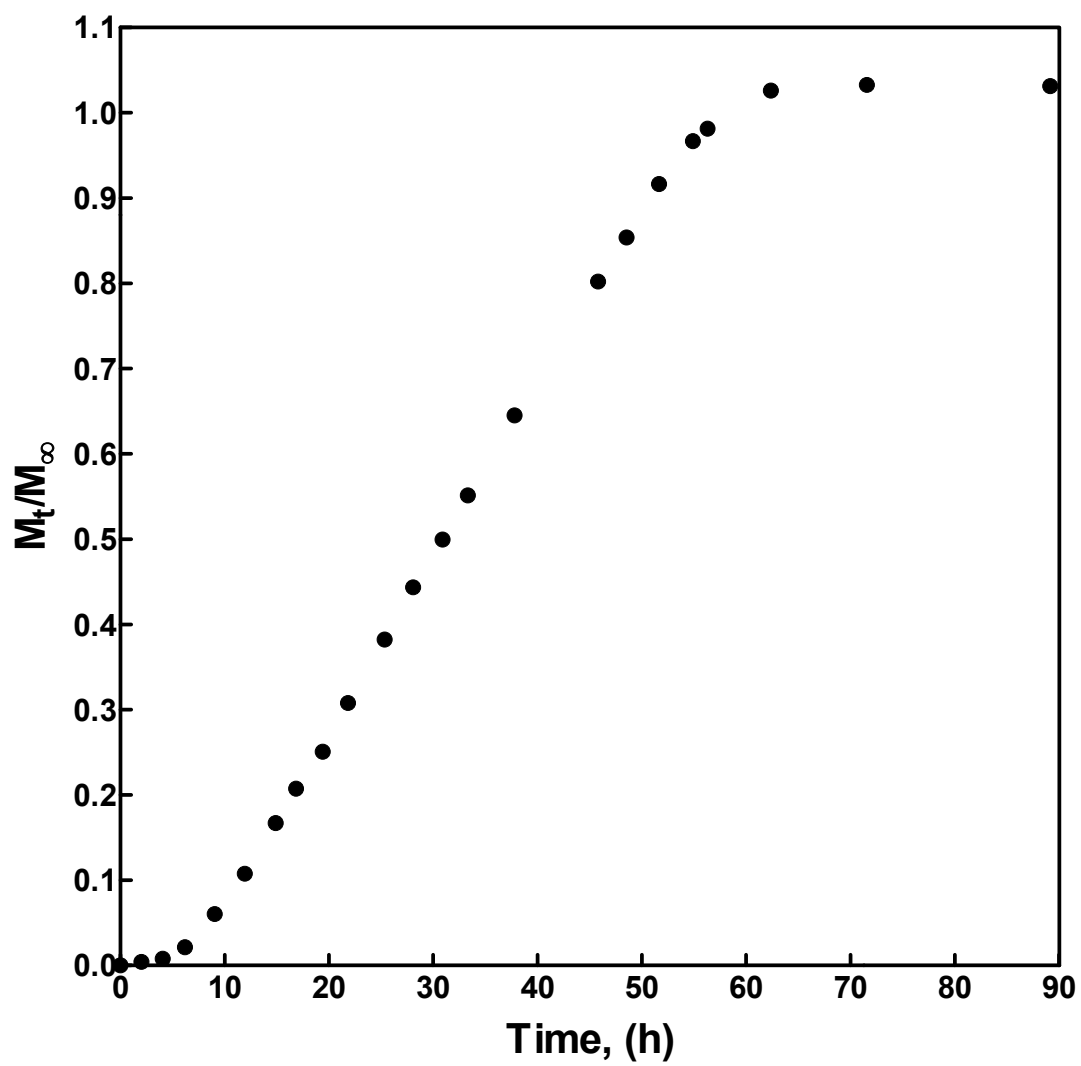
Figure 5.11: Uncrosslinked PMMA Disc with 0.5 wt % initiator annealed for 117 days and swollen in methanol at 22°C.
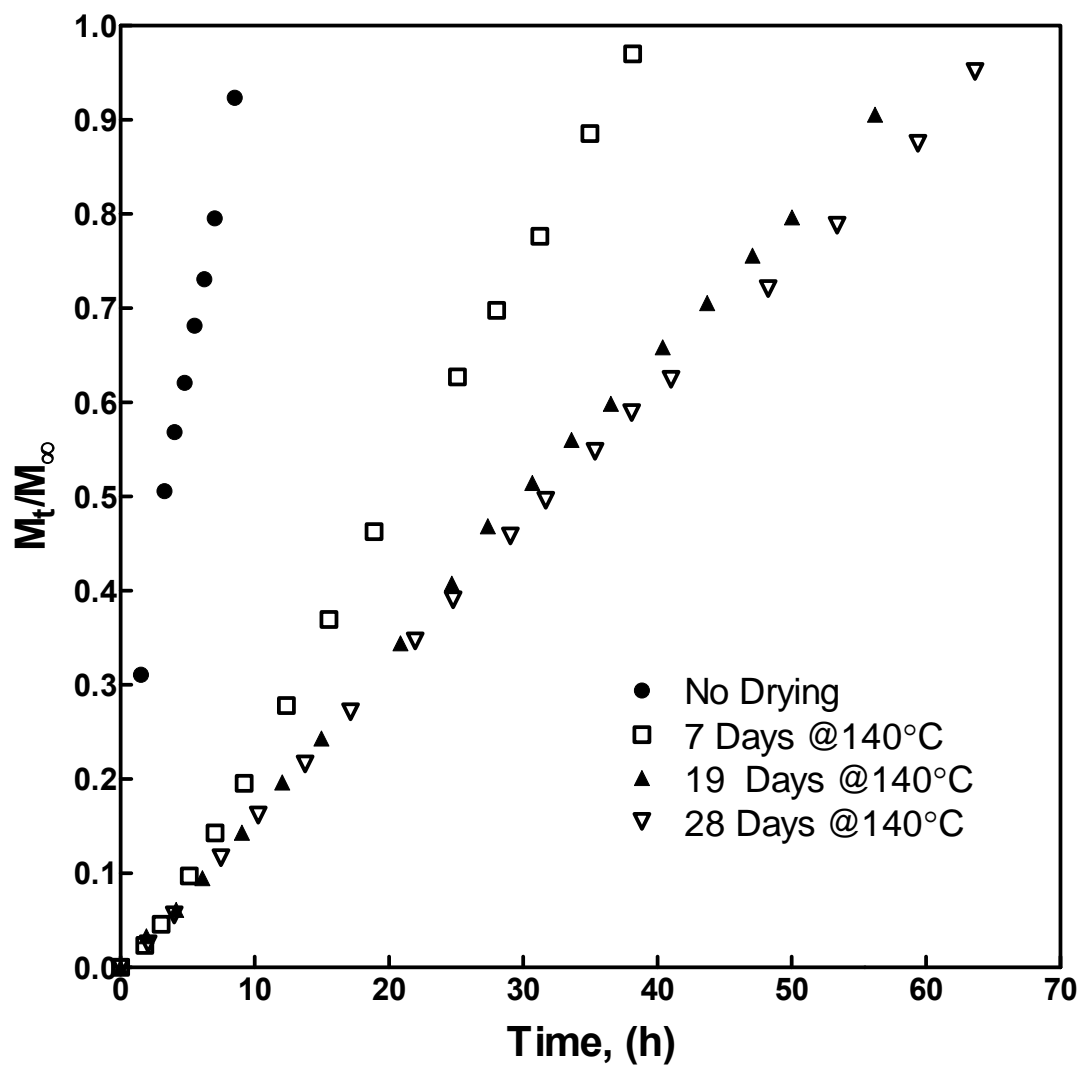
Figure 5.12: Effect of drying time on PMMA discs with 2.29 mol % crosslinking (EGDMA) dried above T_g (140°C in this instance) and swollen in methanol at 30°C.
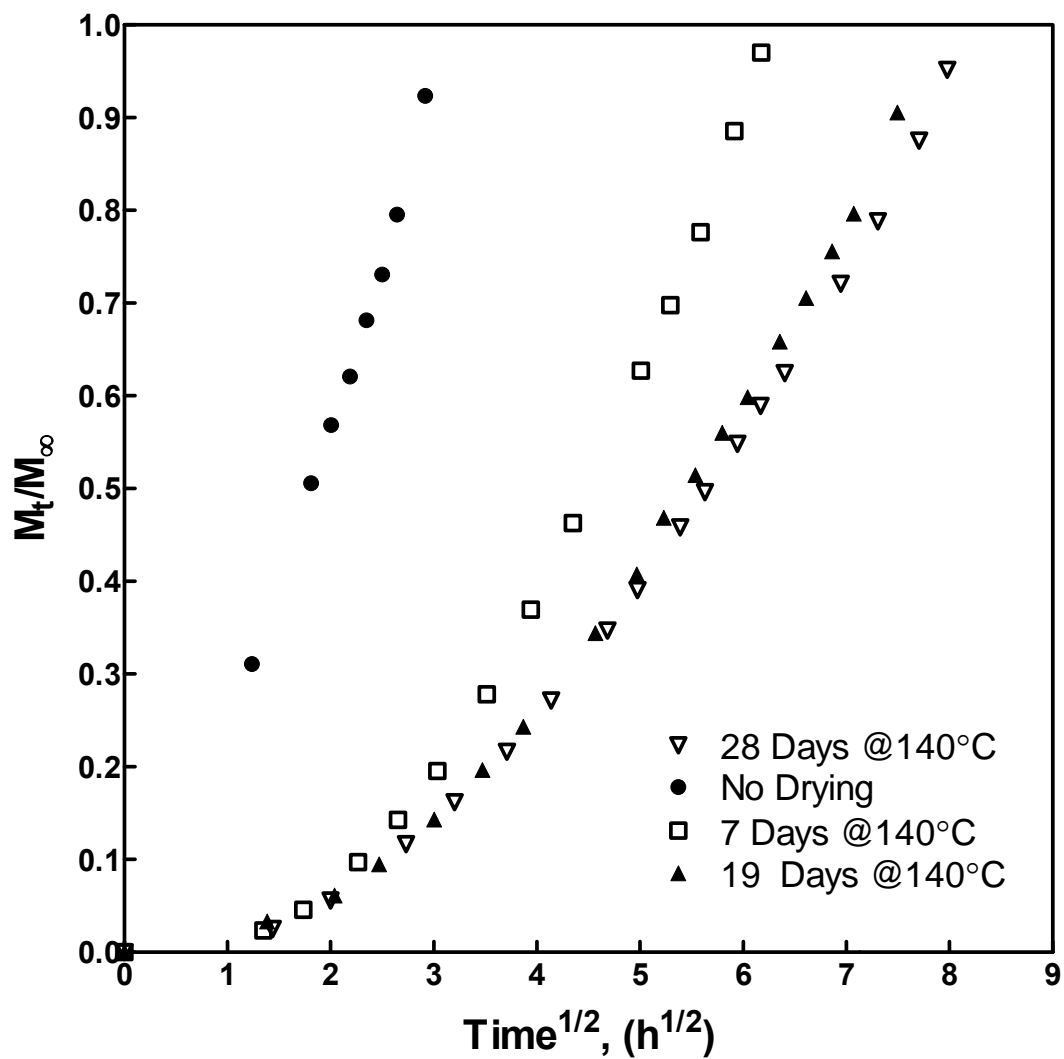
Figure 5.13: Effect of drying time on PMMA discs with 2.29 mol % crosslinking (EGDMA) dried above T_g (140°C in this instance) and swollen in methanol at 30°C.
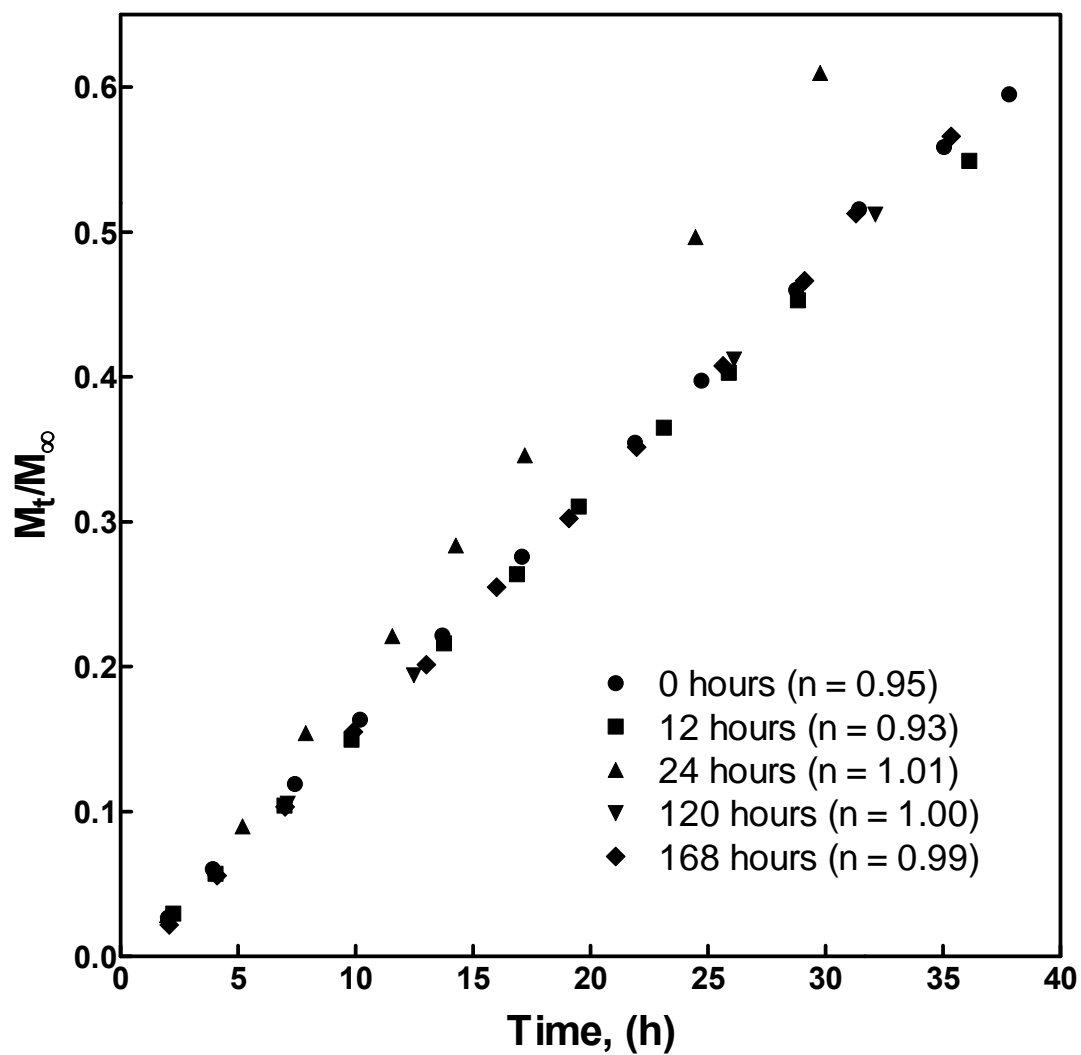
Figure 5.14: Effect of annealing time on PMMA discs with 2.29 mol % crosslinking (EGDMA) annealed at 10°C below T_g (108°C in this instance) after drying above T_g (140°C in this instance) and swollen in methanol at 30°C.
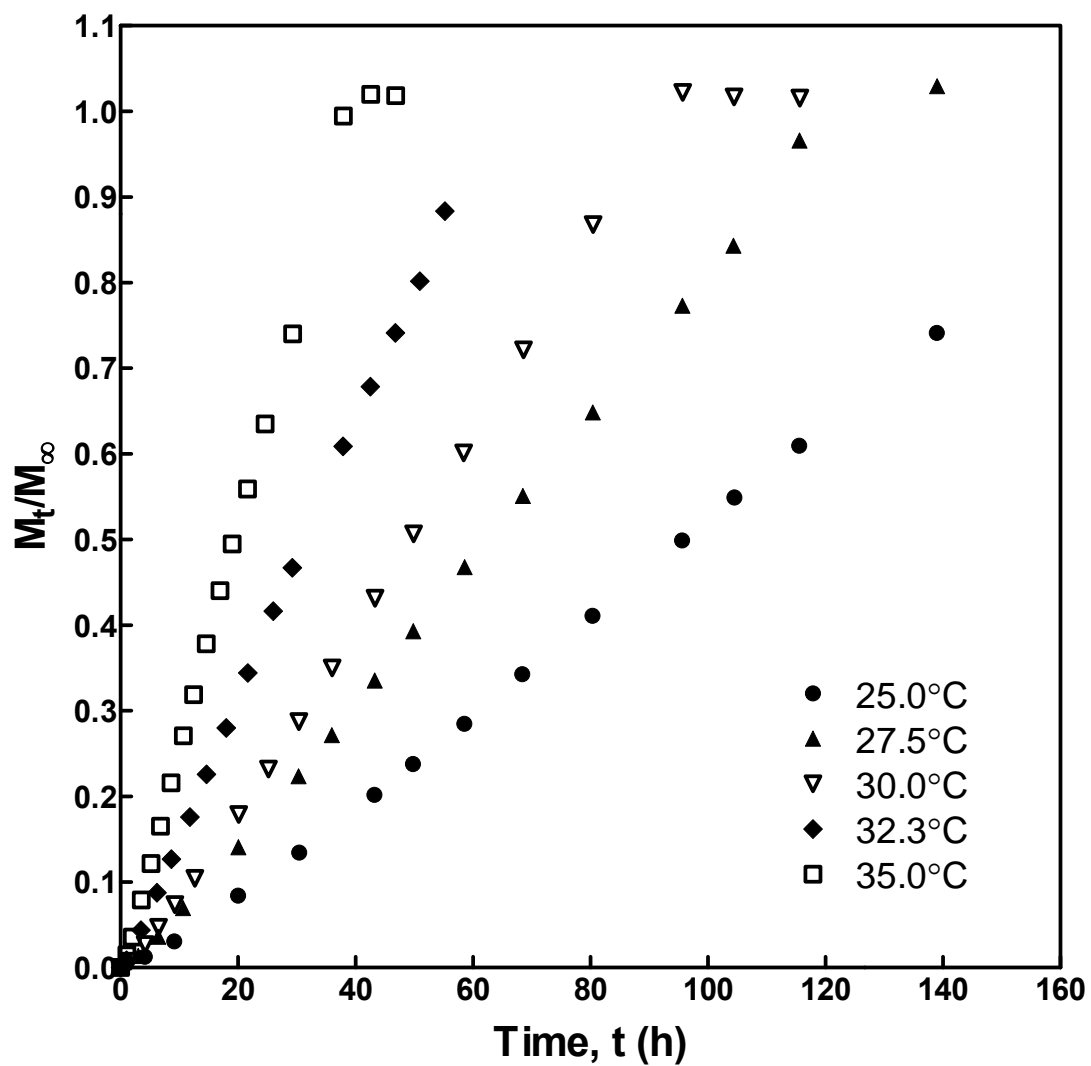
Figure 5.15: Effect of temperature on PMMA discs with 2.29 mol % crosslinking (EGDMA) and swollen in methanol.
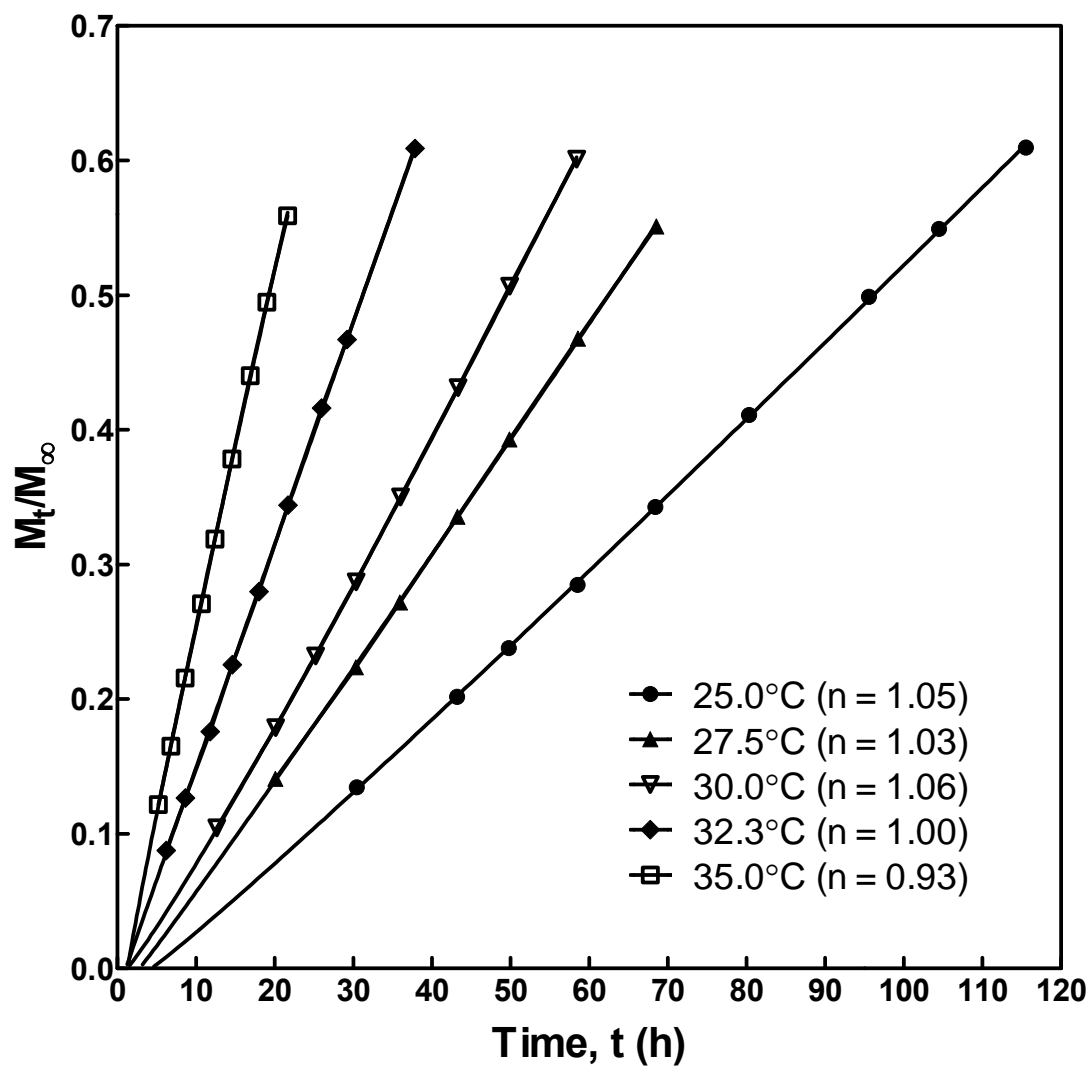
Figure 5.16: Power-law model analysis of temperature effect on PMMA discs with 2.29 mol % crosslinking (EGDMA) and swollen in methanol.
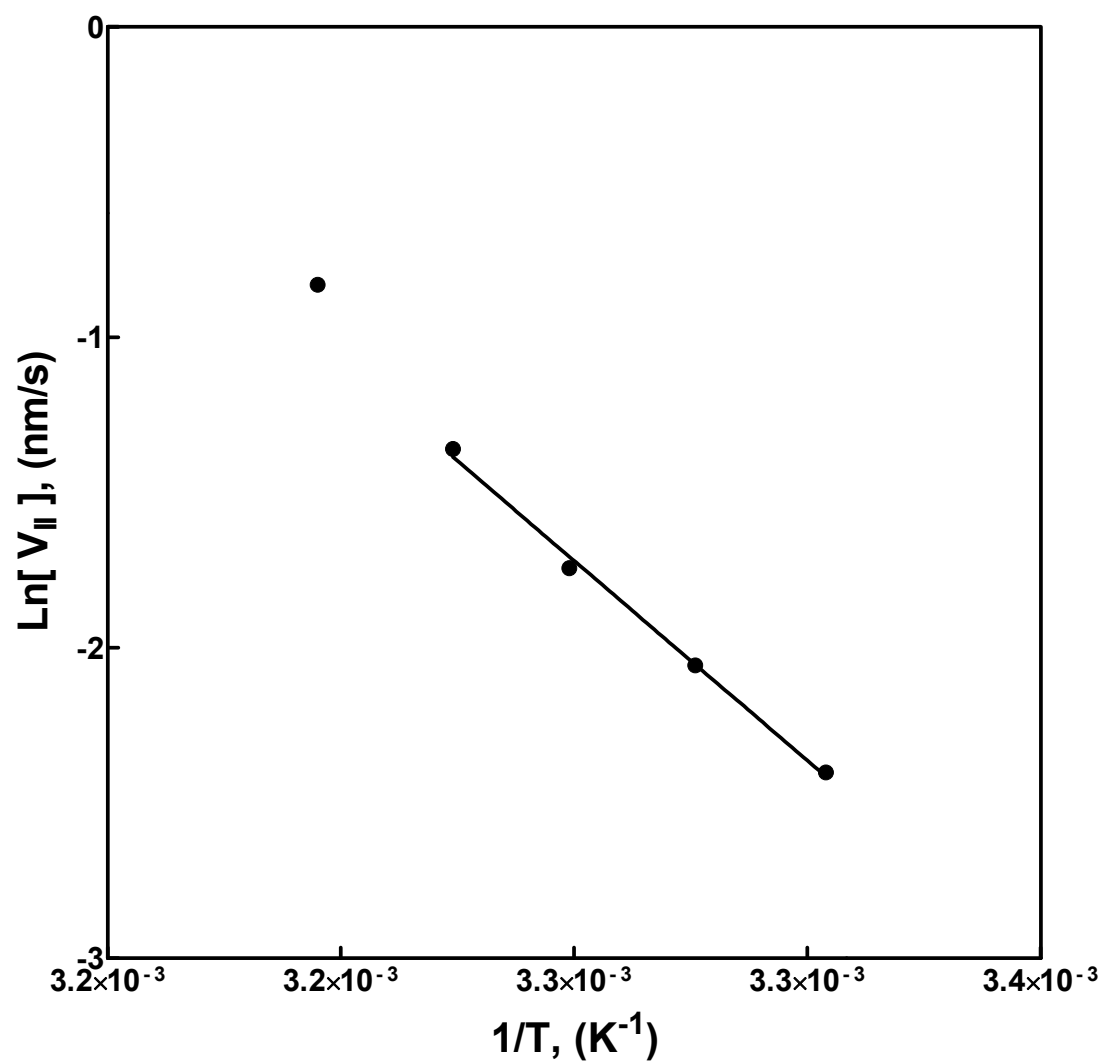
Figure 5.17: Arrhenius plot of the effect of temperature on the Case II front velocity, V_{II}, for PMMA discs with 2.29 mol % crosslinking (EGDMA) swollen in methanol.
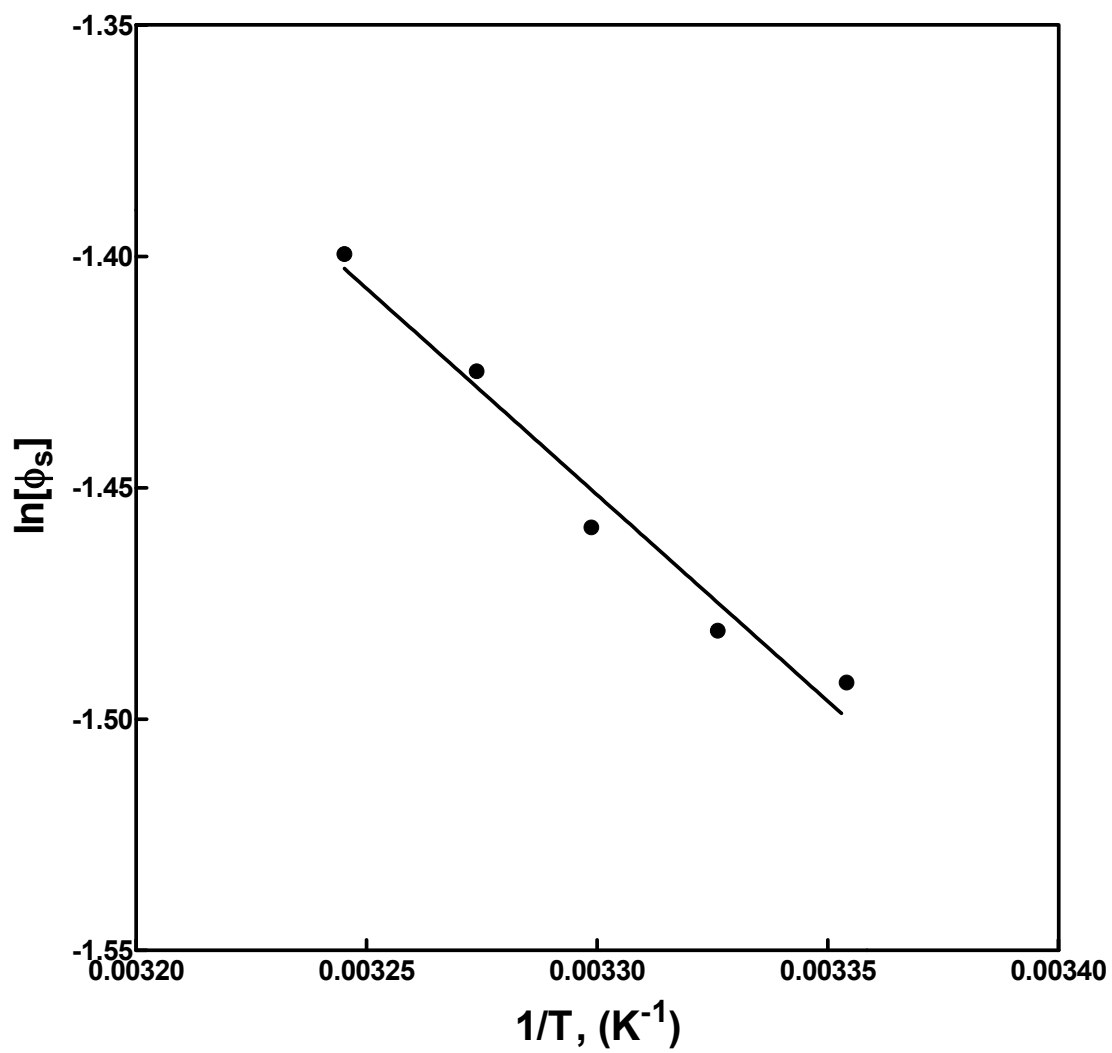
Figure 5.18: Effect of temperature on the equilibrium penetrant volume fraction, ϕ_s, for PMMA discs with 2.29 mol % crosslinking (EGDMA) swollen in methanol.
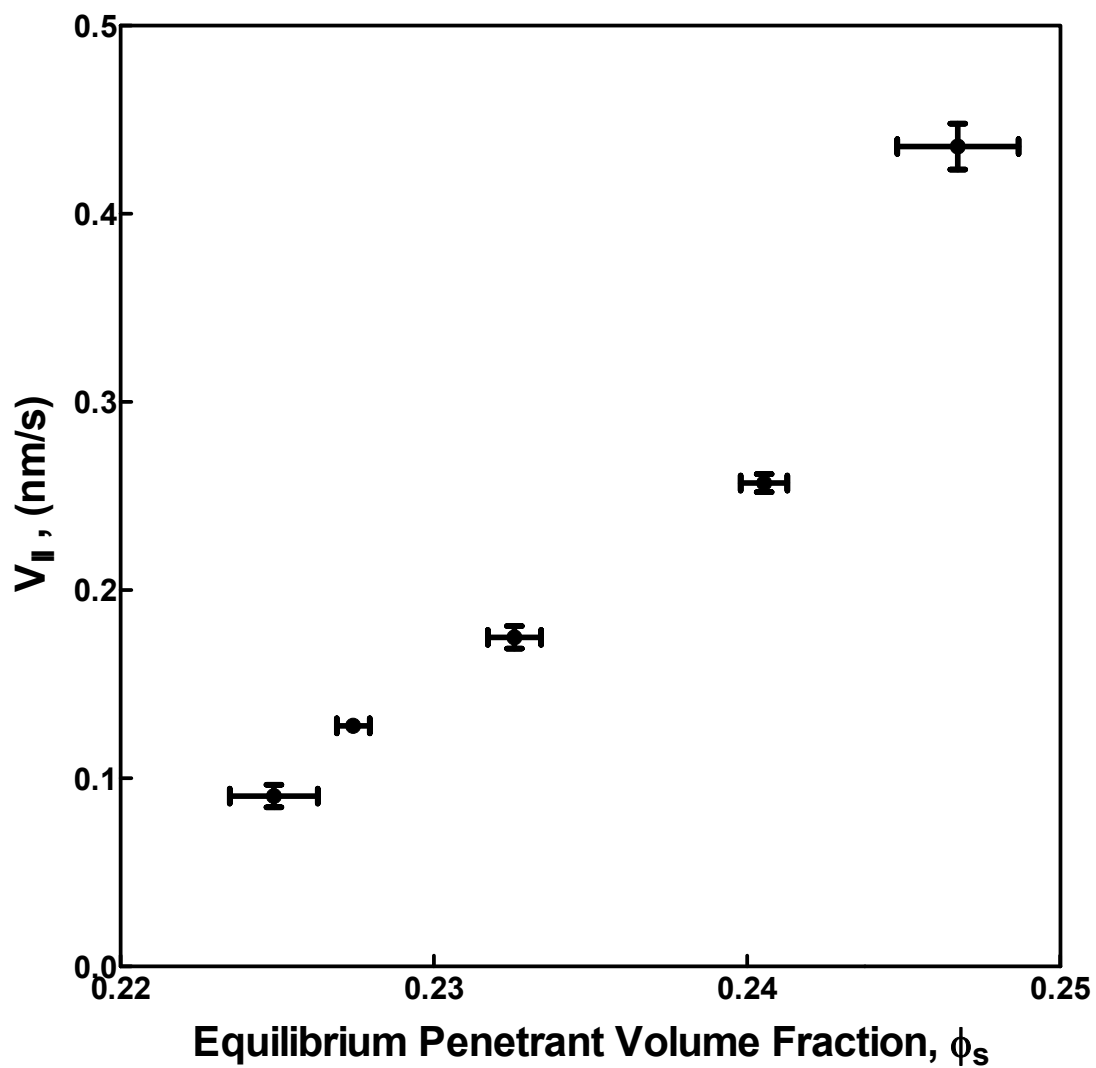
Figure 5.19: Case II front velocity, V_{II}, plotted versus the equilibrium penetrant volume fraction, ϕ_s, for PMMA discs with 2.29 mol % crosslinking (EGDMA) swollen in methanol at varying temperatures.
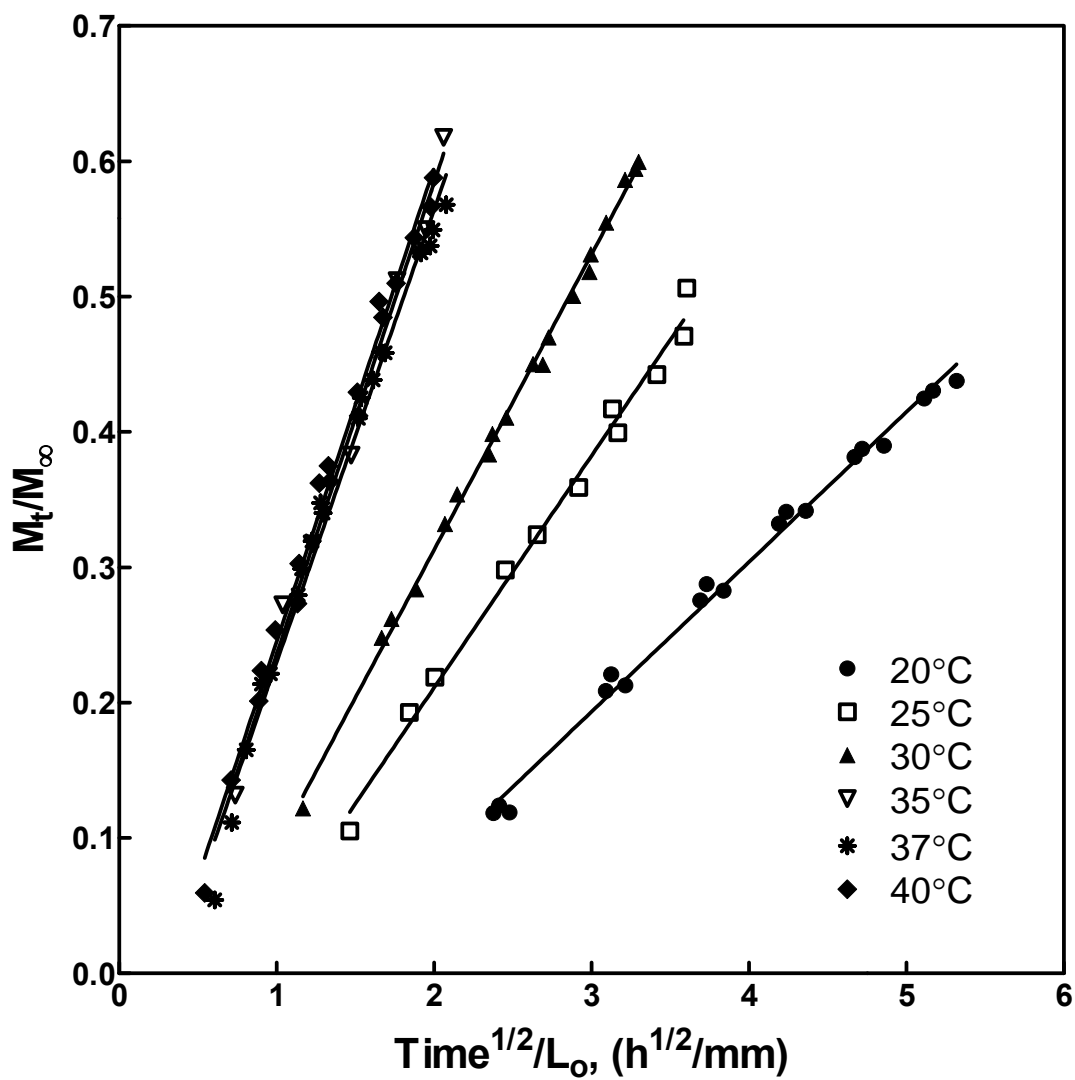
Figure 5.20: Effect of temperature on PMMA discs with 2.29 mol % crosslinking (EGDMA) dried/annealed for 24 hours at 10°C below T_g and swollen in methanol (linear regressions shown).
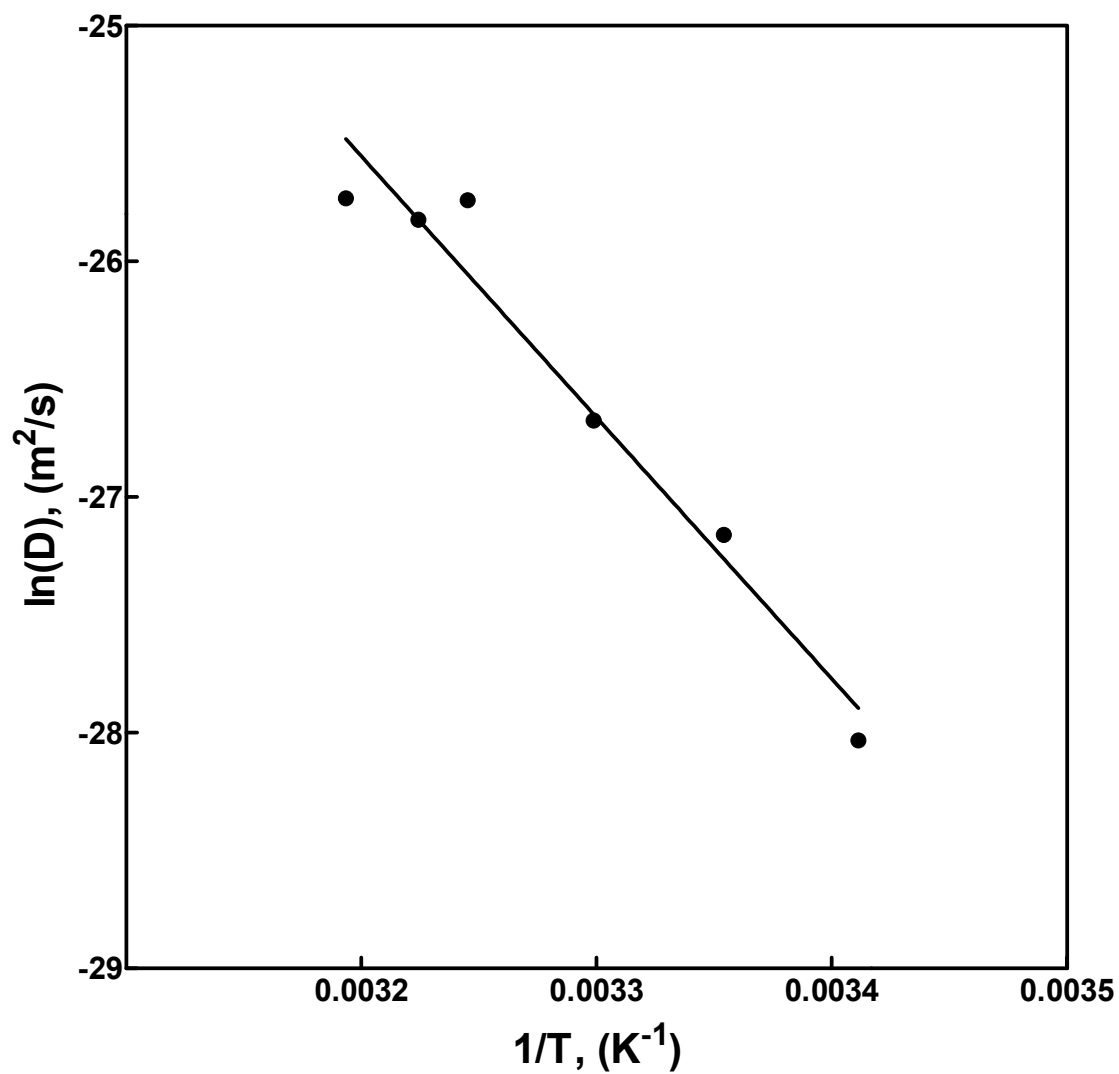
Figure 5.21: Arrhenius plot of the effect of temperature on the binary diffusion coefficient for PMMA discs with 2.29 mol % crosslinking (EGDMA) dried/annealed for 24 hours at 10°C below T_g and swollen in methanol.
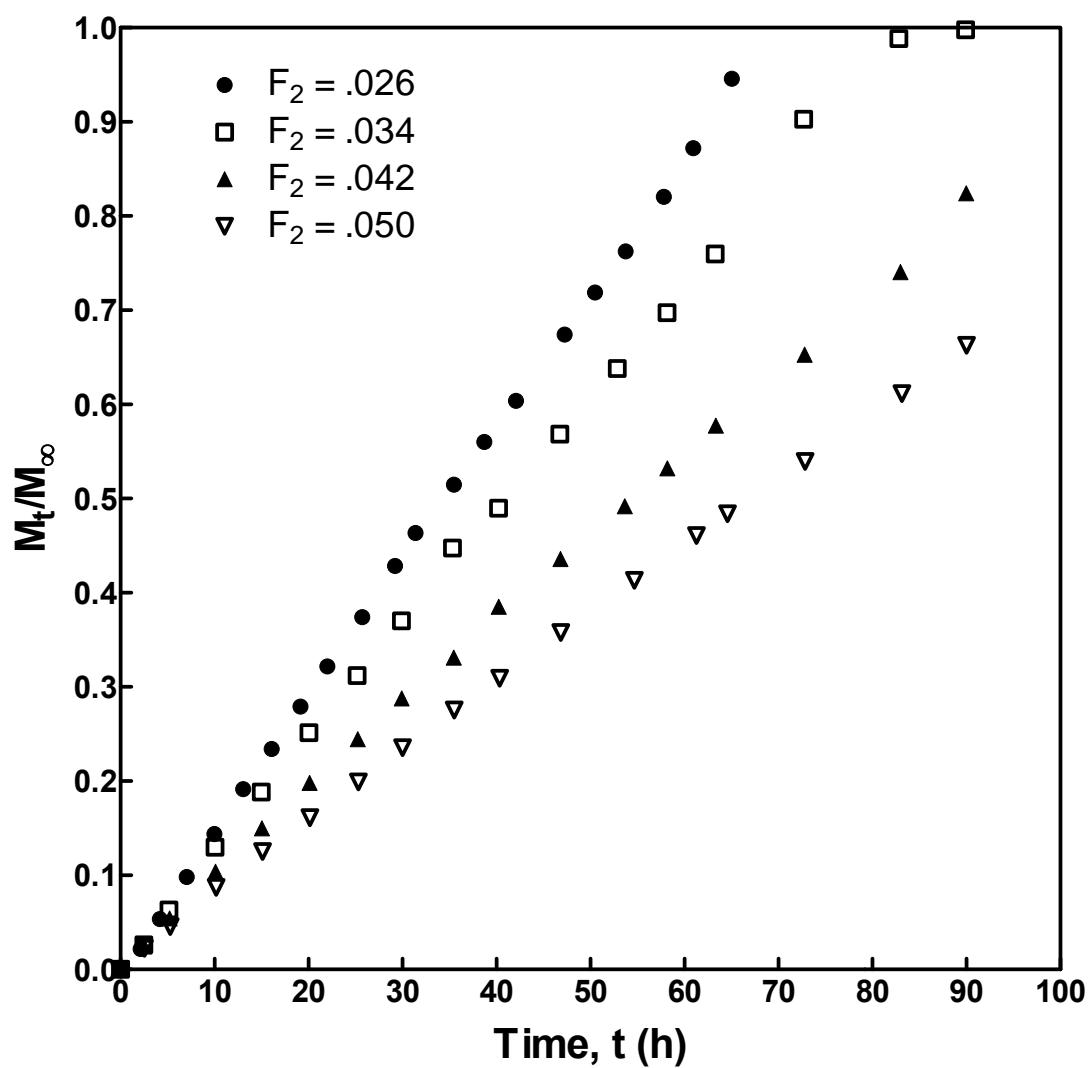
Figure 5.22: Effect of low degrees of copolymer crosslinking (F_2) on penetrant transport for PMMA discs crosslinked with EGDMA (Series 2) and swollen in methanol at 30°C.
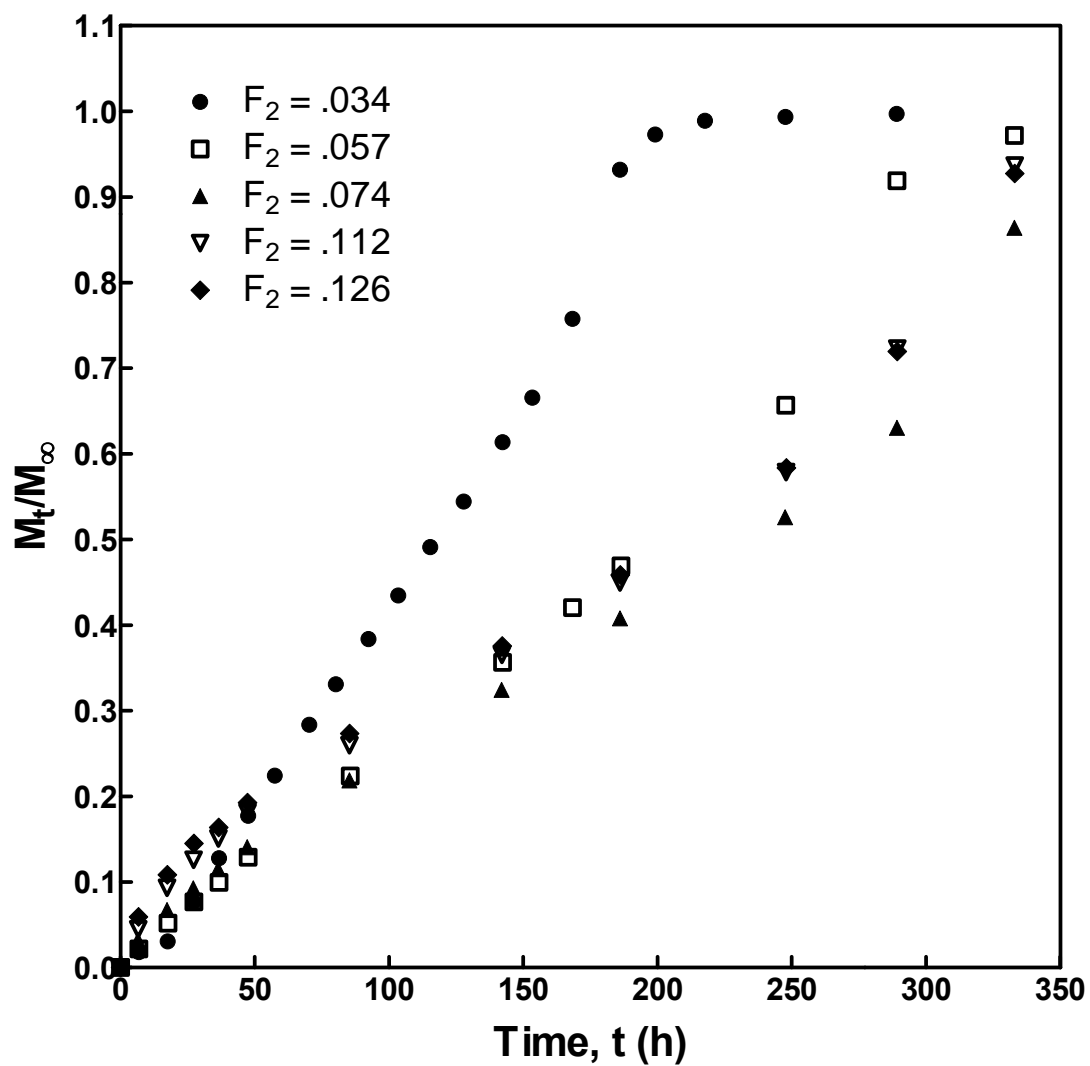
Figure 5.23: Effect of high degrees of copolymer crosslinking (F_2) on penetrant transport for PMMA discs crosslinked with EGDMA (Series 1) and swollen in methanol at 25°C.
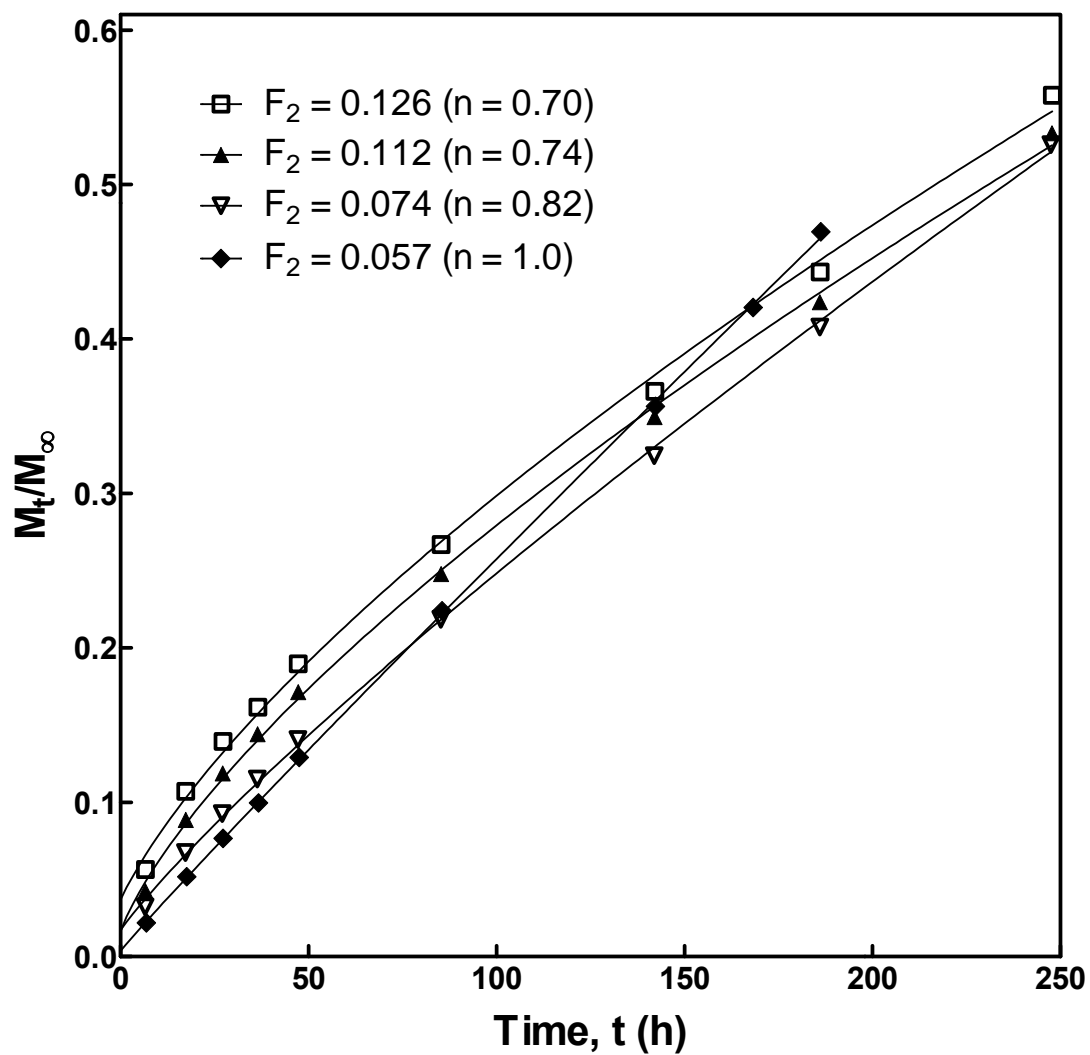
Figure 5.24: Power-law analysis of the effect of high degrees of copolymer crosslinking (F_2) on penetrant transport for PMMA discs crosslinked with EGDMA (Series 1) and swollen in methanol at 25°C.
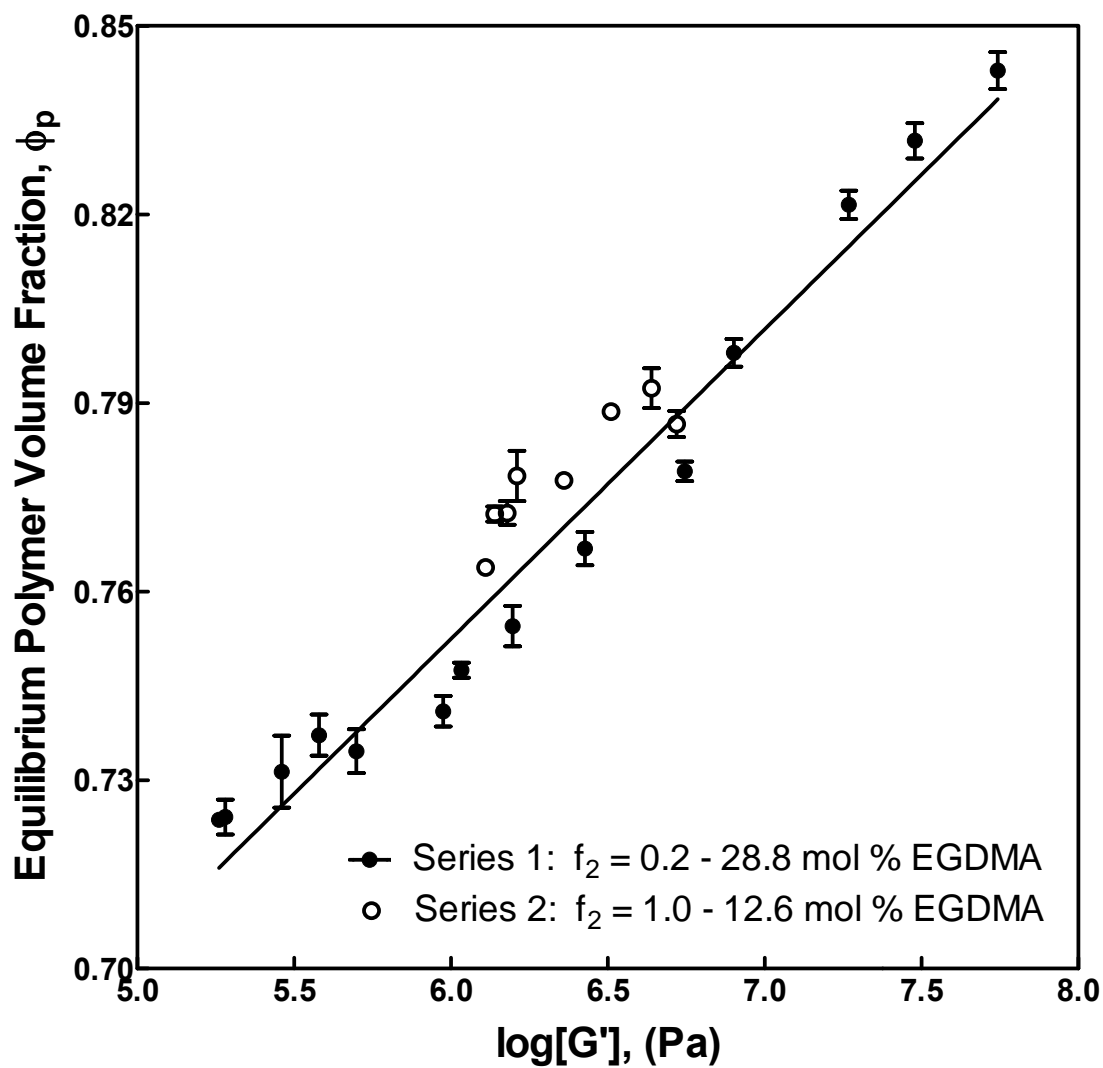
Figure 5.25: The variation of equilibrium polymer volume fraction, ϕ_p, plotted against the shear storage modulus, G', in PMMA discs crosslinked with EGDMA (Series 1 and 2) and swollen in methanol at 25°C.
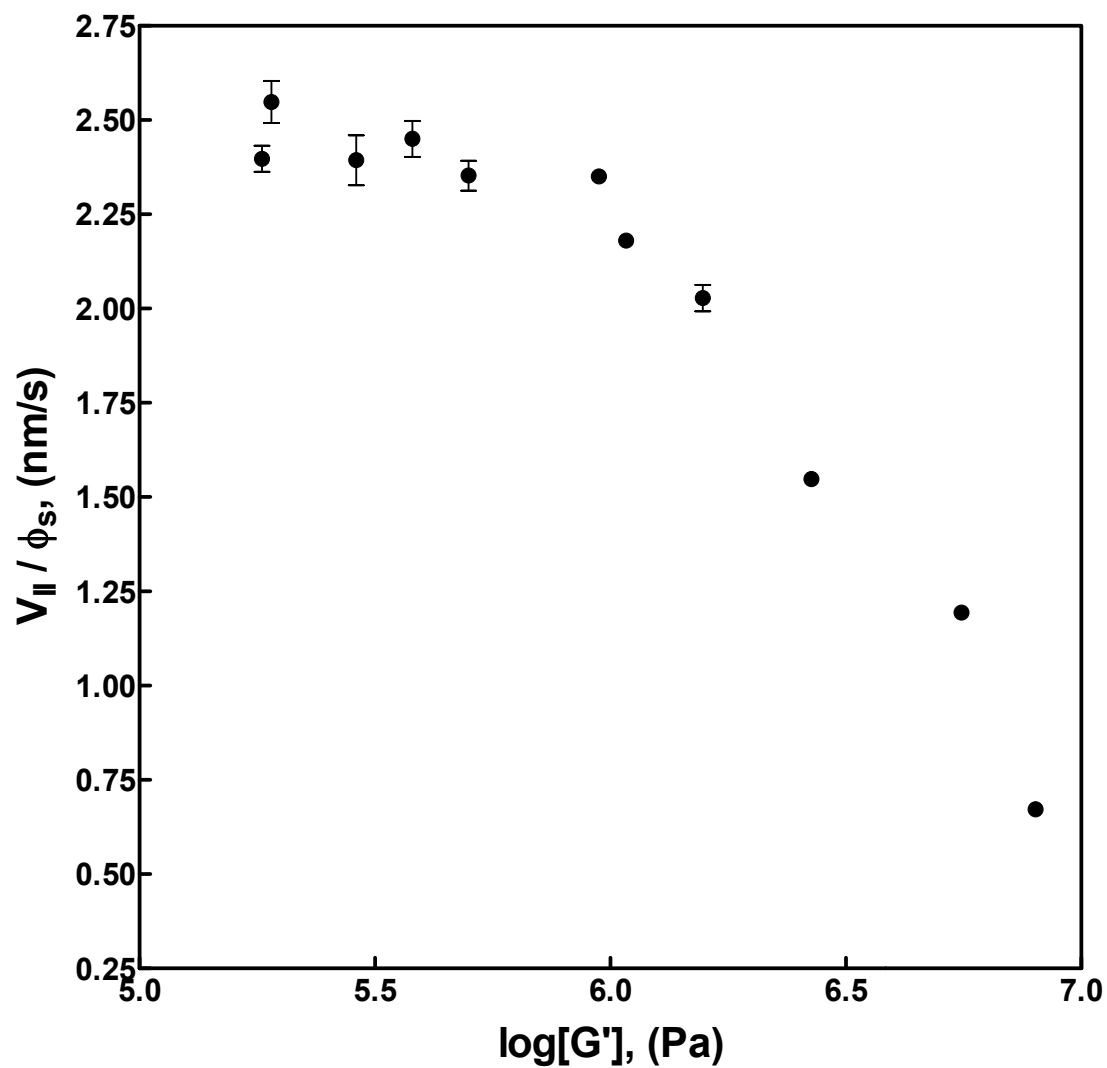
Figure 5.26: Normalized (by ϕ_s) Case II front velocity, V_{II}, versus the shear storage modulus, G', in PMMA discs crosslinked with EGDMA (Series 1) and swollen in methanol at 25°C.
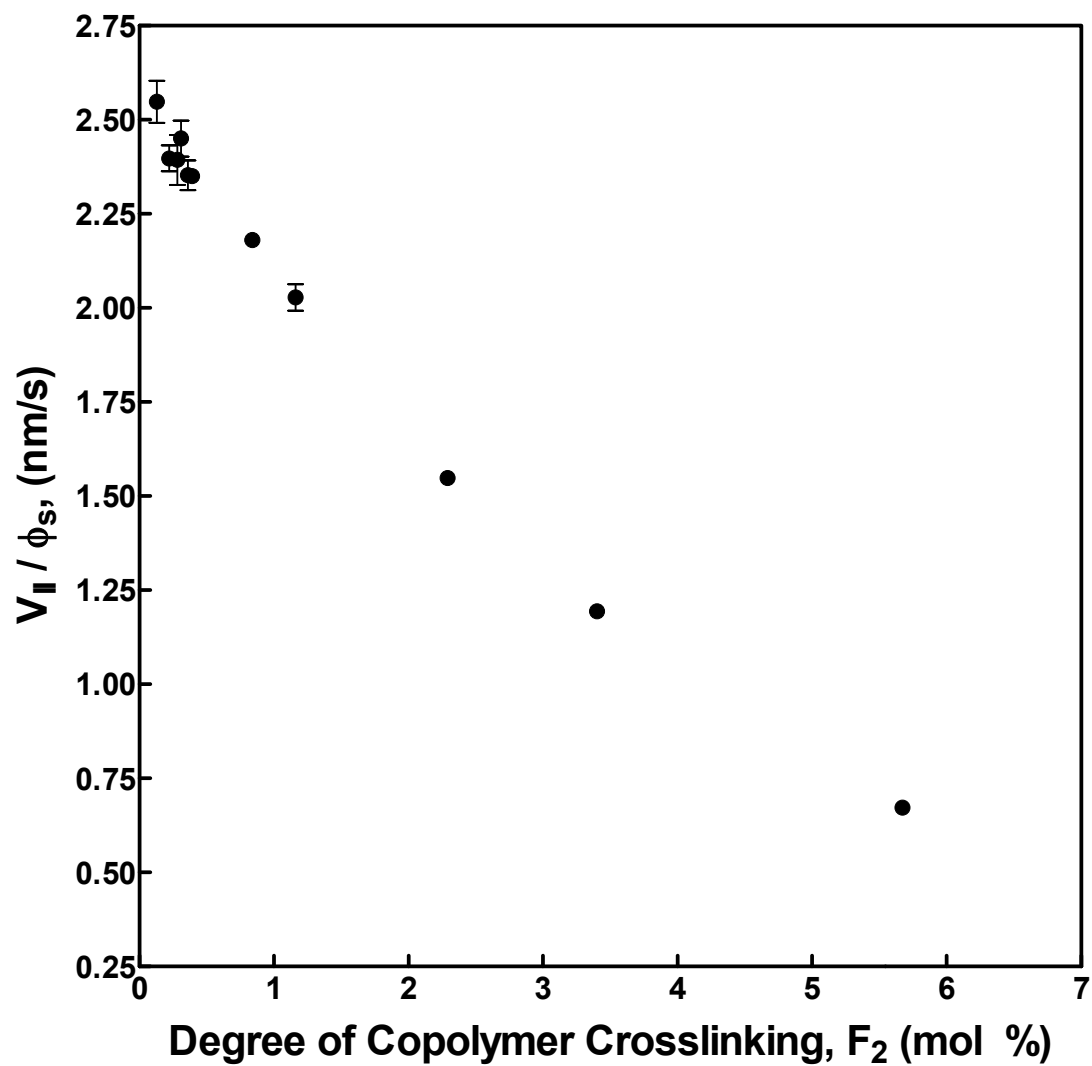
Figure 5.27: Normalized (by ϕ_s) Case II front velocity, V_{II}, versus the degree of copolymer crosslinking, F_2, in PMMA discs crosslinked with EGDMA (Series 1) and swollen in methanol at 25°C.
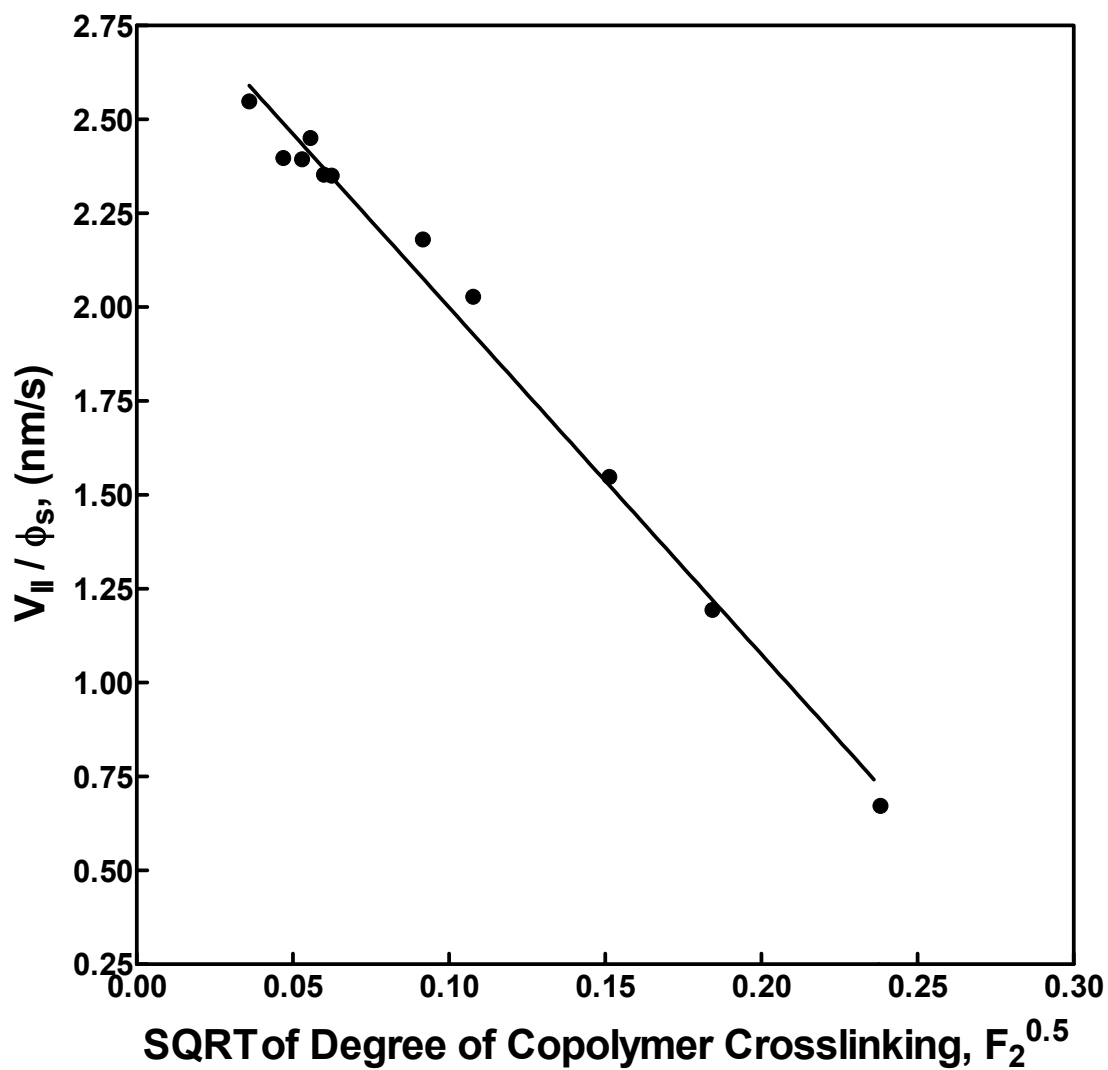
Figure 5.28: Normalized (by ϕ_s) Case II front velocity, V_{II}, versus the square root of the degree of copolymer crosslinking, $F_2^{0.5}$, in PMMA discs crosslinked with EGDMA (Series 1) and swollen in methanol at 25°C.
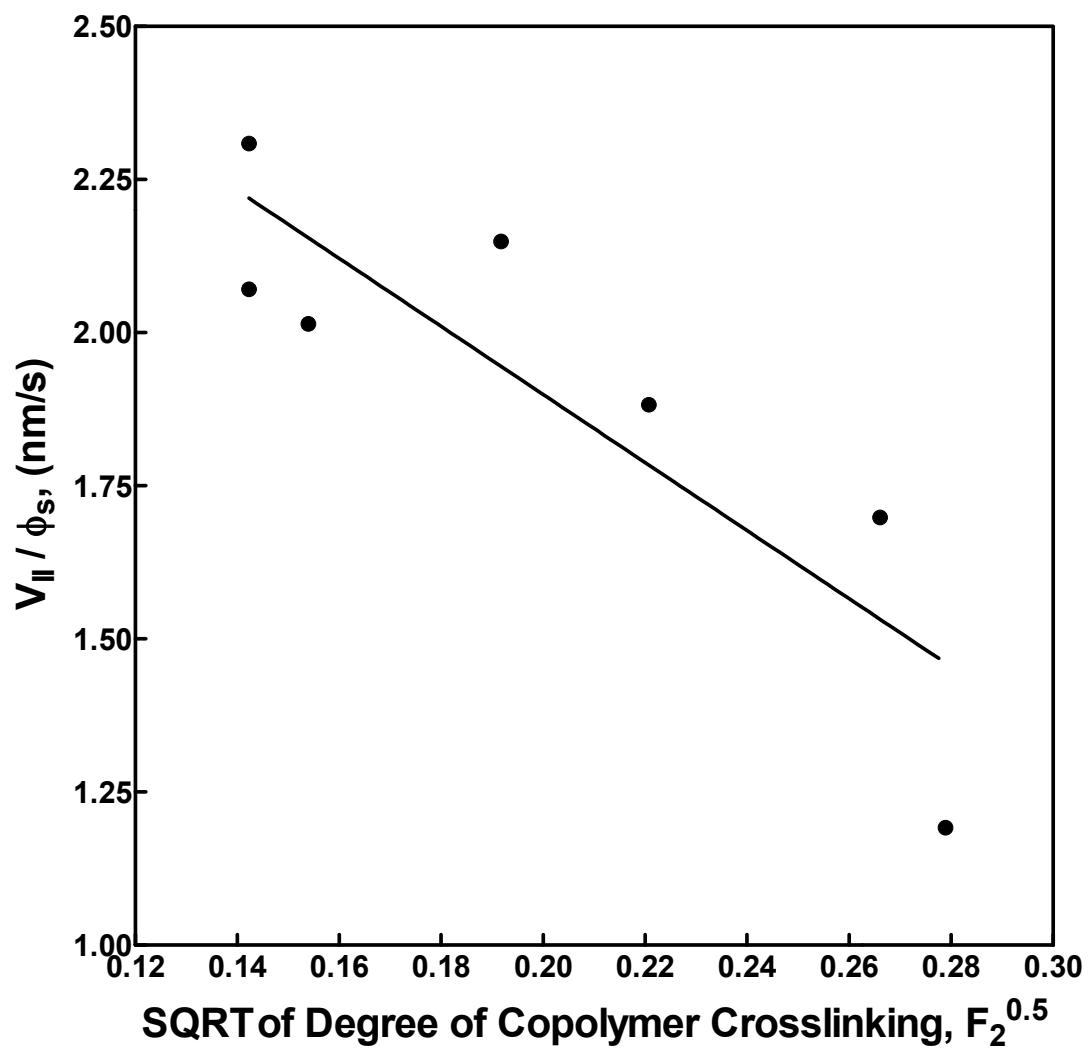
Figure 5.29: Normalized (by ϕ_s) Case II front velocity, V_{II}, versus the square root of the degree of copolymer crosslinking, $F_2^{0.5}$, in PMMA discs crosslinked with EGDMA (Series 2) and swollen in methanol at 30°C.
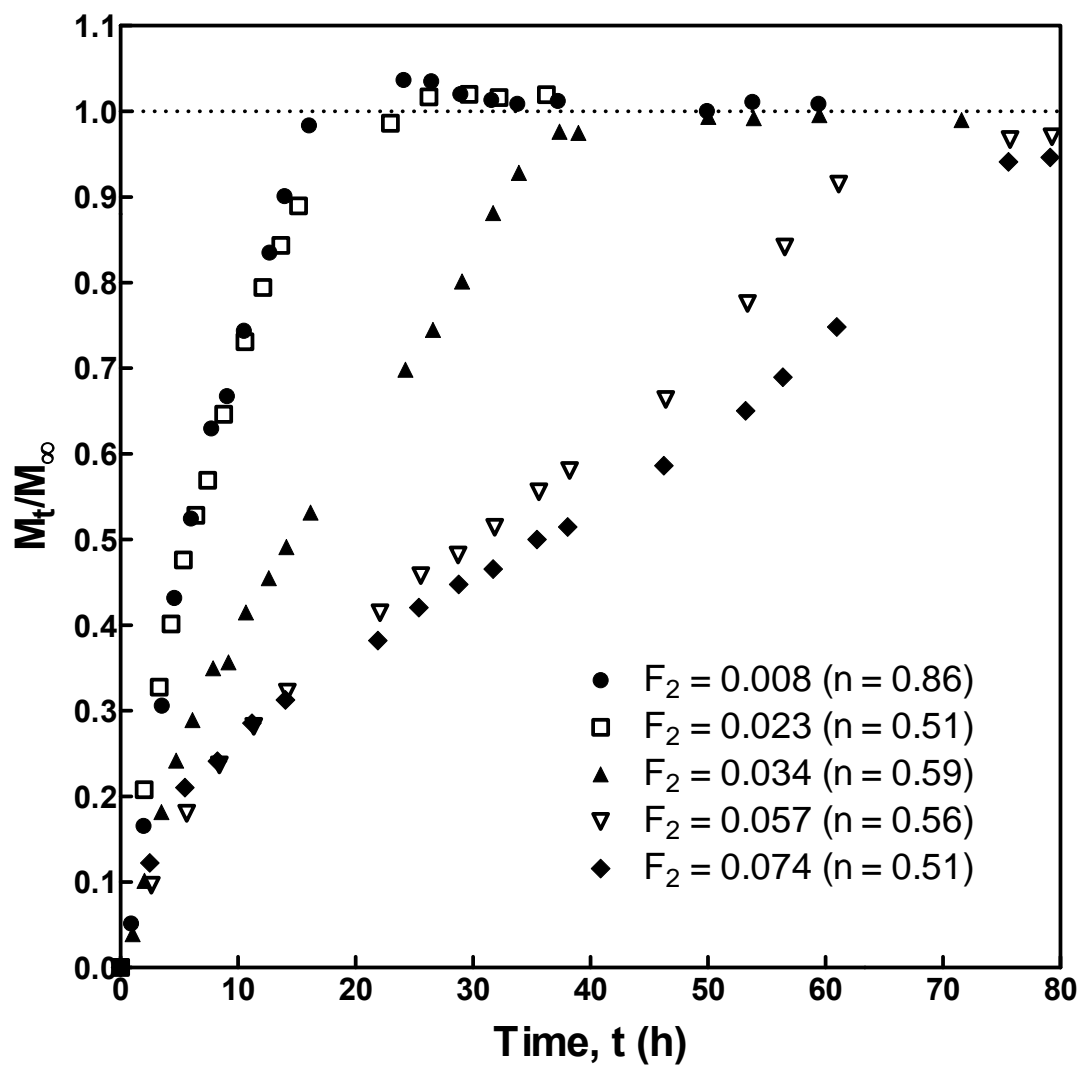
Figure 5.30: Effect of copolymer crosslinking (F_2) on penetrant transport for PMMA discs crosslinked with EGDMA, dried/annealed for 24 hours at 10°C below T_g, and swollen in methanol at 30°C.
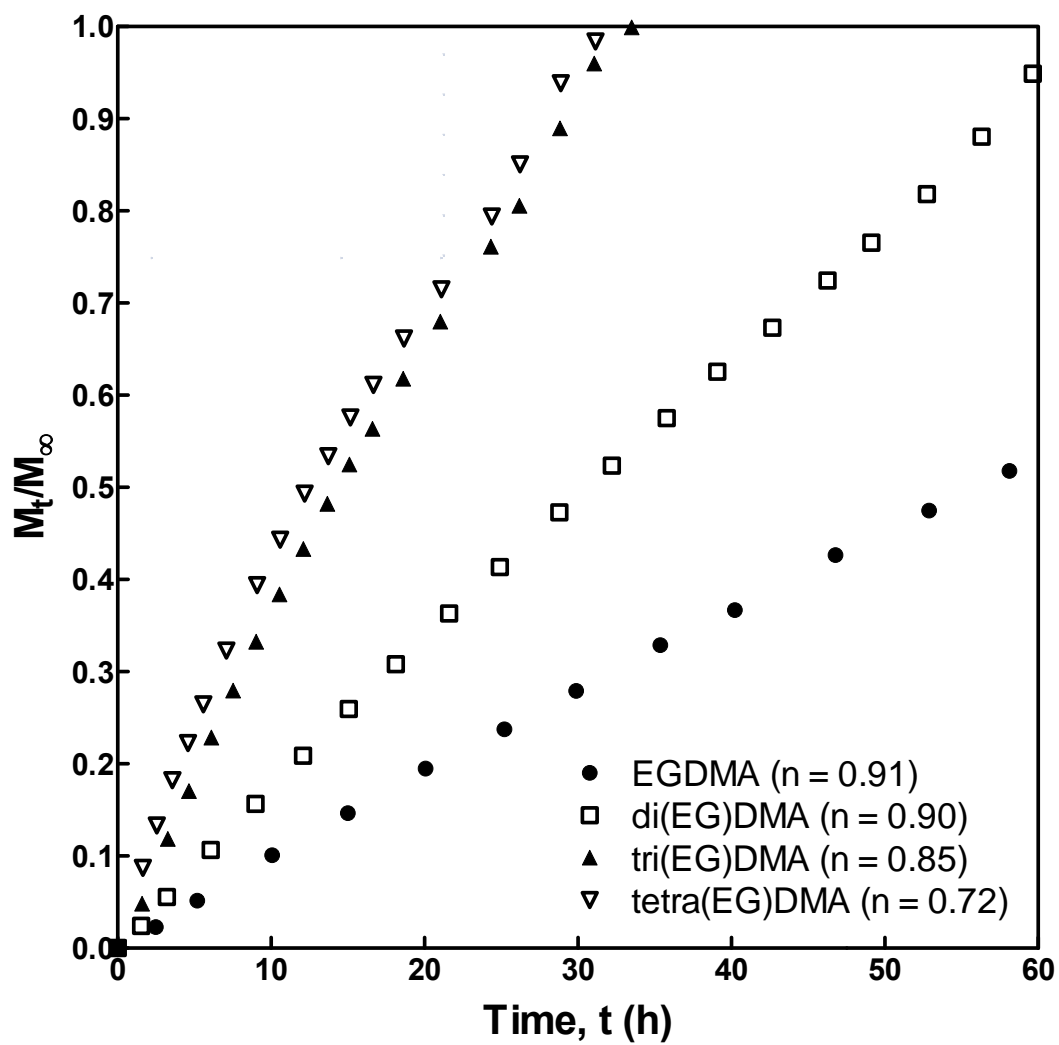
Figure 5.31: Effect of crosslinker bridge length on penetrant transport for PMMA discs crosslinked with 3.4 mol % multi(EG)DMAs and swollen in methanol at 30°C.
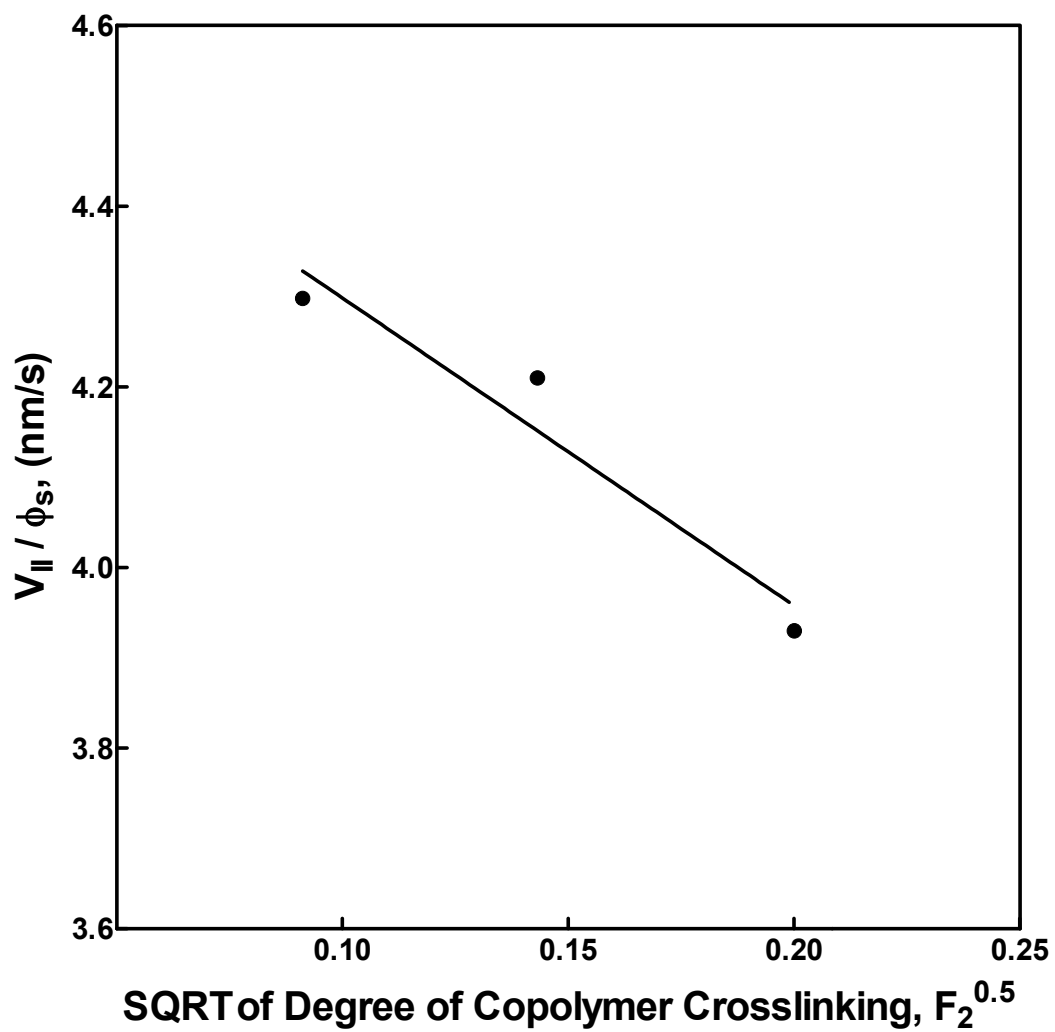
Figure 5.32: Normalized (by ϕ_s) Case II front velocity, V_{II}, versus the square root of the degree of copolymer crosslinking, $F_2^{0.5}$, in PMMA discs crosslinked with di(EG)DMA (and swollen in methanol at 30°C.
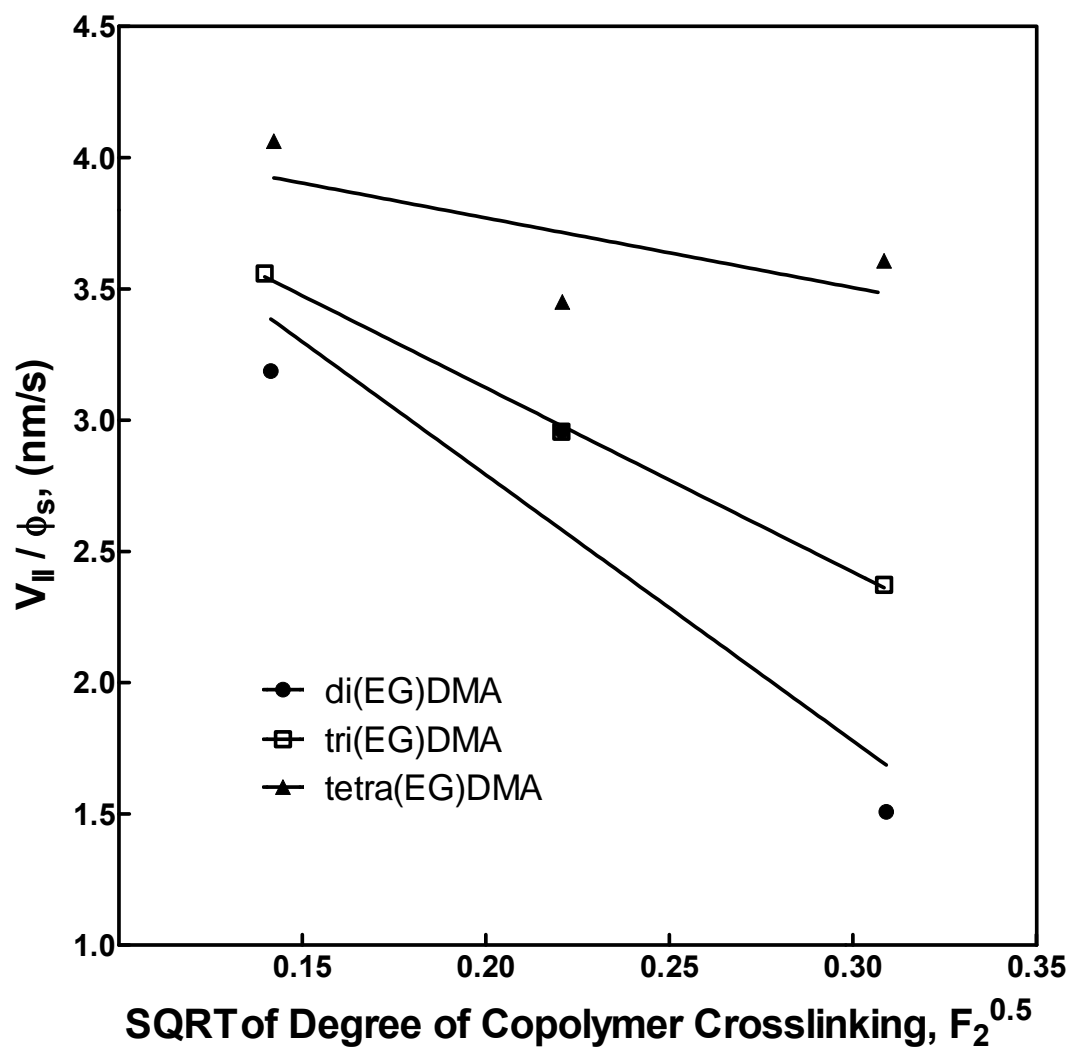
Figure 5.33: Normalized (by ϕ_s) Case II front velocity, V_{II}, versus the square root of the degree of copolymer crosslinking, $F_2^{0.5}$, in PMMA discs crosslinked with multi(EG)DMAs and swollen in methanol at 25°C.
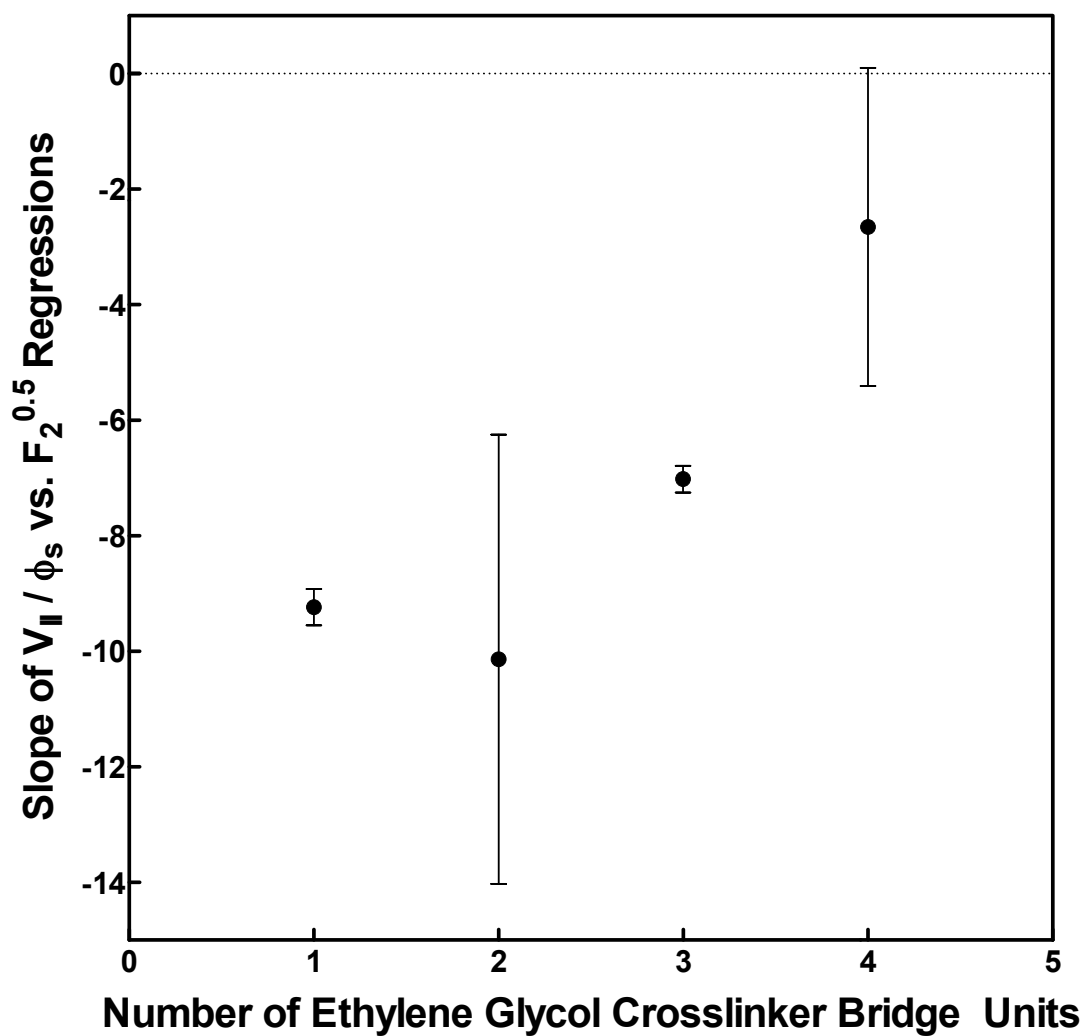
Figure 5.34: Slopes of normalized (by ϕ_s) Case II front velocity, V_{II}, versus the square root of the degree of copolymer crosslinking, $F_2^{0.5}$, for PMMA discs crosslinked with multi(EG)DMAs and swollen in methanol at 25°C.

Chapter 6: In situ Dynamics of Penetrant Transport as Revealed by High-Resolution X-Ray Computed Tomography

INTRODUCTION

While the qualitative features of Case II transport have been studied experimentally and in great detail, there have been very few *in situ* investigations concerning the mechanistic features of anomalous transport. A key experimental complication in examining this transport behavior is that information on the time-dependent penetrant concentration profiles within a polymer sample must be gathered to validate the observed mechanism. This was originally accomplished by adding iodine into methanol prior to sorption into glassy poly(methyl methacrylate), freezing the transport process at a time interval, microtoming the sample into thin slices, and determining the methanol concentration profile by measuring the iodine concentration in each slice [1]. While yielding valuable mechanistic information, this process was very time-consuming, required the destruction of one sample at each time point, and offered many opportunities for experimental error.

More recently, nuclear magnetic resonance (NMR) has been utilized for non-destructive, real-time collection of concentration profiles [2, 3]. However, limitations of the technique include low spatial resolution (typically 70 μm or more), a required cylindrical sample geometry of 5 mm in diameter or less, and image collection times of 10 minutes or greater. A recent review by Vesely [4] summarized nicely the typical experimental techniques that have been used previously to study diffusion of liquids in polymers. In this investigation, a new procedure for the detailed study of diffusion in polymers, including the collection of time-dependant concentration profiles, was developed and used to image anomalous transport of methanol into plasticized poly(methyl methacrylate).

High resolution X-ray computed tomography (CT) is a non-invasive method capable of visualizing features in the interior of opaque solid objects and obtaining digital information on their 3-D structure by mapping the variations in X-ray attenuation (closely related to density) within those objects. While CT has found widespread application in the medical and geological fields, it is used primarily to image stationary objects that are not changing in time. For this investigation, the CT procedures were adapted to obtain real and computerized profiles of polymeric discs slowly swelling in compatible penetrants.

The basic principle in CT is that an X-ray source emits X-rays in the form of a single beam (1st generation), a fan beam (2nd and 3rd generations), or a cone beam or collimated, thick parallel beam (volume scanning), these beams pass through the sample being scanned at a variety of angular orientations, and a series of detectors measures the extent to which the X-rays have been attenuated (absorbed or deflected) by the sample [5]. Information can thus be collected for a given sample in the form of horizontal slices of the material, which can then be stacked and a 3-dimensional image can be digitally reconstructed using software programs. Additional information on the CT technology, its typical applications, and the specific capabilities of the instrument used in this investigation have been discussed by Ketcham and Carlson [5].

MATERIALS AND METHODS

Sample Preparation

Homopolymers of methyl methacrylate (MMA) (Sigma-Aldrich, St. Louis, MO) and copolymers of MMA and pentabromobenzyl acrylate (PBBA) (Sigma-Aldrich) were synthesized using an *iniferter*-mediated, thermally-initiated free radical polymerization and were designated PMMA and P(MMA-co-PBBA), respectively. The crosslinking agent used was ethylene glycol dimethacrylate (EGDMA) (Sigma-Aldrich). PBBA and EGDMA were used as received, and MMA was passed through a pre-packed inhibitor removal column (Sigma-Aldrich) to remove hydroquinone prior to polymerization. All MMA

monomer was used within two weeks of inhibitor removal. The monomer molar feed ratios were 97.5:2.5 MMA:EGDMA for PMMA and 97.3:0.2:2.5 MMA:PBBA:EGDMA for P(MMA-co-PBBA). Lauroyl peroxide (Fluka/Sigma-Aldrich) was added as a thermal initiator in the amount of 0.5 wt % of the total monomer content. Tetraethylthiuram disulfide (TED) (Sigma-Aldrich) was added as an *iniferter* compound in a 1:1 molar ratio with the thermal initiator.

The components were prepared in a cylindrical glass reaction vessel which was silinized prior to use with Siliclad™ (Gelest, Morrisville, PA). The mixture was placed in an oxygen-free environment inside a sealed glove box and bubbled with nitrogen for 5 min to remove dissolved oxygen. The vessel was then sealed and placed in a water bath maintained at 60°C and allowed to polymerize for 48 hours. Following synthesis, the polymer cylinders (approximately 12.6 mm in diameter) were sliced into discs with a nominal thickness of 1 mm by a Isomet™ Low-Speed Saw with diamond wafering blades (Buehler®, Lake Bluff, IL), polished to remove surface defects by an abrasive slurry (Novus #2 Fine Scratch Remover, Savage, MN), and dried in a vacuum oven for 24 hours at 10°C below the glass transition temperature.

Gravimetric Studies

Discs of PMMA and P(MMA-co-PBBA) were suspended in methanol (Certified ACS Grade, Fisher Scientific, Pittsburgh, PA) in a glass jar on a raised aluminum mesh that occluded less than 3% of the lower disc surface. The glass jars were placed in a water bath set at 22°C and allowed to absorb methanol. Weight measurements were taken at time intervals of approximately 2.5 hours by removing a disc from methanol, drying the surface with a paper towel, and recording both the weight in air and the weight in a non-solvent (water) using an Ohaus Analytical Plus balance (Ohaus, Pine Brook, NJ). The measurements were taken in two ways. First, a set of 10 discs from the same cylinder was immersed in methanol at the same time and a different disc was measured at each time point, such that each disc was measured only once. Second, sets

of three discs, each set from one cylinder, were immersed at the same time and all discs were measured at each time point. Additionally, thickness and diameter measurements were taken both prior to immersion in methanol and once the discs had reached equilibrium using a digital caliper (Brown and Sharpe, North Kingstown, RI).

Computed Tomography

The CT experiment was carried out at the High Resolution X-ray CT Facility in the Department of Geological Sciences at The University of Texas at Austin. For this work, a volume scanning method using a collimated, thick parallel beam was chosen to promote rapid scanning, as information can be collected on all slices in a single rotation leading to a scanning time of less than three minutes. As a result, the error involved in imaging a dynamic process can be minimized, while still maintaining sufficient resolution for image clarity. The polymeric disc was immersed in methanol by laying it on low-density foam and was placed in the CT chamber at room temperature (22°C) as shown in Figure 6.1. Once preparation was complete, the sample was scanned, the 3-dimensional images were reconstructed, and the data were analyzed for disc volume and thickness, total sample attenuation, and attenuation profiles within the disc at 30-minute intervals for 12 hours. Additional data were collected after 24 hours and 120 hours to obtain equilibrium values. The CT device (Bio-Imaging Research, Inc., Lincolnshire, Illinois) was run on its ultra-high-resolution mode utilizing a 225 kV tube (Feinfocus FXE-200.20) with an adjustable focal spot with a minimum size of <10 µm at 8 W total load. The slice thickness was set at 27 µm, which led to approximately 37 slices of the dry polymeric disc. The 3-dimensional images were reconstructed from the raw CT data using Amira®, an image processing program, image artifacts were removed, and the images were sent through noise-reduction programs for visual clarity.

RESULTS AND DISCUSSION

In preliminary experiments for this investigation, discs of PMMA were first synthesized without the dopant comonomer PBBA. Since methanol is not a good solvent for PMMA and at equilibrium the volume fraction of methanol in the swollen polymer was around 0.2, the difference in X-ray attenuation in the dry (immediately upon immersion in methanol) and equilibrium states was only a 2.5 % decrease. Since the concentration profiles were determined by inference directly from the attenuation profiles within the polymer discs, a greater separation between initial and final states was desired. To this end, 1.0 wt % of PBBA was added to the PMMA discs. This monomer was chosen due to its highly attenuating substituent group structure (a benzene ring with five bromine atoms attached) and its favorable reactivity ratios with methyl methacrylate (r_{MMA} = 2.0 and r_{PBBA} = 0.9) [6]. This small addition of a dopant comonomer doubled the ultimate change in sample X-ray attenuation. However, this addition introduced an additional concern, namely that chains of P(MMA-co-PBBA) will have greater barriers to rotation and likely decrease the rate of polymer relaxation.

To answer this concern, samples were synthesized both with and without the PBBA dopant, keeping all other variables constant. The resulting polymer cylinders were cut into discs and used to perform gravimetric sorption studies for comparison. Figure 6.2 shows the fractional mass uptake curves for PMMA and P(MMA-co-PBBA) samples. The first 60 % of the fractional mass uptake of these curves were then fit to a time-shifted version of the power law model:

$$\frac{M_t}{M_\infty} = k(t - \tau)^n \qquad (6.1)$$

where t is time, τ is the induction time, M_t is the mass of penetrant sorbed at a time t, M_∞ is the equilibrium mass of penetrant sorbed, k is a kinetic constant (k can be related directly to the binary self-diffusion constant for Fickian transport dynamics), and n is the

power law exponent. The power law exponents obtained were 0.66 and 0.71 for the neat PMMA and doped PMMA, respectively. A value of 0.5 would indicate Fickian transport dynamics; a value of 1.0, Case II dynamics; and everything in between, anomolous tranpsort. Thus, incorporation of the dopant comonomer had only a slight impact on the observed behavior, shifting the transport dynamics towards the Case II regime. This was expected, since a more rigid chain backbone increases the polymer's characteristic relaxation time and heightens the concentration dependence of the binary diffusion coefficient. Similarly, the overal rate of sorption slowed slightly, with the kinetic constant dropping from 0.1 from 0.13 upon incorporation of the dopant. Thus, the incoporation of the dopant comonomer did not significantly affect the tranport mechanism or kinetics and comparisons of this experiment to others with neat PMMA were appropriate.

Additionally, intergral sorption experiments were performed using both a triplicate repeat and a single-use data collection method. The triplicate method required far fewer samples and experimental effort; however, the question remained as to whether or not removing the polymer discs briefly for weighing at regular intervals had a significant effect on the transport process. Figure 6.3 shows a comparison of these two modes and validates the accuracy of the triplicate data collection method under the conditions encountered in this thesis. It is reasonable to say that sorption profiles will only be altered by this method when the loss of penetrant to evaporation is significant compared to the mass gained between measurements. Thus, so long as meaurements are not taken too frequently use of the triplicate method will be appropriate.

The resulting reconstructed 3-D images (sliced in half to visualize the interior of the polymeric discs) are shown in Figures 6.4-6.8 for 0-12 hours, 23.5 hours, and 5 days after sample immersion. In these images, the attenuation values (and thus the density of the material) scales from light blue (low) to a darker blue (high). At time 0:00, the polymer disc displayed a uniform higher density since the disc was completely dry and

homogeneous. After six and eight hours, the persistence of a dry polymer core could be seen along with advancing fronts of higher methanol concentrations. After 12 hours, the inner, dry core had completely disappeared. The total attenuation of the swelling disc was related to the total mass of the disc at any time. Thus, a fractional mass uptake curve and equilibrium swelling values were constructed and compared to the average gravimetric results of 9 separate discs from the same P(MMA-co-PBBA) cylinder. The equilibrium CT and gravimetric data compared favorably as shown in Table 6.1; however, there was significant noise present in the non-equilibrium CT fractional mass uptake measurements due to the difficulty in determining the true physical boundary of swollen polymer and pure methanol with a fixed slice thickness of 27 μm.

Dynamic values for disc expansion over the course of the experiment are shown in Figure 6.9. Initially, the thickness expanded at a rate that was 5.4 times the rate of expansion of the diameter, highlighting the often highly anisotropic nature of swelling in glassy polymers. Around nine hours into the transport process, this trend reversed, and the diameter began to expand at a greater rate than the disc thickness. This shift in the expansion behavior corresponded very closely with the observed disappearance of the dry inner polymer core. Thus, the traditional contention that the dry core restricts the manner in which the polymer disc may expand and causes the anisotropic nature was validated. Additionally, the disc thickness expanded first well beyond its equilibrium value before gradually receding, even as the diameter continued to expand.

This anisotropic nature could also explain the appearance of overshoots in the sorption process, where the system at some point contains more methanol than its equilibrium structure can accommodate. In this particular case, the 24 hour CT values indicated a methanol content that was 8 % higher than the ultimate equilibrium value. After 24 hours, the disc thickness expansion was still 25 % higher than its equilibrium value, the diameter was still below its equilibrium value, and the system volume expansion was 6 % greater than its ultimate value. The dimensional swelling data thus corroborated the existence of the overshoot and indeed showed how this was created

144

as a result of the inherent anisotropy in anomalous transport mechanisms in glassy polymers. Finally, the dimensional data indicated an induction period of 45 minutes before swelling began. This was in agreement with induction times measured from fractional mass uptake data from both CT and gravimetric sorption experiments.

Penetrant concentration profiles in the disc were obtained by normalizing the average attenuation values with respect to the difference between the state at any point in time and the dry state and dividing this number by the ultimate difference in attenuation between the dry and fully swollen states. The concentrations at each slice were averaged over the interior region of the disc to reduce noise while avoiding the inclusion of edge effects. These profiles were then compared to the expected Fickian profiles, where the diffusion coefficient was obtained by forcing the gravimetric results to fit the power law model with an exponent of 0.50. The value of the diffusion coefficient was then calculated as 1.362×10^{-12} m^2/s and used in the rigorous solution of Fick's 2nd Law with appropriate boundary conditions [7].

The resulting concentration profile curves for 4-12 hours after immersion are shown in Figures 6.10-6.18. As noted in the 3-dimensional images, there was a dry core that was maintained until it began to disappear around 9 hours into the sorption process. This dry core was the result of advancing fronts marking a boundary between dry polymer and polymer containing just over 50 % of its equilibrium methanol mass. This type of front behavior was reminiscent of case II transport. However, these results showed continued swelling behind the advancing fronts that appeared to follow Fickian dynamics and accounted for the additional 50 % of the eventually absorbed methanol. This type of behavior could then be called anomalous transport, being a blend of both Fickian and non-Fickian dynamics.

The data indicated that at a critical penetrant concentration region the mechanism of transport quickly changed from non-Fickian to Fickian behavior. This was consistent with the notion that as the local methanol concentration in the polymer increased, the polymer chains gained more mobility and the characteristic relaxation

145

time decreased. At some point, this trend led to a separation of the diffusion and relaxation processes, whereby chain relaxation began to occur quickly enough to no longer restrict the transport process. In this case, it was most likely due to a glass/rubber transition at the critical methanol concentration. It can also be easily seen that the concentration profiles in the disc are off-center. This was the result of the polymer disc being placed on low-density foam. While this did not eliminate the diffusion of methanol into the bottom of the disc, it effectively reduced the overall surface area available for diffusion. This led to a reduced rate of penetrant transport into the bottom of the disc relative to the top, but did not affect the observed trends or transport mechanisms.

Thomas and Windle have previously shown increasingly anomalous penetrant transport profiles for methanol in PMMA when the temperature of the experiment was increased [1]. In their case, the departure from purely Case II transport was a result of the greatly increased speed of the advancing sorption fronts relative to the decrease in diffusional resistance in the swollen polymer behind the advancing fronts. Thus, the concentration of methanol at the sorption front could not be maintained and decreased throughout the experiment as the fronts advanced. The concentration profiles thus showed a Case II front that decreased in magnitude and velocity as the experiment proceeded and behaved as expected once the fronts had met. At the highest temperatures they tested, the Case II front was almost non-existent, yet the system still displayed a sharp, inwardly-advancing front.

In this experiment, the 24 hr period of sample drying removed only a portion of the unreacted monomer, leaving approximately 1.5 wt % methyl methacrylate. Samples that were dried for 6 months showed purely Case II transport and those without any drying exhibited a power-law exponent of 0.58, close to Fickian transport. The presence of the monomer plasticized the polymer chains and caused a glass/rubber transition at a lower penetrant concentration than was seen in dry PMMA. Since purely Case II transport for methanol in PMMA has been shown to occur regardless of whether the

146

swollen polymer is in the rubbery or glassy state [8], one might still expect to see a Case II front in this experiment. However, no evidence of a true Case II front was seen. It is possible that the fronts are in reality sharper than the data would lead us to believe, since there is a bleeding effect in CT images that broadens such abrupt transitions. However, no decline was noticed in the transition concentration behind the advancing front, and the concentration of methanol in the center of the polymer was still very low after the dry core had disappeared (Figure 6.16).

The observed concentration profiles were consistent with a two-regime transport with highly concentration-dependant transport kinetics in the glassy regime and Fickian transport in the rubbery regime. In the glassy regime, the local polymer relaxation kinetics and diffusion kinetics were both rapidly changing as the penetrant both plasticizes the polymer chains and increased the fractional free volume. This rapid change created a sharp, visible front that propagated through the polymer preceded by a significant Fickian precursor until the precursors met in the center and the dry polymer core disappeared. This behavior approached that of Case II transport; however, the plasticizing effect of the unreacted monomer present in the polymer reduced the relaxational resistance and allowed for a deformation-free transport process to occur. This experiment also indicated that the presence of the dry polymer core was necessary for the continued propagation of the sharp fronts, as once the precursors met the fronts ceased inward propagation and the continued swelling appeared to be Fickian in nature. In this experiment, since the Fickian precursors were very significant in magnitude, the sharp advance of the non-Fickian fronts was halted with just over 50 % of the total sorption process completed.

CONCLUSIONS

High-resolution X-ray computed tomography was successfully adapted to produce detailed information on the mechanistic features of swelling glassy polymers *in situ*. For the particular case discussed, where a PMMA disc with 1 wt % pentabromobenzyl acrylate incorporated into the chain structure and 1.5 wt % of unreacted monomer was swollen in methanol at 22°C, the CT technique clearly showed its anomalous mechanism and anisotropic nature. In addition, excellent agreement in equilibrium sorption values between the gravimetric and CT studies was found, thus validating the accuracy of the CT techniques described.

The PMMA and methanol combination at room temperature is one of the classic instances where Case II transport can be seen; however, the presence of unreacted monomer plasticized the polymer, thus reducing its relaxational resistance to expansion. This resulted in a departure from deformation-driven Case II dynamics to highly concentration dependant transport kinetics in the glassy regime and Fickian kinetics in the rubbery regime. This experiment shed light on one of many scenarios that can lead to anomalous transport kinetics, broadly defined as any transport behavior lying seemingly between the two extremes of Fickian and Case II dynamics and having a fitted power-law exponent between 0.5 and 1.0.

As an experimental means for visualizing penetrant transport profiles in glassy polymers, CT compared favorably with the previous state-of-the-art method utilizing solid-state, spin-echo NMR techniques. Both require expensive equipment that is not extensively available and specialized knowledge of data analysis procedures, but the edge in this regard and in cost to run an individual experiment goes to NMR. However, the improved sample resolution, decreased size and geometry restrictions, and faster data collection rates make CT a very powerful tool for such applications.

REFERENCES

1. Thomas, N. and A.H. Windle, *Transport of Methanol in Poly(Methyl Methacrylate).* Polymer, 1978. **19**(3): p. 255-265.
2. Cranitch, L., D.J.T. Hill, and A.K. Whittaker, *A study of the swelling of copolymers of NIPAM and DMA with water by NMR imaging.* Applied Magnetic Resonance, 2007. **32**(1-2): p. 51-62.
3. Weisenberger, L.A. and J.L. Koenig, *NMR Imaging of Solvent Diffusion in Polymers.* Applied Spectroscopy, 1989. **43**(7): p. 1117-1126.
4. Vesely, D., *Diffusion of liquids in polymers.* International Materials Reviews, 2008. **53**(5): p. 299-315.
5. Ketcham, R.A. and W.D. Carlson, *Acquisition, optimization and interpretation of X-ray computed tomographic imagery: applications to the geosciences.* Computers & Geosciences, 2001. **27**(4): p. 381-400.
6. Merfeld, G.D., T.T. Maa, K. Chan, and D.R. Paul, *Synthesis and blends of pentabromobenzyl acrylate copolymers.* Polymer, 2000. **41**(2): p. 663-674.
7. Crank, J., *The Mathematics of Diffusion*. 2nd ed. 1975, New York: Oxford University Press. p. 47.
8. Thomas, N.L. and A.H. Windle, *A Deformation Model for Case-II Diffusion.* Polymer, 1980. **21**(6): p. 613-619.

Table 6.1: Comparison of gravimetric and CT equilibrium swelling ratios for methanol sorption in P(MMA-co-PBBA) discs at 22°C.

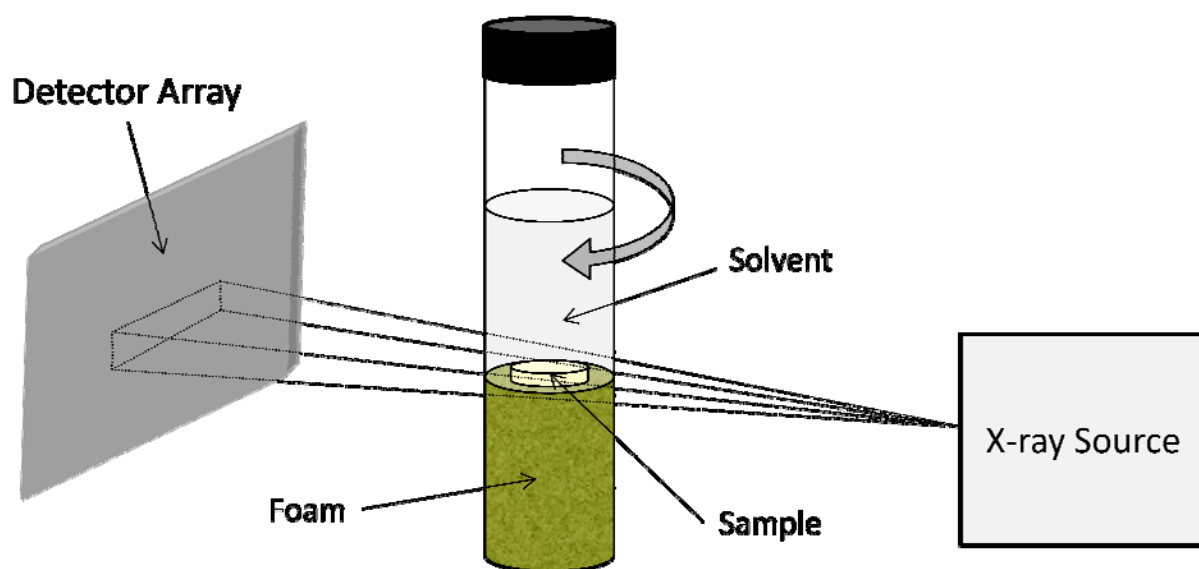|	Gravim. Data	CT Data	Difference (%)
q (weight swelling)	1.139	1.152	1.128
Q (volume swelling)	1.199	1.190	-0.756
Diameter Expansion	1.037	1.051	1.332
Thickness Expansion	1.079	1.077	-0.185

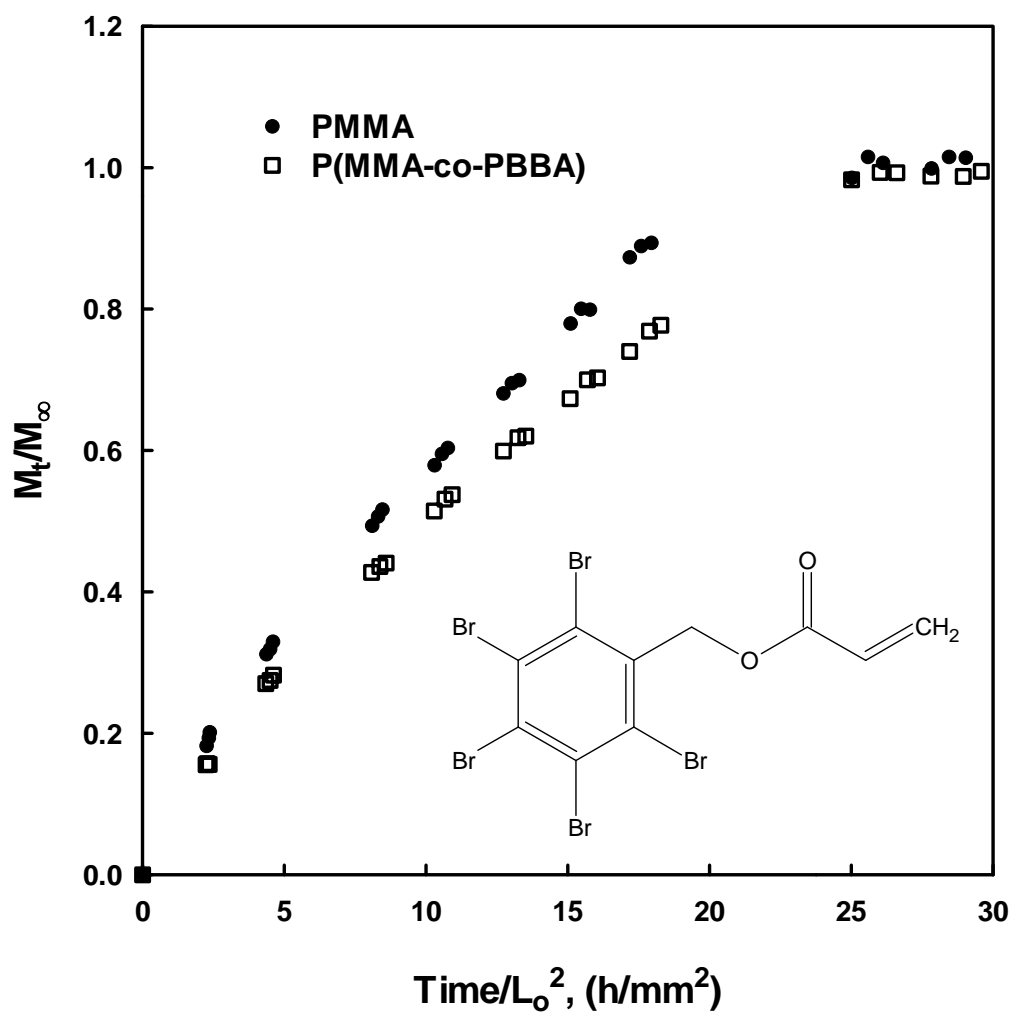Figure 6.1: Representative diagram of CT experimental procedure.

Figure 6.2: Comparison of gravimetric swelling results for PMMA and a PMMA copolymer with 1 wt % pentabromobenzyl acrylate (structure shown).
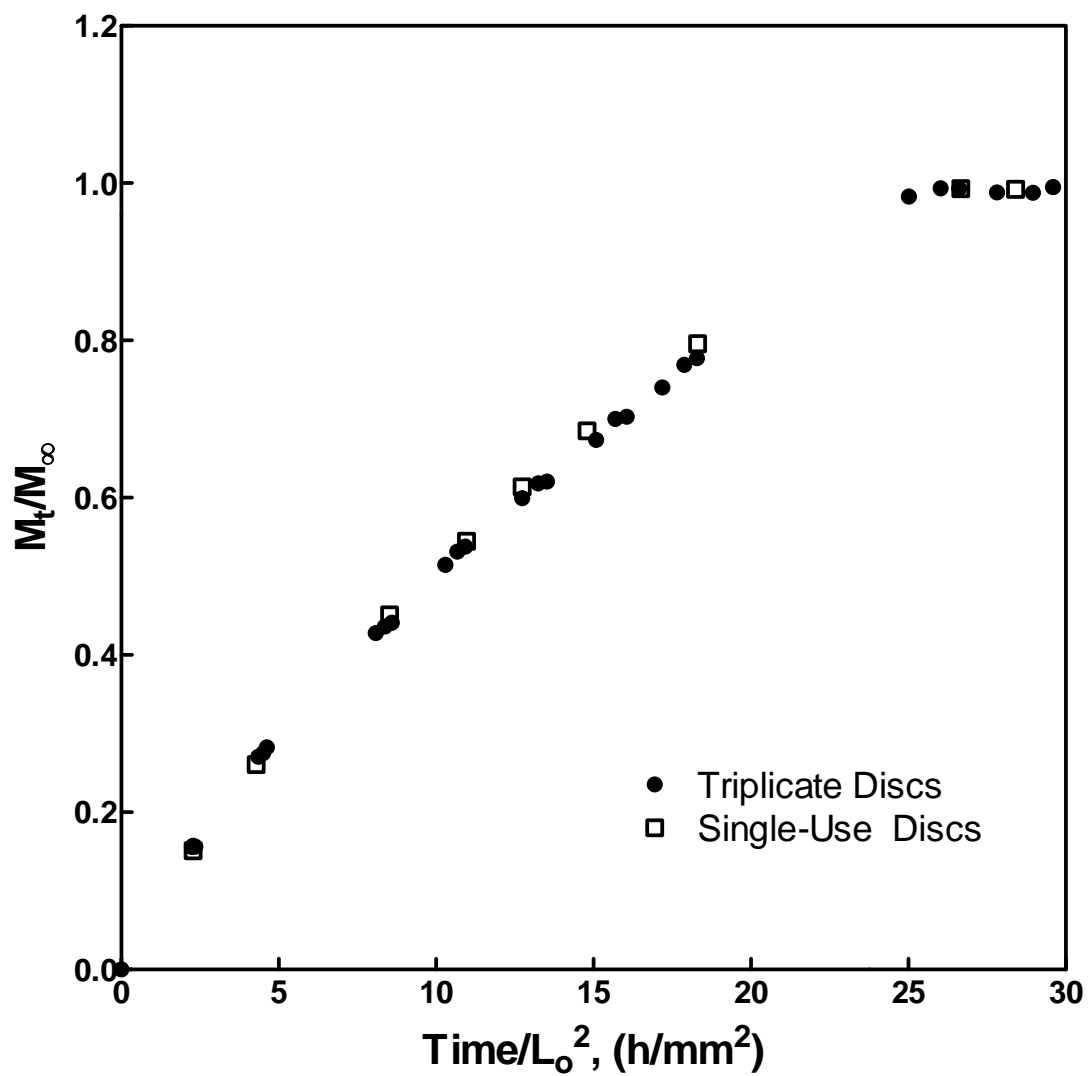
Figure 6.3: Comparison of triplicate and single-use-disc gravimetric methods for P(MMA-co-PBBA) discs with 2.5 mol % EGDMA dried for 24 hours and swollen in methanol at 22°C.

Figure 6.4: Computer-processed CT images for a P(MMA-co-PBBA) disc swelling in methanol at 22°C after 0, 1, and 2 hours.
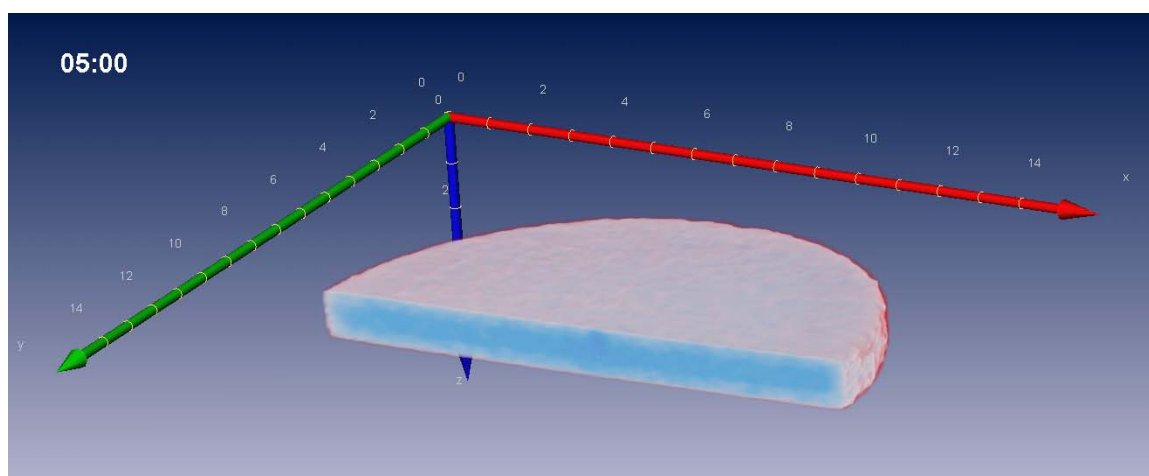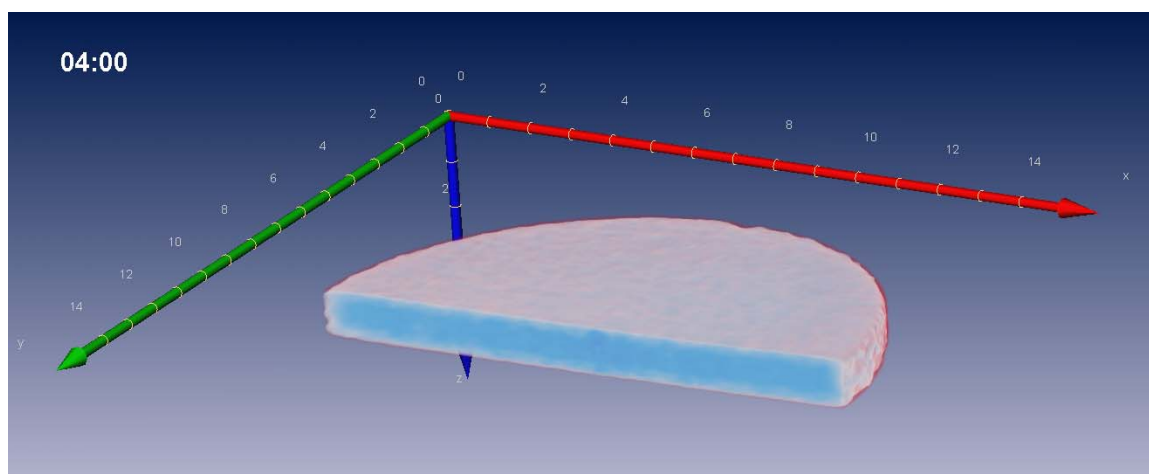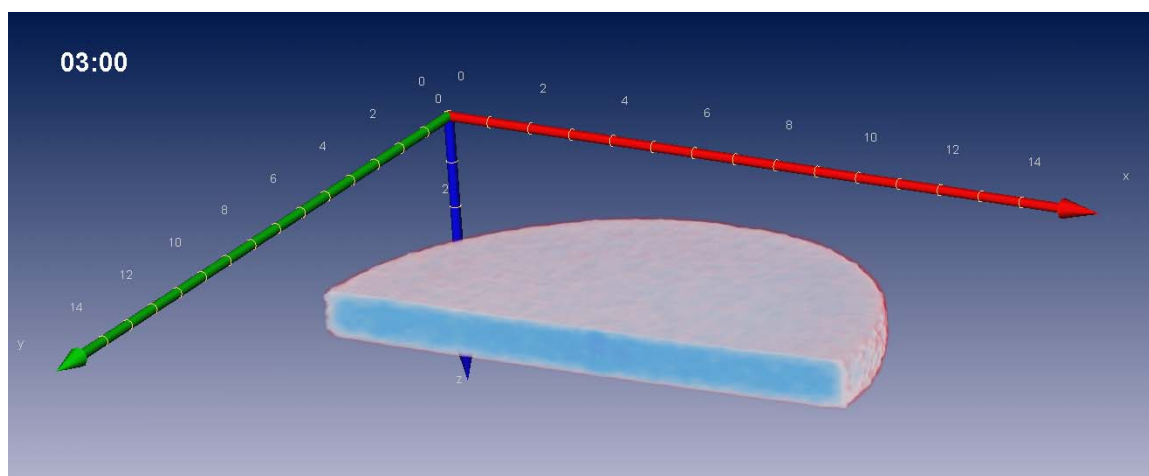
Figure 6.5: Computer-processed CT images for a P(MMA-co-PBBA) disc swelling in methanol at 22°C after 3, 4, and 5 hours.
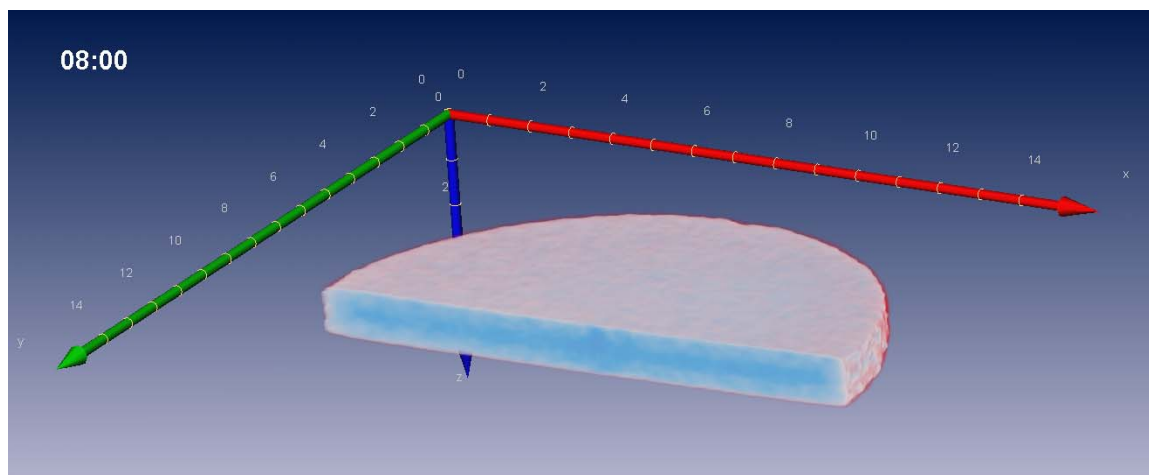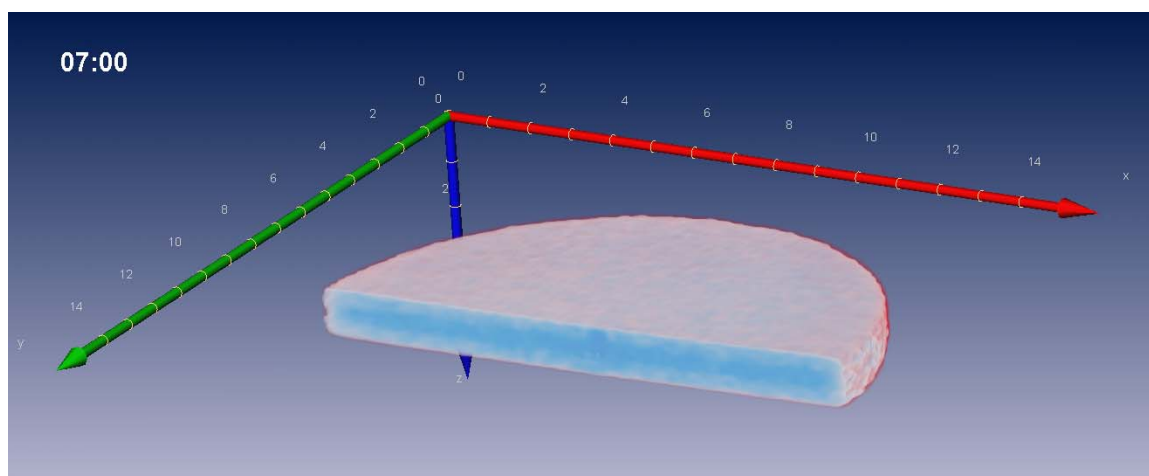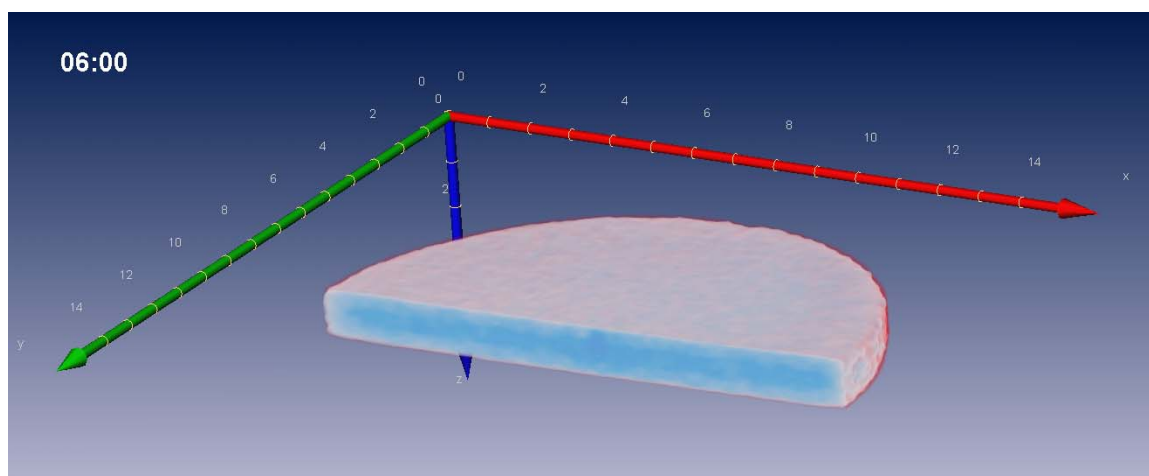
Figure 6.6: Computer-processed CT images for a P(MMA-co-PBBA) disc swelling in methanol at 22°C after 6, 7, and 8 hours.
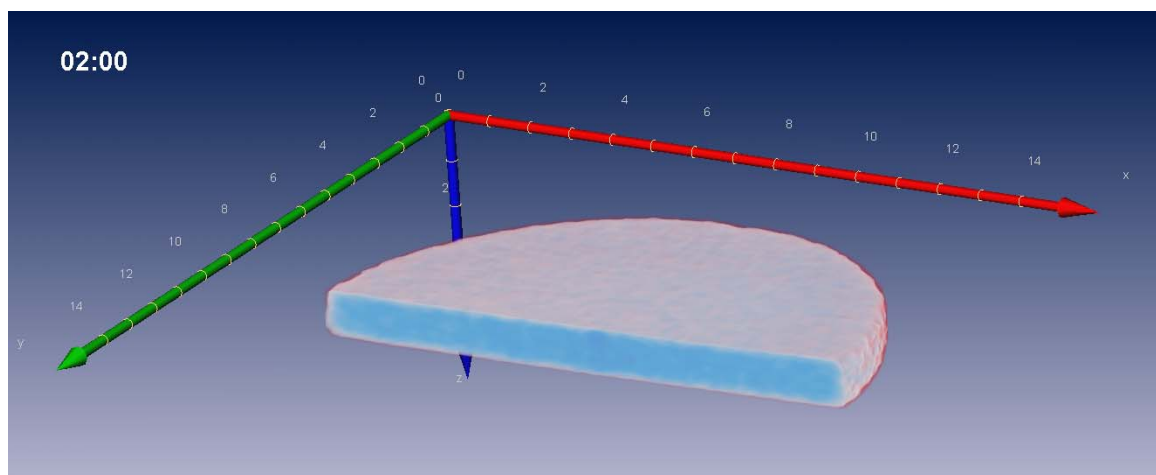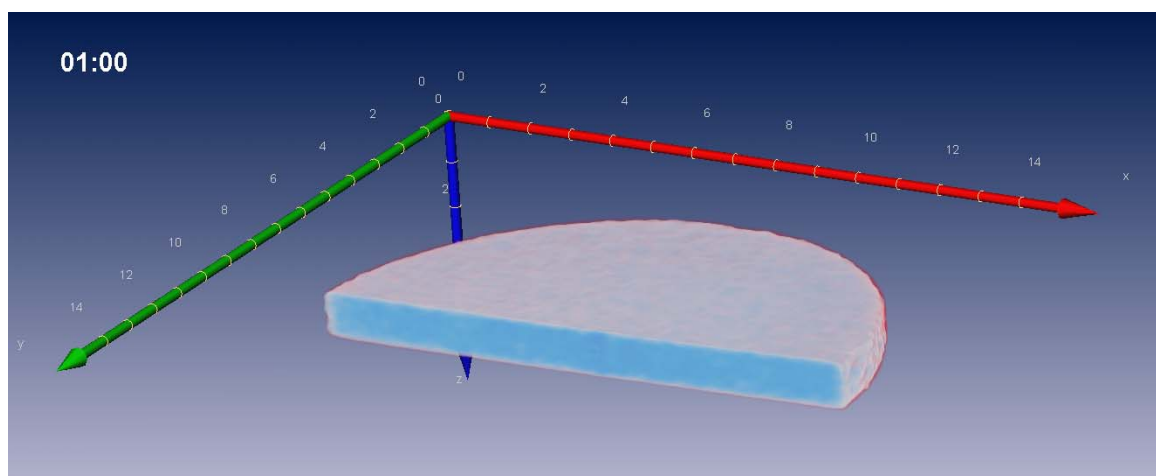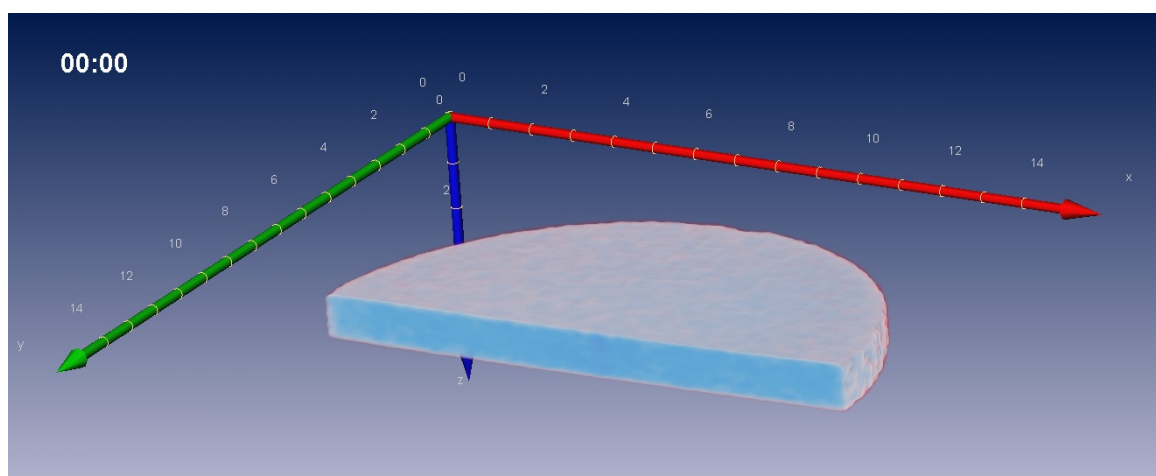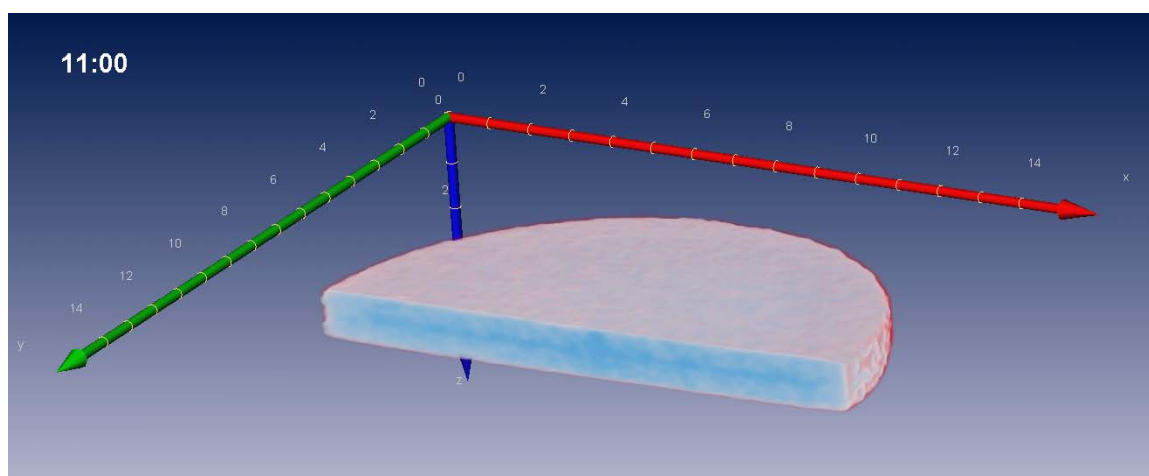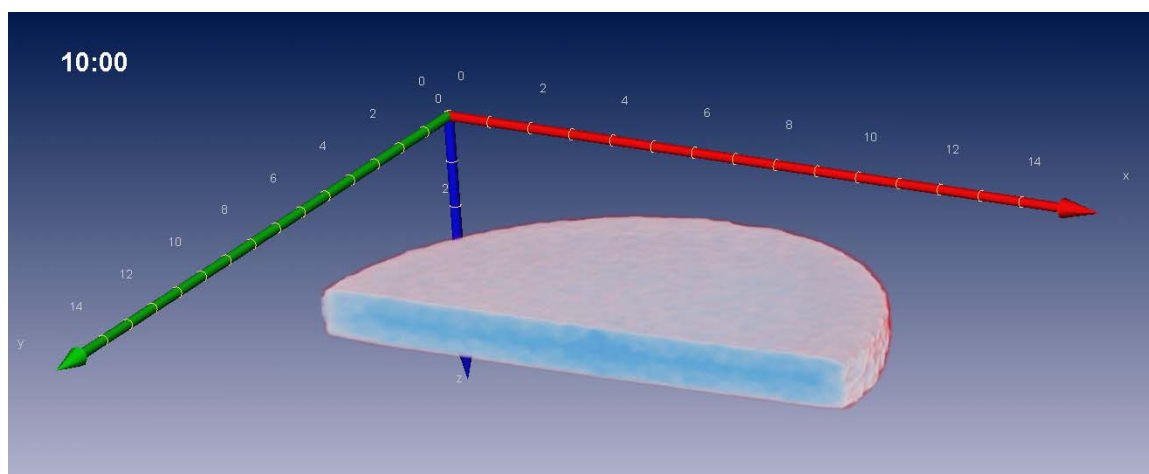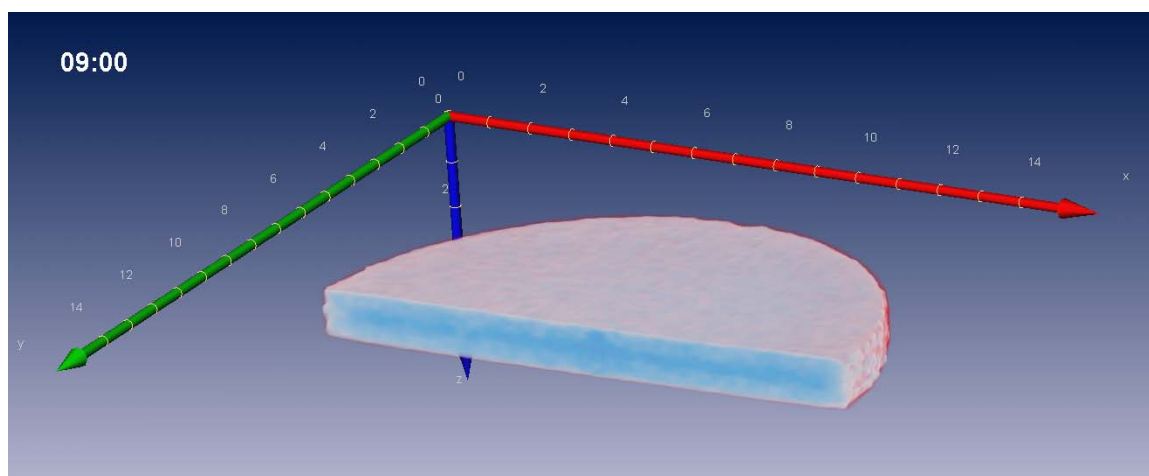
Figure 6.7: Computer-processed CT images for a P(MMA-co-PBBA) disc swelling in methanol at 22°C after 9, 10, and 11 hours.
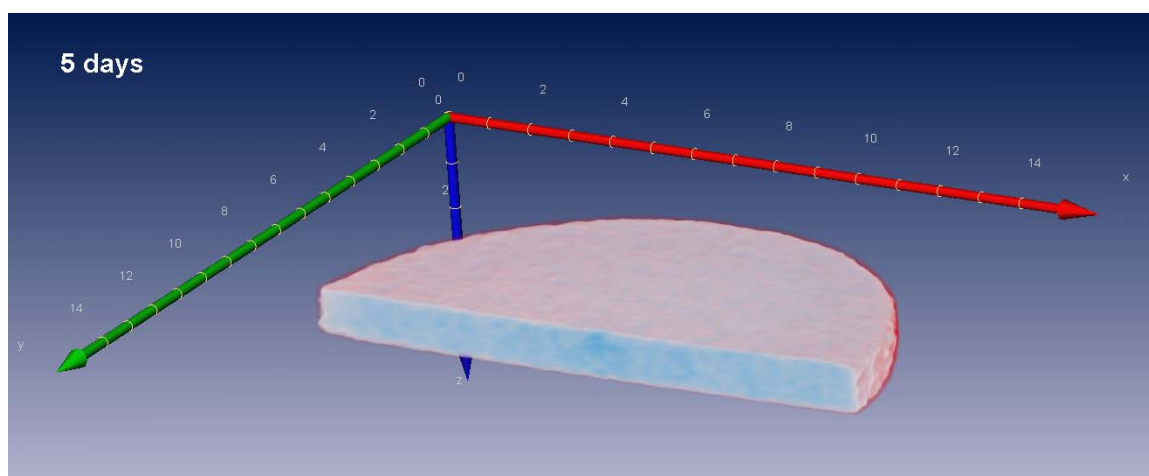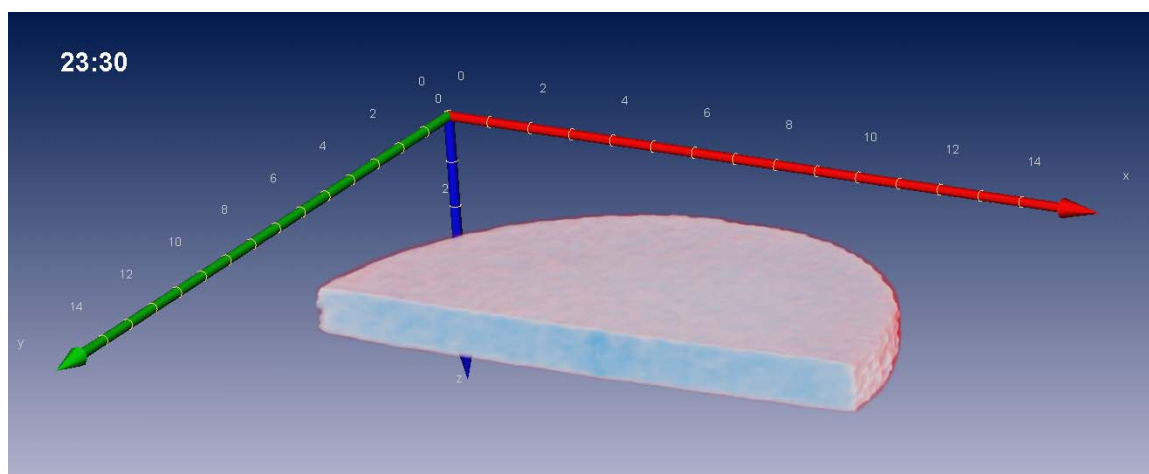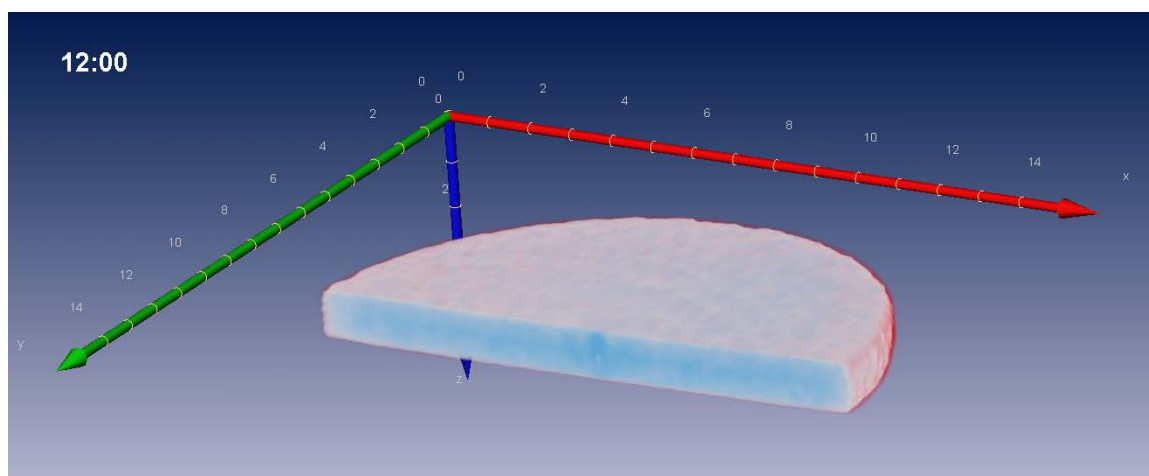
Figure 6.8:   Computer-processed CT images for a P(MMA-co-PBBA) disc swelling in methanol at 22°C after 12 hours, 23.5 hours, and 5 days.
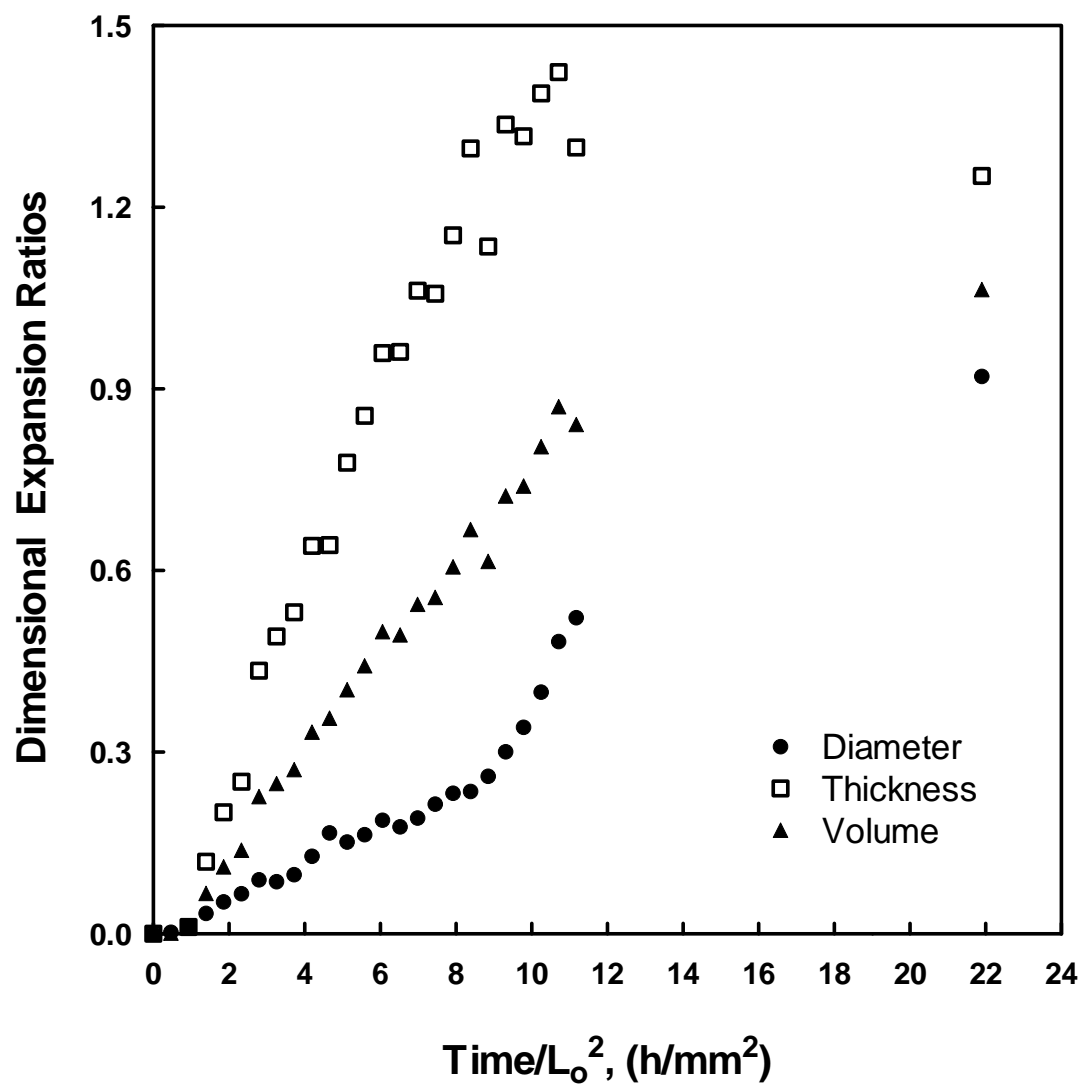
Figure 6.9: Dimensional changes during swelling of a P(MMA-co-PBBA) disc in methanol at 22°C (CT Data).
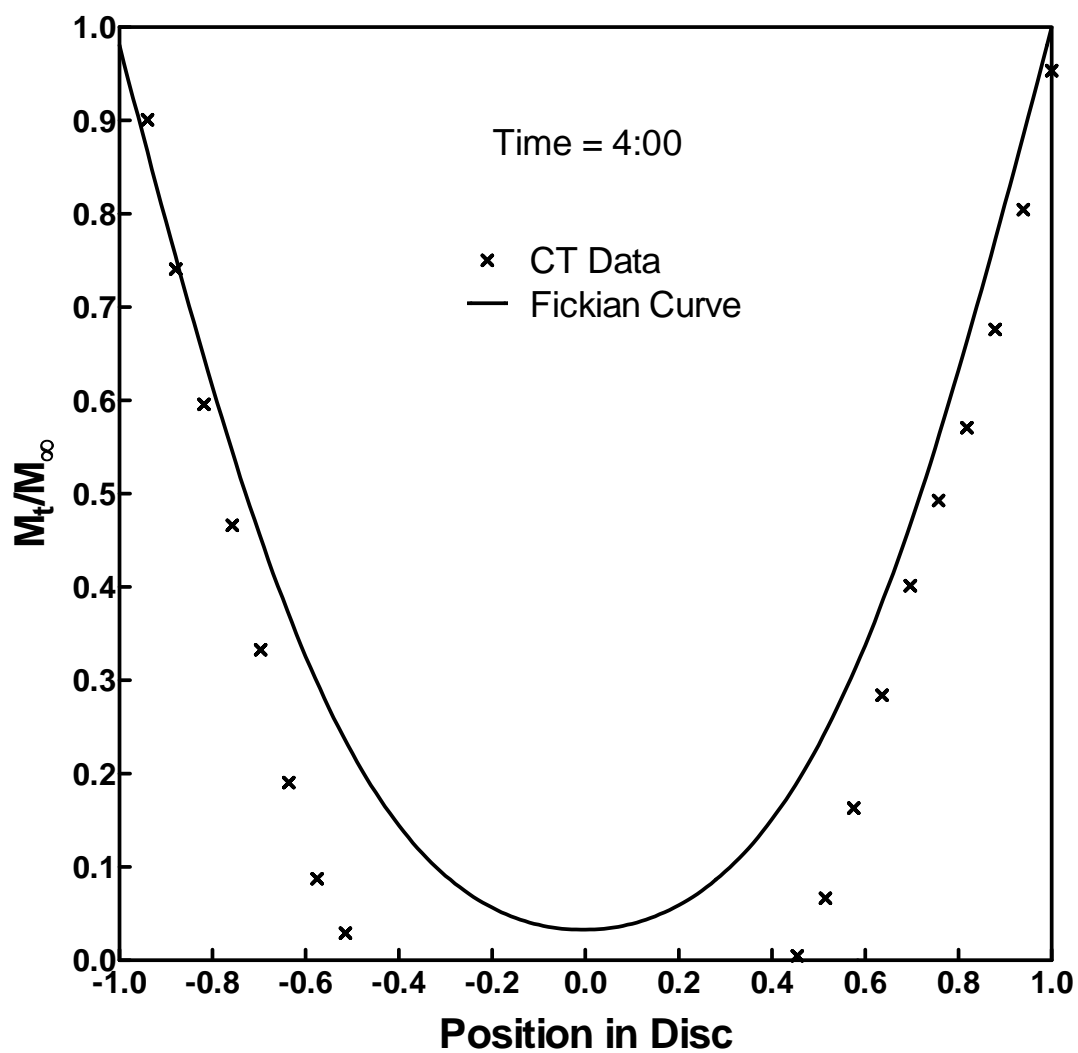
Figure 6.10: Comparison of the solvent concentration profile through a PMMA disc swelling in methanol at 22°C with the expected Fickian profile after four hours.
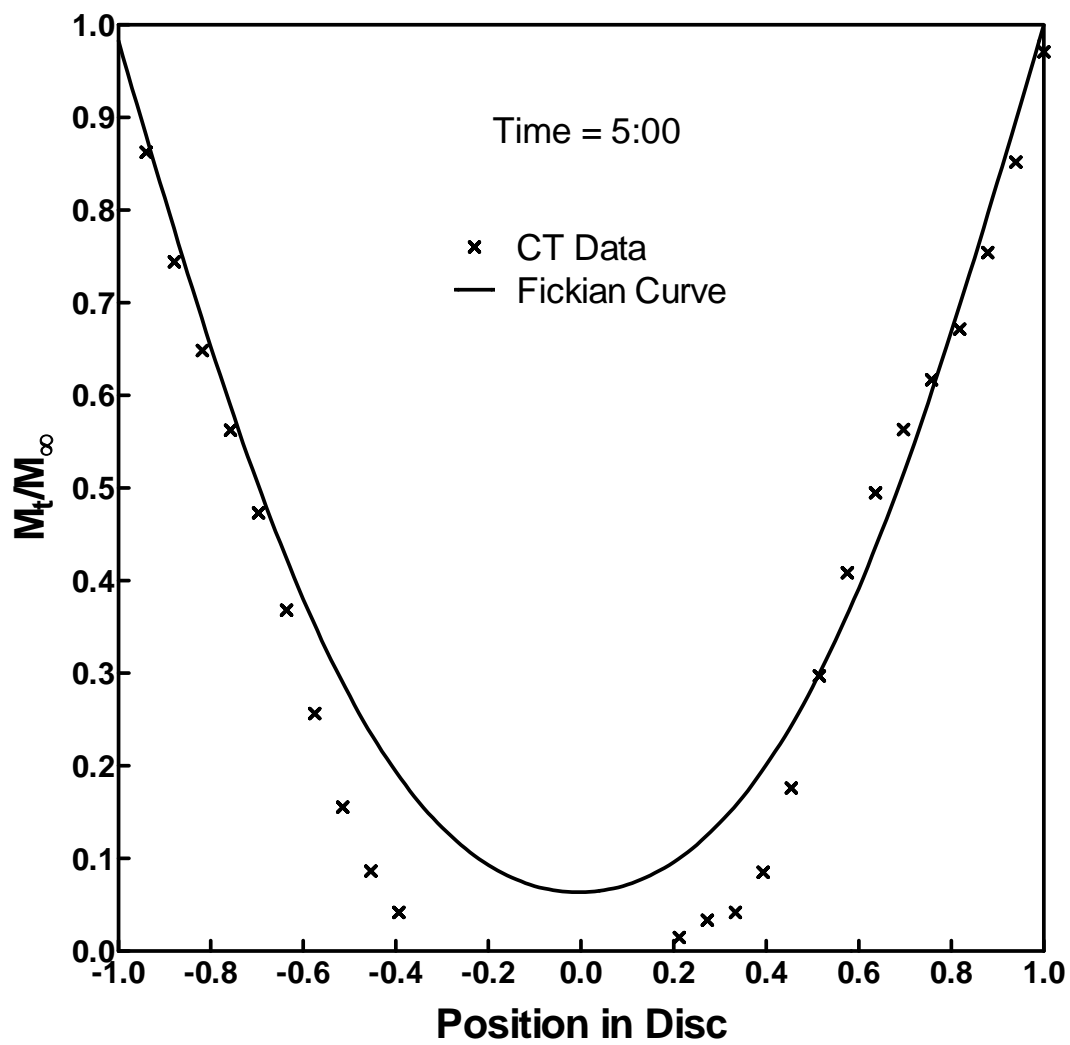
Figure 6.11: Comparison of the solvent concentration profile through a PMMA disc swelling in methanol at 22°C with the expected Fickian profile after five hours.
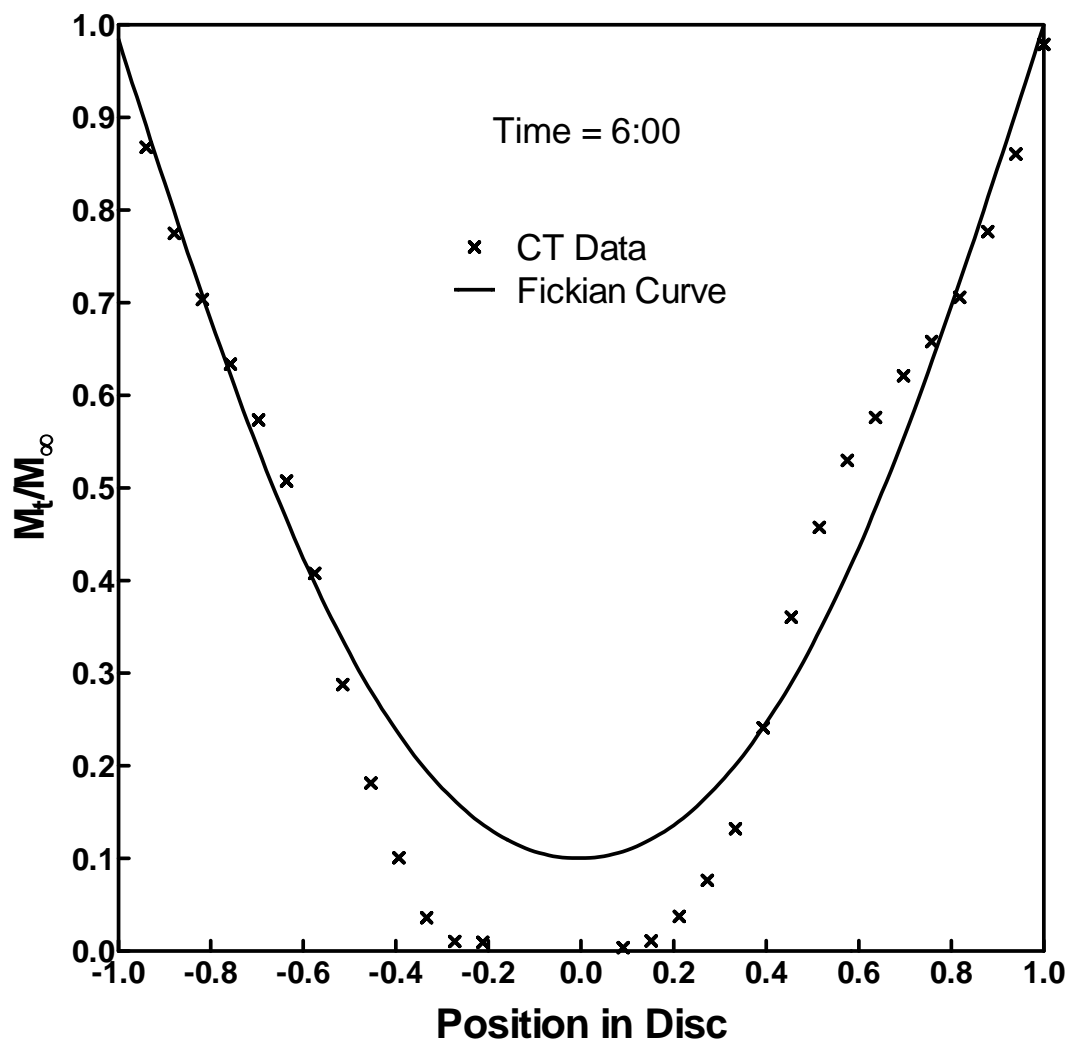
Figure 6.12: Comparison of the solvent concentration profile through a PMMA disc swelling in methanol at 22°C with the expected Fickian profile after six hours.
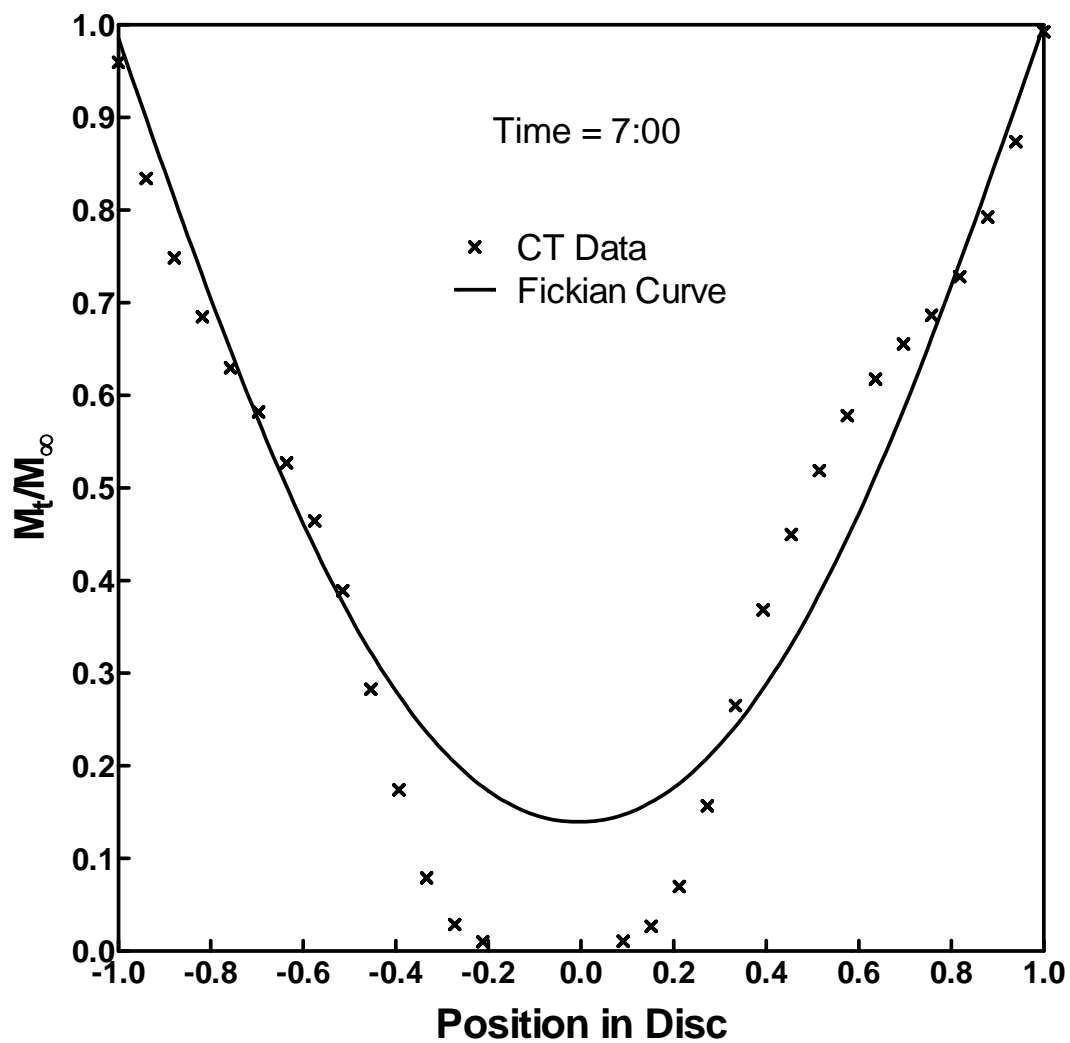
Figure 6.13: Comparison of the solvent concentration profile through a PMMA disc swelling in methanol at 22°C with the expected Fickian profile after seven hours.
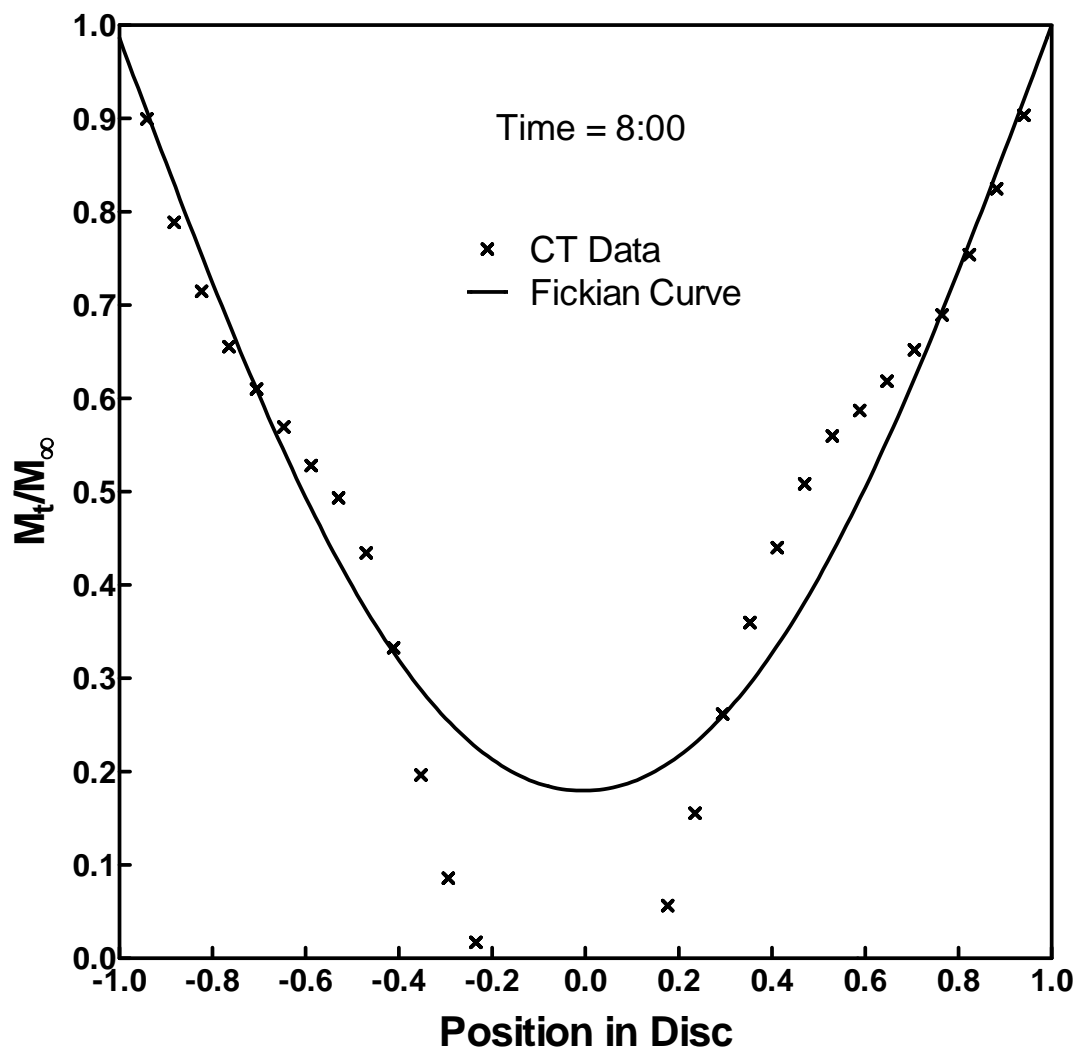
Figure 6.14: Comparison of the solvent concentration profile through a PMMA disc swelling in methanol at 22°C with the expected Fickian profile after eight hours.
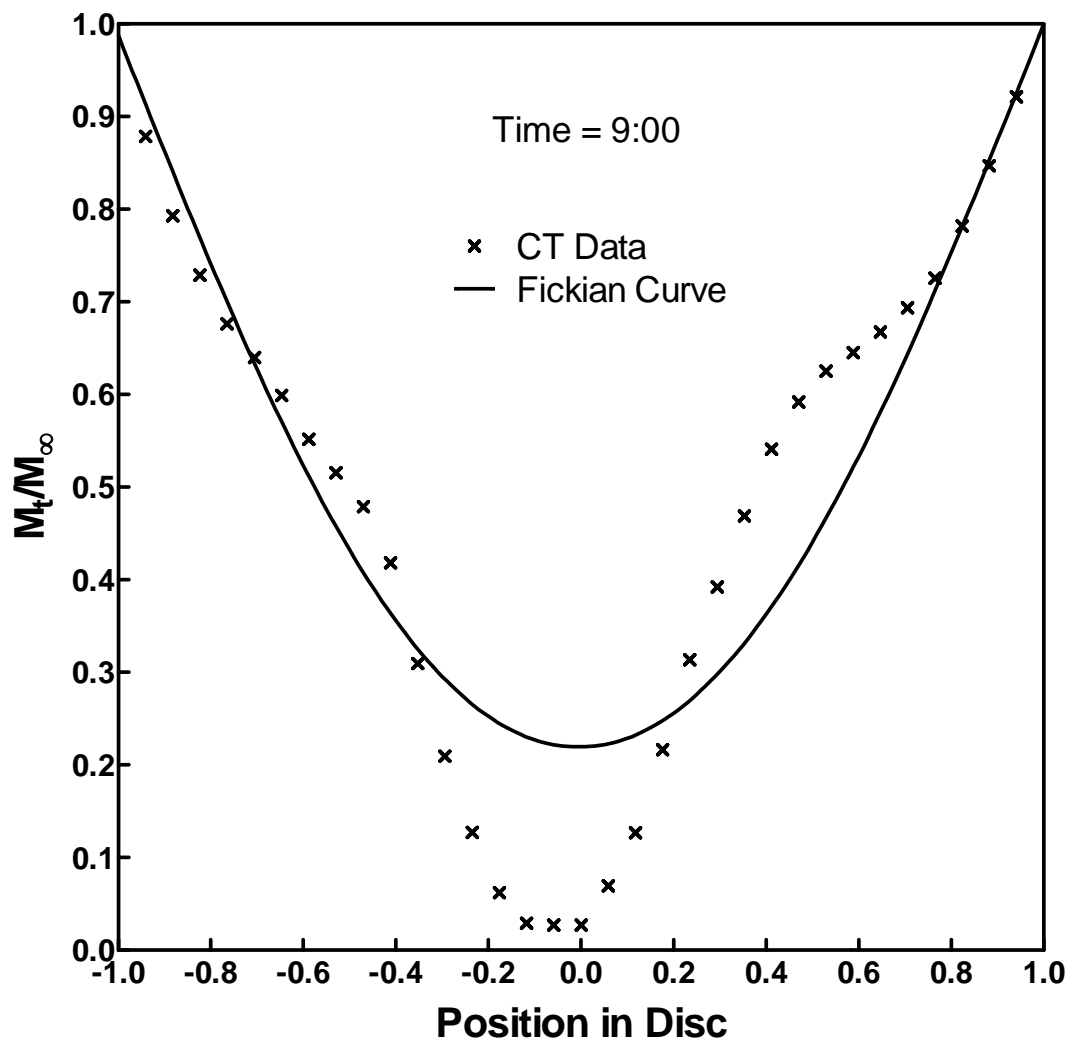
Figure 6.15: Comparison of the solvent concentration profile through a PMMA disc swelling in methanol at 22°C with the expected Fickian profile after nine hours.
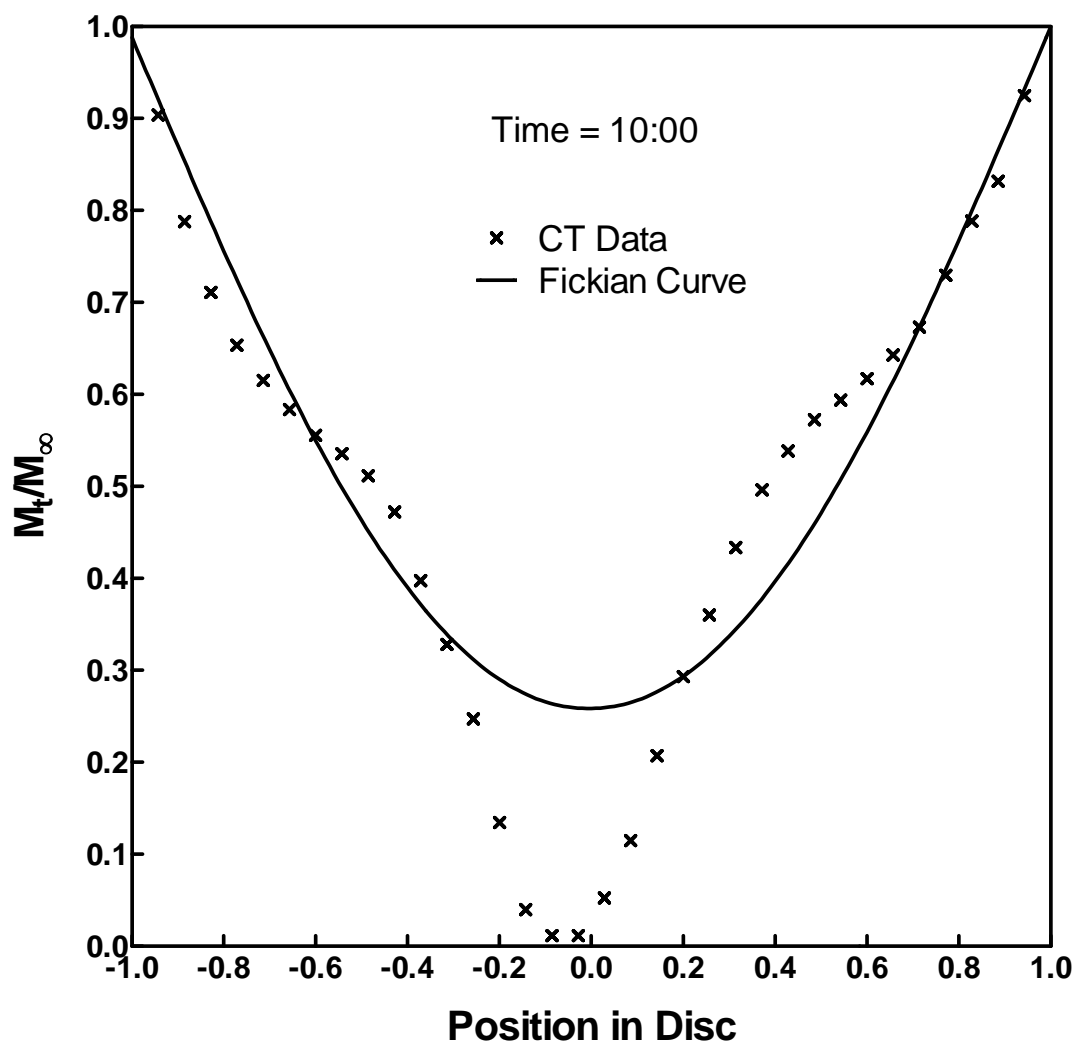
Figure 6.16: Comparison of the solvent concentration profile through a PMMA disc swelling in methanol at 22°C with the expected Fickian profile after ten hours.
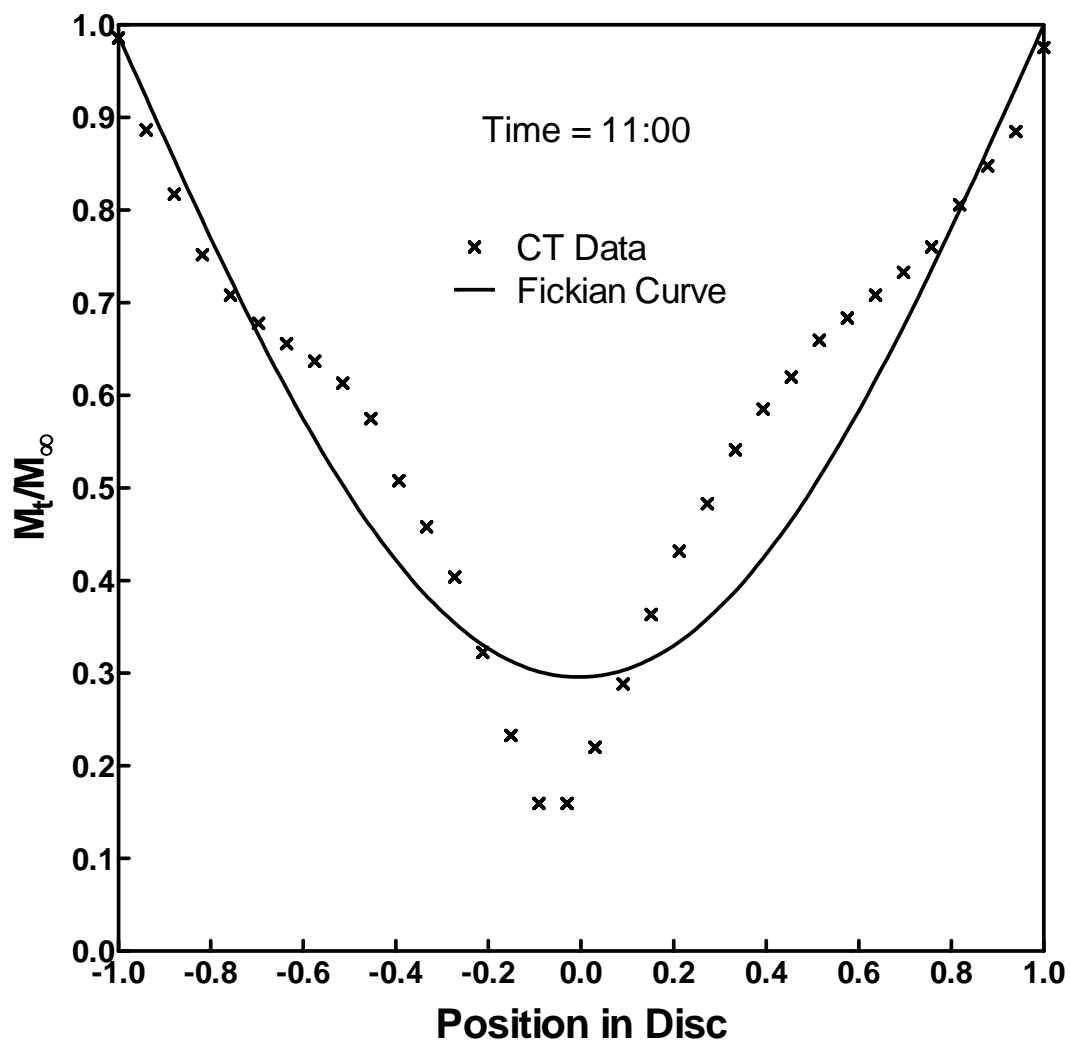
Figure 6.17: Comparison of the solvent concentration profile through a PMMA disc swelling in methanol at 22°C with the expected Fickian profile after eleven hours.
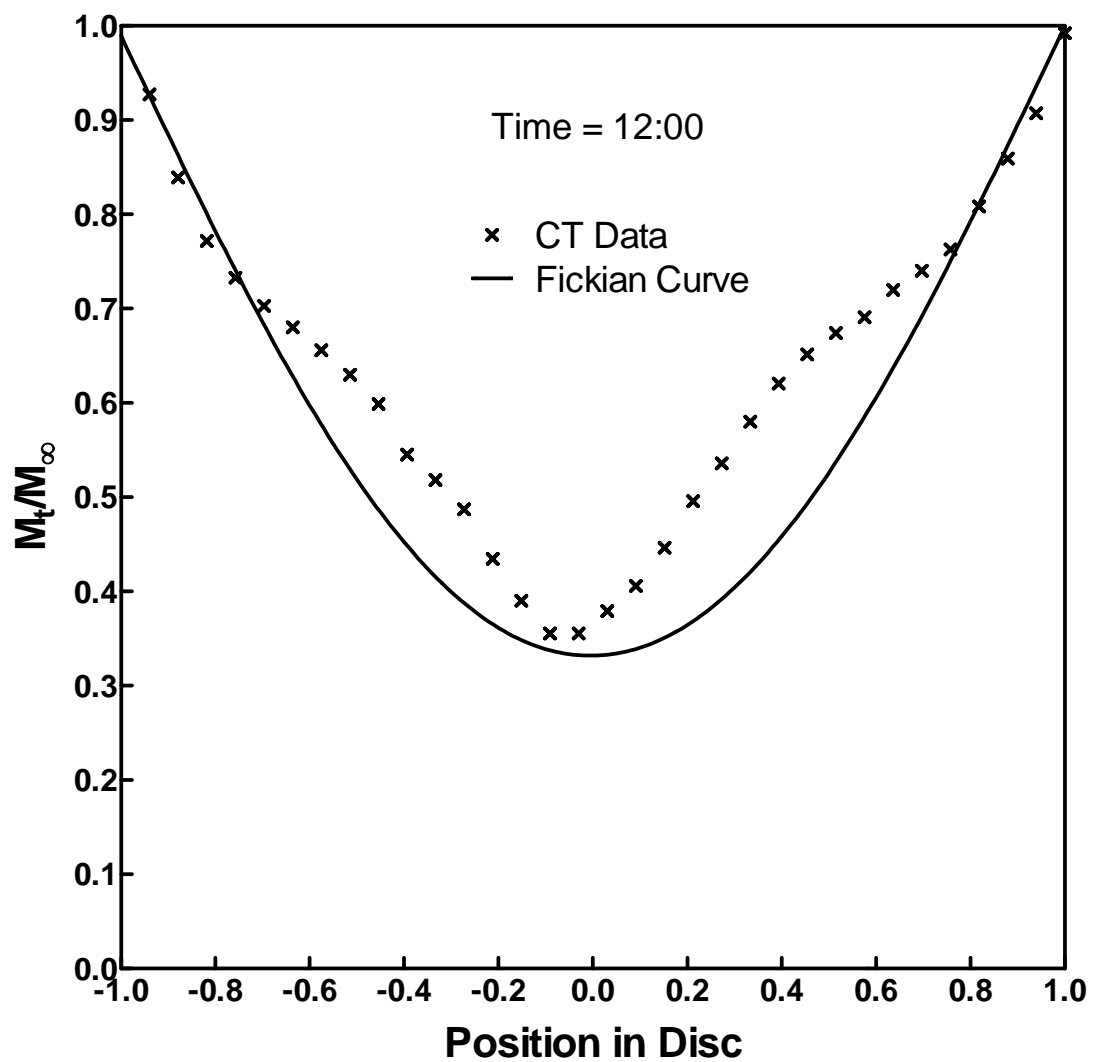
Figure 6.18: Comparison of the solvent concentration profile through a PMMA disc swelling in methanol at 22°C with the expected Fickian profile after twelve hours.

Chapter 7: Penetrant Transport into Glassy Poly(2-Hydroxyethyl Methacrylate) and Poly(Vinyl Alcohol)

INTRODUCTION

In addition to studying the transport behavior of a model system for Case II and anomalous transport (PMMA-methanol), it was desired to investigate sorption in additional polymer-penetrant systems. To this end, poly(2-hydroxyethyl methacrylate) (PHEMA) and poly(vinyl alcohol) (PVA) were chosen for investigation. PHEMA is a similar, though now hydrophilic, polymer to PMMA. PVA on the other hand is a semi-crystalline, hydrophilic polymer, which afforded the ability to investigate the effects of both the degree of crosslinking and the degree of crystallinity on the penetrant transport process.

MATERIALS AND METHODS

Poly(2-Hydroxyethyl Methacrylate) Preparation

Homopolymers of 2-hydroxyethyl methacrylate (HEMA) (Sigma-Aldrich, St. Louis, MO) were synthesized using an *iniferter*-mediated, thermally-initiated free radical polymerization. The crosslinking agent used was ethylene glycol dimethacrylate (EGDMA) (Sigma-Aldrich). EGDMA was used as received, and HEMA was passed through a pre-packed inhibitor removal column (Sigma-Aldrich) to remove hydroquinone prior to polymerization. All HEMA monomer was used within two weeks of inhibitor removal. Benzoyl Peroxide (Sigma-Aldrich) was added as a thermal initiator in the amount of 0.5 wt % of the total monomer content. Tetraethylthiuram disulfide (TED) (Sigma-Aldrich) was added as an *iniferter* compound in a 1:1 molar ratio with the thermal initiator.

The components were prepared in a cylindrical glass reaction vessel which was silanized prior to use with Siliclad^TM (Gelest, Morrisville, PA). The mixture was placed in an oxygen-free environment inside a sealed glove box and bubbled with nitrogen for 5

min to remove dissolved oxygen. The vessel was then sealed and placed in a water bath maintained at 60°C and allowed to polymerize for 48 hours (~1.7 initiator half-lives). Following synthesis, the polymer cylinders (approximately 25 mm in diameter) were sliced into discs with a nominal thickness of 1 mm by a Isomet™ Low-Speed Saw with diamond wafering blades (Buehler®, Lake Bluff, IL), polished to remove surface defects by an abrasive slurry (Novus #2 Fine Scratch Remover, Savage, MN), and dried and annealed in a vacuum oven prior to use.

Poly(Vinyl Alcohol) Preparation

Samples of poly(vinyl alcohol) (PVA) were prepared by a solvent casting procedure on commercially purchased material. To this end, PVA with a weight average molecular weight of 124,000 – 186,000 g/mole was purchased in powder form (Sigma-Aldrich). Solutions of 10 wt % PVA in water were then prepared and poured into 0.5 cm deep Teflon™ wells. Crosslinking of the films was next carried out by the addition of glutaraldehyde (Sigma-Aldrich) in the presence of sulfuric acid (Sigma-Aldrich) as a catalyst and methanol (Sigma-Aldrich) as a quenching agent at 75°C for 25 min. All chemicals were used as received and their structures are shown in Figure 7.1. The PVA gels were then dried slowly in an incubator at 37°C until a constant weight was obtained. The resulting films were approximately 0.2 mm thick and were prepared for characterization (3 cm x 3 cm) and penetrant transport studies (1 cm x 1 cm).

Characterization

The thermal properties of the polymer samples were characterized by differential scanning calorimetry (Perkin Elmer DSC 7, Perkin Elmer, Waltham, MA) using a heat/cool/heat method. A sample of each polymer batch to be tested was cut into a small section with tin snips or a cork borer. Once ready, 10-15 mg samples were placed into the DSC, heated from 50°C to 180°C (or higher temperatures as needed), and then cooled back to 50°C at a rate of 10°C/min in order to erase any thermal histories present

in the polymer and to remove moisture that might interfere with the signal. The samples were then heated a second time from 50°C to 180°C and the glass transition temperature, T_g, was determined as the halfway point during the change in heat capacity of the polymer associated with the transition from glass to rubber (1/2 ΔC_p method). Additionally, for PVA films, the degree of crosslinking was determined from integration of the melting peak divided by the sample mass and dividing the resulting heat of melting, ΔH_m, value obtained by the heat of melting of 100 % crystalline PVA (138.6 J/g) [1].

X-ray diffraction (XRD) experiments were also performed on PVA films to evaluate the degree of crystallinity, crystalline domain size, and lamellar spacing. The scanning angle, θ, was altered and the degree of X-ray diffraction (at a wavelength, λ, of 1.54 Å) was measured. The lamellar thickness, t, was then calculated by means of the Scherrer Equation [2]:

$$t = \frac{0.9\lambda}{B\cos\theta}$$
(7.1)

where B is the half-width at the half-height (in rad). The overall degree of crystallinity was then determined by integration of the peak area.

Finally, dynamic mechanical analysis (DMA 983, TA Instruments, and New Castle, DE) was used to determine basic mechanical properties of PHEMA samples. Rectangular samples (~2 mm x 8 mm x 20 mm) were cut for each polymer to be tested. Once prepared, the samples were placed into the DMA device and the device was run on resonant mode from 60°C to 180°C (or higher temperatures as needed). In this manner, the shear storage modulus, G'; the shear loss modulus, G''; the onset T_g based on G'; and the tanδ peak T_g were determined.

Gravimetric Studies

Discs of PHEMA and films of PVA were suspended in ethanol and/or ultra-pure water (Certified ACS Grade, Fisher Scientific, Pittsburgh, PA) in glass jars on a raised aluminum mesh that occluded less than 3% of the lower disc/film surface. The glass jars were placed in a constant-temperature water bath or a refrigerator and allowed to absorb penetrant. Weight measurements were taken at time intervals by removing a disc/film from the penetrant, drying the surface with a paper towel, and recording the weight in air using an Ohaus Analytical Plus balance (Ohaus, Pine Brook, NJ). For each PHEMA experiment, sets of three discs were immersed at the same time and all discs were measured at each time point. For each PVA experiment, sets of three films were immersed at the same time and each film was measured in turn and the order repeated until swelling was complete. Additionally, thickness and diameter measurements were taken both prior to immersion and once the discs/films had reached equilibrium using a digital caliper (Brown and Sharpe, North Kingstown, RI). Data analysis was performed on integral sorption studies as discussed in Chapter 5.

RESULTS AND DISCUSSION

Characterization of Poly(2-Hydroxyethyl Methacrylate)

Dynamic mechanical analysis experiments were performed on the synthesized polymers after drying and annealing in order to determine both the thermal and mechanical properties of the samples prior to use in sorption investigations. For this investigation, the critical aspect of the polymer's T_g was not its absolute value, but the rate at which the T_g changed with changing network structure. The variation of the values of the glass transition temperature with increasing crosslinker feed compositions (from 3.9 – 26.1 mol %) determined from both the shear storage modulus, G', and the peak of the tanδ curve are shown in Figure 7.2. Even though the absolute value of the T_g differs for each method, increasing the crosslinking density by incorporating more

crosslinking moieties affects each method in the same, linear manner. This behavior is generally expected and predicted by the Fox-Loshaek Equation [3] (Equation 4.4).

As discussed in Chapter 4, entanglements act as temporary, physical crosslinks in the rubbery state. However, as chemical crosslinks are added to the network structure, some of these entanglements will become entrapped, thereby creating permanent physical crosslinks that add to the effective crosslinking density of the polymer. As the degree of chemical crosslinking continues to increase, eventually all of the entanglements present will be locked into place and contribute to polymer properties. Thus, shear modulus profiles like that shown in Figure 7.3 were expected from theory [4]. Additionally, when the latter portion of the curve in Figure 7.3 was fit to a linear profile (shown), the y-intercept returned a value of the molecular weight between entanglements in the uncrosslinked state, M_e^0, for the polymer samples used in this study. The resulting value of M_e^0 was 1,720 g/mol and was utilized in this investigation to determine the extent of chemical crosslinking.

Finally, DMA analysis was performed to determine M_c using rubber elasticity theories as discussed in chapter 4 (Equations 4.31 - 4.32). The M_c values thus calculated were used to calculate a mol % of crosslinker incorporated into the polymer chains (F_2). The resulting typical crosslinking efficiency of the crosslinker feed composition was 39 %. Figure 7.4 compares DMA-calculated values of M_c for PHEMA crosslinked with EGDMA with the expected value based on theoretical calculations with a crosslinking efficiency of 39 %.

Penetrant Transport in Poly(2-Hydroxyethyl Methacrylate)

PHEMA discs with varying degrees of crosslinking were first immersed in ultra-pure water at 30°C and the transport dynamics were determined in an analogous manner to studies with PMMA in Chapter 5. Transport at 30°C and 25°C showed purely Fickian dynamics, so the temperature was lowered below ambient by placing the discs in a refrigerator at approximately 8°C. The resulting fractional mass uptake profiles are

shown in Figure 7.5. Even at this reduced temperature, the behavior was Fickian in nature (shown in Figure 7.6 where n = 0.5 in all cases). Since the freezing point of water prevented a further substantial lowering of the temperature in order to observe non-Fickian behavior, the penetrant molecule was instead altered.

Figure 7.7 shows profiles and power-law model analyses of ethanol sorption in the PHEMA discs with varying degrees of crosslinking (F_2) at 25°C. The transport process was essentially Case II in nature for all samples except the highest degree of crosslinking (F_2 = 0.140). It was expected that the scaling relationship found for methanol sorption into PMMA would be further validated by these studies. In Figure 7.8, once again a linear dependence of the Case II front velocity on the square root of the degree of copolymer crosslinking ($F_2^{0.5}$) was returned. The shift from Case II towards anomalous transport at very high degrees of crosslinking was also expected to follow the same behavior as PMMA showed in Chapter 5. However, full sorption profiles were not able to be examined and equilibrium polymer volume fractions could not be accurately measured, as the PHEMA discs all substantially fractured at around 18 - 20 wt % sorption of ethanol.

Characterization of Poly(Vinyl Alcohol)

The primary quantity of interest in investigations performed with PVA was the degree of crystallinity. Figure 7.9 presents DSC thermograms for varying degrees of crosslinking of PVA films with glutaraldehyde. As can be seen in the graph, the melting peak increased in magnitude as the degree of crosslinking was increased. These results were furthered analyzed in Table 7.1 and degrees of crystallinity are reported. The degree of crystallinity increased as the degree of crosslinking increased. This result was at first counter-intuitive. One would expect the formation of crystalline domains to become more difficult as additional crosslinks are added to the network structure and impede chain motion. However, crystallization is a kinetic process, and in this case the increase in crosslinking led to a slower drying rate and a longer drying time. In the end

this resulted in the fulfillment of a greater portion of the crystalline capacity in the PVA films with higher degrees of crosslinking.

Additional characterization of the crystalline structure was accomplished though XRD studies. Figure 7.10 presents XRD profiles for PVA films (3 cm x 3 cm) crosslinked with 2.5 mol % glutaraldehyde with varying annealing times at 100°C. As expected, the degree of crystallinity increased with annealing time, though the quantification of this effect was less successful, as seen in Table 7.2, and DSC data was relied upon for this metric. Even with no annealing, the degree of polymer crystallinity was substantial and led to limited control over this parameter. Additionally, Table 7.2 lists the crystalline lamellar thicknesses determined by XRD. Annealing time had a negligible effect on the lamellar thickness and the value is between 30 and 56 Å.

Penetrant Transport in Poly(Vinyl Alcohol)

Figure 7.11 presents the effects of crosslinking on PVA films swollen in water at 30°C. The transport behavior was Case II in nature for the first 60 % of swelling. However, the samples with lower degrees of crosslinking fractured significantly before equilibrium was obtained. When the rate of mass uptake versus the square root of the degree of crosslinking was plotted, the now expected linear relationship was returned (Figure 7.12). Finally, the effect of long-time annealing on the penetrant transport process of water in PVA films at 30°C is presented in Figure 7.13. Basically, as the polymer was annealed, the degree of crystallinity was increased. Since crystalline regions act as physical crosslinks and do not otherwise participate in the sorption process, this led to a decrease in the degree of penetrant uptake and a decrease in the rate of initial sorption.

CONCLUSIONS

Discs of poly(2-hydroxyethyl methacrylate) were synthesized by an *iniferter*-mediated, thermally-initiated, free radical polymerization mechanism with varying degrees of crosslinking with EGDMA. Samples were successfully characterized by DMA and a molecular weight between entanglements of 1,720 g/mol and a crosslinking efficiency of 39 % were elucidated. Integral sorption kinetics for water into PHEMA samples were Fickian for all conditions tested. Sorption kinetics for ethanol, though, displayed primarily Case II dynamics with the now expected dependence of the Case II front velocity on the square root of the degree of crosslinking and showed a similar trend away from Case II transport at the highest degrees of crosslinking.

Solvent-cast films of poly(vinyl alcohol) crosslinked in solution with glutaraldehyde were fabricated, annealed to increase crystallinity, were characterized by DSC and XRD to analyze crystallinity, and the transport dynamics of water sorption at 30°C were investigated. Once again the direct dependence of the rate of mass uptake, related to the Case II front velocity, on the square root of the degree of crosslinking in the polymer was demonstrated. Additionally, while the degree of crystallinity was shown to increase with crosslinking and annealing, no conclusive quantitative analyses could be performed for two reasons. First, the solvent-casting procedure for formation of the crosslinked polymer films introduced around 25 wt % crystallinity to the PVA films. Thus, the degree of crystallinity began high and its subsequent increase was limited. Second, when melting and rapid quenching of the polymer samples was attempted, the degree of crystallinity was never successfully lowered below 20 wt %. Add to this the fact that the melting and degradation temperatures are very near one another, and the end result was that only a qualitative correlation could be determined.

REFERENCES

1. *Polymer Handbook*. Third ed, ed. J. Brandrup and E.H. Immergut. 1989, New York: John Wiley & Sons.
2. Alexander, L.E., *X-Ray Diffraction Methods in Polymer Science*. 1979, New York: Robert E. Krieger Publishing Company.
3. Fox, T.G. and S. Loshaek, *Influence of Molecular Weight and Degree of Crosslinking on the Specific Volume and Glass Temperature of Polymers.* Journal of Polymer Science, 1955. **15**: p. 371-390.
4. Ferry, J.D., *Viscoelastic Properties of Polymers*. 3rd ed. 1980, New York: John Wiley & Sons.

Table 7.1: Percent crystallinity for PVA films with varying feed crosslinking compositions, f_2, determined by DSC.

PVA Crosslinking, f_2 (mol %)	ΔCp (J/g°C)	ΔH (J/g)	PVA Crystallinity (wt %)
1.98	1.1	33.7	24.3
4.88	1.0	31.2	22.5
9.52	1.6	32.4	23.4
13.95	N/A	48.3	34.9
18.18	1.7	51.6	37.2

Table 7.2: Percent crystallinity and lamellar thicknesses for PVA films with varying annealing times at 100°C determined by XRD.

Annealing Time (100°C)	Lamellar Thickness, t (Å)	Percent Crystallinity (%)
No Annealing	31.1	77.9
60 min	52.6	98.1
120 min	53.9	85.6
1 day	55.7	97.1
2 days	30.4	78.2
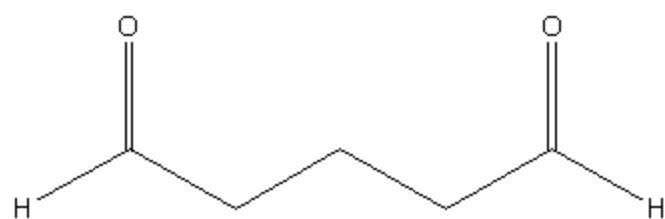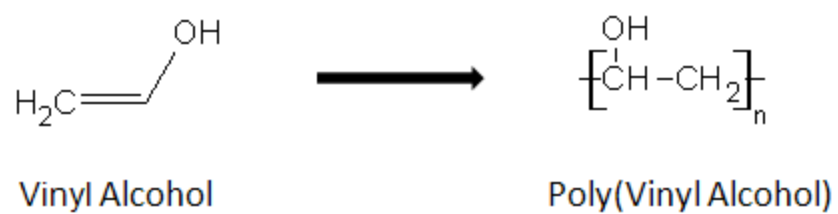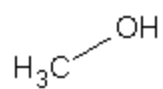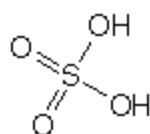
Figure 7.1: Materials used in the preparation of crosslinked poly(vinyl alcohol) films.
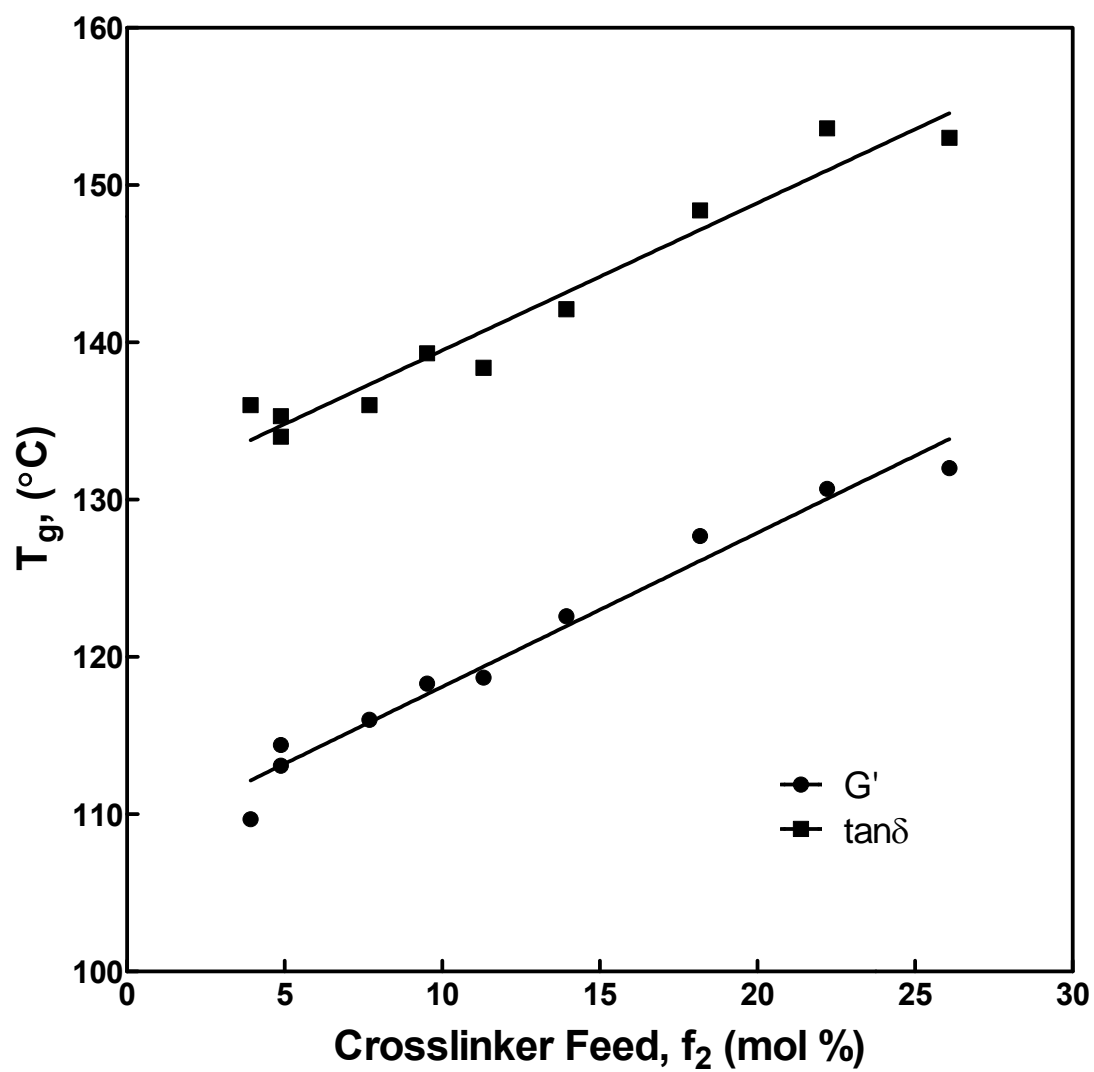
Figure 7.2: Values of T_g determined for PHEMA with varying molar crosslinker feed compositions (f_2) by DMA (G' and tanδ).
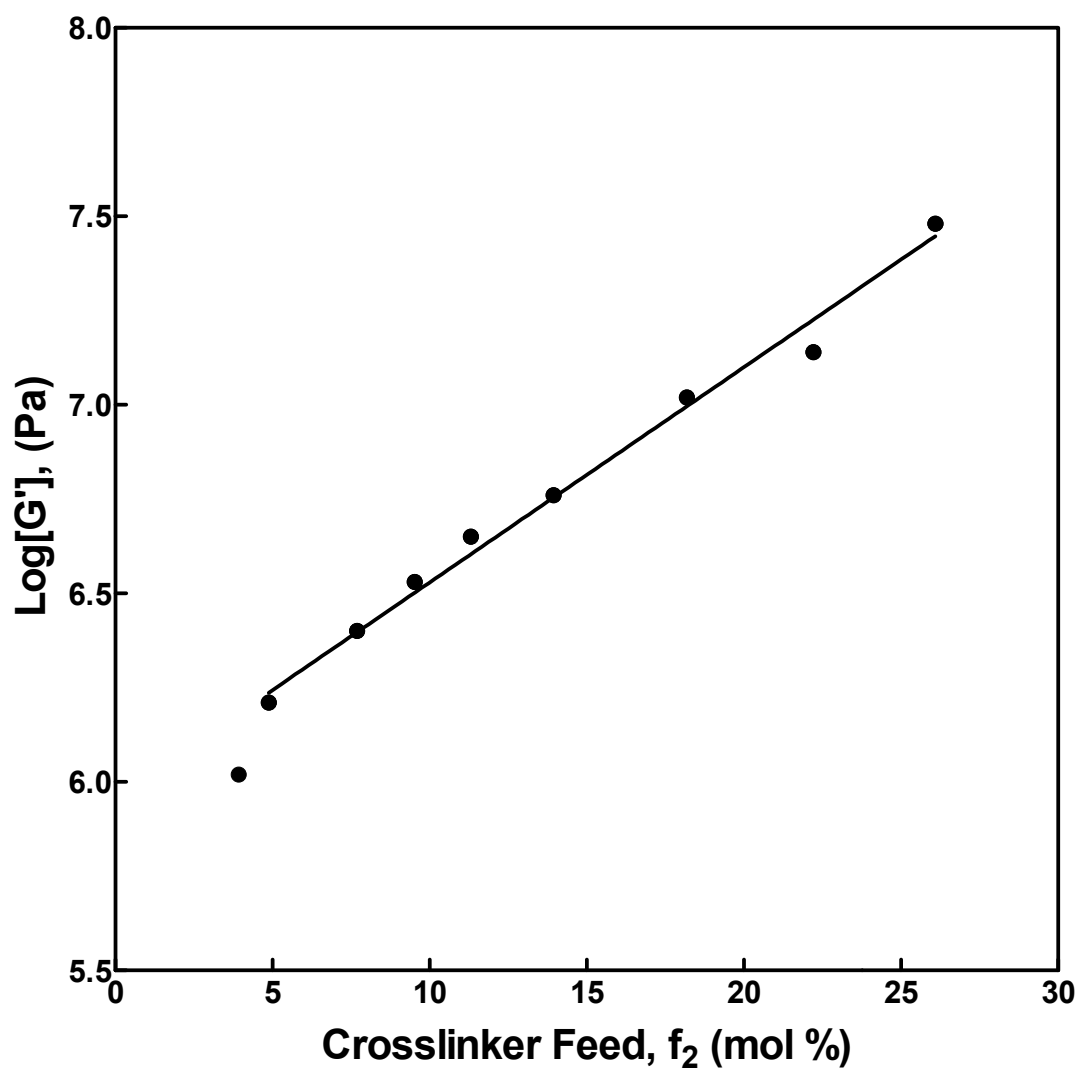
Figure 7.3: Values of the rubbery plateau shear storage modulus determined by DMA for PHEMA crosslinked with EGDMA with varying crosslinker feed compositions (f_2).
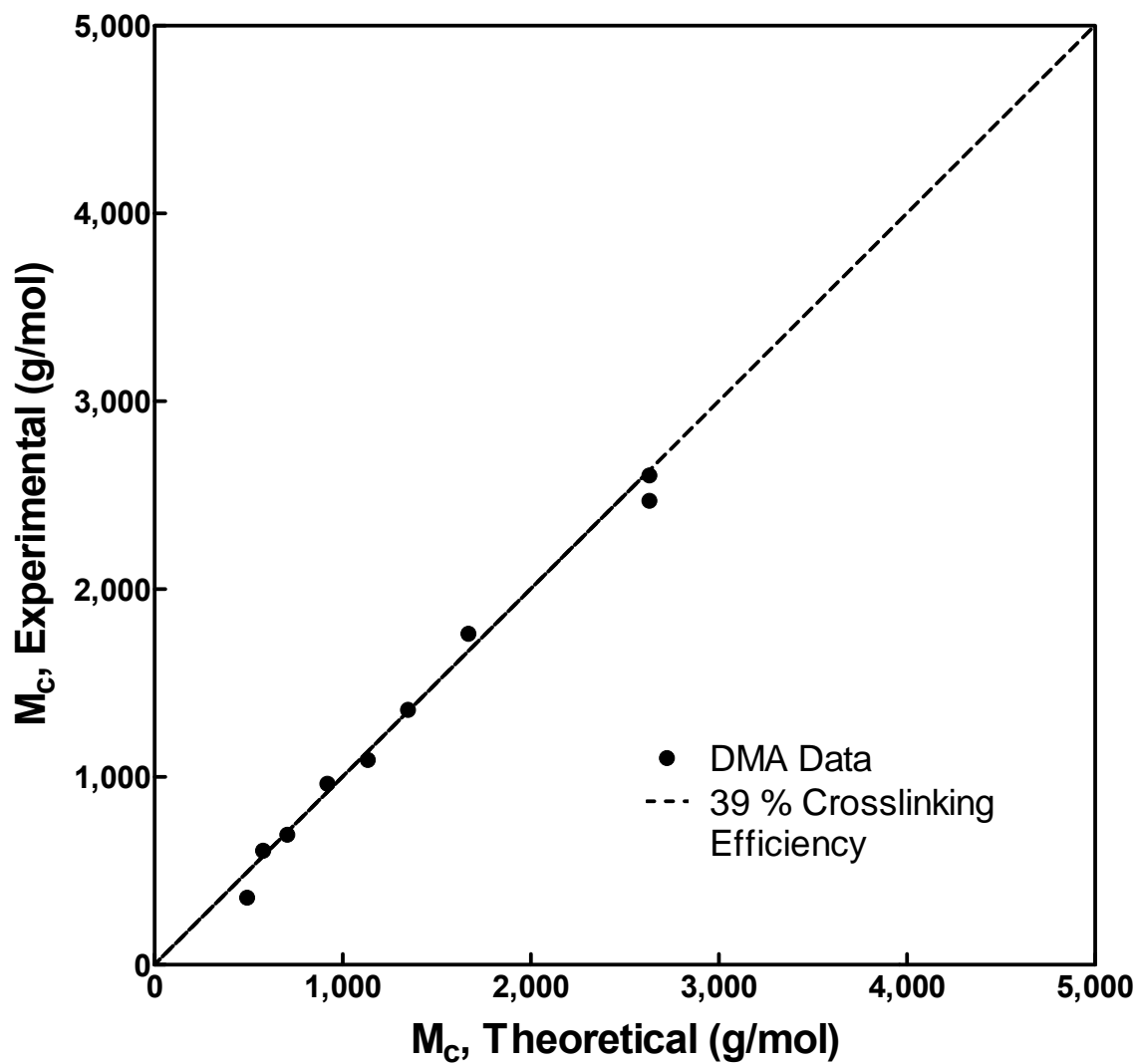
Figure 7.4: Comparison of molecular weights between crosslinks derived from DMA G′ measurements and theoretical molecular weights between crosslinking with a crosslinking efficiency of 39 % for PHEMA crosslinked with EGDMA.
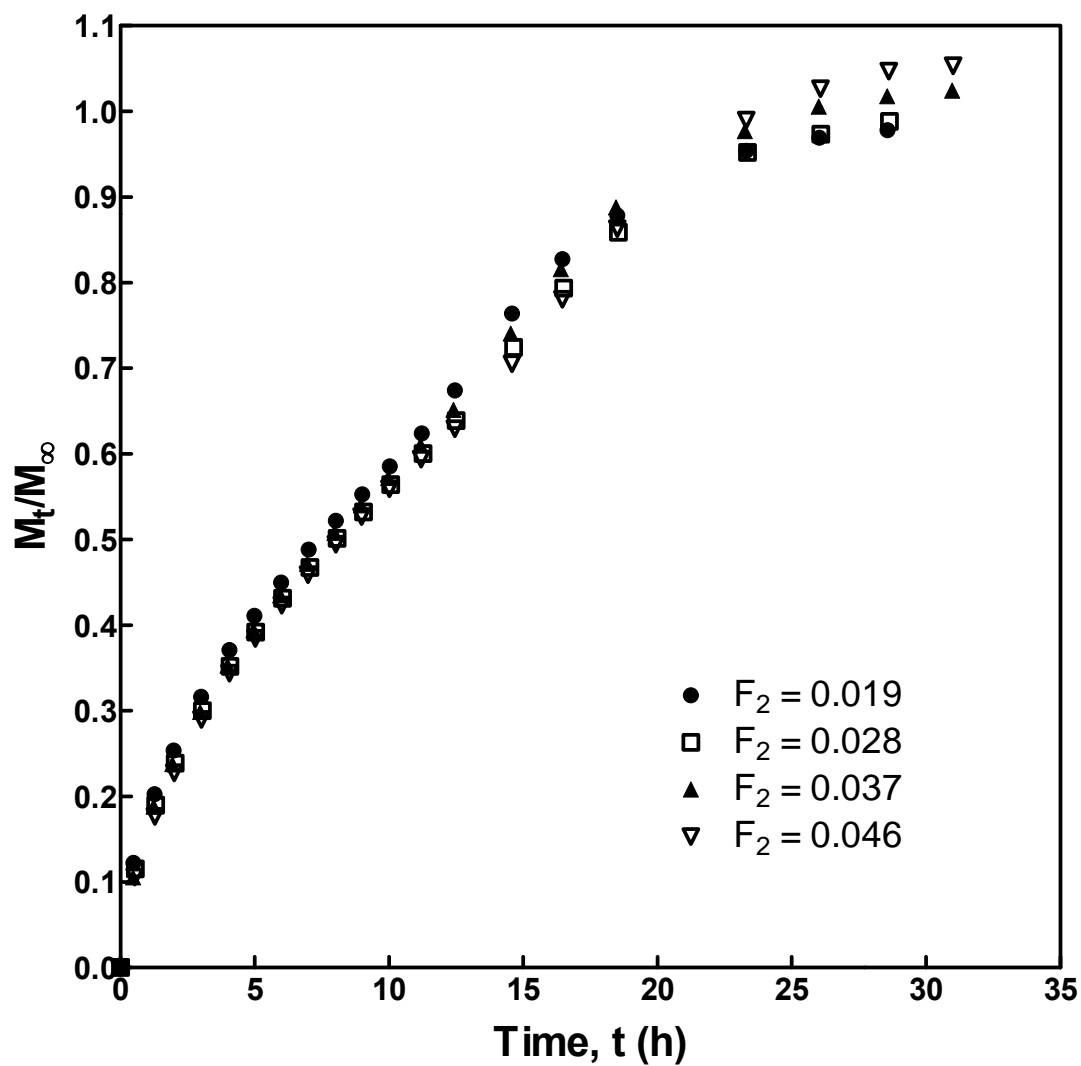
Figure 7.5: The effect of degree of copolymer crosslinking (F$_2$) on the integral sorption dynamics of PHEMA discs crosslinked with EGDMA and swollen in water at 8°C.
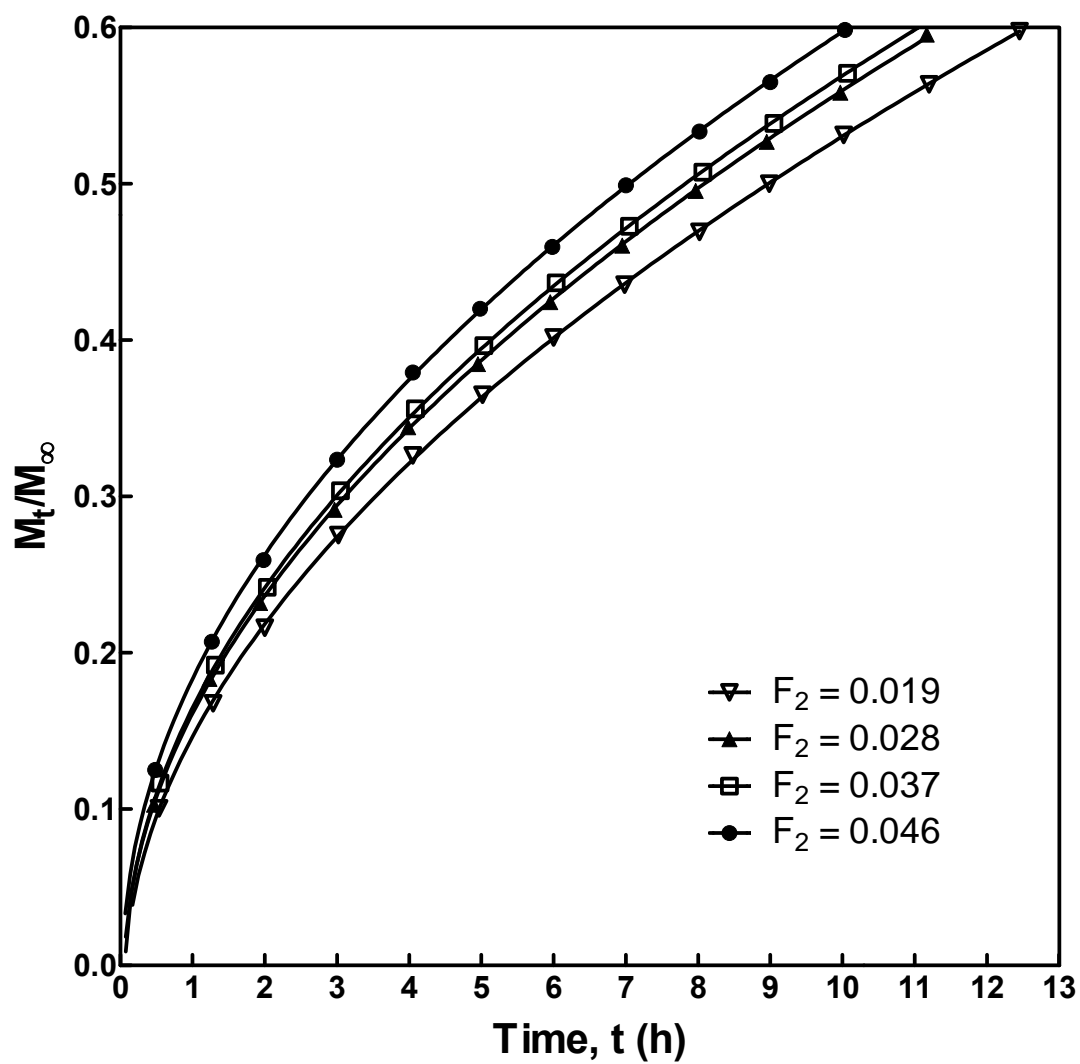
Figure 7.6: Power-law model analysis of the effect of the degree of copolymer crosslinking (F_2) on the integral sorption dynamics of PHEMA discs crosslinked with EGDMA and swollen in water at 8°C.
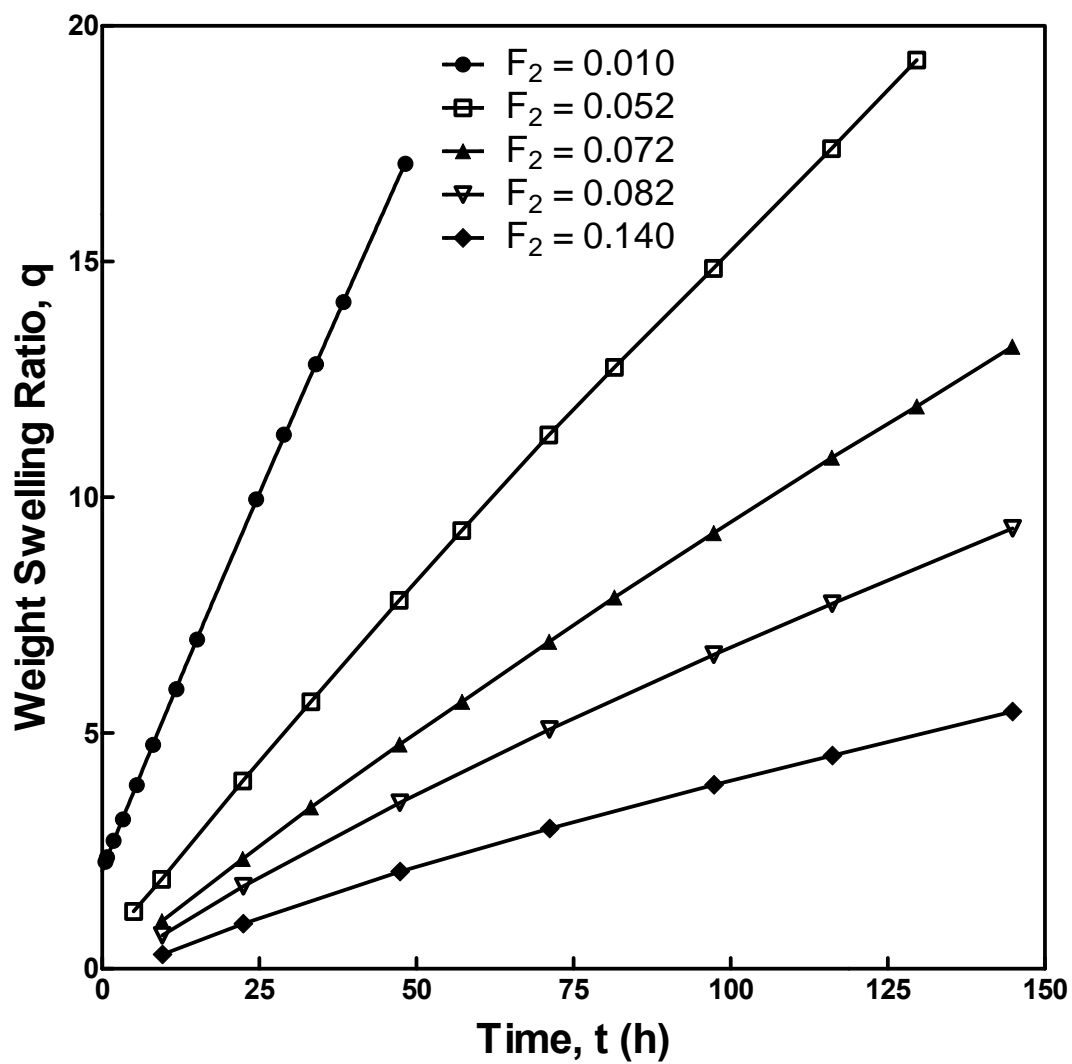
Figure 7.7: Power-law model analysis of the effect of degree of copolymer crosslinking (F_2) on the integral sorption dynamics of PHEMA discs crosslinked with EGDMA and swollen in ethanol at 25°C.
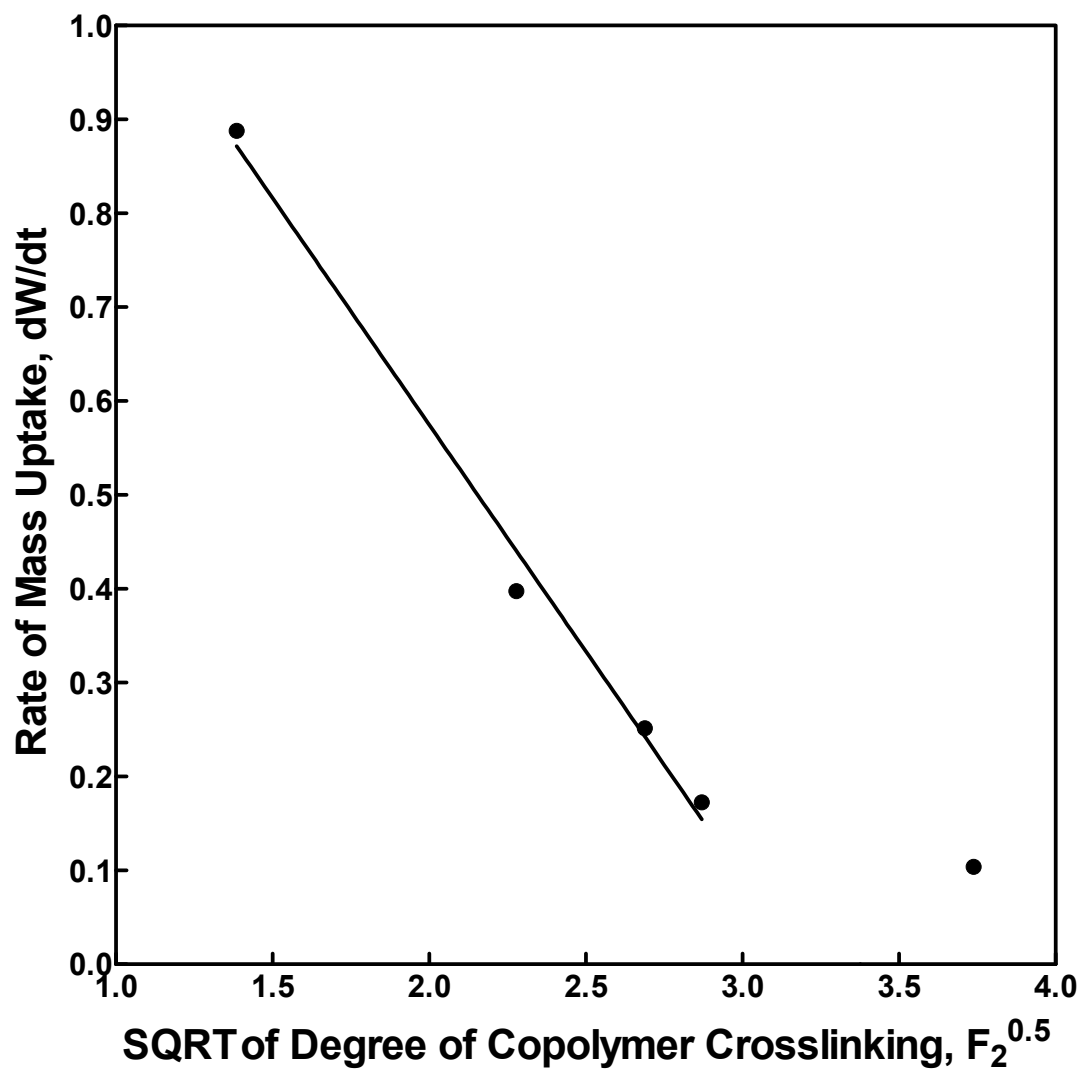
Figure 7.8: Rate of mass uptake versus the square root of the degree of copolymer crosslinking, $F_2^{0.5}$, in PHEMA discs crosslinked with EGDMA and swollen in ethanol at 25°C.
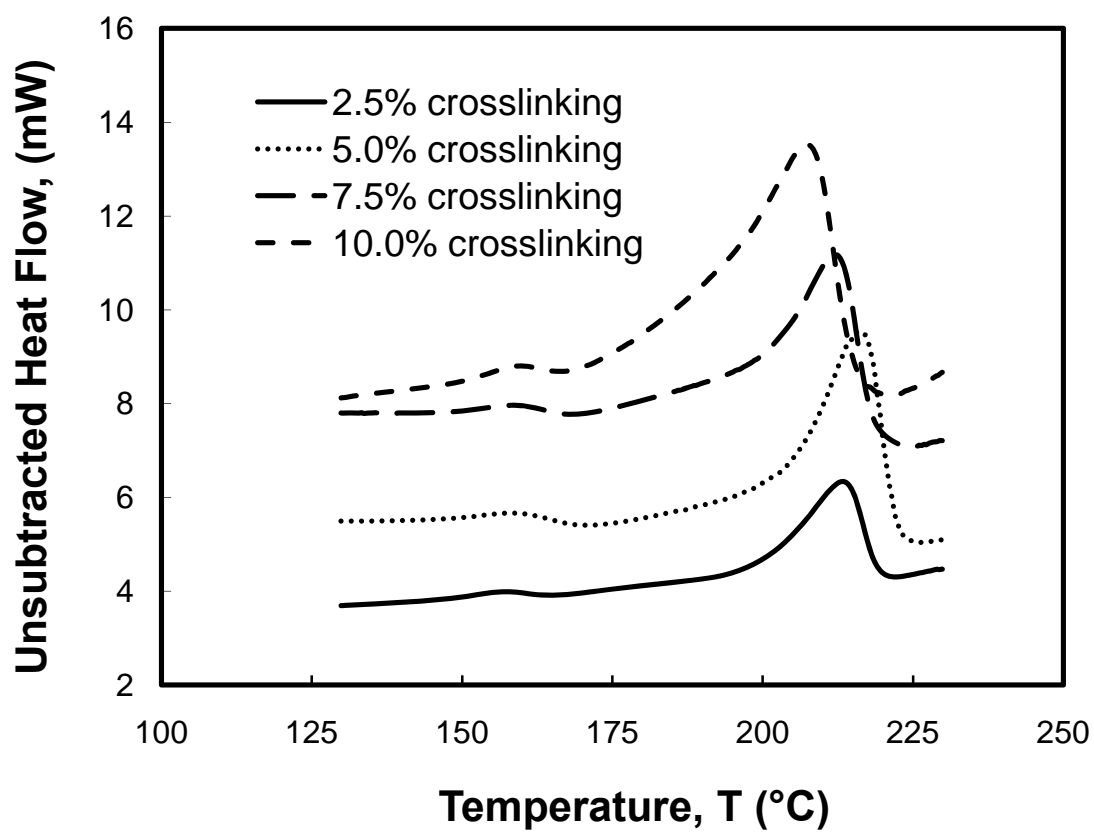
Figure 7.9: DSC thermograms for PVA crosslinked with varying molar glutaraldehyde feed compositions (mol %).
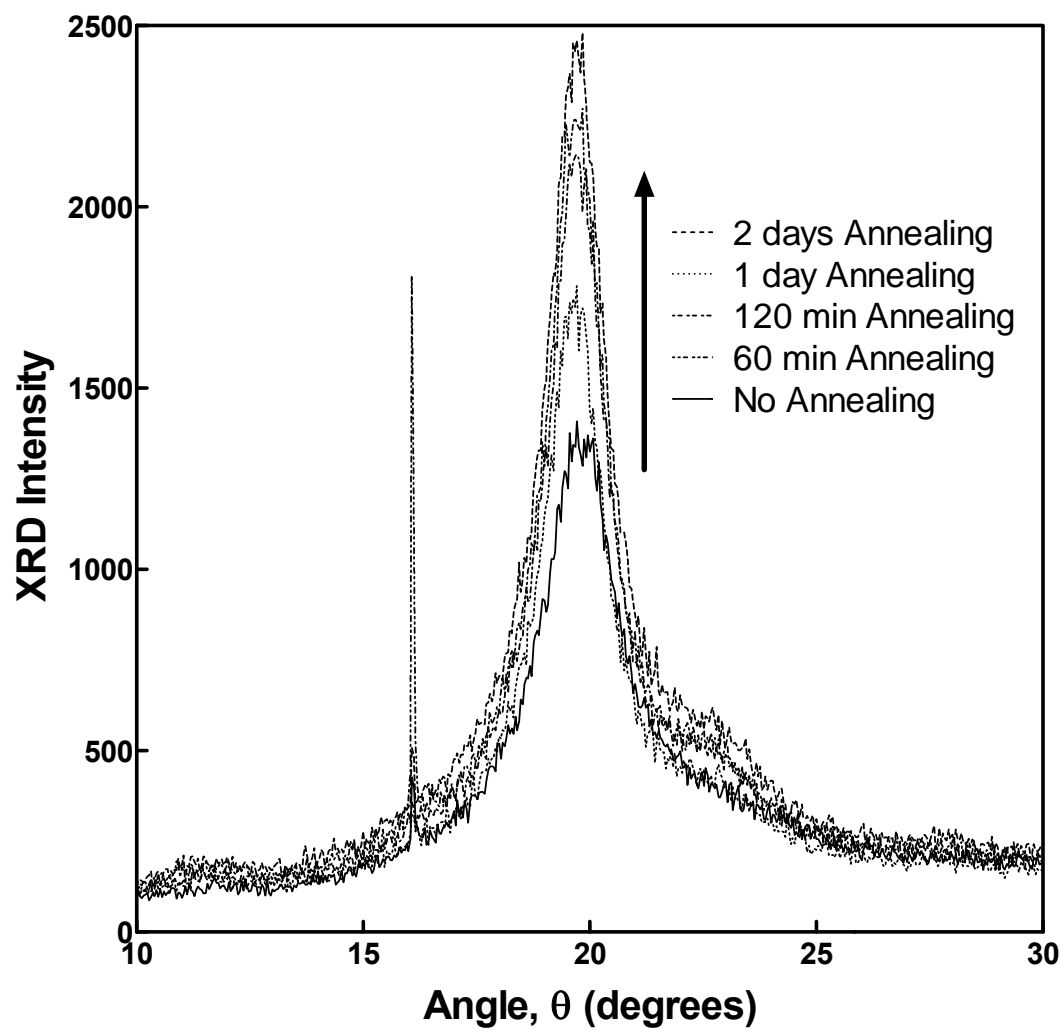
Figure 7.10: XRD Patterns for PVA crosslinked with a 2.5 mol % glutaraldehyde feed composition and annealed for varying times at 100°C.
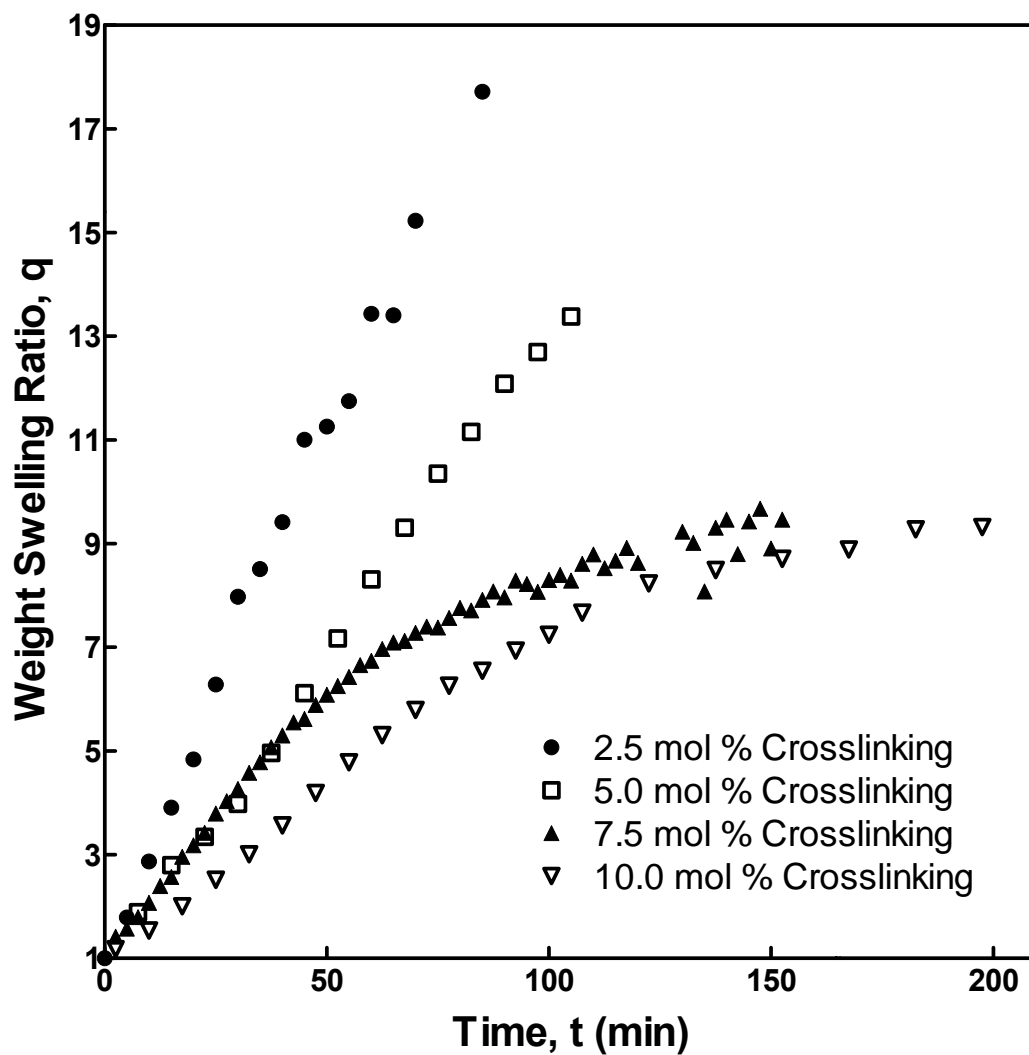
Figure 7.11: The effect of the mol % of glutaraldehyde feed during crosslinking on the integral sorption dynamics of PVA swollen in water at 30°C.
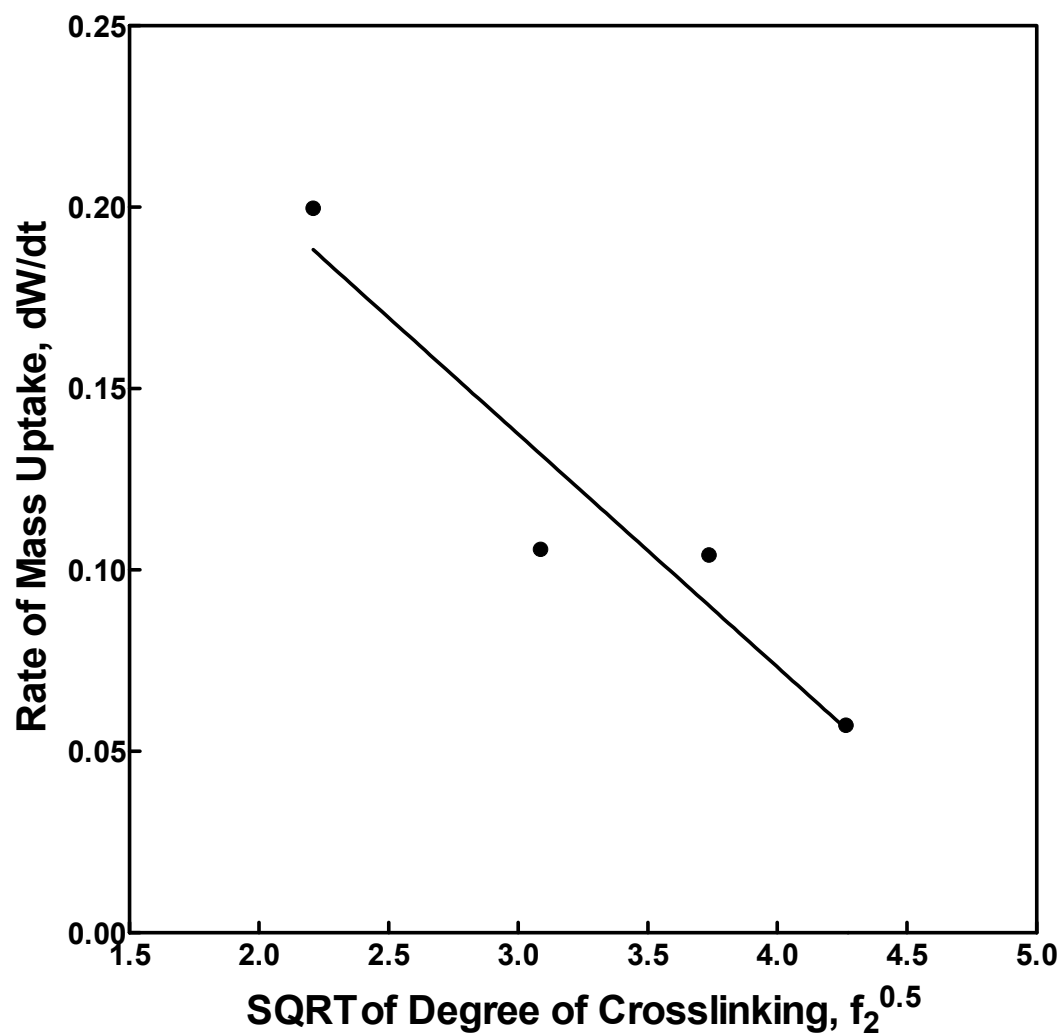
Figure 7.12: Rate of mass uptake versus the square root of the degree of crosslinking based on feed ratios, $f_2^{0.5}$, in PVA discs crosslinked with glutaraldehyde and swollen in water at 30°C.
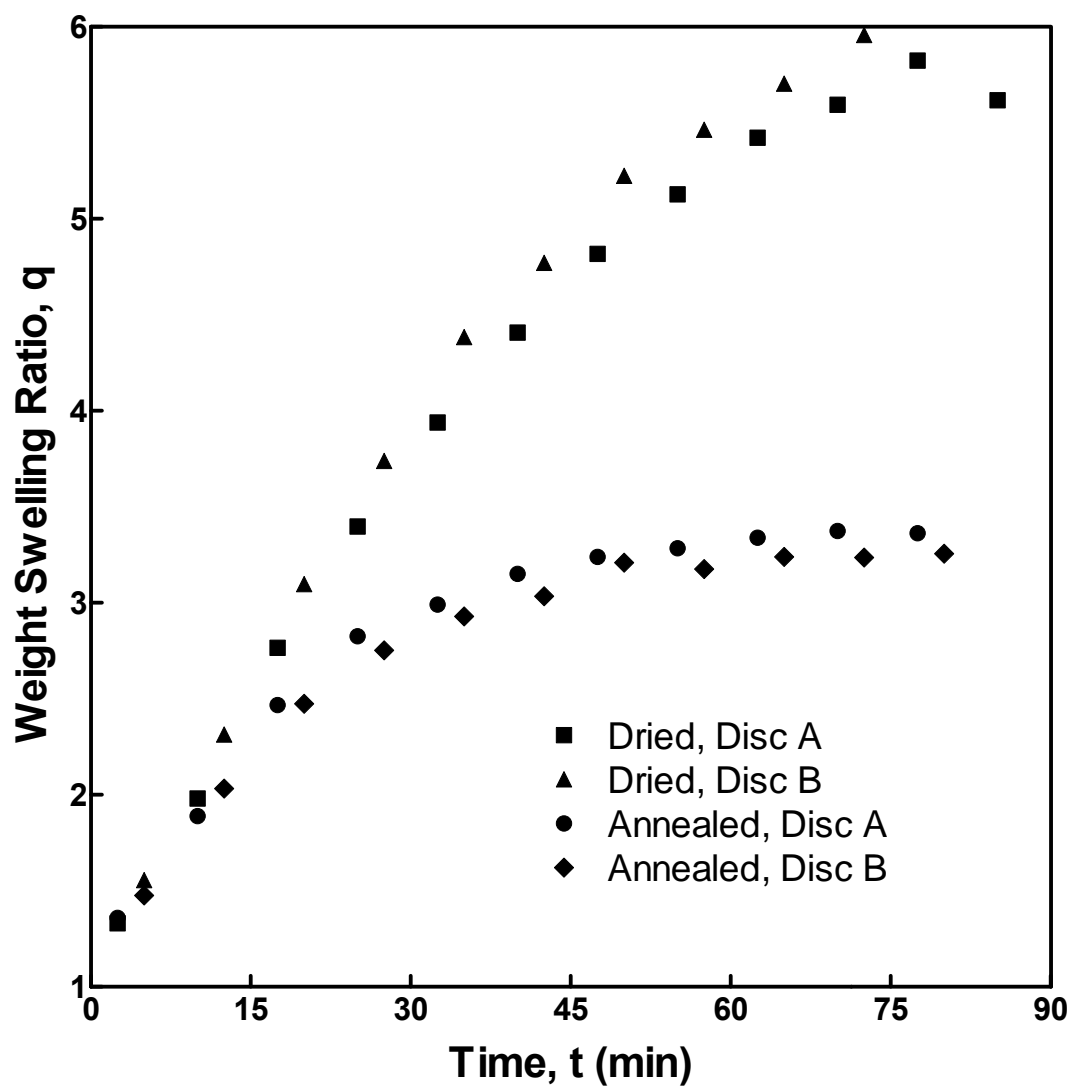
Figure 7.13:   The effect of annealing on the integral sorption dynamics of PVA crosslinked with 2.5 mol % glutaraldehyde and swollen in water at 30°C.

Chapter 8: Conclusions

Samples of poly(methyl methacrylate) (PMMA) were synthesized via an *iniferter*-mediated, thermally-initiated free radical polymerization procedure to produce polymers with controlled variations in network structure by altering the comonomer feed ratios of dimethacrylate crosslinkers and changing the crosslinking interchain bridge length. The polymers produced were characterized by differential scanning calorimetry (DSC), dynamic mechanical analysis, and equilibrium sorption studies along with appropriate calculations based on the comonomer reactivity ratios. The thermal, mechanical, and network properties were thus determined, and the efficiency of crosslinking was shown to be on average 40 %.

Additionally, samples of amorphous and semi-crystalline hydrophilic polymers were prepared. Poly(2-hydroxyethyl methacrylate) (PHEMA) was synthesized and characterized in an analogous manner to PMMA. Poly(vinyl alcohol) (PVA) was prepared from a powder, crosslinked in solution, and solvent-cast to produce thin films. The semi-crystalline properties of PVA were analyzed by DSC and X-ray diffraction techniques.

The penetrant transport dynamics of small molecules into these glassy polymers (methanol, ethanol, and water for PMMA, PHEMA, and PVA, respectively) were investigated by gravimetric sorption techniques. Case II transport was observed in each case when appropriate experimental conditions were used. The rate of Case II transport, or the Case II front velocity, was found to scale with the square root of the degree of polymer crosslinking for each system. As a result of the interrelation of the network parameters, this was equivalent to saying that the front velocity scaled with the molecular weight between crosslinks to the -0.5 power and with the polymer mesh size.

The ability to control the rate and mechanism of penetrant transport simply through alteration of the basic polymer network structure was demonstrated. Increasing the degree of crosslinking moved systems from Fickian or pseudo-Fickian

193

behavior to Case II transport. Increasing the crosslinking interchain bridge length was drove transport from Case II behavior towards Fickian dynamics. In addition, the transport rate and mechanism were in some cases altered without noticeably affecting the glass transition temperature, mechanical moduli, or equilibrium penetrant uptake of the polymer systems.

The practical implications of these investigations are evident. Appropriate alteration of these two basic polymer variables will allow practitioners to tune the nature and rate of sorption of small molecules into polymeric materials and devices. In particular, materials that are frequently exposed to penetrants that can cause crazing and cracking could be improved by utilizing a longer crosslinking bridge to move the polymer away from these extreme anomalous effects (or even adding a long-bridge crosslinker to an initially uncrosslinked polymer). Obviously, such procedures will find little utility in commodity plastics, where melt processing of polymers is commonly employed. However, polymeric devices made through *in situ* syntheses, such as those often found in many high-tech applications including microelectronics, microfluidics, and biomaterial synthesis, could benefit from the findings of this investigation.

Finally, high-resolution X-ray computed tomography was adapted in a novel manner to image the dynamic penetrant process of methanol into plasticized PMMA. Through this non-destructive, *in situ* technique, the time-dependent concentration profiles, dimensional swelling, and equilibrium sorption parameters were determined. The particular system investigated showed an anomalous transport mechanism with highly-concentration dependent diffusion in the glassy domain and Fickian diffusion in the rubbery domain.

To summarize, a fundamental investigation into the effects of material properties on the appearance and rates of anomalous and Case II transport was successfully performed and the objectives set forth in Chapter 3 were largely met. Given that control over the polymer network structure was desired, samples of glassy polymers were synthesized and/or prepared in house with hydrophilic, hydrophobic,

and semi-crystalline properties. The sorption behavior of small penetrant molecules into dry, glassy polymer was investigated through traditional gravimetric and novel computed X-ray tomography methodologies. The effects of the polymer network structure on the transport process were determined; crosslinking was shown to be a means by which to tune the observed penetrant transport to the desired behavior; and evidence was presented showing that control over the rate of Case II front propagation belongs solely to the glassy state, or the initial state at low degrees of penetrant sorption.

The primary novel contributions to the field by this thesis were that: (i) a straightforward, scaled control over V_{II} was demonstrated through altering the degree of crosslinking, (ii) an ability to control both the mechanism and rate of transport through modification of the interchain crosslinking bridge length was shown, (iii) similarities between dry and monomer-plasticized PMMA in relation to activation energies and behavior at high values of F_2 were observed, and (iv) high resolution X-ray computed tomography was introduced and validated as a powerful technique for the study of penetrant transport in polymers.

Recommendations for future experimental efforts in this field are centered on predicting when the transitions from anomalous to Case II and from Case II to crazing/cracking occur. Using gravimetric methods for integral sorption studies of organic vapors in common polymers, such as PMMA and polystyrene, the penetrant activity could easily be adjusted. In this way, the effects of the penetrant driving force, or the osmotic suction created during the propagation of a Case II front, could be related to material properties at critical activities when plastic deformation fronts will first be established and when material failure will begin to occur. The ability to predict material failure *a priori* when in contact with certain penetrant activities would be a tremendous achievement in terms of its broad applicability and usefulness to both commercial and academic endeavors. Additionally, insight would be gained into the

interrelation of Case II and anomalous transport, which would further aid efforts to develop an all-encompassing theory for penetrant transport in glassy polymers.

References

DIPPR 801 Database of Physical and Thermodynamical Properties of Pure Chemicals, BYU DIPPR Thermodynamical Properties Laboratory. Web. May 2010.

Abgrall, P. and A.M. Gue, *Lab-on-chip technologies: making a microfluidic network and coupling it into a complete microsystem - a review.* Journal of Micromechanics and Microengineering, 2007. **17**(5): p. R15-R49.

Alexander, L.E., *X-Ray Diffraction Methods in Polymer Science*. 1979, New York: Robert E. Krieger Publishing Company.

Alfrey, T., E.F. Gurnee, and W.G. Lloyd, *Diffusion in Glassy Polymers.* Journal of Polymer Science, Part C: Polymer Symposia, 1966. **12**: p. 249-261.

Argon, A.S., R.E. Cohen, and A.C. Patel, *A mechanistic model of case II diffusion of a diluent into a glassy polymer.* Polymer, 1999. **40**(25): p. 6991-7012.

Arnould, D. and R.L. Laurence, *Size Effects on Solvent Diffusion in Polymers.* Industrial & Engineering Chemistry Research, 1992. **31**(1): p. 218-228.

ASTM Standard D3125-97 (2001), *Monomethyl Ether of Hydroquinone in Colorless monomeric Acrylate Esters and Acrylic Acid.* ASTM International, West Conshohocken, PA, 2001, DOI: 10.1520/D3125-97R01, w ww.astm.org.

Bagley, E. and F.A. Long, *Two-stage Sorption and Desorption of Organic Vapors in Cellulose Acetate.* Journal of the American Chemical Society, 1955. **77**(2172-2178).

Baird, B.R., H.B. Hopfenberg, and V. Stannett, *The Effect of Molecular Weight and Orientation on the Sorption of n-Pentane by Glassy Polystyrene.* Polymer Engineering and Science, 1971. **11**(4): p. 274-283.

Bowman, C.N. and N.A. Peppas, *Polymers for Information-Storage Systems .2. Polymerization Kinetics for Preparation of Highly Cross-Linked Polydimethacrylates.* Journal of Applied Polymer Science, 1991. **42**(7): p. 2013-2018.

Brandrup, J. and E.H. Immergut, eds. *Polymer Handbook*. Third ed. 1989, John Wiley & Sons: New York.

Brandrup, J., E.H. Immergut, and E.A. Grulke, eds. *Polymer Handbook*. 4th ed. 1999, John Wiley & Sons: New York.

197

Brannon-Peppas, L. and N.A. Peppas, *Solute and Penetrant Diffusion in Swellable Polymers .9. The Mechanisms of Drug Release from Ph-Sensitive Swelling-Controlled Systems.* Journal of Controlled Release, 1989. **8**(3): p. 267-274.

Brannon-Peppas, L. and N.A. Peppas, *Equilibrium Swelling Behavior of Dilute Ionic Hydrogels in Electrolytic Solutions.* Journal of Controlled Release, 1991. **16**(3): p. 319-330.

Brazel, C.S. and N.A. Peppas, *Modeling of drug release from swellable polymers.* European Journal of Pharmaceutics and Biopharmaceutics, 2000. **49**(1): p. 47-58.

Cayot, N., C. Dury-Brun, T. Karbowiak, G. Savary, and A. Voilley, *Measurement of transport phenomena of volatile compounds: A review.* Food Research International, 2008. **41**(4): p. 349-362.

Chaterji, S., I.K. Kwon, and K. Park, *Smart polymeric gels: Redefining the limits of biomedical devices.* Progress in Polymer Science, 2007. **32**(8-9): p. 1083-1122.

Chen, J.K., S.W. Kuo, H.C. Kao, and F.C. Chang, *Thermal properties, specific interactions, and surface energies of PMMA terpolymers having high glass transition temperatures and low moisture absorptions.* Polymer, 2005. **46**(7): p. 2354-2364.

Cranitch, L., D.J.T. Hill, and A.K. Whittaker, *A study of the swelling of copolymers of NIPAM and DMA with water by NMR imaging.* Applied Magnetic Resonance, 2007. **32**(1-2): p. 51-62.

Crank, J. and G.S. Park, *Diffusion in High Polymers: Some Anomalies and their Significance.* Transactions of the Faraday Society, 1951. **47**: p. 1072-1084.

Crank, J. and G.S. Park, *Diffusion in Polymers*. 1968, New York: Academic Press.

Crank, J., *The Mathematics of Diffusion*. 2nd ed. 1975, New York: Oxford University Press. p. 47.

de Jong, J., R.G.H. Lammertink, and M. Wessling, *Membranes and microfluidics: a review.* Lab on a Chip, 2006. **6**(9): p. 1125-1139.

Durning, C.J., D.A. Edwards, and D.S. Cohen, *Perturbation analysis of Thomas and Windle's model of case II transport.* AIChE Journal, 1996. **42**(7): p. 2025-2035.

E., H.G., *Copolymerization*. 1964, New York: Interscience Publishers.

Enscore, D.J., H.B. Hopfenberg, V.T. Stannett, and A.R. Berens, *Effect of Prior Sample History on N-Hexane Sorption in Glassy Polystyrene Microspheres.* Polymer, 1977. **18**(11): p. 1105-1110.

Ferry, J.D., *Viscoelastic Properties of Polymers.* 3rd ed. 1980, New York: John Wiley & Sons.

Flory, P.J., *Thermodynamics of High-Polymer Solutions.* Journal of Physical Chemistry, 1942. **10**: p. 51-61.

Flory, P.J. and R. Rehner, Jr., *Statistical Mechanics of Crosslinked Polymer Networks. I. Rubberlike Elasticity.* Journal of Chemical Physics, 1943. **11**: p. 521.

Flory, P.J. and W.R. Krigbaum, *Thermodynamics of High Polymer Solutions.* Annual Review of Physical Chemistry, 1951. **2**: p. 383-402.

Fox, T.G. and S. Loshaek, *Influence of Molecular Weight and Degree of Crosslinking on the Specific Volume and Glass Temperature of Polymers.* Journal of Polymer Science, 1955. **15**: p. 371-390.

Frisch, H.L., *Sorption and Transport in Glassy-Polymers - Review.* Polymer Engineering and Science, 1980. **20**(1): p. 2-13.

Fujita, H. and A. Kishimoto, *Diffusion-Controlled Stress Relaxation in Polymers. II. Stress Relaxation in Swollen Polymers.* Journal of Polymer Science, 1958. **28**(118): p. 547-567.

Gall, T.P., R.C. Lasky, and E.J. Kramer, *Case-II Diffusion - Effect of Solvent Molecule Size.* Polymer, 1990. **31**(8): p. 1491-1499.

Geyer, K., J.D.C. Codee, and P.H. Seeberger, *Microreactors as tools for synthetic chemists - The chemists' round-bottomed flask of the 21st century?* Chemistry - A European Journal, 2006. **12**(33): p. 8434-8442.

Gunther, A. and K.F. Jensen, *Multiphase microfluidics: from flow characteristics to chemical and materials synthesis (vol 6, pg 1487, 2006).* Lab on a Chip, 2007. **7**(7): p. 935-935.

Haeberle, S. and R. Zengerle, *Microfluidic platforms for lab-on-a-chip applications.* Lab on a Chip, 2007. **7**(9): p. 1094-1110.

Hansen, C.M., *Hansen Solubility Parameters: A User's Handbook*. 2nd ed. 2007, Boca Raton: CRC Press.

Harmon, J.P., S. Lee, and J.C.M. Li, *Methanol Transport in PMMA - the Effect of Mechanical Deformation.* Journal of Polymer Science Part A - Polymer Chemistry, 1987. **25**(12): p. 3215-3229.

Hartley, G.S., *Diffusion and Swelling of High Polymers. Part I. The Swelling and Solution of a High Polymer Solid Considered as a Diffusion Process.* Transactions of the Faraday Society, 1946. **42**: p. B006-B011.

Hartley, G.S., *Diffusion and Swelling of High Polymers. Part III. Anisotropic Swelling in Oriented Polymer Film.* Transactions of the Faraday Society, 1949. **45**: p. 820-832.

Hassan, M.M. and C.J. Durning, *Effects of polymer molecular weight and temperature on Case II transport.* Journal of Polymer Science Part B-Polymer Physics, 1999. **37**(22): p. 3159-3171.

Hayes, M.J. and G.S. Park, *Diffusion of Benzene in Rubber. I. Low Concentrations of Benzene.* Transactions of the Faraday Society, 1955. **51**: p. 1134-42.

Holley, R.H., H.B. Hopfenberg, and V. Stannett, *Anomalous Transport of Hydrocarbons in Polystyrene.* Polymer Engineering and Science, 1970. **10**(6): p. 376-382.

Hopfenberg, H.B. and H.L. Frisch, *Transport of Organic Micromolecules in Amorphous Polymers.* Journal of Polymer Science, Part B: Polymer Letters, 1969. **7**(6): p. 405-409.

Hopfenberg, H.B., R.H. Holley, and V. Stannett, *The Effect of Penetrant Activity and Temperature on the Anomalous Diffusion of Hydrocarbons and Solvent Crazing in Polystyrene Part I: Biaxially Oriented Polystyrene.* Polymer Engineering and Science, 1969. **9**(4): p. 242-249.

Hopfenberg, H.B., R.H. Holley, and V. Stannett, *The Effect of Penetrant Activity and Temperature on Anomalous Diffusion of Hydrocarbons and Solvent Crazing in Polystyrene .1. Biaxially Oriented Polystyrene.* Polymer Engineering and Science, 1969. **9**(4): p. 242-&.

Hopfenberg, H.B. and V. Stannett, in *Physics of Glassy Polymers*, R.N. Haward, Editor. 1973, Applied Science: London.

Hopfenberg, H.B., L. Nicolais, and E. Drioli, *Relaxation Controlled (Case Ii) Transport of Lower Alcohols in Poly(Methylmethacrylate).* Polymer, 1976. **17**(3): p. 195-198.

Hu, G.Q. and D.Q. Li, *Multiscale phenomena in microfluidics and nanofluidics.* Chemical Engineering Science, 2007. **62**(13): p. 3443-3454.

Huggins, M.L., *Some Properties of Solutions of Long-chain Compounds.* Journal of Physical Chemistry, 1942. **46**: p. 151-158.

Jacques, C.H.M. and H.B. Hopfenberg, *Vapor and Liquid Equilibria in Glassy Polyblends of Polystyrene and Poly(2,6-Dimethyl-1,4-Phenylene Oxide) .1.* Polymer Engineering and Science, 1974. **14**(6): p. 441-448.

Jacques, C.H.M. and H.B. Hopfenberg, *Kinetics of Vapor and Liquid Transport in Glassy Polyblends of Polystyrene and Poly (2,6-Dimethyl 1,4-Phenylene Oxide) .2.* Polymer Engineering and Science, 1974. **14**(6): p. 449-455.

Jacques, C.H.M., H.B. Hopfenberg, and V.T. Stannett, *Super Case II Transport of Organic Vapors in Glassy Polymers.* Abstracts of Papers of the American Chemical Society, 1974: p. 51-51.

Joshi, S. and G. Astarita, *Diffusion-Relaxation Coupling in Polymers Which Show 2-Stage Sorption Phenomena.* Polymer, 1979. **20**(4): p. 455-458.

Kambour, R.P., E.E. Romagosa, and C.L. Gruner, *Swelling, Crazing, and Cracking of an Aromatic Copolyether-Sulfone in Organic Media.* Macromolecules, 1972. **5**(4): p. 335-&.

Kambour, R.P., C.L. Gruner, and E.E. Romagosa, *Solvent Crazing of Dry Polystyrene and Dry Crazing of Plasticized Polystyrene.* Journal of Polymer Science Part B-Polymer Physics, 1973. **11**(10): p. 1879-1890.

Kannurpatti, A.R., S.X. Lu, G.M. Bunker, and C.N. Bowman, *Kinetic and mechanistic studies of iniferter photopolymerizations.* Macromolecules, 1996. **29**(23): p. 7310-7315.

Kazmaier, P.M., K.A. Moffat, M.K. Georges, R.P.N. Veregin, and G.K. Hamer, *Free-Radical Polymerization for Narrow-Polydispersity Resins - Semiempirical Molecular-Orbital Calculations as a Criterion for Selecting Stable Free-Radical Reversible Terminators.* Macromolecules, 1995. **28**(6): p. 1841-1846.

Ketcham, R.A. and W.D. Carlson, *Acquisition, optimization and interpretation of X-ray computed tomographic imagery: applications to the geosciences.* Computers & Geosciences, 2001. **27**(4): p. 381-400.

King, G., *Sorption of Vapours by Keratin and Wool.* Transactions of the Faraday Society, 1945. **41**: p. 325-332.

Kokes, R.J., F.A. Long, and J.L. Hoard, *Diffusion of Acetone into Polyvinyl Acetate above and below the Second-Order Transition.* Journal of Chemical Physics, 1952. **20**(11): p. 1711-1716.

Kovac, J., *Modified Gaussian Model for Rubber Elasticity.* Macromolecules, 1978. **11**(2): p. 362-365.

Kwei, T.K. and H.M. Zupko, *Diffusion in Glassy Polymers. I.* Journal of Polymer Science, Part A-2: Polymer Physics, 1969. **7**(5): p. 867-877.

Lambrinos, P., M. Tardi, A. Polton, and P. Sigwalt, *The Mechanism of the Polymerization of Normal-Butyl Acrylate Initiated with N,N-Diethyl Dithiocarbamate Derivatives.* European Polymer Journal, 1990. **26**(10): p. 1125-1135.

Langer, R. and N.A. Peppas, *Advances in biomaterials, drug delivery, and bionanotechnology.* AIChE Journal, 2003. **49**(12): p. 2990-3006.

Langer, R. and D.A. Tirrell, *Designing materials for biology and medicine.* Nature, 2004. **428**(6982): p. 487-492.

Lee, P.I., *Temperature-Dependence of Methanol Transport in Spherical PMMA Beads.* Polymer, 1993. **34**(11): p. 2397-2400.

Lee, S.B. and T.M. Fu, *Methanol Transport in Cross-Linked Poly(Methyl Methacrylate).* Polymer, 1995. **36**(20): p. 3975-3978.

Long, F.A. and D. Richman, *Concentration Gradients for Diffusion of Vapors in Glassy Polymers and their Relation to Time Dependent Diffusion Phenomena.* Journal of the American Chemical Society, 1960. **82**: p. 513-519.

Loshaek, S. and T.G. Fox, *Cross-linked Polymers. I. Factors Influencing the Efficiency of Cross-linking in Copolymers of Methyl Methacrylate and Glycol Dimethacrylates.* Journal of the American Chemical Society, 1953. **75**: p. 3544.

Loshaek, S., *Crosslinked Polymers. II. Glass Temperatures of Copolymers of Methyl Methacrylate and Glycol Dimethacrylates.* Journal of Polymer Science, 1955. **15**: p. 391-404.

Losi, E., R. Bettini, P. Santi, F. Sonvico, G. Colombo, K. Lofthus, P. Colombo, and N.A. Peppas, *Assemblage of novel release modules for the development of adaptable drug delivery systems.* Journal of Controlled Release, 2006. **111**(1-2): p. 212-218.

Luo, N., A.T. Metters, J.B. Hutchison, C.N. Bowman, and K.S. Anseth, *A methacrylated photoiniferter as a chemical basis for microlithography: Micropatterning based on photografting polymerization.* Macromolecules, 2003. **36**(18): p. 6739-6745.

Lustig, S.R., *A Continuum Thermodynamics Theory for Transport in Polymer/Fluids Systems*, in *Chemical Engineering*. 1989, Purdue University.

Manga, J.D., A. Polton, M. Tardi, and P. Sigwalt, *Living Character of the Polymerization of Butyl Acrylate Initiated by a Model N,N-Diethyldithiocarbamate.* Journal of Macromolecular Science-Pure and Applied Chemistry, 1995. **A32**: p. 695-703.

Mao, R.S., Y. Liu, M.B. Huglin, and P.A. Holmes, *Determination of Monomer Reactivity Ratios in the Cross-Linking Copolymerization of Methyl-Methacrylate with Ethylene Dimethacrylate.* Macromolecules, 1995. **28**(20): p. 6739-6744.

Merfeld, G.D., T.T. Maa, K. Chan, and D.R. Paul, *Synthesis and blends of pentabromobenzyl acrylate copolymers.* Polymer, 2000. **41**(2): p. 663-674.

Michaels, A.S., H.J. Bixler, and H.B. Hopfenberg, *Controllably Crazed Polystyrene - Morphology and Permeability.* Journal of Applied Polymer Science, 1968. **12**(5): p. 991-&.

Nicolais, L., E. Drioli, H.B. Hopfenberg, and D. Tidone, *Characterization and Effects of N-Alkane Swelling of Polystyrene Sheets.* Polymer, 1977. **18**(11): p. 1137-1142.

Nicolais, L., E. Drioli, H.B. Hopfenberg, and G. Caricati, *Diffusion-Controlled Penetration of Polymethyl Methacrylate Sheets by Monohydric Normal Alcohols.* Journal of Membrane Science, 1978. **3**(2-4): p. 231-245.

Nicolais, L., E. Drioli, H.B. Hopfenberg, and A. Apicella, *Effects of Orientation on the Penetration, Crazing, and Dissolution of Polystyrene by N-Hexane.* Polymer, 1979. **20**(4): p. 459-464.

Odian, G., *Principles of Polymerization*. 4th ed. 2004, Hoboken, NJ: John Wiley & Sons, Inc.

Otsu, T. and M. Yoshida, *Role of Initiator-Transfer Agent-Terminator (Iniferter) in Radical Polymerizations - Polymer Design by Organic Disulfides as Iniferters.* Makromolekulare Chemie, Rapid Communications, 1982. **3**(2): p. 127-132.

Otsu, T., T. Matsunaga, A. Kuriyama, and M. Yoshioka, *Living Radical Polymerization through the Use of Iniferters - Controlled Synthesis of Polymers.* European Polymer Journal, 1989. **25**(7-8): p. 643-650.

Otsu, T. and A. Matsumoto, *Controlled Synthesis of Polymers Using the Iniferter Technique: Developments in Living Radical Polymerization*. Advances in Polymer Science. Vol. 136. 1998, New York: Springer. 75-137.

Otsu, T., *Iniferter concept and living radical polymerization.* Journal of Polymer Science, Part A: Polymer Chemistry, 2000. **38**(12): p. 2121-2136.

Peppas, N.A. and L.M. Lucht, *Macromolecular Structure of Coals. I. The Organic Phase of Bituminous Coals as a Macromolecular Network.* Chemical Engineering Communications, 1984. **30**(3-5): p. 291-310.

Peppas, N.A. and K.G. Urdahl, *Anomalous Penetrant Transport in Glassy-Polymers .7. Overshoots in Cyclohexane Uptake in Cross-Linked Polystyrene.* Polymer Bulletin, 1986. **16**(2-3): p. 201-207.

Peppas, N.A. and A.R. Khare, *Preparation, Structure and Diffusional Behavior of Hydrogels in Controlled-Release.* Advanced Drug Delivery Reviews, 1993. **11**(1-2): p. 1-35.

Peppas, N.A., P. Bures, W. Leobandung, and H. Ichikawa, *Hydrogels in pharmaceutical formulations.* European Journal of Pharmaceutics and Biopharmaceutics, 2000. **50**(1): p. 27-46.

Peppas, N.A., *Intelligent biomaterials as pharmaceutical carriers in microfabricated and nanoscale devices.* MRS Bulletin, 2006. **31**(11): p. 888-893.

Peppas, N.A., J.Z. Hilt, A. Khademhosseini, and R. Langer, *Hydrogels in biology and medicine: From molecular principles to bionanotechnology.* Advanced Materials, 2006. **18**(11): p. 1345-1360.

Peterlin, A., *Diffusion in a Network with Discontinuous Swelling.* Polymer Letters, 1965. **3**: p. 1083-1087.

Rehberg, C.E. and C.H. Fisher, *Properties of Monomeric and Polymeric Alkyl Acrylates and Methacrylates.* Journal of Industrial and Engineering Chemistry, 1948. **40**: p. 1429-33.

Ritger, P.L. and N.A. Peppas, *Transport of Penetrants in the Macromolecular Structure of Coals .4. Models for Analysis of Dynamic Penetrant Transport.* Fuel, 1987. **66**(6): p. 815-826.

Rodriguez, F., C. Cohen, C.K. Ober, and L.A. Archer, *Principles of Polymer Systems*. 5th ed. 2003, New York: Taylor & Francis.

Rosen, B., *Time-Dependent Tensile Properties. Part III. Microfracture and Non-Fickian Vapor Diffusion in Organic Glasses.* Journal of Polymer Science, 1961. **49**: p. 177-188.

Sekkar, V., K. Narayanaswamy, K.J. Scariah, P.R. Nair, K.S. Sastri, and H.G. Ang, *Evaluation by various experimental approaches of the crosslink density of urethane networks based on hydroxyl-terminated polybutadiene.* Journal of Applied Polymer Science, 2007. **103**(5): p. 3129-3133.

Sinclair, G.W. and N.A. Peppas, *Analysis of Non-Fickian Transport in Polymers Using Simplified Exponential Expressions.* Journal of Membrane Science, 1984. **17**(3): p. 329-331.

Situma, C., M. Hashimoto, and S.A. Soper, *Merging microfluidics with microarray-based bioassays.* Biomolecular Engineering, 2006. **23**(5): p. 213-231.

Thomas, N. and A.H. Windle, *Discontinuous Shape Changes Associated with Case-2 Transport of Methanol in Thin Sheets of PMMA.* Polymer, 1977. **18**(11): p. 1195-1195.

Thomas, N. and A.H. Windle, *Transport of Methanol in Poly(Methyl Methacrylate).* Polymer, 1978. **19**(3): p. 255-265.

Thomas, N.L. and A.H. Windle, *A Deformation Model for Case-II Diffusion.* Polymer, 1980. **21**(6): p. 613-619.

Thomas, N.L. and A.H. Windle, *Diffusion Mechanics of the System PMMA-Methanol.* Polymer, 1981. **22**(5): p. 627-639.

Thomas, N.L. and A.H. Windle, *A Theory of Case-II Diffusion.* Polymer, 1982. **23**(4): p. 529-542.

Treloar, L.R.G., *The Physics of Rubber Elasticity*. 3rd ed. 1975, New York: Oxford University Press.

Turner, S.R. and R.W. Blevins, *Photoinitiated Block Copolymer Formation Using Dithiocarbamate Free-Radical Chemistry.* Macromolecules, 1990. **23**(6): p. 1856-1859.

Vesely, D., *Diffusion of liquids in polymers.* International Materials Reviews, 2008. **53**(5): p. 299-315.

Vrentas, J.S., C.M. Jarzebski, and J.L. Duda, *Deborah Number for Diffusion in Polymer-Solvent Systems.* AIChE Journal, 1975. **21**(5): p. 894-901.

Vrentas, J.S. and J.L. Duda, *Diffusion in Polymer-Solvent Systems .3. Construction of Deborah Number Diagrams.* Journal of Polymer Science Part B-Polymer Physics, 1977. **15**(3): p. 441-453.

Ward, J.H. and N.A. Peppas, *Kinetic gelation modeling of controlled radical polymerizations.* Macromolecules, 2000. **33**(14): p. 5137-5142.

Ward, J.H., R. Bashir, and N.A. Peppas, *Micropatterning of biomedical polymer surfaces by novel UV polymerization techniques.* Journal of Biomedical Materials Research, 2001. **56**(3): p. 351-360.

Ward, J.H., A. Shahar, and N.A. Peppas, *Kinetics of 'living' radical polymerizations of multifunctional monomers.* Polymer, 2002. **43**(6): p. 1745-1752.

Weisenberger, L.A. and J.L. Koenig, *NMR Imaging of Solvent Diffusion in Polymers.* Applied Spectroscopy, 1989. **43**(7): p. 1117-1126.

Zaki, O., B. Abbes, and L. Safa, *Non-Fickian diffusion of amyl acetate in polypropylene packaging: Experiments and modelling.* Polymer Testing, 2009. **28**(3): p. 315-323.

Zaremskii, M.Y., A.V. Olenin, Y.S. Garina, S.I. Kuchanov, V.B. Golubev, and V.A. Kabanov, *Mechanism of Photoinitiated Radical Polymerization of Styrene in the Presence of Benzyldithiocarbamate Iniferter.* Vysokomolekulyarnye Soedineniya Seriya A, 1991. **33**(10): p. 2167-2175.

Zhang, C.S., D. Xing, and Y.Y. Li, *Micropumps, microvalves, and micromixers within PCR microfluidic chips: Advances and trends.* Biotechnology Advances, 2007. **25**(5): p. 483-514.

Zhou, Q.Y., A.S. Argon, and R.E. Cohen, *Enhanced Case-II diffusion of diluents into glassy polymers undergoing plastic flow.* Polymer, 2001. **42**(2): p. 613-621.

Vita

Adam K. Ekenseair is from Fayetteville, Arkansas. He received his B.S. in Chemical Engineering from the University of Arkansas at Fayetteville in May 2005. As an undergraduate, he performed research under the direction of Professor Edgar C. Clausen on compound extraction and quantification from Mimosa and fermentation of grape pomace. He also attended two NSF-REU programs working on "Fabrication of Nylon-6 and PET Nanocomposites" with Dr. Thanasis Papathanasiou at the University of South Carolina and on "Catalytic Oxidation of Alkenes" with Dr. Kerry Dooley at Louisiana State University.

After graduation, Adam joined the University of Texas at Austin as a National Defense Science and Engineering Graduate Fellow and a National Science Foundation Graduate Research Fellow working with Professor Nicholas A. Peppas.

Permanent Address: 1908 Albury Cv. Apt. C, Austin, TX 78758

This dissertation was typed by the author